UNIVERSITÉ DE STRASBOURG

ÉCOLE DOCTORALE MSII

Laboratoire ICube – Département Mécanique (D-M)

THÈSE présentée par :

Sonja KALLIO

soutenue le : **14 Septembre 2022**

pour obtenir le grade de : **Docteur de l'université de Strasbourg**

Discipline/ Spécialité : ENERGETIQUE

Management de l'énergie des systèmes de micro-cogénération basés sur des énergies renouvelables dans le contexte des smart grids

Energy management of renewable energy-based micro-cogeneration systems in the context of smart grids

THÈSE dirigée par :

SIROUX Monica	Professeur, INSA Strasbourg ICUBE Université de Strasbourg

RAPPORTEURS :

MÉNÉZO Christophe	Professeur, Université Savoie-Mont Blanc
SALAGNAC Patrick	Professeur, Université de La Rochelle

AUTRES MEMBRES DU JURY :

BENNACER Rachid	Professeur, ENS CACHAN Université Paris-Saclay

“One, remember to look up at the stars and not down at your feet. Two, never give up work. Work gives you meaning and purpose and life is empty without it. Three, if you are lucky enough to find love, remember it is there and don't throw it away.”

— Stephen Hawking

ACKNOWLEDGMENTS

As a part of the ACA-MODES project, this thesis received the support and funding from Interreg V Rhin Supérieur which I want to acknowledge gratefully. I want to thank all the ACA-MODES project partners from Germany and Switzerland, who were creating this project from the beginning, for their support and co-operation during these three years. The global pandemic COVID-19 gave us difficult and special conditions to implement this project and, for me, to write this thesis but we managed it in the best way.

A special acknowledge to my thesis supervisor Professor Monica SIROUX for her suggestions, contributions and continuous encouragement to believe in myself as a researcher. I want to thank her for giving me this opportunity to write my thesis in Strasbourg, France.

I want to express my gratitude to the jury members, Professor Christophe MÉNÉZO, Professor Patrick SALAGNAC and Professor Rachid BENNACER for their patience to read and evaluate this thesis. I appreciate your commitment and remarks which are invaluable to me.

I want to thank the technical staff of the ICUBE laboratory for their invaluable help in realizing the solar microgrid experimental set-up used in this thesis.

I'm grateful to all my colleagues at INSA Strasbourg and ICUBE laboratory that I got this opportunity to get to know you and be part of this multi-cultural atmosphere.

Last but not least, I want to thank my family in Finland for their continuous support and Jukka VASTARANTA for standing on my side during this part of our life long journey.

TABLE OF CONTENTS

Page

LIST OF FIGURES

Page

LIST OF TABLES

Page

NOMENCLATURE

A	Area	m^2
$\dot{C}$	Exergy cost rate	€/h
c	Specific cost of exergy unit	€/kWh
CHP	Combined Heat and Power	
CPC	Compound Parabolic Collector	
DHW	Domestic Hot Water	
DNI	Direct Normal Irradiation	W/m^2
E	Energy	J, kWh
ETC	Evacuated Tube Collector	
Ex	Exergy	J, kWh
$\dot{E}x$	Exergy flow	W, kW
f	Quality factor	-
FPC	Flat-Plate Collector	
G	Solar irradiation	W/m^2
GHI	Global Horizontal Irradiation	W/m^2
GTI	Global Tilted Irradiation	W/m^2
h	Specific enthalpy	J/kg
HREMS	Home Renewable Energy Management System	
HRES	Hybrid Renewable Energy System	
Ir	Exergy irreversibility rate	W, kW
$\dot{m}$	Mass flow rate	kg/s, kg/h
P	Electrical power	W, kW
p	Pressure	hPa
PES	Primary Energy Savings	
PV	Photovoltaic	
PVT	Photovoltaic-Thermal	
Q	Thermal energy	J, kWh
R	Reliability	
RAI	Relative Avoided Irreversibility	
RH	Relative Humidity	%
s	Specific entropy	J/kgK
SHC	Solar Heat Collector	
SOC	State Of Charge	
T	Temperature	K, °C
$\dot{Z}$	Initial investment rate	€/h
WS	Wind Speed	m/s
w	Weighting factor	

Greek letters

ε	Emissivity	
σ	Stefan–Boltzmann constant	$W/m^2/K^4$
β	Temperature coefficient	
ψ	Exergy conversion coefficient	
Ω	Exergy destruction rate	
η	Energy efficiency	
Ƶ	Exergy efficiency	
δ	Maximum power correction factor	

Subscripts

a	Ambient
B	Battery
b	Boiler
CHP	Combined Heat and Power
d	Exergy destruction
el	Electric
fuel, f	Energy/Exergy fuel
g	Grid
I	Initial investment cost
i	flow
irr	Irradiation
k	k^{th} component
Load	Electrical load
loss	Energy loss
NOCT	Nominal Operating Cell Temperature
OM	Operation and maintenance costs
Product, p	Energy/Exergy product
pv	Photovoltaic
ref	Reference
STC	Standard Test Conditions
t	time
th	Thermal

ABSTRACT

Increasing energy demand and the ambitious primary energy and CO_2 reduction targets of the European Union have increased interest in renewable energy-based micro-cogeneration systems that produce heat and power simultaneously from a single fuel source for on-site use of buildings. Although these systems operate at high energy efficiency, deeper efficiency analysis is required to reveal hidden inefficiencies. The exergy analysis combines the first and second law of thermodynamics and is used to define, in addition to the quantity, the quality of energy supply. The exergy analysis has been mainly applied in industrial processes that are significantly different in nature compared to building energy systems. However, this thesis aims to apply the exergy method to the micro-cogeneration and hybrid renewable energy systems on the building microgrids by performing energy, exergy and exergo-economic analysis, and exergy based design optimization. The aim is also to investigate the impact of different meteorological conditions on the results of the exergy analysis and to find out if the results differ from the energy analysis. Additionally, different energy management methods for the hybrid renewable energy system are studied by realizing an experimental set-up of a residential solar microgrid. The experimental set-up aims to collect the weather and PV production data to study different machine learning-based forecasting methods to be used in the advanced control methods.

To apply the exergy method, the simulation platforms for the solar and biomass-based micro-cogeneration systems and the hybrid renewable energy system were built into Matlab/Simulink for a dynamic simulation purpose. First, a single photovoltaic-thermal (PVT) collector was modelled to conduct energy and exergy analysis under different climate conditions and to perform exergy-based design optimization of the collector. Next, the model was used for exergy optimization of a multi-stage PVT collector. The second simulation model was built for a biomass-fueled micro-cogeneration system to conduct the energy and exergy analysis. Finally, these models were coupled to form a novel hybrid renewable energy system (HRES) for a residential building and studied in terms of energy, exergy and exergo-economics. Again, different weather conditions were considered. At the application level, the energy management strategies were investigated by the experimental set-up and linear programming optimization model in Matlab. The different PV production forecasting models were built into Matlab as well.

The exergy analysis applied to the PVT collectors brought new information on the efficiency and design variables compared to the energy approach. The thermal exergy efficiency was maximized by decreasing the mass flow rate and by increasing the inlet temperature that are both opposite if compared to maximizing the thermal energy efficiency, which led to high mass flow rate and low inlet temperature. The exergy method was also applied to the biomass-fueled ÖkoFEN Stirling engine micro-CHP unit. The results revealed high thermal inefficiency of the system, although the thermal energy efficiency was 98%. However, the micro-CHP was an improvement in terms of the primary energy saving and relative avoided irreversibility if compared to the reference system. The exergo-economic analysis applied to the novel HRES indicated a high variation in the specific costs of the energy products over a year. The different weather conditions had an impact on the value of the heat products due to varying ambient temperatures. The HRES reduced strongly primary energy use and costly irreversibility. The system was economically viable in each investigated location, although the average yearly electricity costs were higher than the current electricity price from the grid. However, the grid prices are expected to increase in the future, which can make the system more viable from the energy autonomy point of view. Finally, the experimental data from the solar microgrid was used to train machine learning-based PV power prediction models for the advanced energy management methods that require future information. The results showed that the artificial neural network model with the data from the micro-inverters led to the most accurate future forecast of PV production.

As a conclusion, this research provides deeper knowledge of the energy efficiency in renewable energy-based micro-cogeneration systems in the domestic microgrids. It highlights the importance of moving from the energy quantity-based evaluation of the building energy systems to the quality-based evaluation. The research results show that maximizing the exergy efficiency leads to different operational conditions than maximizing the energy efficiency. To understand the real monetary value of the energy products of the HRES in a residential microgrid, the significance of the exergo-economic costing method is demonstrated for the HRES under different climate conditions. This research also provides operational data of a solar microgrid which is essential for further studies of energy management and PV modelling in this thesis.

Résumé

En français

Management de l’énergie des systèmes de micro-cogénération basés sur des énergies renouvelables dans le contexte des smart grids

Introduction

La région métropolitaine tri-nationale du Rhin supérieur (TMR) est située à la frontière rhénane de trois pays européens : la France (Alsace), l'Allemagne (Bade-Wurtemberg, partie sud de la Rhénanie-Palatinat) et la Suisse (cantons de Bâle-Ville, Bâle-Campagne, Argovie, Jura et Soleure). Dans le cadre de la "stratégie climatique et énergétique pour le TMR", l'exploitation transfrontalière du TMR vise à réduire les émissions de CO_2 de 80 % par rapport à 2000 et la consommation d'énergie primaire de 35 % d'ici 2050. Dans le TMR, les laboratoires de recherche ont une grande opportunité d'étudier et de développer un fonctionnement transfrontalier et respectueux du réseau des systèmes d'énergie renouvelable hybrides décentralisés dans le contexte du smart grid. Dans cette optique, le projet innovant transfrontalier ACA-MODES est développé dans le cadre du programme INTERREG V Rhin supérieur. Cette thèse fait partie de ce projet dont l'objectif principal est d'optimiser les systèmes énergétiques hybrides décentralisés en termes de fonctionnement transfrontalier, d'efficacité énergétique et de conception.

Les objectifs ambitieux de réduction de l'énergie primaire et du CO_2 fixés par le TMR et l'UE nous encouragent à révéler les inefficacités cachées grâce à l'analyse exergétique des systèmes énergétiques des bâtiments. En combinant la première et la deuxième loi de la thermodynamique, l'accent mis sur les quantités d'énergie et les réductions d'énergie primaire peut être étendu à l'aspect qualitatif de l'approvisionnement énergétique des bâtiments.

Cette thèse est motivée par la volonté de concevoir des systèmes énergétiques plus efficaces et durables pour les bâtiments. Dans ce but, l’analyse exergétique et exergo-économique est étudiée et réalisée dans le contexte de la micro-cogénération et des systèmes hybrides d’énergie renouvelable. L’autre motivation de cette thèse est d’étudier différentes méthodes de management de l‘énergie et de prévision de la production énergie solaire. La gestion optimale de l'énergie et les méthodes de prévision précises permettent un contrôle plus efficace du système et l'utilisation des énergies renouvelables dans les systèmes hybrides d'énergie renouvelable. Dans ce but, un dispositif expérimental basé sur des panneaux photovoltaïques est réalisé au cours de cette thèse afin de recueillir des données météorologiques

et de étudier le fonctionnement des panneaux photovoltaïques PV à l'aide des méthodes de machine learning.

Chapitre 1. Etat de l'art : Micro-cogénération et la méthode exergétique dans le contexte des micro-réseaux

Le chapitre 1 présente l'état de l'art de la méthode exergétique dans le contexte des micro-réseaux. Tout d'abord, les problèmes et les enjeux de la consommation d'énergie dans L'Union Européenne (UE) avec les objectifs de réduction sont présentés et discutés. Les systèmes énergétiques décentralisés plus efficaces dans les micro-réseaux de bâtiments sont considérés comme l'une des mesures clés pour atteindre l'objectif de réduction de la consommation d'énergie de l'UE.

Les micro-réseaux résidentiels dans le contexte des smart grids devraient inclure la production d'énergie la plus efficace qui est réalisée par la micro-cogénération. Les unités de micro-cogénération contrôlables et fluctuantes, telles que la biomasse et le solaire, peuvent former un système hybride d'énergie renouvelable dans lequel les unités se soutiennent mutuellement et où un système de stockage d'énergie étendus ne sont pas absolument nécessaires. Ce chapitre présente donc une étude approfondie des systèmes de micro-cogénération et des systèmes énergétiques hybrides composés d'un système de micro-cogénération alimenté en combustible et de technologies solaires.

La méthode exergétique est utilisée pour révéler les inefficacités cachées des composants du système énergétique. Les indicateurs d'exergie sont présentés avec la méthode de l'analyse exergétique. De plus, l'exergie des différents types de technologies dans les micro-réseaux est présentée et discutée. Enfin, une méthode combinant l'exergie et la valeur monétaire, appelée exergo-économie, est présentée afin de disposer d'une méthode de calcul des coûts plus rationnelle pour évaluer les systèmes hybrides d'énergie renouvelable dans les micro-réseaux.

1.1 Micro-cogénération et systèmes hybrides d'énergie renouvelable

Les systèmes de micro-cogénération produisent simultanément de la chaleur et de l'électricité à partir d'une seule source de combustible, avec un rendement élevé d'environ 85 à 95 %. Ces systèmes sont définis comme ayant une puissance électrique inférieure à 15kW. Les

avantages de la micro-cogénération par rapport à la production d'énergie séparée par convection sont présentés dans la figure 1-1.

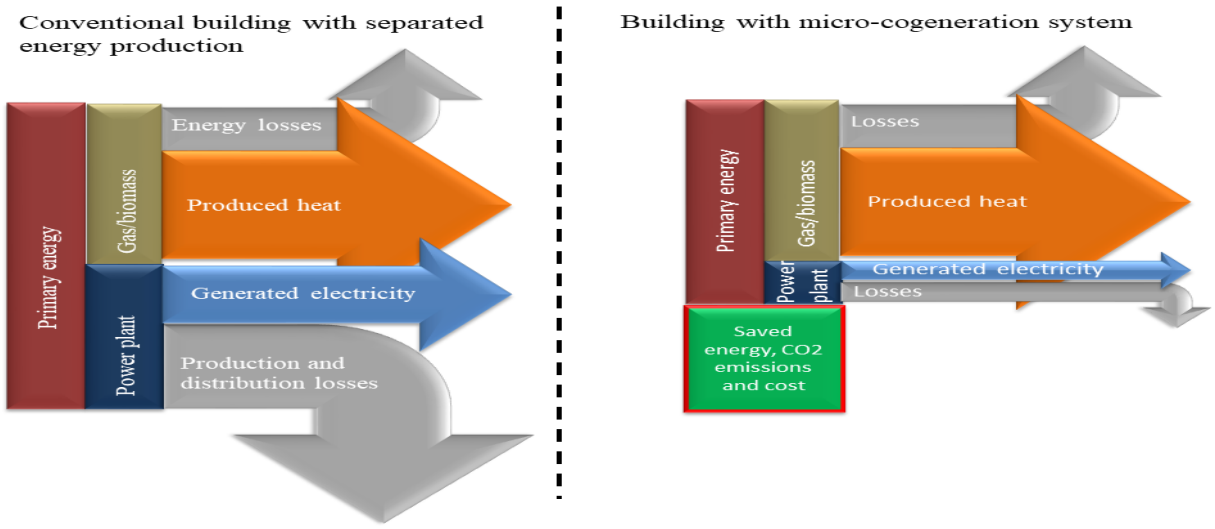

Figure 1-1 : *Comparaison entre la production conventionnelle d'énergie séparée et la micro-cogénération.*

Les systèmes de micro-cogénération alimentés par des combustibles suivants sont disponibles sur le marché :

Pile à combustible : Ces systèmes ont un rendement électrique élevé, de faibles émissions et un fonctionnement silencieux. Ils fonctionnent selon un processus non combustible pour produire de la chaleur et de l'électricité à partir d'hydrogène, de gaz naturel ou de biogaz. Le processus de conversion énergétique de la pile à combustible ne produit que de la chaleur et de l'eau comme sous-produit, ce qui en fait le moteur le plus propre en termes de conversion énergétique. Le désavantage de la pile à combustible reste un coût d'investissement très élevé, une courte durée de vie et la difficulté de produire le combustible avec une énergie sans émissions de CO_2.

Moteur à combustion interne : Ces systèmes sont les plus développés et les plus éprouvés des technologies de moteurs à combustion. Cependant, ils ne peuvent pas utiliser directement les combustibles solides, tels que la biomasse, mais la gazéification peut être utilisée pour produire un gaz de synthèse approprié à partir de la biomasse. En général, ces moteurs sont alimentés par du gaz naturel et présentent le meilleur rendement parmi les technologies de moteurs.

Moteur Stirling : Cette technologie de moteur principal est basée sur la source de chaleur extérieure permettant d'utiliser une large gamme de combustibles renouvelables, tels que la biomasse, le biogaz et le solaire. Les moteurs Stirling offrent le potentiel de fonctionnement le plus silencieux par rapport aux autres moteurs, un ratio puissance/chaleur adapté aux applications de bâtiment et de faibles besoins de maintenance. L'unité disponible sur le marché de la société ÖkoFEN est étudiée dans cette thèse.

Cycle Rankine Organique (ORC) : L'ORC est le deuxième moteur principal avec le processus de combustion externe et une grande variété de combustibles provenant de la géothermie, du solaire ou de la biomasse. Grâce à l'utilisation d'un fluide organique comme fluide de travail, l'ORC peut fonctionner à des températures de vaporisation plus basses pour dilater la vapeur dans une turbine. Les systèmes de micro-cogénération basés sur l'ORC sont bien étudiés par les chercheurs et les entreprises. Cependant, la disponibilité de ces systèmes sur le marché est encore limitée.

Outre les systèmes de micro-cogénération à combustible et contrôlables, le capteur **photovoltaïque-thermique** (PVT) est un système de micro-cogénération à base solaire qui intègre les composants du panneau photovoltaïque (PV) et du capteur de chaleur solaire en une seule unité afin d'améliorer le rendement total. Le PVT utilise le panneau PV pour produire de l'électricité et, comme sous-produit, de la chaleur utile est produite en refroidissant le PV avec un fluide réfrigérant. Le refroidissement diminue la température de fonctionnement du panneau PV, ce qui augmente le rendement électrique. Un système de cogénération à base solaire peut également être formé en installant séparément des panneaux photovoltaïques et des capteurs de chaleur solaire. Cependant, les principaux avantages des capteurs PVT sont l'amélioration de 'utilisation de la zone d'installation, l'augmentation du rendement énergétique total et l'augmentation de la durée de vie des cellules PV.

Par définition, **le système hybride d'énergie renouvelable** (HRES) couple deux ou plusieurs sources d'énergie renouvelables avec ou sans source d'énergie conventionnelle et stockage d'énergie pour satisfaire une certaine demande énergétique. Le système HRES produit de la chaleur et de l'électricité et peut faciliter l'autonomie énergétique d'un micro-réseau. Pour étudier le HRES résidentiel le plus efficace, les systèmes de micro-cogénération alimentés par la biomasse et l'énergie solaire sont intégrés dans cette thèse, comme le montre la figure 1-2

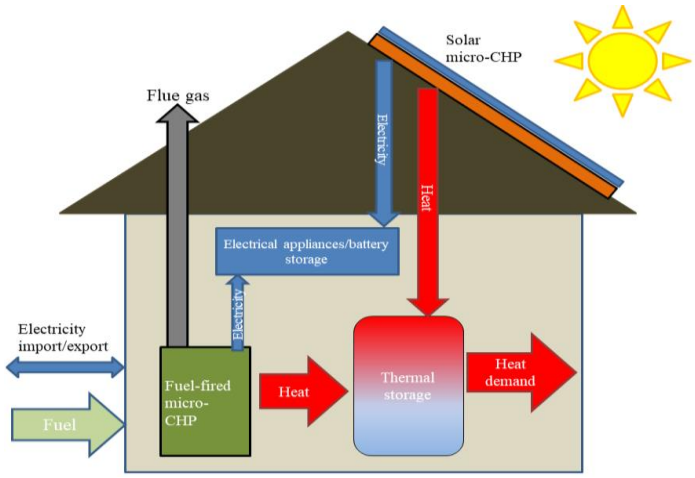

Figure 1-2 : *Les flux d'énergie dans le micro-réseau résidentiel, y compris les systèmes de micro-cogénération alimentés au combustible et à l'énergie solaire.*

1.2 Méthode d'exergétique

Les systèmes de micro-cogénération et les systèmes hybrides d'énergie renouvelable peuvent être évalués par la méthode d'exergétique qui est basée sur deuxième loi de la thermodynamique et combinée avec l'analyse énergétique. La première loi de la thermodynamique (analyse de l'énergie) quantifie la quantité d'énergie qui peut changer de forme mais dont la quantité totale reste constante dans le système. Selon la deuxième loi de la thermodynamique, la qualité de l'énergie existe également. La qualité de l'énergie est détruite dans tout processus de conversion énergétique. La quantité de qualité détruite peut être utilisée comme une deuxième mesure de l'efficacité des processus de conversion de l'énergie.

En termes de systèmes de cogénération, l'électricité est considérée comme une exergie pure car elle peut être transférée directement en travail. Cependant, l'exergie de l'énergie thermique dépend de la différence de température entre la chaleur et son environnement, qui est utilisée pour extraire du travail. La figure 1-3 et 1-4 présente l'évaluation énergétique et exergétique de différents types de technologies. En raison de la production simultanée de chaleur et d'électricité dans le système de cogénération, le rendement exergétique est le plus élevé, même si le rendement énergétique peut être identique.

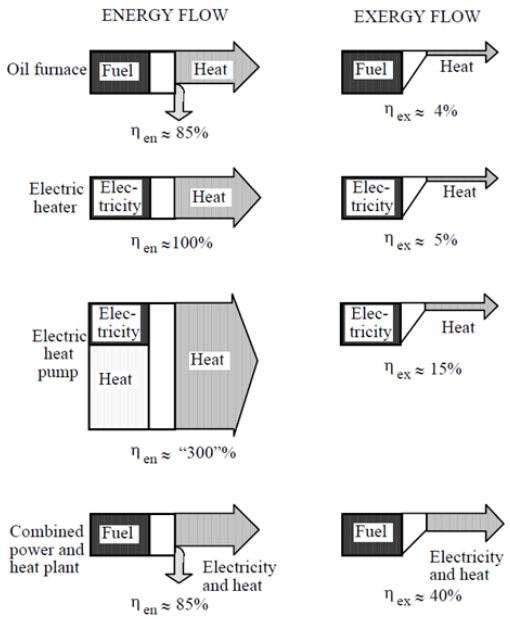

Figure 1-3 : *Efficacité énergétique et exergétique de différents dispositifs de conversion d'énergie [81].*

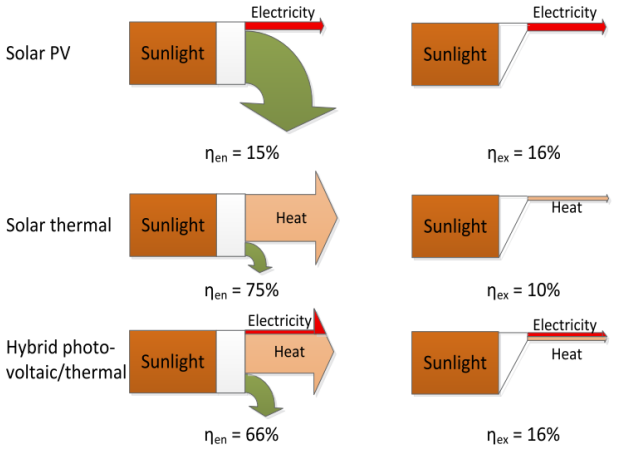

Figure 1-4 : *Efficacité énergétique et exergétique de différents systèmes de conversion de l'énergie solaire [83].*

L'économie de l'énergie est un domaine qui combine l'énergie et l'économie pour définir les valeurs monétaires des différents produits énergétiques. Cependant, une méthode de calcul des coûts plus rationnelle consiste à combiner l'exergie avec la valeur monétaire, car l'exergie indique la valeur de l'énergie. Cette méthode s'appelle l'exergo-économie et il attribue des valeurs monétaires aux flux d'exergie du système considéré, tel que le système hybride d'énergie renouvelable.

La figure 1-5 présente le bilan exergo-économique du $k^{ème}$ composant ou du système complet. Le système reçoit une certaine exergie d'entrée, ainsi que des flux de coûts exégétiques et non exergétiques. En sortie, certains produits énergétiques, tels que la chaleur et l'électricité, et les coûts des produits exergétiques en résultent. Le coût de la destruction d'exergie dans la figure 1-5 peut être calculé également ou mis à zéro, ce qui transfère le coût de destruction directement aux produits.

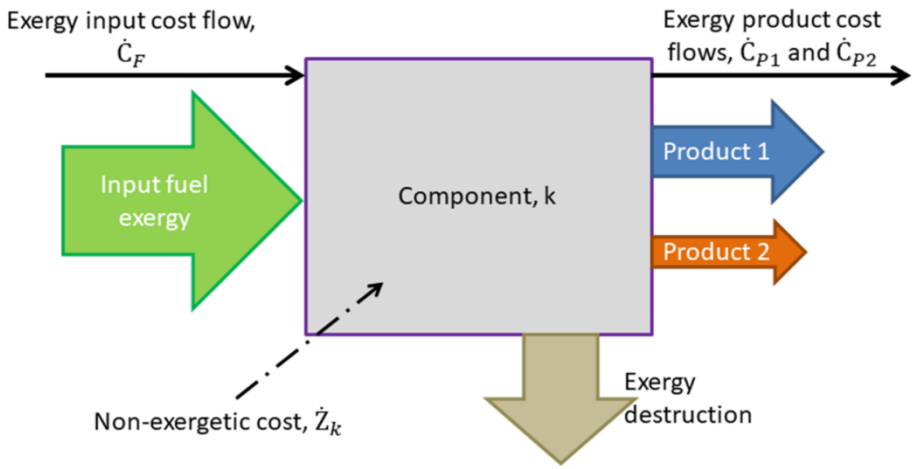

Figure 1-5 : *Le bilan exergo-économique de la k^{ème} composante.*

L'exergo-économie est utilisée pour calculer la valeur monétaire spécifique des produits énergétiques du système en considérant la destruction coûteuse de l'exergie du combustible et les coûts non exergétiques. Ces coûts spécifiques du produit peuvent être utilisés pour la tarification et récupérés par la vente des produits. D'autre part, ces coûts peuvent être récupérés en générant des économies par l'utilisation sur place des produits.

Chapitre 2. Analyse énergétique et optimisation exergétique d'un capteur thermique photovoltaïque dans différentes conditions climatiques

Le chapitre 2 présente une modèle dynamique du capteur photovoltaïque-thermique (PVT) construit dans Matlab/Simulink qui est utilisé pour effectuer une analyse énergétique et exergétique des performances de capteur dans deux conditions climatiques européennes différentes.

Le fonctionnement du capteur PVT est un compromis car l'efficacité électrique du panneau PV diminue quand la température de fonctionnement du capteur augmente. D'autre part, l'augmentation de la température de fonctionnement entraîne une augmentation du rendement thermique. Pour cette raison, un problème d'optimisation multi-objectif est formulé pour trouver une solution de compromis pour une conception PVT.

La conception du capteur PVT est optimisée en termes d'efficacité exergétique thermique et électrique en utilisant un algorithme d'intelligence artificielle appelé « Non-Dominated

Sorting Genetic Algorithm-II » (NSGA-II). Les variables de décision suivantes sont utilisées dans l'optimisation multi-objectif bidimensionnelle du capteur PVT : le débit massique du réfrigérant, la température d'entrée, l'épaisseur de la lame d'air entre le verre de couverture et le module PV et l'épaisseur de l'isolation.

Sur la base du front de Pareto obtenu, trois conceptions différentes de PVT sont sélectionnées et comparées aux performances d'un panneau photovoltaïque (PV). La comparaison est utilisée pour révéler si le PVT est toujours compétitif avec la production électrique du panneau, après avoir maximisé son efficacité exergétique thermique, car la performance thermique du PVT a un impact négatif sur sa performance électrique.

2.1 Performance du capteur PVT dans deux conditions climatiques différentes

Des simulations horaires ont été réalisées avec le modèle PVT dynamique dans Matlab/Simulink dans deux conditions climatiques différentes.

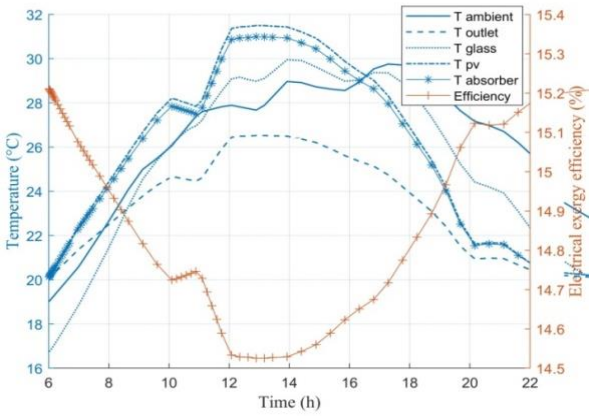

Figure 2-1 : *Le rendement exergétique, la surface PVT, la sortie du fluide et la température ambiante pendant un jour d'été.*

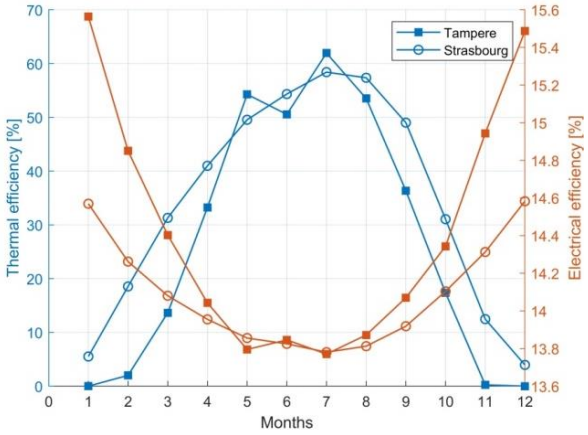

Figure 2-2 : *Efficacités électriques et thermiques mensuelles sur un an à Tampere et Strasbourg.*

La température de fonctionnement de la cellule PV a un impact fort sur son efficacité électrique. La figure 2-1 montre la simulation des températures de la couche PVT sur une journée et comment l'efficacité électrique diminue lorsque les températures augmentent, et vice versa. Cela conduit à la conclusion que les rendements électrique et thermique ne peuvent pas être maximisés en même temps, mais qu'il faut trouver une solution de compromis.

La figure 2-2 montre les rendements thermiques et électriques mensuels sur deux endroits. Les résultats montrent qu'il n'y a pas de différence significative entre les sites

sélectionnés en termes de performance énergétique maximale. L'efficacité électrique présente les valeurs les plus faibles pendant les mois d'été en raison des températures de fonctionnement plus élevées. La figure 2-3 présente les efficacités exergétiques thermiques et électriques mensuelles des deux endroits. Le résultat principal est que l'efficacité exergétique thermique prend des valeurs très basses dans les deux endroits par rapport à l'efficacité énergétique thermique. Dans l'emplacement nord, l'énergie thermique a l'exergie la plus élevée. La production annuelle totale d'énergie et d'exergie est respectivement, de 7,8 % et 1,27 % plus élevée à Strasbourg qu'à Tampere.

Le fonctionnement du capteur PVT et du panneau PV est comparé à l'aide de modèles de simulation dans Matlab/Simulink. Ceci est illustré dans la figure 2-4. L'effet de refroidissement du capteur PVT réduit la température maximale de fonctionnement à 30 °C par rapport à 48 °C du panel PV. Cela permet d'obtenir un rendement électrique supérieur de 1.1 point de pourcentage dans le capteur PVT. Ensuite, le facteur de remplissage (r_c) du capteur PVT est varié de 0.6 à 1 et comparé au panel PV. Les résultats montrent que le facteur de remplissage n'a qu'une faible influence sur la température de fonctionnement du capteur PVT. Le capteur PVT avec un facteur de remplissage de 0.8 à 1 est compétitif ou meilleur par rapport au panel PV.

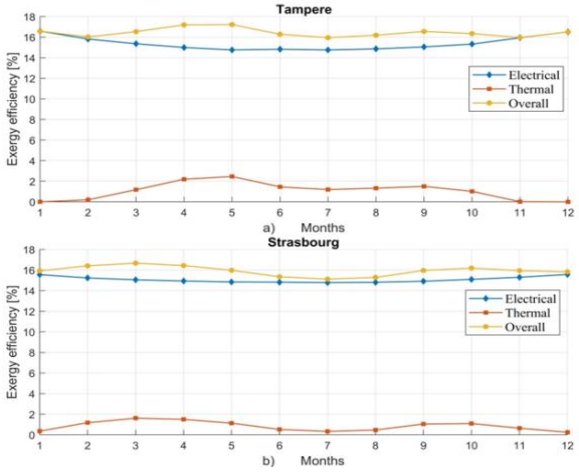

Figure 2-3 : *Efficacité exergétique thermique, électrique et mensuelle globale à a) Tampere et b) Strasbourg*

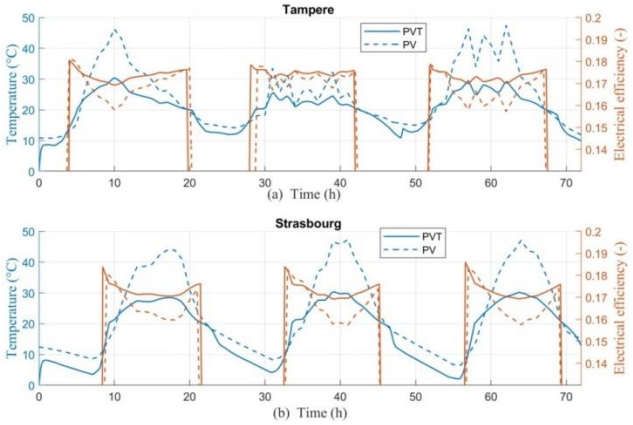

Figure 2-4 : *Les températures de fonctionnement des cellules PV et le rendement électrique a) à Tampere et b) à Strasbourg pendant les trois jours d'été.*

2.2 Optimisation multi-objectifs du capteur PVT

L'optimisation multi-objectifs basée sur la simulation de la conception du capteur PVT est réalisée dans Matlab/Simulink avec l'algorithme NSGA-II. Les conditions stables

d'irradiation solaire de 500 W/m^2, de température ambiante de 16 °C et de vitesse du vent de 2 m/s sont utilisées dans l'optimisation. Sur la base de l'analyse de sensibilité, les variables de décision suivantes sont sélectionnées pour optimiser simultanément les efficacités exergétiques thermique et électrique : débit massique, température d'entrée, épaisseur de la lame d'air et épaisseur de l'isolation.

Le résultat est un front de Pareto dans la figure 2-5 qui montre trois niveaux de solution pour la conception : la solution axée sur l'électricité, la solution axée sur l'exergie thermique et la solution de compromis. La solution axée sur l'électrique est caractérisée par un débit massique élevé, une épaisseur de la lame d'air plus faible, une température d'entrée basse et une épaisseur d'isolation faible. La solution axée sur l'exergie thermique est caractérisée par un débit massique faible, une température d'entrée élevée, une lame d'air et une isolation plus épaisse. La figure 2-6 montre que les trois solutions de conception PVT sont compétitives avec le panel PV en termes de production d'électricité, bien que la solution thermique présente la température de fonctionnement la plus élevée. Toutefois, les températures de fonctionnement maximales mensuelles restent inférieures par rapport à celles du panel PV.

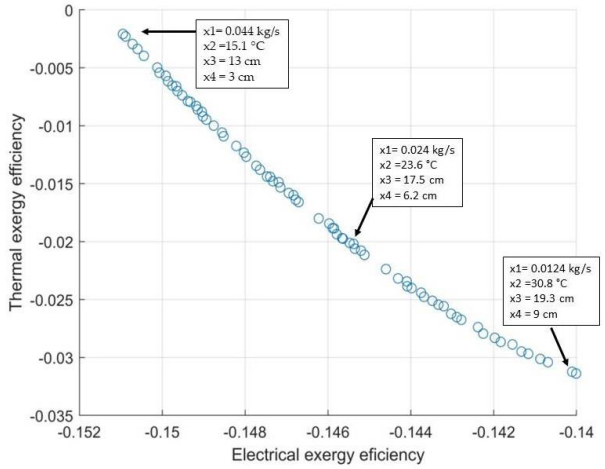

Figure 2-5 : *Efficacité exergétique thermique, électrique et mensuelle globale à a) Tampere et b) Strasbourg.*

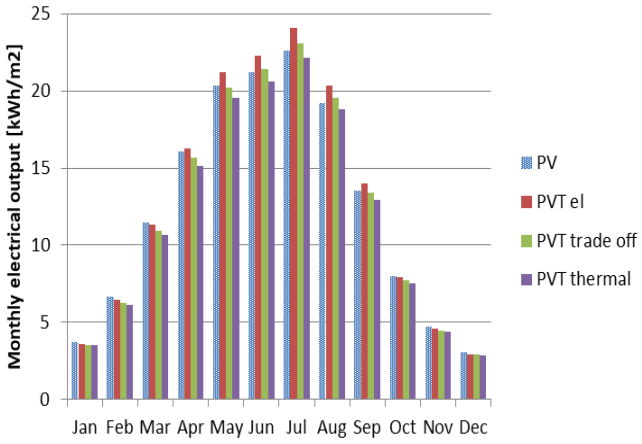

Figure 2-6 : *Rendement électrique mensuel du panel PV et trois conceptions optimales de PVT.*

Chapitre 3. Optimisation exergétique d'un système de micro-cogénération solaire à multi-étages

Dans le chapitre 3, le modèle PVT du chapitre 2 est développé pour présenter un capteur PVT multi-étages avec N collecteurs présenté dans la figure 3-1. Tout d'abord, le modèle est

présenté et l'étude paramétrique détaillée est menée dans des conditions météorologiques stables. L'objectif de l'étude paramétrique est de révéler la relation entre le débit massique, le nombre de capteurs et la température d'entrée et les rendements énergétiques et exergétiques.

Ensuite, l'optimisation de la conception du capteur PVT à plusieurs étages est réalisée pour trois conditions météorologiques différentes en conditions stables selon le débit massique, le nombre de capteurs PVT et la température d'entrée. L'optimisation multi-objectifs bidimensionnelle vise à maximiser simultanément l'efficacité exergétique thermique et électrique. La conception du capteur PVT à plusieurs étages est optimisée en utilisant un algorithme d'intelligence artificielle appelé « Non-Dominated Sorting Genetic Algorithm-II » (NSGA-II) en Matlab. Comme résultats, un front de Pareto est obtenu et la méthode du point idéal est utilisée pour sélectionner la solution optimale finale pour chaque condition climatique.

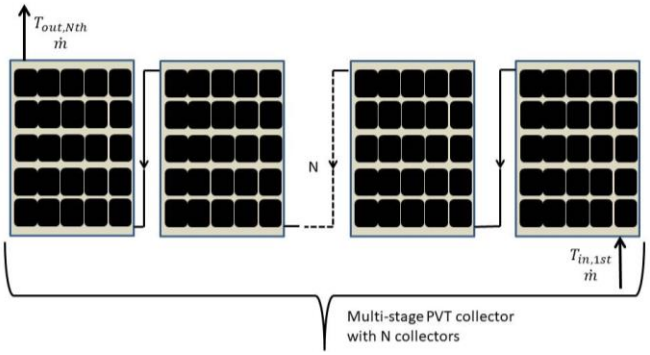

Figure 3-1 : *Le principe de fonctionnement du capteur PVT multi-étages.*

3.1 L'étude paramétrique

L'étude paramétrique est réalisée dans les conditions météorologiques suivantes : irradiation solaire 800 W/m^2, température ambiante de 25 degrés et vitesse du vent de 1 m/s. Dans la figure 3-2, le débit massique est augmenté, ce qui augmente l'efficacité électrique et diminue l'efficacité exergétique thermique. Cela révèle la nature du compromis de l'opération du capteur PVT. Dans la figure 3-3, la température d'entrée est augmentée, ce qui augmente l'efficacité exergétique thermique mais diminue l'efficacité énergétique thermique.

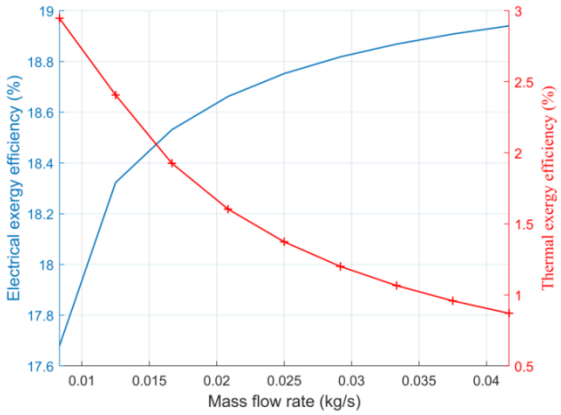

Figure 3-2 : *Variation de l'efficacité exergétique thermique et électrique en fonction du débit massique du fluide de refroidissement.*

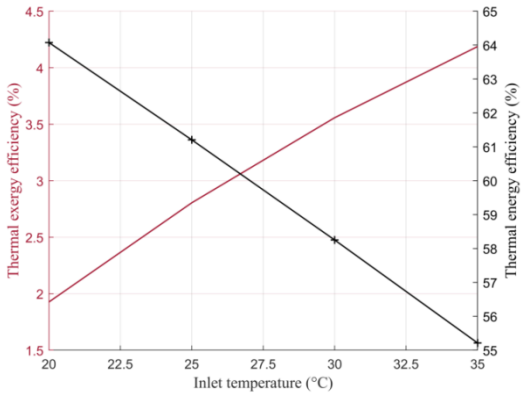

Figure 3-3 : *Variation de l'efficacité exergétique thermique et de l'efficacité de l'énergie thermique en fonction de la température d'entrée du fluide de refroidissement.*

Si le nombre de capteurs PVT en série est augmenté, la température de sortie du fluide de refroidissement augmente mais le rendement électrique diminue en raison de la température de fonctionnement plus élevée. Dans la figure 3-4, le nombre de capteurs augmente, ce qui augmente l'efficacité exergétique thermique jusqu'à un certain point. En même temps, l'efficacité thermique est seulement diminuée parce que la surface totale des capteurs augmente relativement plus que la température de sortie gagnée. La figure 3-5 montre que l'augmentation de la température d'éntrée réduit la nécessité d'augmenter le nombre de capteurs PVT en série en termes d'efficacité exergétique thermique. Si la température d'entrée est réduite, un nombre plus élevé de capteurs PVT est nécessaire pour atteindre la même efficacité exergétique thermique.

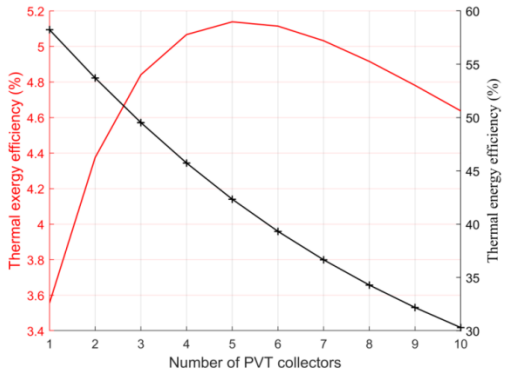

Figure 3-4 : *La variation de l'efficacité exergétique thermique et de l'efficacité énergétique thermique en fonction du nombre de capteurs PVT en série.*

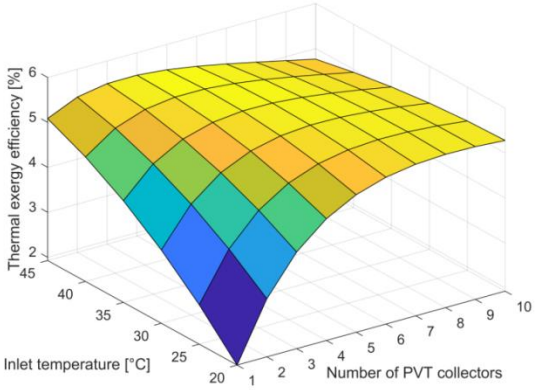

Figure 3-5 : *La variation de l'efficacité exergétique thermique en fonction de la température d'entrée de fluide de refroidissement et du nombre de capteurs PVT.*

3.2 Optimisation multi-objectifs du capteur PVT multi-étages

L'optimisation multi-objectifs est réalisée dans trois conditions météorologiques différentes en conditions stables : froid, moyen et chaud. L'objectif est de voir l'impact des conditions sur le front de Pareto de la figure 3-7. La figure 3-6 présente l'ensemble des solutions optimales dans les conditions moyennes en termes d'efficacité exergétique totale. L'efficacité exergétique totale maximale dans l'ensemble des solutions optimales est de 21.87% et ceci est obtenu avec une température d'entrée de 31 °C, 4 capteurs en série et un débit massique de 0.0269 kg/s.

La figure 3-7 présente les fronts de Pareto dans chaque condition climatique. Le front de Pareto comprend plusieurs solutions optimales et le processus de prise de décision est utilisé pour trouver la solution optimale finale pour chaque condition climatique. La méthode du point idéal est utilisée pour définir les solutions optimales finales présentées dans la figure 3-7. Dans le cas de conditions moyennes, cette solution est un peu différente de celle de la figure 3-6 qui maximise l'efficacité énergétique globale.

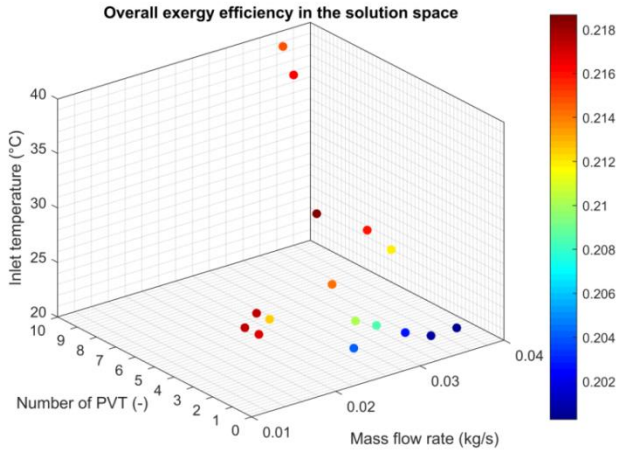

Figure 3-6 : *L'ensemble des solutions optimales dans les conditions moyennes en termes d'efficacité énergétique totale.*

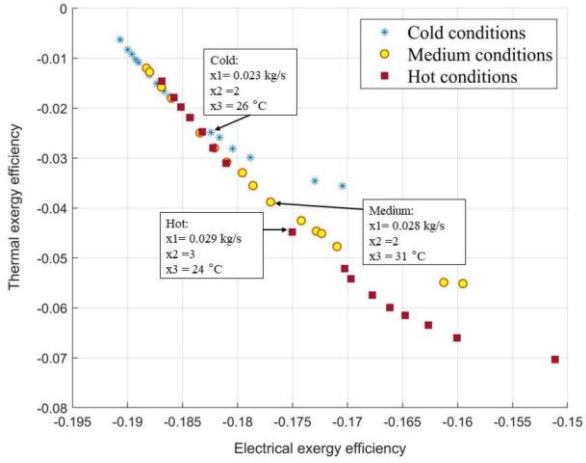

Figure 3-7 : *Le front optimal de Pareto pour les efficacités exergétiques thermique*

Les fronts de Pareto de la figure 3-7 varient en fonction des conditions météorologiques, mais ils se chevauchent également. La gamme des solutions optimales dans l'espace objectif est définie par les conditions météorologiques. La gamme la plus petite est obtenue avec les

conditions froides tandis que les conditions chaudes ont la gamme la plus large. Le nombre optimal de capteurs PVT en série varie de 2 à 4 en fonction des conditions climatiques.

Chapitre 4. Analyse énergétique et exergétique d'une unité de micro-cogénération la biomasse

Le chapitre 4 présente un modèle dynamique d'un système de micro-cogénération (micro-CHP) alimenté par de la biomasse et un moteur Stirling, construit dans Matlab/Simulink. Le système est présenté dans la figure 4-1 et les volumes de contrôle du modèle dans la figure 4-2. Les données expérimentales sont utilisées pour caractériser le modèle. Le modèle est utilisé pour mener une analyse énergétique et exergétique du système avec différentes températures d'entrée.

De plus, une étude comparative entre le micro-CHP et un système de référence de production séparée de chaleur et d'électricité est menée. Dans cette comparaison, deux indicateurs principaux sont utilisés : les économies d'énergie primaire (PES) et l'irréversibilité évitée relative (RAI). L'indicateur PES basé sur l'énergie révèle l'énergie primaire économisée lors de l'utilisation de la cogénération par rapport au système de référence. L'indicateur RAI basé sur l'exergie considère la destruction d'exergie générée ou l'irréversibilité du processus de conversion d'énergie. Il montre la différence relative de l'irréversibilité générée par la cogénération et le système de référence.

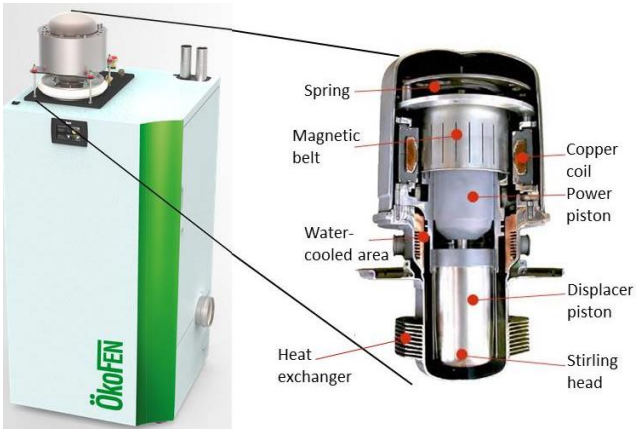

Figure 4-1 : *Unité de micro-cogénération ÖkoFEN alimentée par la biomasse et le moteur Stirling.*

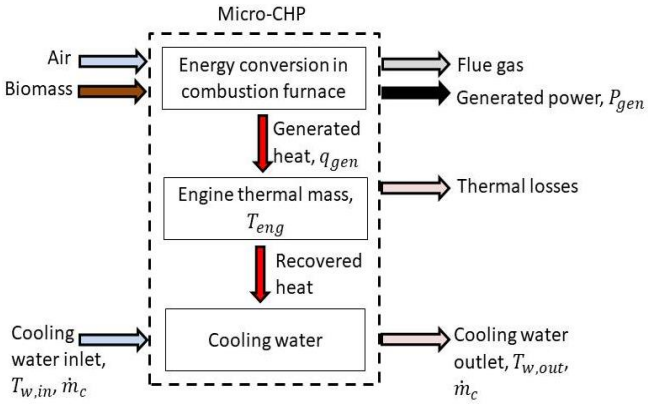

Figure 4-2 : *Les volumes de contrôle du modèle, ainsi que les flux d'énergie et de masse dans le système.*

4.1 Analyse exergétique

Tout d'abord, le système micro-CHP est modélisé dans Matlab/Simulink et l'estimateur de paramètres est utilisé pour estimer les masses thermiques du moteur et de l'eau de réfrigération et les coefficients de transfert de chaleur spécifiques. Le modèle est utilisé pour effectuer une analyse énergétique et exergétique en conditions stables de la micro-CHP fonctionnant au mode d'opération maximum.

Les résultats de l'analyse sont présentés dans la figure 4-3 et la figure 4-4. La température d'entrée du flux d'eau de réfrigération est de 15 °C. Les résultats montrent que l'efficacité thermique et électrique est de 98 % et 7 %, respectivement. Cependant, l'efficacité exergétique thermique n'est que de 7.6 % car le système utilise un combustible de haute qualité pour produire de la chaleur à basse température (qualité). Le rendement exergétique électrique est de 6.4 %. Le processus de conversion de l'énergie du système micro-CHP détruit 86 % de l'apport d'exergie. L'analyse exergétique révèle la grande inefficacité du processus par rapport à l'analyse énergétique.

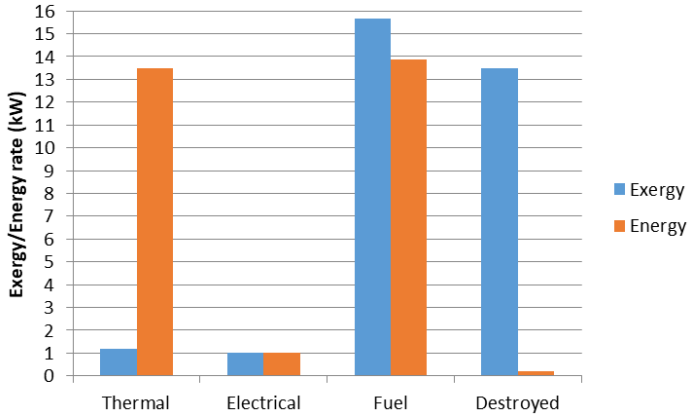

Figure 4-3 : *Les flux d'énergie et d'exergie en mode de fonctionnement maximal.*

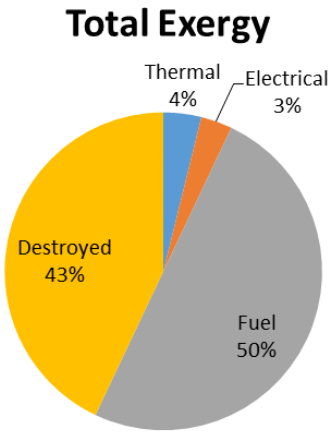

Figure 4-4 : *L'exergie totale est divisée en exergie du combustible, de la destruction et des produits thermiques et électriques.*

L'efficacité exergétique thermique de la micro-CHP peut être augmentée en augmentant la température d'entrée de 15 °C à 40 °C et 60 °C. Avec une température d'entrée de 40 °C, l'efficacité exergétique thermique passe de 7.6 % à 13.5 %. Ceci peut être réalisé en connectant la micro-CHP avec un stockage d'énergie thermique.

4.2 L'étude comparative

Le système de micro-cogénération est comparé à un système de référence comprenant la production séparée de chaleur et d'électricité par une chaudière à gaz naturel et le raccordement au réseau électrique.

La figure 4-5 présente les indicateurs de comparaison lorsque la température d'entrée de la micro-CHP est de 15 °C et que l'efficacité du système de référence varie. Les résultats montrent que la micro-CHP crée des économies d'énergie primaire (PES) de 14% à 30% selon l'efficacité du système de référence. Cependant, l'indicateur RAI n'est positif que si le rendement de la chaudière est inférieur à 95%. En termes d'indicateur RAI, la micro-CHP est une amélioration par rapport au système de référence dans tous les cas si la température d'entrée est augmentée à 40 °C.

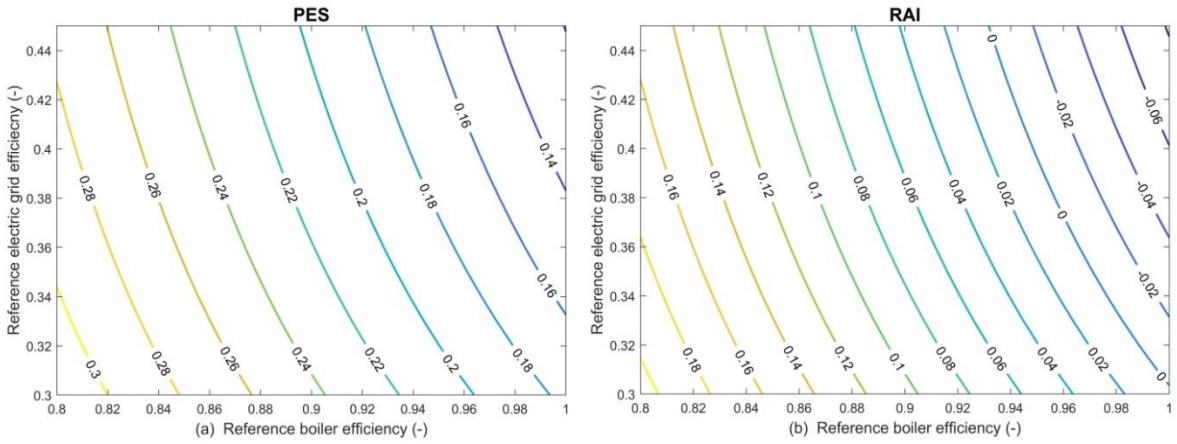

Figure 4-5 : *Les courbes de niveau de a) PES et b) RAI en fonction de l'efficacité de réseau électrique et de l'efficacité thermique de la chaudière.*

Chapitre 5. Systèmes hybrides d'énergie renouvelable basés sur la cogénération

Le chapitre 5 présente une analyse des systèmes d'énergie renouvelable hybrides et une étude de cas pour optimiser la taille du système d'énergie solaire hybride en termes de fiabilité thermique et électrique et de coûts d'investissement initiaux. L'étude de cas est utilisée comme un raisonnement pour l'hybridation des systèmes de micro-cogénération à base de combustible et d'énergie solaire. Ce type de système hybride peut fournir une énergie 100% renouvelable et indépendante des conditions météorologiques.

Les avantages et les désavantages des systèmes de micro-cogénération alimentés par des énergies renouvelables suivants sont évalués : moteur Stirling, capteur photovoltaïque-thermique

et cycle organique de Rankine. Ensuite, les travaux de recherche sur l'hybridation des systèmes de micro-cogénération solaire et à combustible dans la littérature sont présentés et les principaux résultats sont résumés.

L'hybridation des systèmes de micro-cogénération contrôlables et fluctuants, comme le solaire et la biomasse, peut être une meilleure solution que l'hybridation de la cogénération fluctuante avec des stockages d'énergie seulement. Le revue de la littérature sur les systèmes énergétiques hybrides montre que l'hybridation de la micro-cogénération alimentée en combustible et des technologies solaires permet d'augmenter l'autoconsommation, de surmonter les problèmes d'intermittence de la production solaire, de réduire la consommation d'énergie primaire et les coûts.

5.1 L'étude de cas

Un modèle dynamique du champ PVT combiné au stockage thermique et électrique et à la demande énergétique du bâtiment résidentiel est construit en Matlab/Simulink. Le système, dans la figure 5-1, est utilisé pour satisfaire la demande en eau chaude sanitaire et en électricité des appareils électriques dans les conditions météorologiques de Strasbourg, France. La conception du système est optimisée avec l'algorithme d'optimisation multi-objectif NSGA-II de Matlab. L'objectif de l'optimisation est de maximiser l'autoconsommation sur l'année avec un coût d'investissement initial minimal. L'optimisation est basée sur les profils horaires de la demande et le fonctionnement du système.

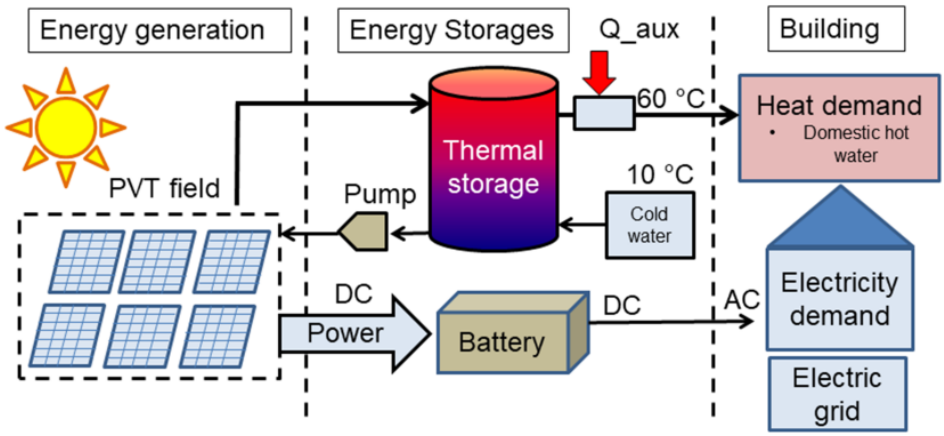

Figure 5-1 : *La disposition du système de l'étude de cas.*

Un problème d'optimisation tridimensionnel est formulé pour maximiser la fiabilité thermique et électrique et minimiser les coûts d'investissement initiaux. Les variables de décision de l'optimisation sont présentées dans le tableau 1.

Tableau 1 : Les variables de décision pour le problème d'optimisation multi-objectif.

Variable de décision	Limites	Unité
Débit massique, ṁ	$60 \leq x(1) \leq 130$	kg/h
N° de PVT en série, N	$1 \leq x(2) \leq 6$	-
N° de rangs PVT, M	$1 \leq x(3) \leq 6$	-
Capacité de la batterie, C_B	$4 \leq x(4) \leq 14$	kWh
Volume de stockage thermique	$0.1 \leq x(5) \leq 0.4$	m^3

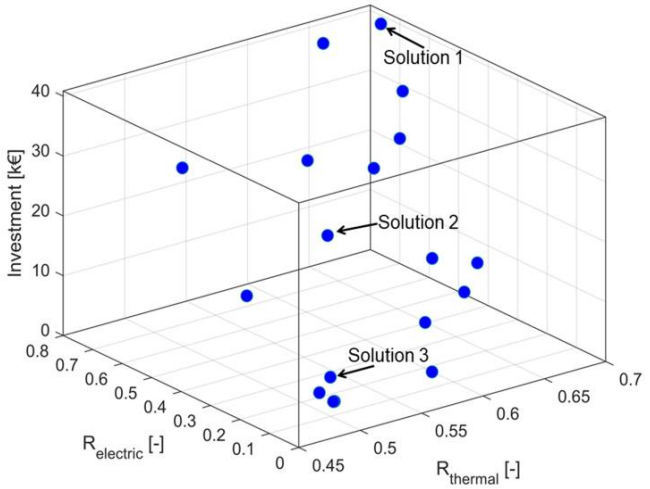

Figure 5-2 : *Le front de Pareto des solutions optimales dans l'espace objectif.*

Le front de Pareto tridimensionnel de la solution optimal est présenté dans la figure 5-2. Trois solutions sont indiquées dans la figure 5-2 et présentées dans le tableau 2. Dans le cadre des contraintes d'optimisation, les résultats montrent que la fiabilité thermique maximale atteinte est de 0.68 et la fiabilité électrique de 0.7. D'après les résultats, la demande horaire en énergie ne peut pas être entièrement satisfaite par le système de micro-cogénération solaire et les stockages d'énergie, mais l'hybridation avec le système alimenté en combustible est nécessaire.

Tableau 2 : Les solutions optimales sélectionnées à partir du front de Pareto.

Solution	ṁ	PVT en	PVT	C_B	V_{TS}	$R_{thermal}$	$R_{electric}$	Inv.

	(kg/h)	série	rangs	(kWh)	(m^3)			(€)
1	108	6	6	14	0.5	0.68	0.7	40877
2	64	6	2	9	0.2	0.57	0.41	18677
3	111	1	3	4	0.1	0.5	0.09	6817

Chapitre 6. Analyse énergétique et exergo-économique d'un système hybride d'énergie renouvelable dans différentes conditions climatiques

Dans le chapitre 6, les systèmes de micro-cogénération contrôlables et fluctuants sont couplés au stockage d'énergie thermique pour former un système hybride d'énergie renouvelable (HRES). Ce système hybride, présenté dans la figure 6-1, est modélisé dans Matlab/Simulink en combinant les modèles précédemment développés de la micro-cogénération Stirling alimentée par la biomasse et des capteurs photovoltaïques-thermiques (PVT). Le système est utilisé pour satisfaire simultanément la demande énergétique résidentielle de chauffage des locaux (figure 6-3), d'eau chaude sanitaire et d'électricité.

L'objectif principal de ce chapitre est de réaliser des analyses dynamiques exergiques et exergo-économiques du système HRES dans trois conditions climatiques différentes et avec les caractéristiques spécifiques des bâtiments définies par l'emplacement. L'analyse exergo-économique est utilisée pour définir le coût spécifique de l'énergie produite par le système dans trois endroits. Les produits énergétiques sont l'électricité, le chauffage des locaux et l'eau chaude sanitaire et les endroits choisis sont Tampere, Finlande ; Strasbourg, France et Barcelona Espagne. En outre, le système HRES est comparé au système de référence dans chaque endroit sélectionné. Les indicateurs PES et RAI sont utilisés pour évaluer le système et les indicateurs économiques suivants sont utilisés pour évaluer la viabilité du système : le délai de récupération simple (SPT) et la valeur actuelle nette (NPV).

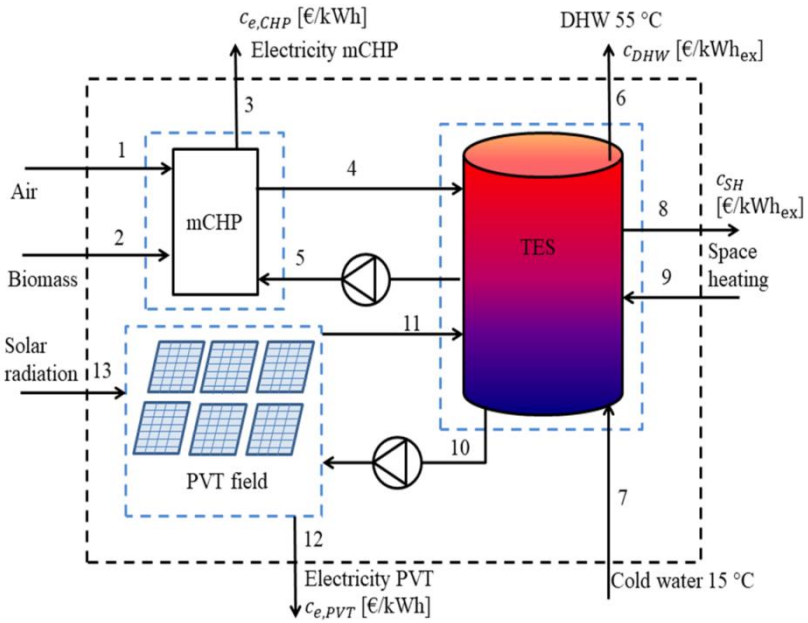

Figure 6-1 : *Le système hybride d'énergie renouvelable.*

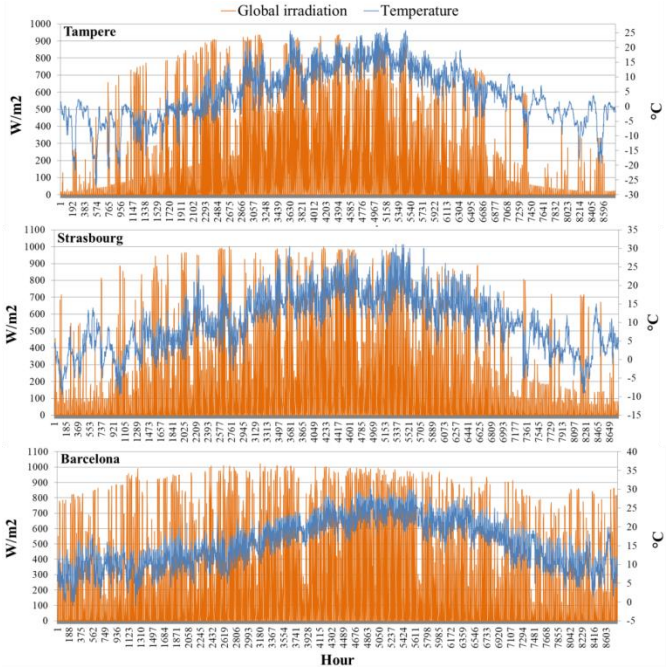

Figure 6-2 : *Le rayonnement solaire horaire et la température ambiante, basés sur les données historiques de chaque endroit.*

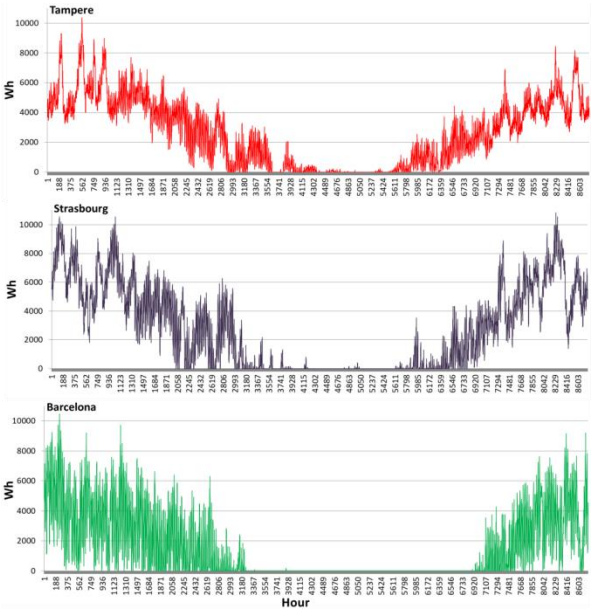

Figure 6-3 : *Les résultats annuels de la charge thermique horaire de chaque endroit.*

6.1 Analyse exergétique

L'objectif de la HRES est d'utiliser une unité de micro-cogénération alimentée par la biomasse pour produire de la chaleur et de l'électricité et de soutenir la production d'énergie avec le système de micro-cogénération solaire. L'analyse exergétique est menée pour voir le fonctionnement dynamique du système, les relations entre les différents produits exergétiques et l'efficacité exergétique totale du système.

La figure 6-4 présente le fonctionnement dynamique du système HRES pendant une journée de printemps et d'été. Pendant ces deux jours, la micro-CHP fonctionne la nuit et l'énergie solaire est produite pendant la journée pour satisfaire la demande en énergie du bâtiment. Pendant la journée de printemps, la micro-CHP doit également fonctionner pendant la journée en raison de la demande de chauffage plus élevée et du gain solaire plus réduit. La destruction d'exergie est significativement élevée dans le système comparé aux produits exergiques comme présenté dans la figure 6-4. La micro-CHP génère une destruction d'énergie coûteuse qui devrait être réduite. La destruction d'énergie dans les capteurs PVT est sans coût.

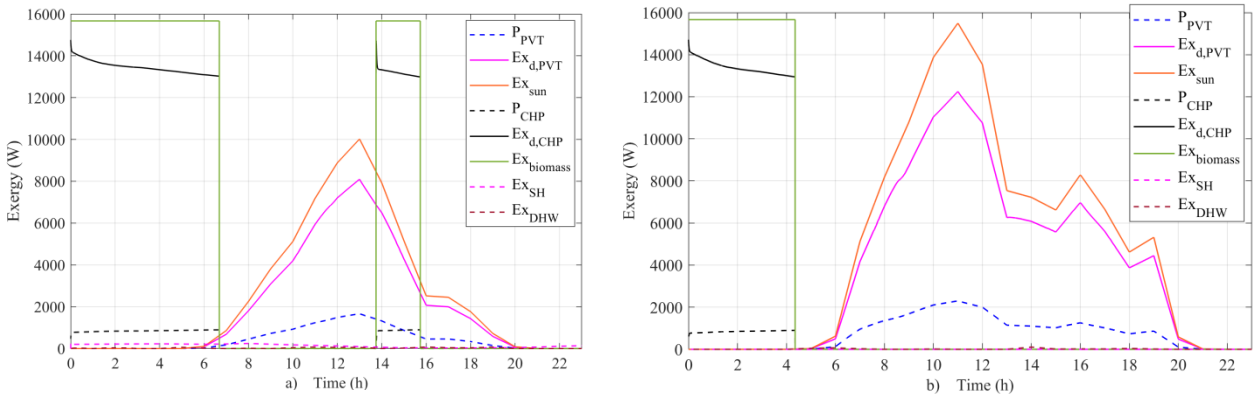

Figure 6-4 : *Les flux de combustible, de produit et d'exergie de destruction pendant deux jours différents à Strasbourg : a) au printemps, b) en été.*

Les différents produits exergétiques du système sont présentés dans la figure 6-5 dans les sites sélectionnés. La plus grande quantité d'exergie est produite par les capteurs PVT. Dans la ville ensoleillée de Barcelone, l'électricité PVT domine les produits électriques, même en janvier. L'hybridation augmente de manière significative la production d'électricité à partir de combustibles libres du système hybride et réduit la destruction coûteuse d'exergie.

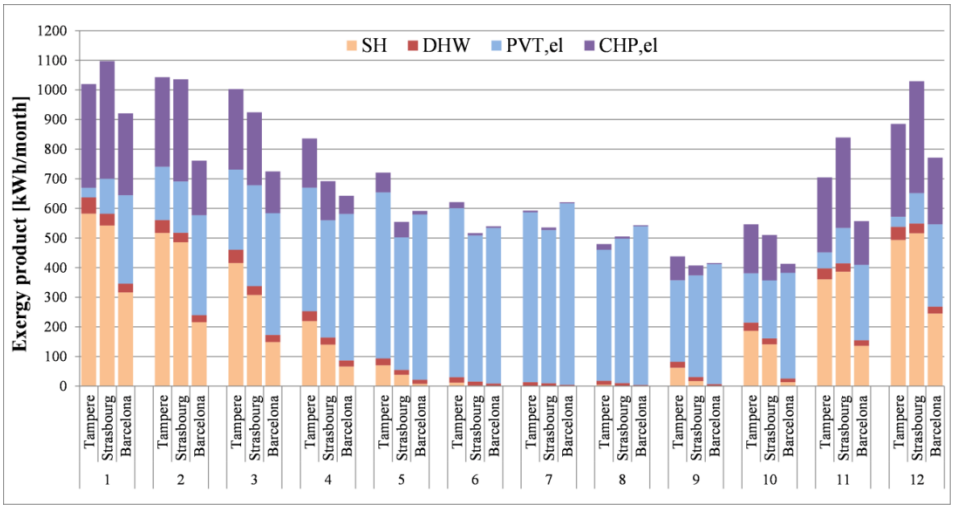

Figure 6-5 : *Les produits exergiques mensuels du système hybride d'énergie renouvelable dans chaque endroit sont divisés pour chaque produit énergétique du système.*

La figure 6-6 présente l'efficacité exergétique totale du HRES. L'efficacité exergétique varie sur l'année de 13% à 16% en fonction des températures de référence mensuelles, du rayonnement solaire et de la demande de chauffage. L'efficacité totale du système peut être proche l'une de l'autre dans différents endroits en raison des taux d'utilisation variables des composants et de l'exergie des produits thermiques.

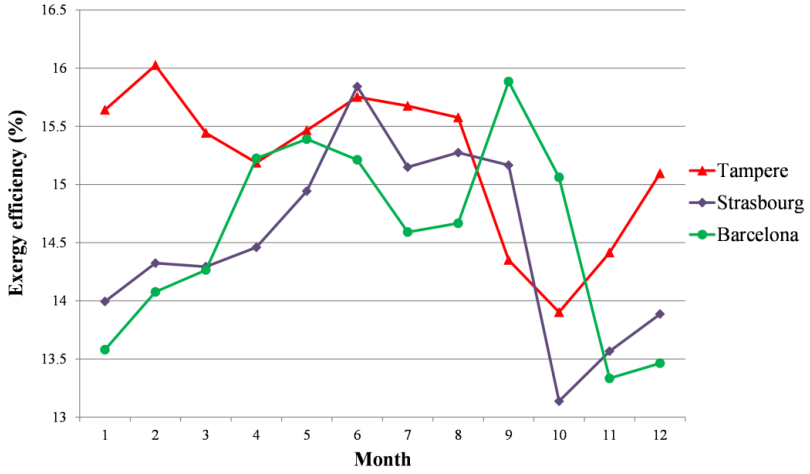

Figure 6-6 : *L'efficacité exergétique mensuel de l'ensemble du système à chaque endroit.*

6.2 Analyse exergo-économique

Le coût spécifique de l'électricité produite par l'unité de micro-cogénération et par le champ PVT forme le coût spécifique de l'électricité produite par le système HRES. Ces coûts dans différents endroits sont présentés dans la figure 6-7. Dans la figure 6-8 est présentée la

sensibilité du coût exergo-économique de l'électricité à la capacité PVT à Strasbourg. Le coût spécifique de l'électricité varie fortement au cours de l'année, avec les valeurs les plus faibles pendant le mois les plus ensoleillés. Dans la région ensoleillée de Barcelone, les coûts sont significativement plus bas pendant les mois d'hiver qu'à Strasbourg et Tampere.

Le HRES original comprend le champ PVT de 3x3 capteurs et la taille du champ varie de ± 33%. Diminuer la quantité de support solaire augmente le coût spécifique de l'électricité relativement plus que d'augmenter la quantité de support solaire.

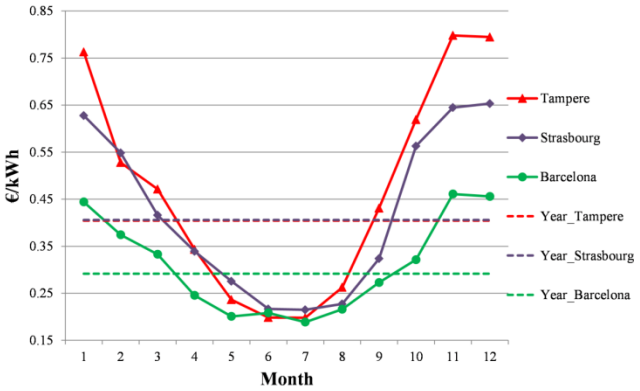

Figure 6-7 : *Les coûts exergo-économiques mensuels et annuels de l'électricité produite par le système énergétique hybride à Tampere, Strasbourg et Barcelone.*

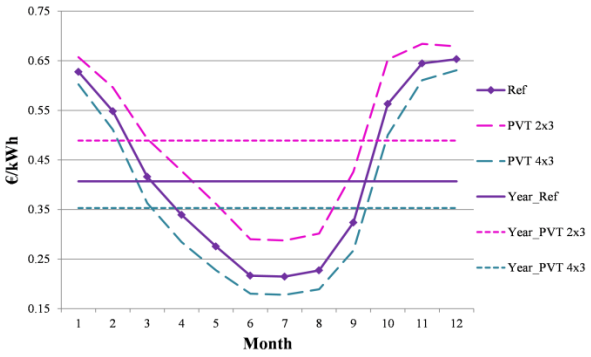

Figure 6-8 : *Les coûts exergo-économiques mensuels et annuels de l'électricité produite par le système énergétique hybride avec différentes capacités PVT.*

Les figures 6-9 et 6-10 présentent les coûts exergo-économiques du chauffage des locaux (SH) et de l'eau chaude sanitaire (DHW) du système. Ces coûts varient également fortement au cours d'une année, les coûts les plus élevés étant observés pendant les mois d'été en raison de la demande faible ou inexistante de chauffage des locaux.

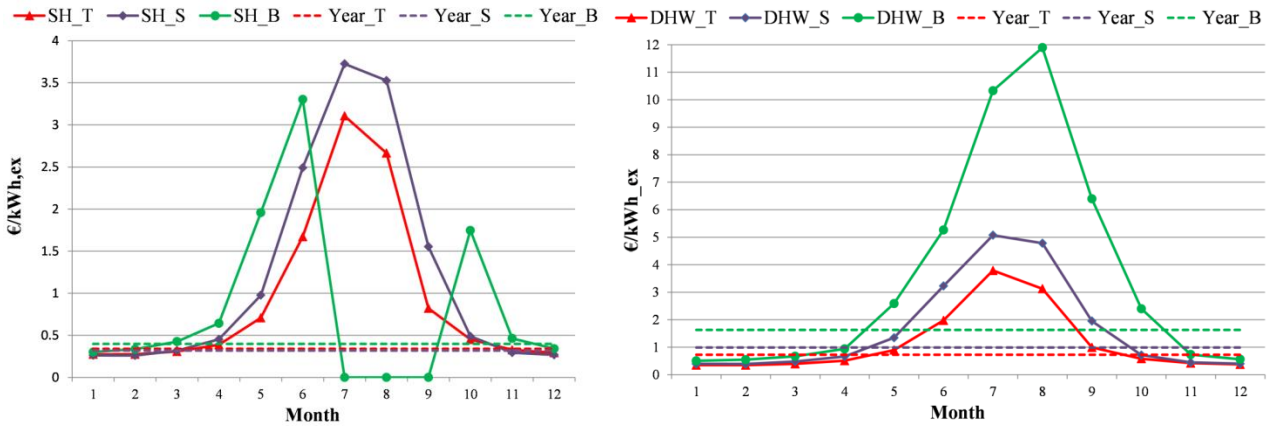

Figure 6-9 : *Les coûts exergo-économiques mensuels et annuels du chauffage des locaux à Tampere, Strasbourg et Barcelone.*

Figure 6-10 : *Les coûts exergo-économiques mensuels et annuels de l'eau chaude sanitaire (DHW) à Tampere, Strasbourg et Barcelone.*

Comme l'électricité, la chaleur n'est pas considérée comme de l'exergie pure et les coûts dans les figures 6-9 et 6-10 sont transférés à l'énergie en utilisant le coefficient de transfert de coûts. Les coûts moyens annuels sont présentés par énergie et par exergie dans le tableau 6-1.

Tableau 6-1 : Les prix unitaires moyens des produits énergétiques dans chaque endroit par énergie et par exergie.

Le produit énergétique	Barcelona	Strasbourg	Tampere	Unit
L'électricité	0.292	0.406	0.404	€/kWh = €/kWh$_{ex}$
Le chauffage des locaux	0.036	0.034	0.044	€/kWh
	0.399	0.319	0.341	€/kWh$_{ex}$
L'eau chaude sanitaire	0.111	0.083	0.075	€/kWh
	1.626	0.987	0.725	€/kWh$_{ex}$

En termes d'autonomie énergétique le coût spécifique de l'électricité reste supérieur au prix de l'électricité du réseau dans chaque endroit. Cela est causé par les coûts d'investissement initiaux élevés des composants du système, en particulier l'unité de micro-cogénération.

6.3 L'analyse comparative

Les indicateurs PES (indicateur énergétique), RAI (indicateur exergique) et économiques sont utilisés pour comparer le fonctionnement de la HRES avec un système de référence comprenant une chaudière à gaz naturel et un réseau électrique.

Les économies mensuelles d'énergie primaire, présentées dans la figure 6-11, sont nettement plus élevées pendant les mois d'été que pendant l'hiver en raison d'une plus grande disponibilité solaire. L'énergie primaire est économisée dans chaque endroit pour chaque mois si le système de référence est remplacé par le HRES.

La figure 6-12 présente l'indicateur mensuel RAI qui révèle l'inefficacité dissimulée du HRES en présentant des valeurs plus faibles que l'indicateur PES. Le RAI est négatif à Tampere en novembre, ce qui indique que le HRES n'évite pas l'irréversibilité par rapport au système de référence en novembre.

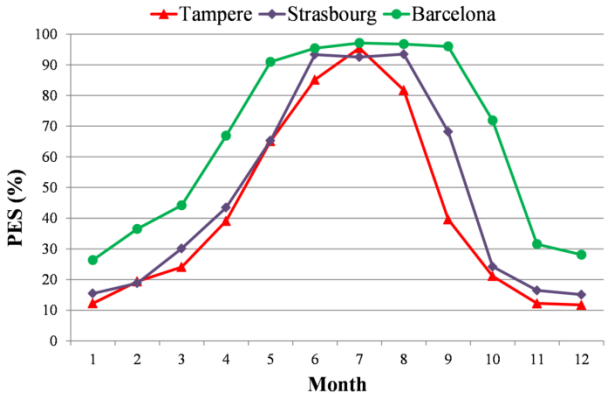

Figure 6-11 : *Les économies mensuelles d'énergie primaire dans chaque endroit.*

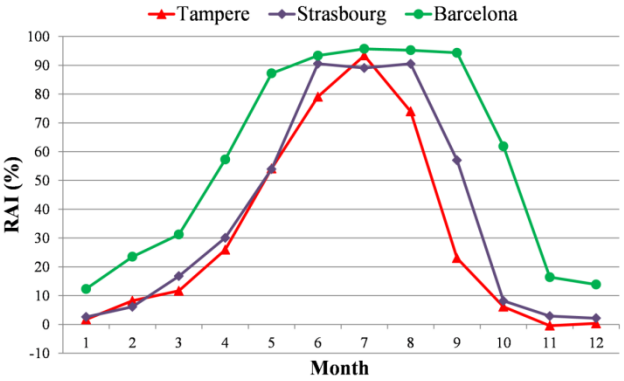

Figure 6-12 : *L'irréversibilité mensuelle relative évitée dans chaque endroit.*

Les indicateurs économiques (le délai de récupération simple SPT et la valeur actuelle nette NPV) sont calculés pour quatre scénarios différents sur chaque site. Les résultats montrent que le HRES est économiquement viable dans chaque endroit dans des circonstances données. La NPV est positive dans chaque endroit et le SPT le plus long de 19.3 and est obtenu à Tampere. Les résultats économiques montrent également que la viabilité est meilleure se l'électricité produite est utilisée 100% sur place.

Chapitre 7. Management de l'énergie renouvelable domestique dans un microgrid solaire

Le chapitre 7 présente les principaux composants d'un micro-réseau solaire résidentiel et le dispositif expérimental du micro-réseau résidentiel PV/batterie réalisé au laboratoire INSA ICUBE à Strasbourg. Le dispositif expérimental est utilisé pour démontrer un système de management de l'énergie renouvelable à domicile (HREMS) basé sur des règles et pour collecter les données opérationnelles du système. Les principaux composants du système sont les panneaux photovoltaïques (PV), le système de stockage par batterie, les micro-onduleurs, la demande locale et la passerelle pour appliquer les stratégies de management de l'énergie.

À la fin du chapitre, l'algorithme de management de l'énergie basé sur l'optimisation est implémenté dans Matlab et son fonctionnement est comparé aux résultats expérimentaux du système de management de l'énergie basé sur des règles.

7.1 Matériaux et méthodes

La typologie de l'installation du dispositif expérimental est présentée dans la figure 7-1. Les quatre panneaux PV DualSun sont connectés à leurs micro-onduleurs pour convertir le courant continu (DC) en courant alternatif (AC). La batterie Enphase AC comprend un onduleur de batterie bidirectionnel et est connectée au côté AC du tableau de distribution. La demande AC des appareils domestiques est utilisée pour décharger la batterie et utiliser directement l'énergie PV. Le surplus de production photovoltaïque est chargé dans la batterie ou injecté dans le réseau.

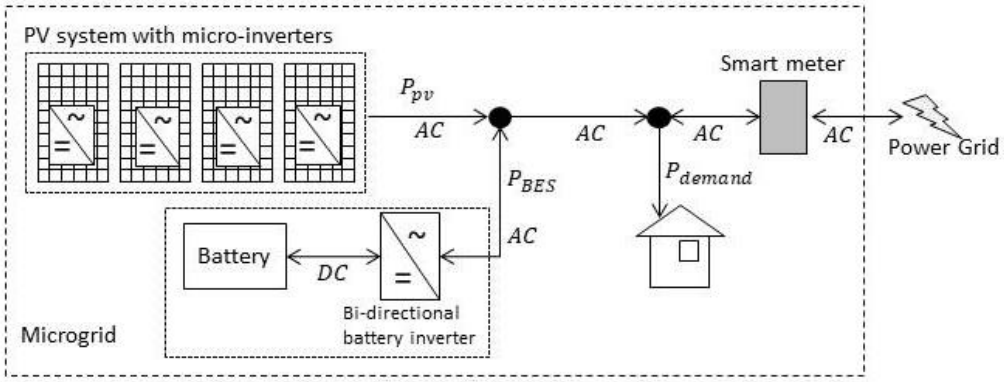

Figure 7-1 : *La topologie du dispositif expérimental du micro-réseau solaire.*

La figure 7-2 présente les panneaux PV et la station météorologique pour collecter les données de la production d'énergie PV et les variables météorologiques, telles que le rayonnement solaire et la température ambiante. La figure 7-3 présente l'installation à l'intérieur du bâtiment, y compris le tableau de distribution, la passerelle et le stockage sur batterie. La batterie a une capacité de 1.2 kWh.

Figure 7-2 : *Les panneaux photovoltaïques installés au laboratoire INSA ICUBE.*

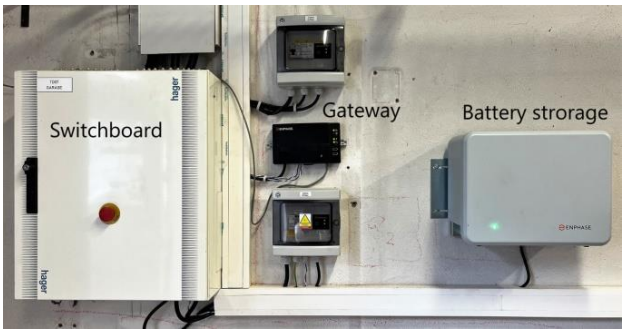

Figure 7-3 : *L'installation dans le garage avec le tableau de distribution, la passerelle et le système de stockage par batterie.*

Enfin, les données du système sont collectées à partir du software basé sur le web qui communique avec la passerelle du système. Dans la figure 7-4 est présenté le workflow pour collecter les données de l'installation.

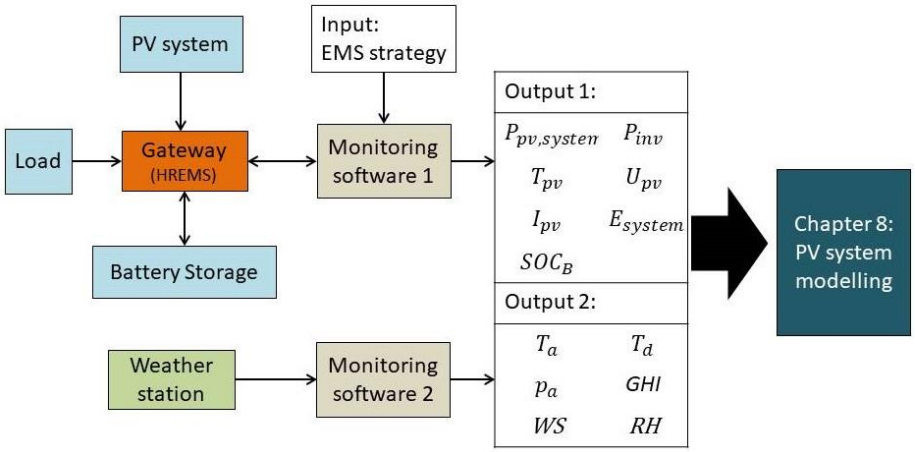

Figure 7-4 : *Le workflow de collecte des données du montage expérimental.*

7.2 Les résultats

Deux stratégies différentes de management de l'énergie basées sur des règles sont appliquées au dispositif expérimental via un software de monitoring basé sur le web : le schéma de temps d'utilisation (TOU) et la maximisation de l'autoconsommation. Le fonctionnement du système dans le cadre de la stratégie TOU est présenté dans la figure 7-5. La stratégie TOU optimise la charge/décharge de la batterie en fonction du prix de l'électricité du réseau pour éviter d'acheter de l'électricité à un prix élevé. Cependant, elle ne prend pas en compte les

informations futures sur la production photovoltaïque ou les prix de l'électricité. Un profil de prix est donné à la passerelle en supposant des pics de prix de 7h00 à 10h00 et de 16h00 à 22h00.

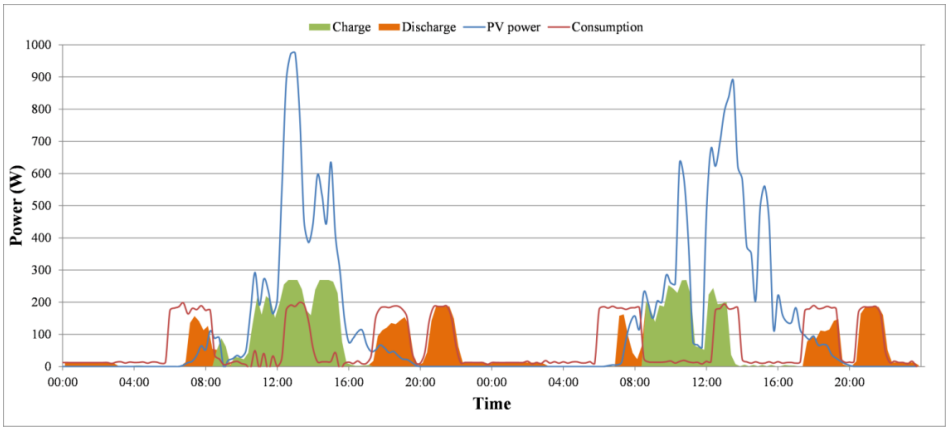

Figure 7-5 : *Fonctionnement du système dans le cadre d'un système de TOU donné le 25.-26.4.2022.*

Un modèle de simulation du dispositif expérimental est implémenté dans Matlab pour contrôler la charge/décharge de la batterie par le système de management de l'énergie basé sur l'optimisation appelé contrôle prédictif de modèle (MPC). L'objectif du problème de contrôle optimal est de minimiser le coût électrique de l'horizon de contrôle. La figure 7-6 présente le fonctionnement du système dans le cadre de la stratégie MPC. On suppose une prédiction parfaite des informations futures pour les 24 heures à venir.

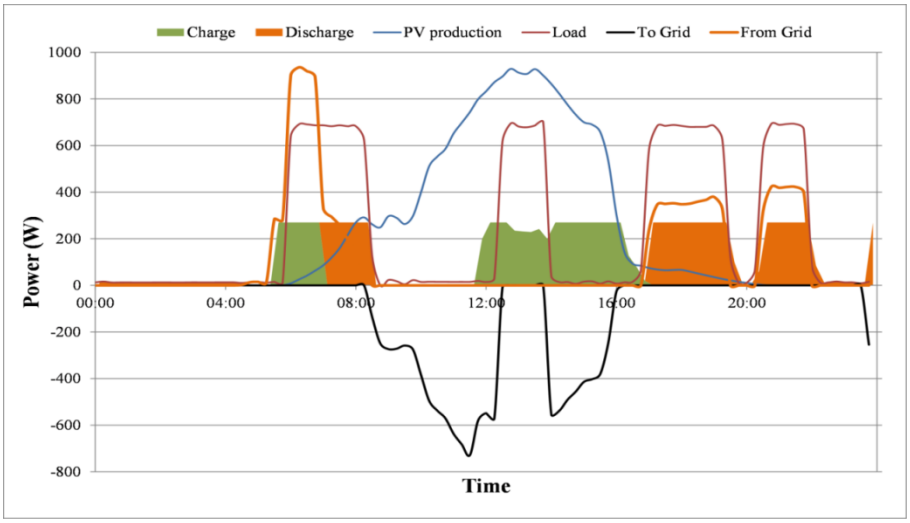

Figure 7-6 : *Les résultats de la simulation du système sous la stratégie MPC le 17 mai 2022.*

Par rapport à la stratégie basée sur des règles, le contrôle optimal permet de charger la batterie pendant la période creuse, juste avant le début de la période de pointe à 7 heures. Dans le même temps, la charge locale est satisfaite par l'électricité du réseau. Pendant la période de pointe, la batterie est déchargée et le prix élevé de l'électricité est évité. Cela est possible parce que le MPC utilise les informations futures de la période de prix élevés à venir de 7h00 à 10h00.

Le coût de fonctionnement du système sous la stratégie MPC est de 0.32 € dans la figure 7-6. Si le système fonctionne avec la stratégie d'autoconsommation maximale, le coût pour le même jour est de 0.39 €. Pour avoir une stratégie MPC réussie, la prédiction PV doit être aussi précise que possible. Les méthodes de prédiction sont étudiées dans le chapitre 8.

Chapitre 8. Prévision de la puissance photovoltaïque pour le contrôle optimal d'un microgrid solaire

Le chapitre 8 présente deux méthodes basées sur la méthode de machine learning pour prédire la production d'énergie PV dans le cadre d'un contrôle optimal. Le dispositif expérimental présenté dans le chapitre 7 est utilisé pour collecter les données de production PV et les données météorologiques pour l'entraînement des modèles. Le processus de collecte des données est présenté dans la figure 8-1.

Dans la modélisation de la prédiction, les méthodes de régression linéaire multiple (MLR) et de réseau neuronal artificiel (ANN) sont utilisées et les performances des modèles sont comparées. De plus, la modélisation est construite selon deux approches : en utilisant les données du micro-onduleur de chaque panneau et les données agrégées de la puissance PV. Les données de training sont collectées pendant 6 mois et les modèles sont entraînés dans Matlab. L'objectif est d'étudier et de comparer différents modèles, mais aussi de comparer différentes données d'entrée en termes de production photovoltaïque. Les données du système sont collectées à partir de deux softwares de monitoring et d'analyse basés sur le web : Enphase Enlighten et WeatherLink.

Pour évaluer et comparer les performances du modèle, les quatre indicateurs de performance suivants sont utilisés : erreur absolue moyenne (MAE), le carré moyen des erreurs (MSE), erreur quadratique moyenne (RMSE) et coefficient de détermination (COD).

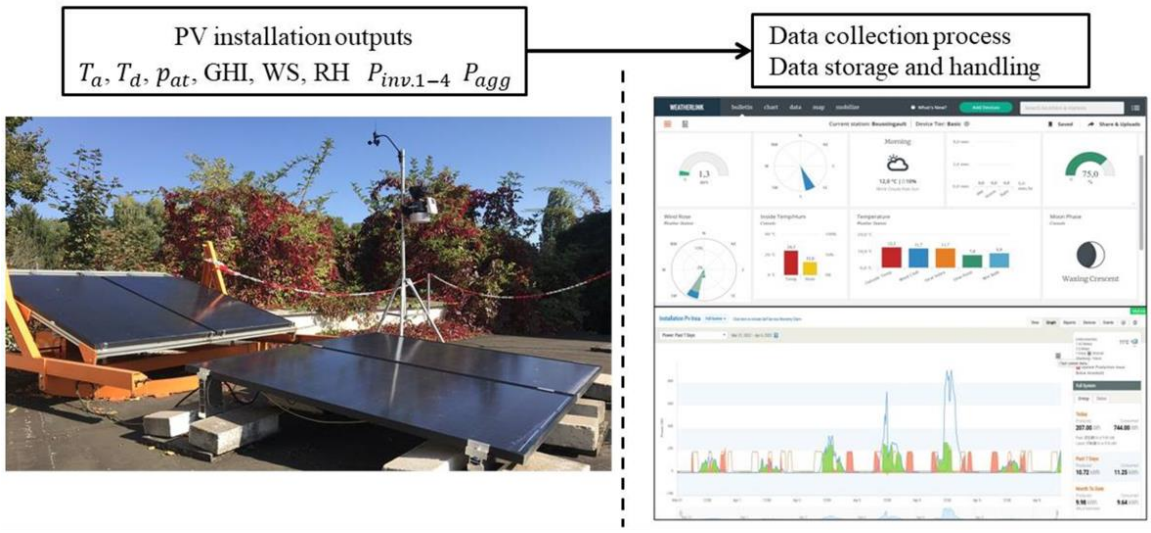

Figure 8-1 : *L'installation PV avec la station météorologique et le processus de collecte des données.*

8.1 Résultats

Pour mettre en évidence de la relation linéaire entre les variables météorologiques et la production d'énergie PV, une analyse de corrélation est effectuée. Les coefficients de corrélation varient de -1 à 1. Les résultats de l'analyse sont présentés dans Tableau 8-1. La corrélation la plus élevée est obtenue entre le rayonnement solaire (GHI et GTI) et la production d'énergie PV, suivie par l'humidité relative et la température ambiante. La température du point de rosée et la pression atmosphérique sont les moins significatives et ne sont pas prises en compte dans la modélisation.

Tableau 8-1 : Les coefficients de corrélation

Variable	Corrélation avec la puissance PV
Température ambiante	0.27
Humidité relative	-0.39
Température du point de rosée	0.01
Vitesse du vent	0.15
Pression atmosphérique	0.11
GHI	0.94

GTI_up	0.94
GTI_down	0.94

Tout d'abord, le modèle MLR est programmé dans Matlab avec les variables météorologiques sélectionnées et les données de production d'énergie PV agrégées. Ensuite, chaque panneau PV est modélisé individuellement et les prédictions sont additionnées pour obtenir une prédiction de l'ensemble du système. La même approche est appliquée au modèle ANN et les résultats de la performance totale sont présentés dans le tableau 8-2. Le modèle ANN avec les données du micro-onduleur montre la meilleure performance totale.

Tableau 8-2 : La comparaison des performances totales des modèles en fonction des différentes méthodes et de l'entrée des données PV.

Modèle		Indicateur de performance			
		MAE	MSE	RMSE	COD (R^2)
MRL	Global	16.32	2161	46.485	0.9074
	Micro-ond.	13.86	1438	37.919	0.9376
ANN	Global	13.34	1517	38.96	0.935
	Micro-ond.	9.87	930	30.497	0.9596

Les deux modèles sont testés pour le jour représentatif qui n'est pas inclus dans les données de training. La figure 8-2 présente la performance du modèle MLR avec les données d'entrée du micro-onduleur. La figure 8-3 présente les résultats obtenus pour le modèle ANN.

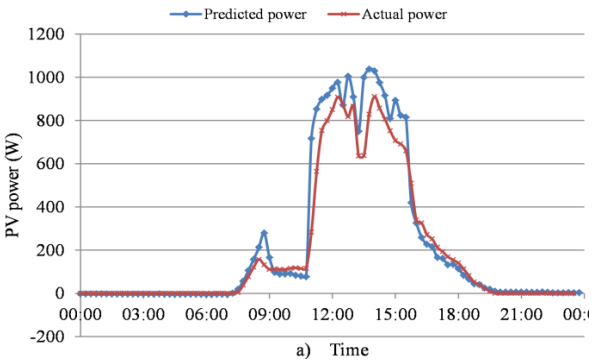

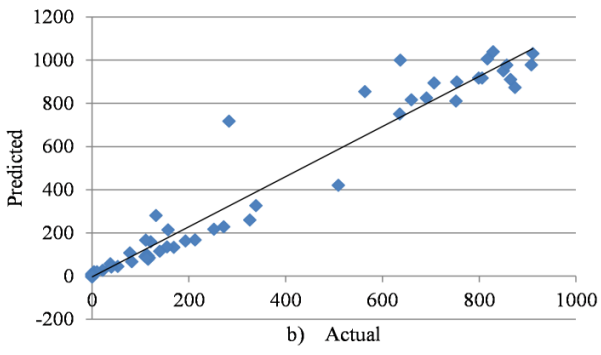

Figure 8-2 : *a) Puissance PV prédite et actuelle en utilisant le modèle MRL basé sur un micro-onduleur. b) Corrélation entre la puissance PV actuelle et prédite et la ligne de tendance linéaire du modèle MRL.*

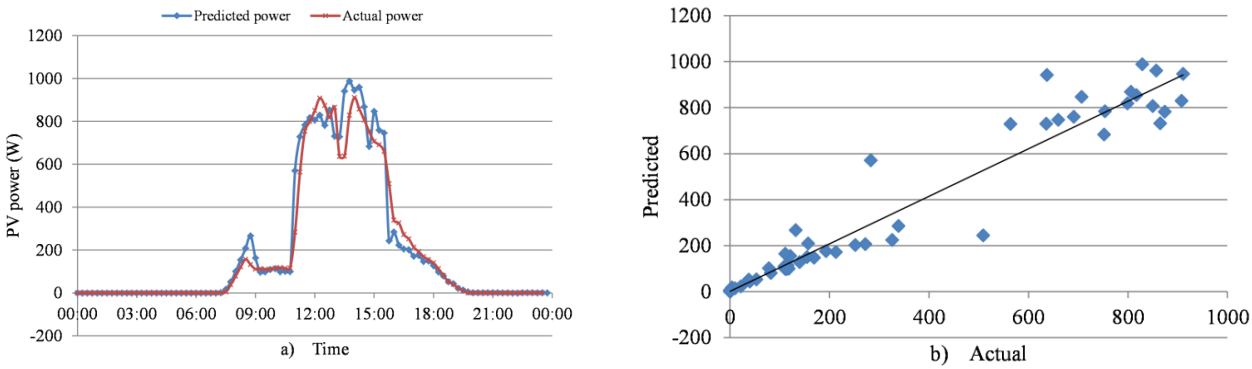

Figure 8-3: *a) Puissance PV prédite et actuelle en utilisant le modèle ANN basé sur le micro-onduleur. b) Corrélation entre la puissance PV actuelle et prédite avec la ligne de tendance linéaire du modèle ANN.*

Conclusions générales et perspectives

Pour réduire la consommation d'énergie primaire et concevoir des systèmes énergétiques plus rationnels pour les bâtiments, il est nécessaire de mener des recherches plus approfondies et plus critiques sur l'efficacité énergétique des technologies énergétiques disponibles. La méthode exergétique combine les première et deuxième lois de la thermodynamique en définissant la quantité et la qualité d'une certaine quantité d'énergie. L'aspect qualitatif peut révéler l'inefficacité cachée des systèmes énergétiques qui ne peut être identifiée par la seule analyse énergétique basée sur la quantité.

La méthode exergétique a été utilisée pour analyser deux composants du système hybride d'énergie renouvelable : les capteurs PVT et le système de micro-cogénération à moteur Stirling alimenté par la biomasse.

L'analyse exergétique a apporté de nouvelles informations sur l'efficacité et les variables de conception du capteur PVT par rapport à l'approche énergétique. L'efficacité exergétique thermique a été maximisée en diminuant le débit massique du liquide de refroidissement et en augmentant la température d'entrée du liquide de refroidissement, ce qui est contraire à la maximisation de l'efficacité énergétique thermique qui a conduit à un débit massique élevé et à une température d'entrée basse. Les résultats ont également montré que la production électrique

du capteur PVT, qui maximise la production d'exergie thermique, est toujours compétitive par rapport à la production du panneau PV.

L'analyse exergétique appliquée à l'unité de micro-cogénération ÖkoFEN à moteur Stirling alimentée par la biomasse a révélé une inefficacité thermique élevée, avec une efficacité exergétique thermique de 7,6 %, alors que l'analyse énergétique a donné une efficacité énergétique thermique de 98 %. L'efficacité exergétique thermique a été augmentée en augmentant la température d'entrée du système. Ce résultat recommande fortement de combiner la micro-CHP avec le stockage de chaleur. Par rapport à un système de référence, la micro-CHP a été une amélioration et est recommandée.

Sur la base de la bibliographie sur les microsystèmes hybrides d'énergie renouvelable, un nouveau système hybride pour les bâtiments a été proposé, comprenant des systèmes de micro-cogénération à base de solaire et de biomasse avec stockage d'énergie pour fournir une énergie 100% renouvelable. L'analyse énergétique, exergétique et exergo-économique dynamique a été menée sur le modèle de système dans trois conditions climatiques différentes afin d'évaluer sa performance exergo-économique et de définir les coûts spécifiques des produits énergétiques. L'hybridation des technologies solaires et de la biomasse a permis de réduire le coût spécifique de l'électricité et d'offrir une production d'énergie continue pour favoriser l'indépendance énergétique du micro-réseau. Les différentes conditions météorologiques ont eu un impact sur les coûts spécifiques des produits énergétiques en raison de la disponibilité variable de l'énergie solaire et du contenu exergétique des produits thermiques qui dépend de la température ambiante. Le coût spécifique de l'électricité a fortement varié sur une année et les prix moyens annuels étaient de 0.29 €/kWh à Barcelone, 0.41 €/kWh à Strasbourg et 0.4 €/kWh à Tampere.

Dans le cadre du projet ACA-MODES, les systèmes énergétiques hybrides complexes nécessitent des méthodes de contrôle avancées pour fonctionner de manière optimale. Le contrôle prédictif de modèle (MPC) a permis de réduire le coût d'exploitation du micro-réseau solaire expérimental par rapport à la méthode de gestion de l'énergie basée sur des règles. Cependant, le MPC nécessite des prévisions futures précises de variables incertaines, telles que la production d'énergie photovoltaïque, pour optimiser le prochain signal de commande du système. Dans cette thèse, les méthodes de machine learning ont été étudiées pour construire un modèle de prédiction de la puissance photovoltaïque. Les données expérimentales du micro-

réseau solaire ont été utilisées pour entraîner les modèles. Le réseau neuronal artificiel avec les données des micro-onduleurs PV a donné le modèle le plus précis.

Dans les travaux futurs, un système solaire hybride combinant différents capteurs solaires, comme le capteur PVT plat en série avec un capteur PVT concentré, devrait être étudié. En ce qui concerne l'unité de micro-cogénération alimentée par la biomasse, l'analyse d'exergie au niveau des composants devrait être menée pour indiquer l'endroit où la destruction d'exergie est la plus élevée dans l'unité. En ce qui concerne le système hybride d'énergie renouvelable, l'optimisation des composants du système, tels que le champ PVT et le stockage d'énergie, doit être réalisée. Une analyse plus approfondie de l'impact de l'énergie solaire sur la viabilité économique de l'installation de micro-cogénération à combustible doit être menée. En outre, l'intégration d'un véhicule électrique dans le système de stockage d'énergie du micro-réseau résidentiel avec un système de management de l'énergie optimal et des modèles de prévision peut être envisagée.

GENERAL INTRODUCTION

1.1 Background

The Tri-national Metropolitan Region Upper Rhine (TMR) is located at the River Rhine border of three European countries: France (Alsace), Germany (Baden-Württemberg, south part of Rhineland-Palatinate) and Switzerland (Cantons of Basel-Stadt, Basel-Landschaft, Aargau, Jura and Solothurn). The region is presented in Figure 1-1 with the local research institutes. In terms of the energy transition, the cross-border operation becomes more important because it creates flexibility in the power grid operation and renewable energy utilization. Due to the country-specific parameters, different energy production methods are more or less favorable depending on the location. The TMR is a good example of the possibilities in the cross-border cooperation of decentralized energy systems. In 2013, the local authorities of the TMR mentioned in their "Climate strategy and energy for the TMR" framework that the future challenges of the area have to be faced together with the cross-border approach. Within this framework, the ambitious energy and climate targets were defined for the first time for the whole Upper Rhine region. These targets aim to reduce, across the whole TMR, emissions by 80% compared to 2000 and primary energy consumption by 35% by 2050 [1]. The long-term objective is to cover all energy use in the TMR with renewable energies after 2050 [1]. The INTERREG programs were started by the European Union in 1989 to finance cross-border projects. In 2015, the association called TRION-climate was founded to create cross-border synergies considering the climate and energy challenges in the TMR.

Figure 1-1: *The map of the Tri-national Metropolitan Region Upper Rhine with the ACA-MODES project partners from France, Germany and Switzerland and their laboratories.*

In the TMR, the research laboratories shown in Figure 1-1 have a great opportunity to investigate and develop a cross-border and grid-friendly operation of the decentralized hybrid renewable energy systems. This thesis has been a part of the ACA-MODES project developed in the INTERREG V Upper Rhine program. The ACA-MODES shorthand stands for "Advanced Control Algorithms for the Management of Decentralized Energy Systems", and it has been an innovative 3-year cross-border project that aims to develop regional sustainability in the TMR. The research focus of the project has been on advanced control algorithms and decentralized multi-energy systems in a built environment. Its main objective has been to optimize the decentralized hybrid energy systems in terms of cross-border operation, energy efficiency and design. For this purpose, the five distributed energy systems of the research consortium have been interconnected to form a smart grid and local energy market to demonstrate the cross-border cooperation in the TMR. The operation of each distributed energy system is managed by model predictive control strategies, and these are linked with the optimization-based energy market mechanisms to optimize the cross-border operation of the smart grid.

The distributed hybrid renewable energy systems (HRES) in the built environment form onsite micro-grids and building owners become prosumers who can produce, store and sell their energy. This increases energy self-sufficiency of the prosumer, stability of the main power grid, better matching between energy production and demand, and reduces primary energy use and

CO_2 emissions. Generally, the HRES consist of renewable energy sources with or without a conventional energy source, and energy storage. These systems produce heat and electricity by the decentralized micro-scale components to satisfy a specific building energy demand. Different HRES configurations can be formed to fulfil buildings' energy demand which accounts for 43% of the final energy consumption in the European Union (EU) [2]. Using micro combined heat and power (micro-CHP) components is a promising solution to fulfil the primary energy and emission reduction targets of the TMR and European Union. These components are defined to have electrical power below 15 kW and the key feature is the capability to produce simultaneously heat and electricity from a single fuel source at high overall efficiency. The micro-CHP components can be fueled by renewable energies, such as solar and biomass.

Currently, the analysis, optimization, costing and control methods of the HRES and different system components are based on the energy flows and the first law of thermodynamics. The primary energy approach is commonly used to reduce fossil fuels and increase the share of renewable energies to satisfy given energy demand. Finally, the aim is to balance the energy quantities between energy supply and demand. However, the quantity-based approach does not give any information about the quality of the energy source or the quality requirements of the demand side. As example, an electric heater can deliver heat at an energy efficiency of 100% or a condensing boiler at 98%. However, the covered heat demand has much lower quality than electricity or wood pellets, and it is not the most efficient and rational way to cover the space heating demand. More attention should be given to matching quality than quantity between energy supply and demand.

Combining the first and second laws of thermodynamics in the system analysis, the quality of energy can be defined. This combined analysis is called "Exergy analysis". A quantity of energy is seen as pure exergy if it can be totally transformed into work. However, often only a part of the energy can be considered as exergy. In each energy conversion process, in contrast to energy, exergy is destroyed due to the irreversibility of the process. Due to this, the high-quality potential of the electricity or wood pellets is lost if these fuels are used directly to cover low-quality space heating demand. Although the energy efficiency could be as high as 98%, the exergy efficiency can drop close to 10%. Due to this, the different components of the domestic HRES should be evaluated carefully using the exergy analysis to reveal quality matching between energy supply and demand. The exergy analysis is common and widely applied in

industrial power plants since the 1970s to increase the overall efficiency and the output of the plant. The exergy analysis has also found its way to analyze building energy systems, as example the Annex 49 Final Report [3]. However, in this case, the target can be to increase the efficiency and output of the energy system but also to reduce the quality of the input energy to maintain still the output which satisfies the energy requirements of the building, such as thermal comfortability. The other significant difference between the power plant and building energy system is the operational temperature level which is really close to the ambient temperature in the micro-sized systems. This highlights the importance of defining the reference temperature, which is used to calculate exergy.

Thermoeconomics are used to combine energy and economics to evaluate the economic viability of the energy systems, and define specific costs of the energy products. The conventional energy-economic analysis is well-established evaluation method, but its weakness is that energy does not tell any information about its value (exergy), and the monetary value should be assigned with the value of a commodity [4]. For example, the same quantities of heat and electricity have different exergy, and we value them differently because they can do different things for us [4]. Due to this, it is more rational to assign the monetary value with quality measure and not quantity measure of energy. The exergo-economic analysis is used to create a relation between the costs and exergy flows of the energy system. In terms of the domestic HRES and micro-grid operation, the exergo-economic costing method can be used to define more rationally and sustainably the specific costs of energy products, such as space heating, domestic hot water and electricity. This is important information when evaluating the economic viability and sustainability of the prosumer's energy self-sufficiency created by the HRES compared to the reference systems, such as the electric grid.

To reduce primary energy use, exergy destruction and CO_2 emissions, the optimal control of the HRES and micro-grid operation is required. The advanced control algorithms can be used to control the operation of complex hybrid energy systems including a high share of fluctuating renewable energies. The main benefit of the advanced control algorithms is that they can directly optimize the control decisions according to the different future forecasts, such as solar availability and energy demand. Compared with conventional rule-based control methods, the predictive control enables more efficient use of fluctuating renewable energies, storage systems and matching between energy supply and demand by shifting energy demands to a more

favorable moment. The Model Predictive Control (MPC) method utilizes an accurate physical model of the system and different forecasts related to the system operation to compute optimal control signals for a specific time horizon, such as 24 hours. The MPC requires a formulation of an optimal control problem to be solved at each time step with the selected optimization method. The successful results of the MPC depend strongly on the accuracy of the physical model but also on the accuracy of the forecasting methods of renewable energies. Deterministic methods can be used to predict solar energy generation but also the model-free artificial intelligence-based machine learning methods offer an alternative way to perform complex prediction tasks by learning from the historical data. Multiple linear regression (MLR) and artificial neural network (ANN) are the machine learning methods that can form a relationship between input and output without any further knowledge of the system.

In this thesis, the decentralized hybrid renewable energy systems based on the micro-cogeneration components are investigated in the context of smart grids and ACA-MODES project. The exergy method is used to analyze and optimize the system components, such as photovoltaic-thermal collectors and biomass-fueled micro-CHP systems. Finally, the energy, exergy and exergo-economic analysis are performed to analyze the dynamic operation of the domestic HRES and define the specific costs of the energy products. Together with applying the exergy method, an experimental application of photovoltaic panels has been realized during this thesis to support the MPC control of the micro-grid with a PV power prediction model based on the measured data.

1.2 Research motivation

The 1970s oil crisis accelerated the utilization of the exergy analysis in the industrial sector to have a more efficient process and energy production. Today, the ambitious primary energy and CO_2 reduction targets of the TMR and the EU are encouraging us to reveal hidden inefficiencies with the exergy analysis in the building energy systems. By combining the first and second laws of thermodynamics, the focus on energy quantities and primary energy reductions can be extended to consider the quality aspect of the energy supply in buildings. Compared to the industrial sector, the building sector has constantly high- and low-quality requirements for the energy demand, such as electricity and space heating, respectively. The exergy analysis can be used to develop and design more efficient hybrid renewable energy

systems but also to find a system which minimizes the quality difference between the supply and demand. In this case, renewable energy-based micro-cogeneration systems, which produce simultaneously low-quality heat and electricity, are highly interesting solutions to be applied to the building sector. Due to this, it is reasonable to further study the micro-cogeneration systems.

The motivation to design the more rational, efficient and sustainable building energy systems drives this PhD thesis. For this purpose, the exergy and exergo-economic analysis are investigated and performed in the context of micro-cogeneration and hybrid renewable energy systems. The other driving motivation of this thesis is to investigate different energy management and solar production forecasting methods. The optimal energy management and accurate prediction methods enable more efficient system control and use of renewable energies in hybrid renewable energy systems. For this purpose, an experimental set-up of photovoltaic panels has been realized during this thesis to gather weather and PV panel operation data for training the machine learning methods for forecasting.

1.3 Objectives

The main objective and novelty of this thesis are to study the exergy method applied to micro-cogeneration and hybrid renewable energy systems in the building sector. Typically, the exergy method has been applied in industrial processes that are significantly different in nature from building energy systems. The exergy method consists of the exergy and exergo-economic analysis, and exergy-based design optimization. The aim is to propose a design optimization method based on exergy and artificial intelligence, and to apply a dynamic exergo-economic analysis as a more rational costing method for the energy products of the residential hybrid renewable energy system. Therefore, the exergy analysis and optimization are performed on the micro-cogeneration system and dynamic exergo-economic analysis is conducted on a proposed novel hybrid renewable energy system.

Additionally, the second objective is to realize an experimental set-up of photovoltaic panels coupled with Lithium-Ion AC battery storage and home energy management system and gather system data to study different machine learning methods for the PV prediction modelling.

To reach the mentioned objectives, the following research questions were formulated:

- Is the exergy approach suitable for the design optimization of the solar micro-cogeneration system?
- If analyzing micro-cogeneration systems, does the exergy approach bring additional information compared to the energy analysis and when especially?
- What is a suitable reference temperature for the exergy analysis when comparing different locations?
- How to perform a dynamic exergy analysis for a HRES in a domestic microgrid? How do the results of the exergy analysis differ for the same system in different locations?
- Is the exergo-economic analysis suitable to define energy prices and viability of the HRES in the different locations?
- Does the hybridization of the fluctuating and controllable cogeneration systems, such as solar and biomass, has an impact on the economic viability of HRES?
- What is the most accurate machine learning PV prediction method for the optimal control problem?

The contributions of this thesis:

- Comprehensive literature review on the hybridization of the solar and fuel-fired micro-cogeneration technologies and the exergy method in the domestic microgrids.
- Proposal of using NSGA algorithm and exergy approach for photovoltaic-thermal collector design optimization.
- Proposal of a novel HRES based on micro-cogeneration for building microgrids.
- Proposal of using exergo-economics approach for pricing energy products of the proposed HRES in a domestic microgrid and economic viability analysis.
- Investigation of the renewable energy systems under different climate conditions.
- Development of the simulation platforms in Matlab/Simulink for a single and multi-stage PVT design exergy optimization and the yearly energy, exergy and exergo-economic simulation of the proposed HRES.
- To realize a solar platform with photovoltaic panels and a Lithium-Ion battery to investigate different PV power forecasting and energy management methods for solar micro-grids.

1.4 Thesis outline

Chapter 1 presents the state-of-art micro-cogeneration technologies and exergy method for the microgrids. First, the solar based technologies are presented and next, the fuel-fired micro-cogeneration systems are reviewed with a comparison of the advantages and disadvantages. These technologies can be utilized to form hybrid renewable energy systems for building microgrids. Due to this, Chapter 1 presents also a literature review on the hybrid renewable energy systems that include a fuel-fired micro-cogeneration unit coupled with solar technologies. After presenting the micro-cogeneration technologies and hybrid systems, the exergy approach for analyzing energy systems is reviewed.

Chapter 2 presents a model of the photovoltaic-thermal (PVT) collector built into Matlab/Simulink, which is used to conduct an energy and exergy analysis on the collector performance in two different European climate conditions. The PVT collector design is optimized in terms of thermal and electrical exergy efficiencies by using an artificial intelligence algorithm called Non-Dominated Sorting Genetic Algorithm-II (NSGA-II). Based on the resulted Pareto front, three different PVT designs are selected and compared to the performance of a photovoltaic (PV) panel. The comparison is used to reveal if the PVT is still competitive with the PV panel electrical output, after maximizing its thermal exergy efficiency because the thermal performance of the PVT has a decreasing impact on its electrical performance.

Chapter 3 presents a novel exergy-based design optimization method for the multi-stage PVT system. The aim of the study is to reveal a compromise solution for a multi-stage PVT design to maximize the overall exergy efficiency under different climate conditions. The parametric study is conducted for the water-based flat-plate PVT system performance. Finally, the decision-making method and process are applied to the results and discussed.

Chapter 4 presents a modelling and steady-state exergy analysis of the biomass-fueled micro-CHP system, which has been previously tested at the INSA Strasbourg laboratory. The operation of the micro-CHP is compared to a reference system.

Chapter 5 presents different hybrid renewable energy systems based on micro-cogeneration. Additionally, a case study is presented in which a design optimization of the PVT/battery/thermal storage system is conducted with the genetic multi-objective optimization method to maximize thermal and electrical reliability and minimize the initial investment costs.

The case study is used to show the need of hybridizing solar technology with fuel-fired micro-cogeneration to have a highly efficient and reliable energy system.

Chapter 6 presents the exergy and exergo-economic analysis of a hybrid renewable energy system consisting of the PVT collectors, biomass-fueled micro-CHP system and thermal energy storage. This chapter combines the previous chapters together to form and analyze the HRES with the exergy method for a residential building in different European locations. In addition to the exergo-economics, the conventional economic parameters, such as simple payback time, net present value and yearly savings are calculated based on the yearly operation of the HRES under different climate conditions.

Chapter 7 and 8 present an introduction to solar microgrids and home renewable energy management methods. Additionally, the realization of the experimental set-up consisting of the photovoltaic panels, Lithium-Ion AC battery and load is presented. Finally, the gathered data from the experimental set-up is used to train a machine learning-based PV power prediction models for the optimal control purpose in Chapter 8.

The redline of the thesis is presented in Figure 1-2.

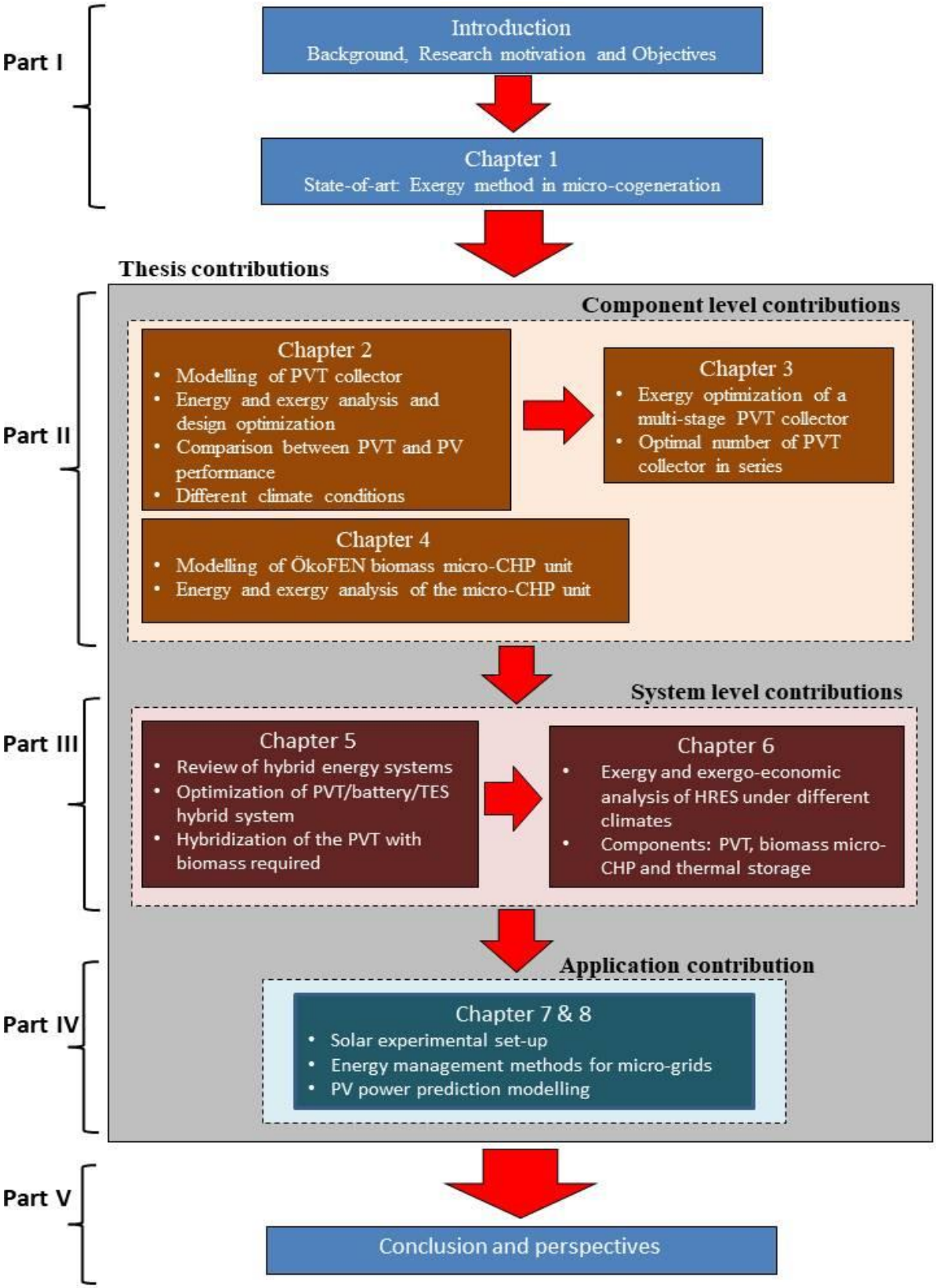

Figure 1-2: *Thesis outline as graphical illustration.*

CHAPTER 1. State-of-art: Micro-cogeneration and exergy method in the context of microgrids

1. Introduction

Access to energy ensures human well-being and economic development for society and prevents poverty. The energy use in Europe has increased strongly with the industrial development and wealth. Due to that, the pressure to reduce the primary energy consumption and CO_2 emission is really strong in Europe. In 2007, the European Council set the following energy and climate change objectives for 2020: greenhouse gas emissions reduction by 20% compared to emissions in 1990, renewable energy share increase to 20% of the energy mix, and to improve energy efficiency by 20% compared to 1990. These targets mean that the European Union (EU) committed itself to reducing energy consumption by 20% by the year 2020. In 2018, the EU set a 2030 target for reducing energy use by 32.5% [5]. In Figure 1-1 is shown the yearly primary energy consumption of the EU-27 and the distance to the 2020 and 2030 targets in 2020.

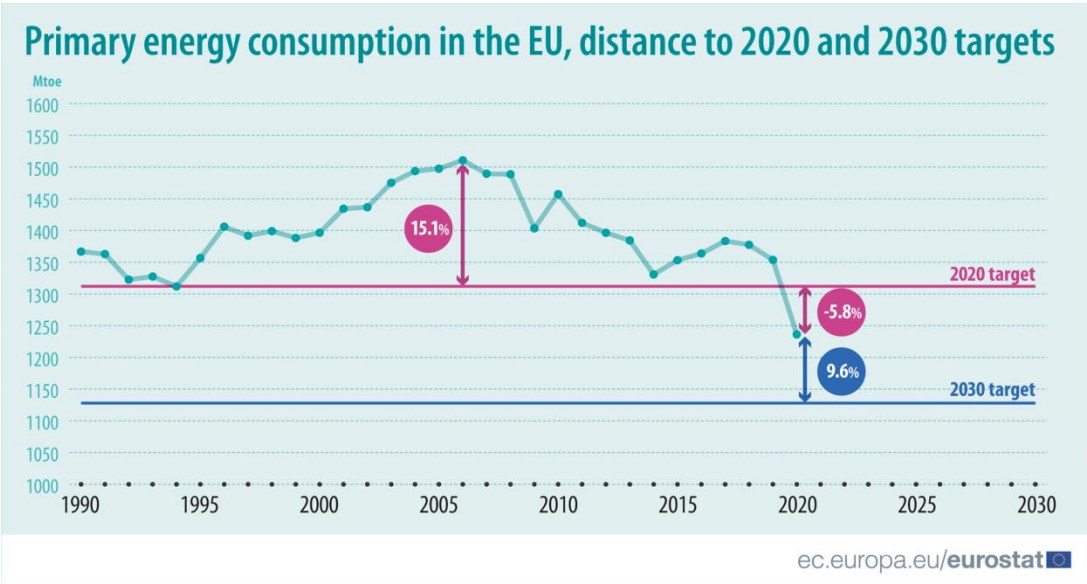

Figure 1-1: *The yearly primary energy consumption of the EU-27 and distance to the 2020 and 2030 targets [5].*

The 2020 target of 1312 Mtoe primary energy consumption was exceeded by -5.8% in 2020. In that year, the energy consumption was strongly influenced by the COVID-19 related restriction, such as travel restrictions and lockdowns, resulting in a sharp decrease in energy consumption [5]. The 2020 energy reduction target was clearly outperformed by 5.8%. In order

to reach the 2030 target, the primary energy consumption of the EU-27 should not exceed 1128 Mtoe in 2030. In 2020, the distance to the 2030 target was 9.6%. Figure 1-1 shows that different energy measures have to be conducted to meet the still demanding saving target of 2030.

One of the promising sectors to apply reduction measures is the building sector which accounts for 43% of the final energy consumption in the European Union (EU) [2]. A large share of the buildings is included in the households sector, which is responsible for 26.3 % of the final energy consumption in the EU, as shown in Figure 1-2. In the households sector, the largest energy end-use is space heating at 66 % followed by water heating as shown in Figure 1-3. However, the share of electrical appliances has increased from 2000 to 2019 and is almost as large as water heating [2]. Hence, the building and space heating efficiency, and more efficient decentralized energy generation technologies in the residential microgrids are seen as the key measures to reach the reduction targets of the EU [6]. Thus, this thesis studies different renewable energy-based micro-cogeneration systems from the exergy point of view and as a part of hybrid renewable energy systems. These systems are highly suitable to produce simultaneously space heating, domestic hot water and electricity to be used within the residential microgrid or sold to the grid.

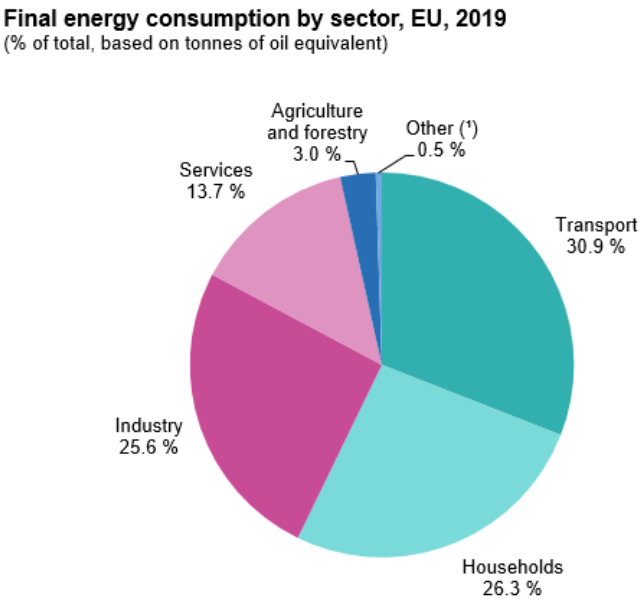

Figure 1-2: *The final energy consumption in the EU by different sectors [7].*

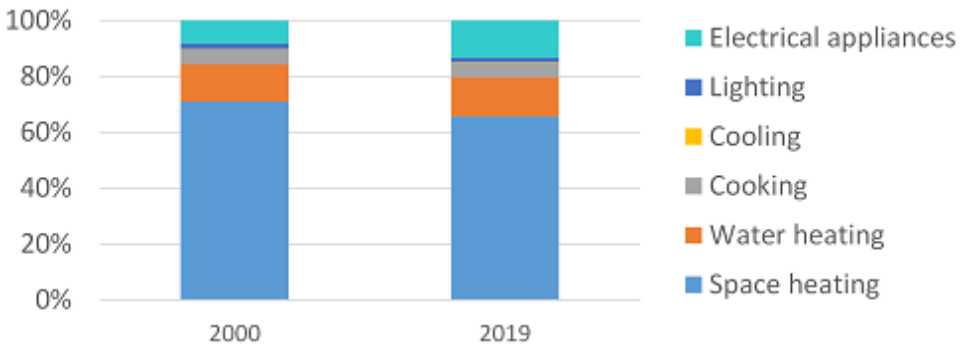

Figure 1-3: *The energy consumption of the households sector by each end-use in 2000 and 2019 [2].*

1.1 Smart Grid

The inflexible conventional power grid enables only one-way communication and supply of electricity from the centralized power plants through the transmission and distribution systems to the end-users [8]. The large transmission lines are used to connect the centralized power plants to the distribution system, which supplies electricity further to all levels of end-users from the industrial to the domestic ones. The operation of the power grid is hierarchical, and it is monitored and controlled manually and centrally by using only a few sensors [8]. The centralized power plants are located far from the end-user and are mainly fossil-fuel-fired. This causes a large share of transmission losses and CO_2 emissions.

The global requirements of decreasing primary energy consumption and CO_2 emissions with the continuously growing electricity demand have led to the need of integrating distributed energy resources (DER), such as renewable energies and energy storage, into the distribution system of the power grid. However, this requires a more flexible and smarter operation of the power grid by integrating information and communication technology to the power grid. The smarter grid integrates DERs and is self-monitoring and –healing through multiple sensors in the grid [8]. It is adaptive and engages the end-users to interact with the power grid through their energy management systems [8]. The smart grid technology enables also the formation of different microgrids within the distribution system of the power grid. The microgrids can work as autonomous systems to produce, store and consume their own electricity and still communicate with the power grid.

The concept of a smart grid came out in the early 2000s to overcome the difficulties of the conventional power grid to apply a two-way supply of electricity to the end-user [9]. The supply of electricity and information through two-way channels is allowed by smart grid

technology, which enables monitoring, control and analysis of energy flows and communication between the prosumer and grid utility company [9]. The bi-directional supply of electricity enables the electricity consumers to become prosumers that produce and store electricity for onsite use and feed the surplus into the main power grid if necessary or economically viable. The reliability of the conventional power grid is decreased by increasing electricity demand and the amount of distributed renewable energy systems in the grid if the smart grid technology is not applied to enable a flexible bi-directional supply of electricity.

1.2 Microgrid

To reduce the CO_2 emission of the conventional power generation, large-scale renewable energy sources (RER), such as wind, solar, hydro and biomass, have been included in the generation mix worldwide since a decade [10]. However, to reduce transmission and distribution losses of the conventional power grid, the small- and micro-scale RER, controllable CHP and other microgeneration and energy storage systems are called distributed energy resources (DERs) and installed close to the consumption point in the distribution system [10]. As a low-voltage (LV) distribution network, a microgrid is used to integrate DERs into the distribution system with the optimal management of the bi-directional power flows between the energy sources, load and the main power grid [10]. The microgrid has the following essential features: local microgeneration, local load and an intelligent energy management system [11]. Typically, the microgrids can operate in grid-connected or off-grid mode. When operating in grid-connected mode, which is usually the case in residential building applications, the microgrid can sell the produced surplus electricity to the main power grid to increase cost savings. This is managed and controlled by the intelligent energy management system. The microgrid can be also totally isolated from the main power grid, such as in the remote areas of mountains or countryside.

At the LV level, the microgrids can have different scales by including neighborhoods or communities of buildings with separated units of DERs or just a building with behind-the-meter DERs. The microgeneration capacity of the microgrid is typically from a few kW to one MW [11]. In Figure 1-4 are presented three low voltage levels of the microgrids defined in [11].

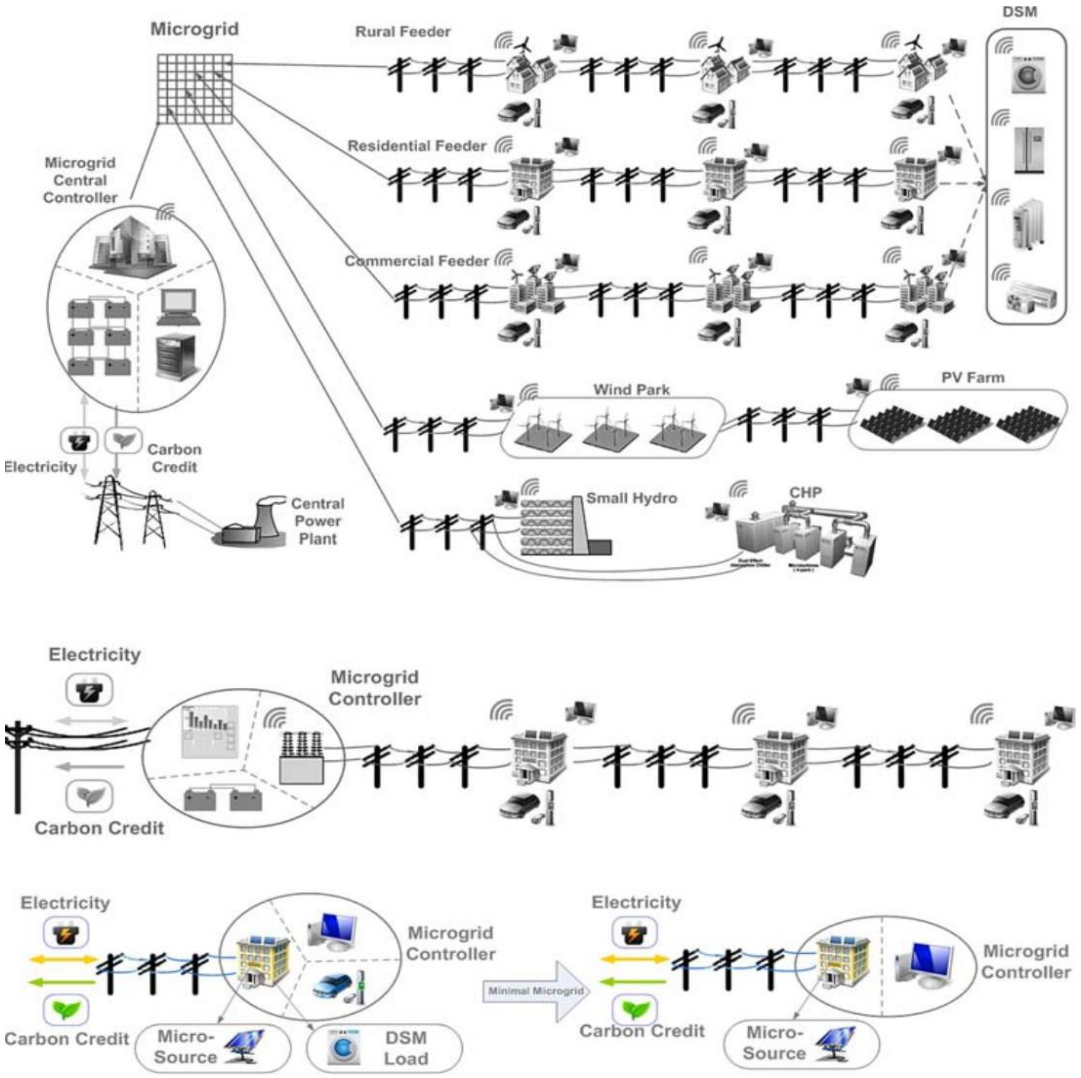

Figure 1-4: *Three levels of microgrids from above: the LV grid, LV feeder and LV house [11]*.

In this thesis, the residential microgrid applications (the LV house in Figure 1-4) are considered with behind-the-meter DERs. The considered DERs are micro-cogeneration systems, solar technologies and energy storage systems which are investigated theoretically and experimentally in terms of exergy method and energy management strategies.

1.3 Definition and benefits of micro-cogeneration

The micro-cogeneration, or combined heat and power (CHP), systems are decentralized energy systems that produce heat and power simultaneously from a single fuel source at high overall efficiency of around 85-95% [12, 13]. These systems produce energy for a prosumer's on-site use, such as domestic hot water, space heating and electricity. The building sector,

especially the residential buildings, is characterized by highly variable energy demand profiles that require a short response time which can be provided by the fuel-fired micro-cogeneration systems [14]. According to the European Parliament, micro-cogeneration refers to the energy systems with electrical power up to 50 kW [15]. However, in the scientific literature, the micro-cogeneration systems are mainly considered in terms of the residential and light commercial buildings and thus, defined to have the electrical power below 15 kW [16–20]. These systems are compact in size and manufactured to be integrated into a building on the prosumer's side of the electric grid as a domestic energy system. The energy flows in the domestic fuel-fired and solar-based micro-cogeneration systems are presented in Figure 1-5 with thermal storage to facilitate the matching of energy demand and production.

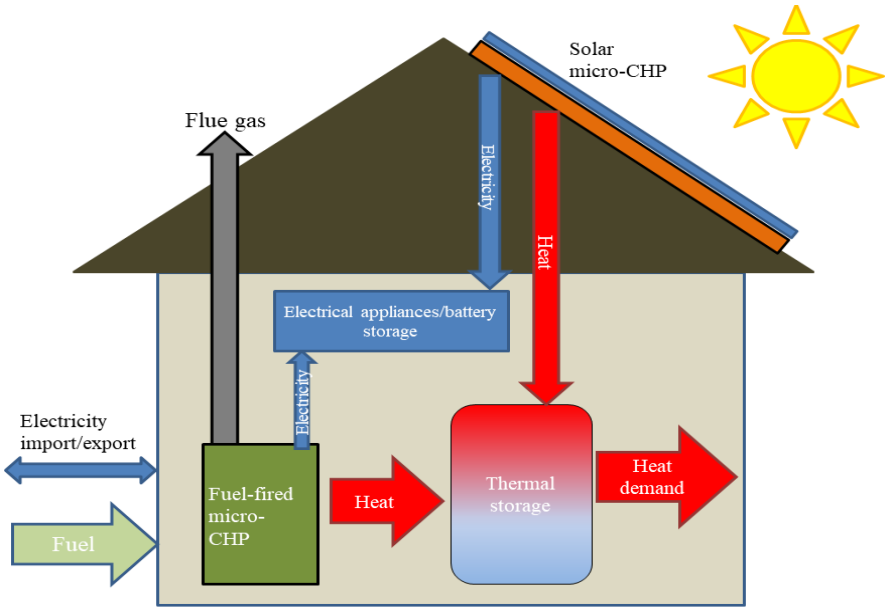

Figure 1-5: *The energy flows in the residential microgrid including fuel-fired and solar based micro-cogeneration systems.*

The utilization of micro-cogeneration systems in buildings has several advantages. In a conventional building, a separate production of heat and electricity is applied. In this case, a natural gas or biomass boiler is used to generate heat on-site and electricity is generated in a large centralized power plant and bought from the electric grid. If the micro-cogeneration system is used, especially, the transmission and distribution losses over long distances are avoided. Additionally, heat is produced at a higher efficiency. Hence, energy, CO_2 emissions and cost savings are generated, which are shown in Figure 1-6.

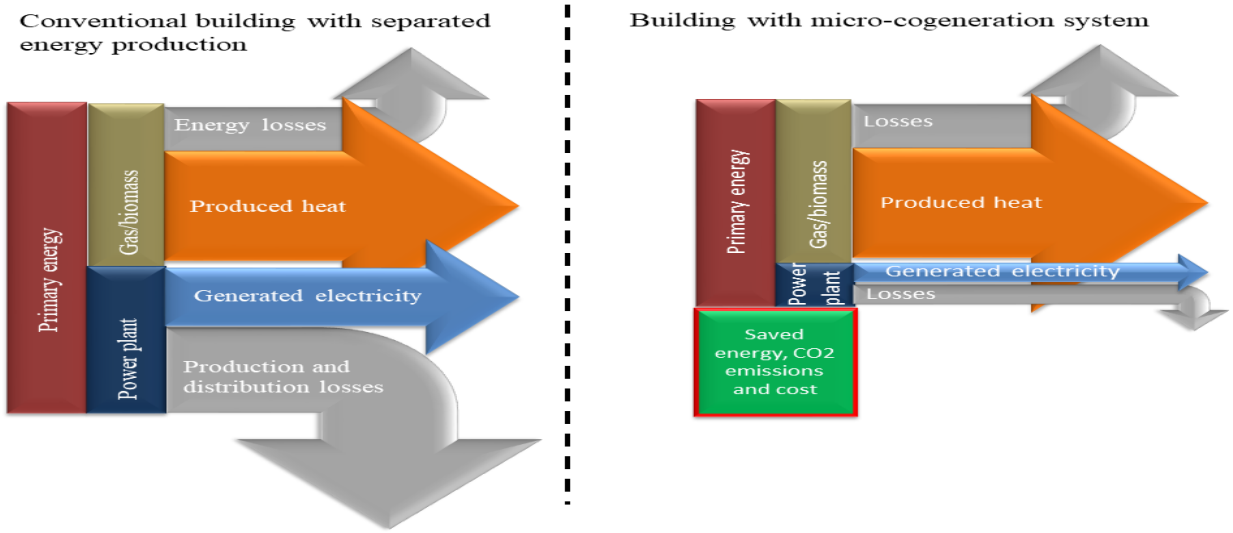

Figure 1-6: *Comparison between conventional separated energy production and micro-cogeneration.*

2. Solar-based micro-cogeneration

Solar energy is free of charge, renewable, inexhaustible and CO_2 emission-free energy source of which utilization causes less harm to the environment than many other sources [21]. From renewable energy sources, solar energy is the most plentiful source, which is freely caught by the earth at a rate of 1.8×10^{14} kW in different forms, such as light and heat [22]. Although the majority of the caught solar energy is lost by reflection, scattering and absorption by clouds, the abundant solar energy could be used to fulfil the global energy demand [22]. The distribution of solar irradiation and its intensity are highly variable over the world, as shown in Figure 1-7. Although solar availability differs between different countries, the same technologies can be used to convert solar energy into useful heat and electricity. However, some of the technologies perform better in conditions with a high share of direct normal irradiation (DNI), and some can convert the diffuse irradiation as well.

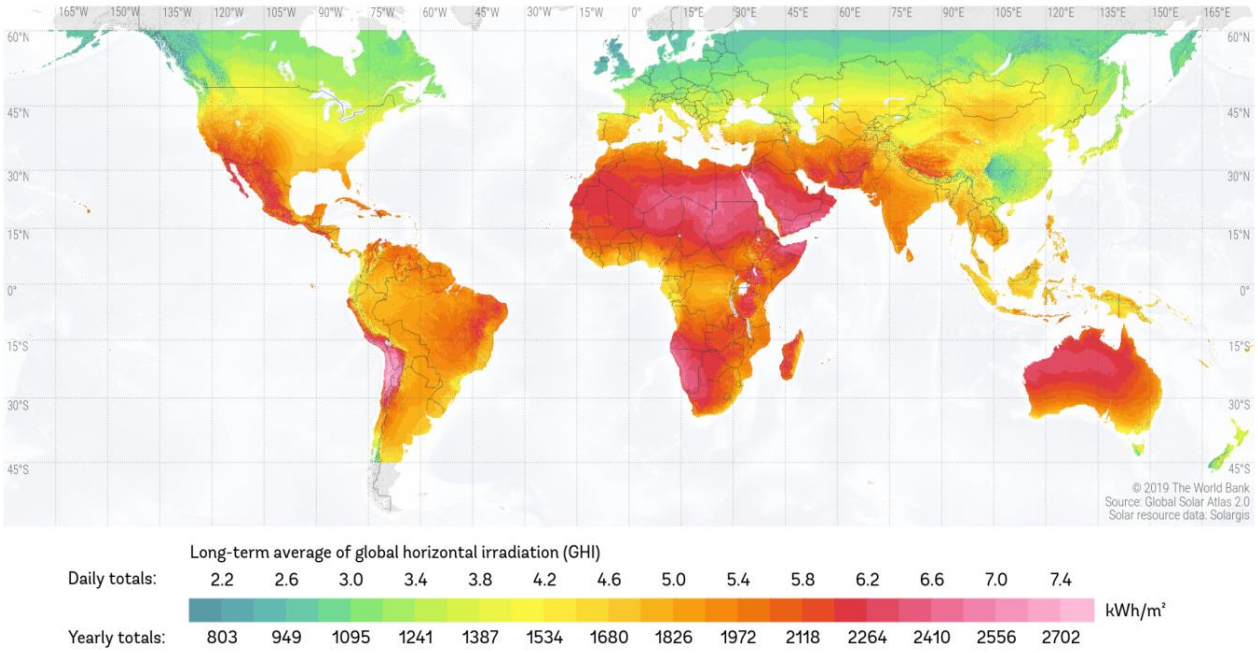

Figure 1-7: *The map of the global horizontal irradiation (GHI) on the earth [23].*

In the building sector, the following solar energy conversion technologies can be integrated into hybrid renewable energy systems and applied to produce domestic hot water (DHW), space heating and electricity: a photovoltaic (PV) panel, solar heat collector (SHC) and photovoltaic-thermal (PVT) collector. The PVT collectors can be used directly to generate heat and electricity simultaneously from the same installed area. Additionally, the PV panels can be combined with solar heat collectors to form a cogeneration system. The utilization of solar energy in these technologies is presented in Figure 1-8.

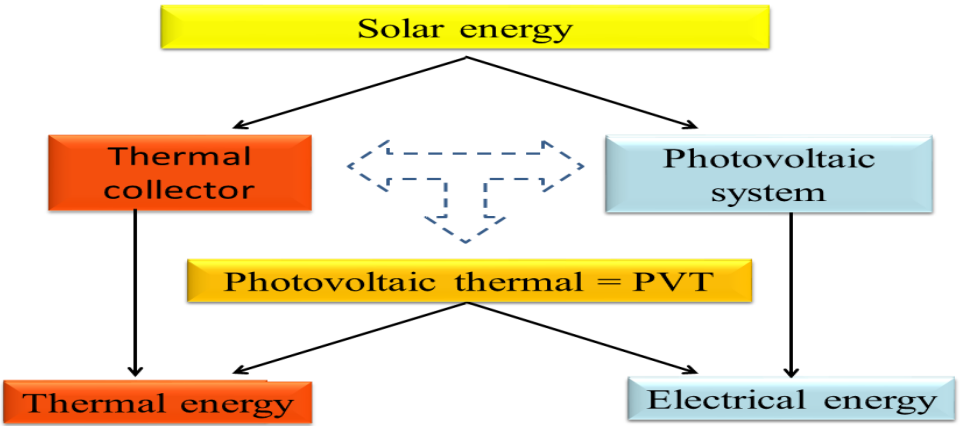

Figure 1-8: *Solar energy technologies.*

This section introduces the mentioned solar technologies that are able to be part of hybrid renewable energy systems in the building sector.

2.1 Photovoltaic panels

Photovoltaic (PV) panels or modules are one of the simplest technologies that can convert solar irradiation into electrical energy. These panels are constructed of several thin PV cells connected in series under a glass cover. The PV cells are made of semiconductor materials, such as silicon, of which electrons are activated by sunlight. These activated electrons move from the lower energy state to the higher one by engendering holes with a positive charge and free electrons with a negative charge, and thus, this phenomenon generates electricity and heat [22]. The process to generate direct-current electricity from sunlight is called the photovoltaic effect. Due to a modular characteristic, several PV panels can be connected in series or parallel to produce higher voltages or currents, respectively, and to form photovoltaic systems of different sizes from watts to megawatts.

Most of the market available PV panels are the first-generation PV cells and are made of monocrystalline and multicrystalline silicon of which electrical efficiencies are between 17-22% and 11-17%, respectively [24]. The difference between the efficiencies is caused by the grains used in the multi-crystalline [25]. The other used semi-conductors are amorphous silicon, cadmium telluride and copper indium gallium selenide that is used in the thin-film PV cells. These cells have typically a lower efficiency of 6 %-13 %, but they allow higher cell operation temperature than crystalline silicon cells and have lower manufacturing costs [24]. The second-generation PV cells are multi-junction thin-film silicon cells and utilize the mixture of gallium indium phosphide, germanium and indium gallium arsenide as a cell material. These cells have significantly high electrical efficiency up to 40 %, and they are less sensitive to higher operating temperatures than the first-generation silicon cells [25]. Both generations of the PV cells are used in the PVT system, and the thermal efficiency of the system is not depending on the used PV cell material [25].

The PV panels are usually connected in series as a solar array, and an inverter or micro-inverters are used to convert DC electricity to AC electricity, which is suitable for building appliances. The PV system can consist of several arrays. In buildings, the PV panels can be coupled with a Lithium-Ion battery as a part of the intelligent home energy management system,

which optimizes the charge and discharge of the battery depending on the solar availability and electricity prices. In this kind of grid-connected micro-grid, the electricity is produced close to the consumption point to avoid transmission and distribution losses. In addition to the battery storage, the electricity can be used directly in the electrical appliances or to heat water in sensible or latent heat storage, such as water or phase change material, respectively.

2.2 Solar heat collectors

The main component of the solar heat collectors is a heat exchanger, which transfers absorbed solar radiation energy into the internal energy of the coolant fluid [26]. The coolant fluid is used to transfer collected heat further to the thermal energy storage, from which it can be taken for the building use when necessary. In the building sector, the solar heat collectors (SHC) are used to generate heat for domestic hot water production, space heating, swimming pool heating and thermally activated cooling devices. The SHCs are dived into two groups: stationary or non-concentrating and concentrating collectors. Usually, in building applications, the coolant fluid is water, non-freezing liquid or air. In high-temperature applications, heat transfer oils are used. The SHCs can be stationary or use single-axis or two-axis tracking to follow the sun position during the day. The tracking systems are usually used in the concentrating collectors.

Stationary, unglazed or glazed flat-plate collectors (FPC) and evacuated tube collectors (ETC) are typically employed to decarbonize heat production in buildings by absorbing direct and diffuse solar radiation. Additionally, compound parabolic collectors (CPC) can be used as stationary or concentrating collectors.

The temperature range of the unglazed FPC varies from 25°C to 50°C and with glazing from 50°C to 100°C due to the better insulation of the absorber plate [24]. The FPCs are the most deployed solar heat collectors with the simplest design consisting of the glazing, riser tubes welded to the absorbing plate, back insulation and casing [26]. The coolant fluid runs by natural or forced circulation in the riser tubes to collect the absorbed heat for further use.

The vacuum-based ETC can reach operating temperatures up to 200°C and can be also employed for high-temperature applications of solar cooling and industrial process [24]. In the ETC, a heat pipe is placed a within vacuum tube which is used to ensure high insulation and to maximize heat transfer with minimum heat losses. A number of the vacuum tubes are connected to the manifold, or heat exchanger, to form a single ETC. The heat transfer process is based on

the evaporating-condensing cycle of the heat transfer fluid in the copper heat pipe [26]. Due to solar heat, the fluid evaporates and moves to the heat sink region in which it condenses and releases its heat to the coolant fluid, such as water, for further use [26]. After returning the fluid to the heat pipe, the cycle is repeated. The small reflectors can be used to concentrate solar radiation onto the vacuum tubes to improve the cost-effectiveness of the ETCs, which are relatively expensive compared to the FPCs [26].

The stationary CPCs operate at the temperatures ranging from 60°C to 240°C depending on the used concentration ratio [26]. The concentration ratio depends on the share of the aperture area to the absorber area and is 1 for FPCs and ETCs but can vary from 1 to 5 for the stationary CPCs [26]. The CPCs use reflectors to catch a wider range of solar radiation angles to the absorber, which is located at the bottom of the reflectors. If the CPC is designed as a panel, the reflectors are small looking like corrugated sheet metal under a glass cover.

In addition to the above-mentioned stationary, FPCs, ETCs and CPCs, the concentrating collectors can be used to increase the intensity of the received solar irradiation and the working fluid operation temperature to satisfy the requirements of high-temperature applications. The intensity of the solar irradiation is increased by using concave reflecting surfaces to focus solar radiation to a smaller absorber area. Such concentrators are single-axis tracking linear Fresnel collector (LFC), compound parabolic collector (CPC) and parabolic trough collector (PTC) of which temperature ranges are 60-250°C, 60-300°C and 60-400°C, respectively [24, 26]. Using of the parabolic dish collector (PDC) or heliostat field collector (HFC) with two-axis tracking results in significantly higher temperatures up to 1500°C and 2000°C, respectively [24]. The PDC can be used to run a Stirling engine to produce electricity but also heat as a by-product and utilized as a micro-cogeneration system for buildings or communities [27, 28]. The main disadvantage of the concentrated SHC technology is that it requires direct solar irradiation and the diffuse part of the irradiation cannot be utilized as in the PV panel, FPC, and ETC [24]. Due to this, it is not suitable to use in locations with a large amount of cloudy days in a year. Additionally, the concentrated collectors require a single- or two-axis tracking system to catch the maximum amount of direct solar irradiation during a day [26]. On the other hand, this enables collecting of solar radiation for a longer period of a day than in the stationary collectors.

In the micro-scale hybrid renewable energy systems applied to buildings, the stationary SHCs are used due to their simplicity and low operation temperature. The collectors are

connected to sensible or latent heat storage to facilitate matching between the heat production and demand. In building applications, thermal storage based on the temperature difference in water is used due to its good heat capacity.

2.3 Photovoltaic-thermal collectors

The photovoltaic-thermal collector is a solar-based micro-cogeneration system which integrates PV and SHC components into a single unit to improve the overall efficiency. The principle of the layers in the PVT collector is presented in Figure 1-9.

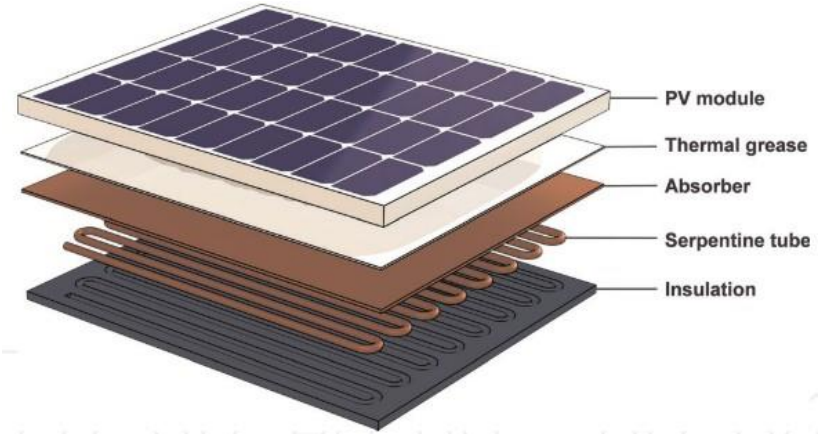

Figure 1-9*: Integration of the PV and SHC components to be a PVT collector [29]*.

The PVT heat exchanger is similar to the fin and tube design of the FPC and is in thermal contact with the PV panel back surface [26]. The PVT utilizes the PV module to produce electricity, and useful heat is produced as a by-product by cooling the module with a coolant fluid, such as water. The cooling effect decreases the operating temperature of the PV module and thus, increases the power generation and electrical efficiency [30]. At the same time, cogeneration increases significantly solar energy utilization and overall system efficiency [30]. The electrical efficiency of the PV panel can decreases by 0.45% for each degree rise in cell temperature of the mono- and multi-crystalline PV cells [26]. For the other semiconductors, such as amorphous silicon, the decrease is 0.25% per degree [26]. The PVT collectors can produce low-temperature heat at 60-80°C, but mainly they produce heat below 50°C which is still suitable for many applications, such as space heating or washing and cleaning processes [26]. The different PVT layers with heat transfer components and energy products are presented in Figure 1-10, and a single collector is further modelled and studied in Chapter 2 of this thesis.

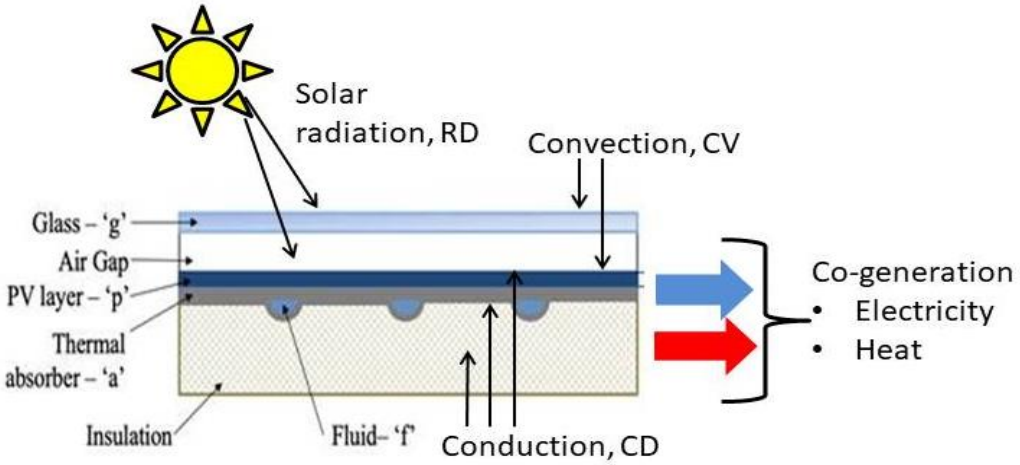

Figure 1-10: *The PVT layers with heat transfer components and energy products.*

Using the PVT collectors, instead of the separated solar technologies, has several advantages, such as architectural uniformity and simplicity to install only one technology type [21]. However, the improved utilization of the installation area, the higher overall energy efficiency and increased lifetime of PV cells compared to the separated production of heat and electricity are the main advantages of the PVT collectors [21, 26].

The working principle of the PVT collector can be utilized with different types of solar input, system configurations, heat extraction arrangements, working fluids and end applications [24, 31]. In terms of system design, the solar input to the PVT collector can be concentrated or non-concentrated. The latter is called a flat-plate PVT collector, which is the simplest and most installed PVT system. Figure 1-11 presents a map of different PVT system implementations. The PVT collector can use different working fluids for heat extraction from the PV module of which the most used are air and water. Due to the higher thermal capacity of water, the water-based PVT collector has better performance than air-cooled collector and hence, is the most used working medium [24, 32]. The heat transfer from the PV module can be improved by using phase change material (PCM) or nano-fluids with adjustable properties. However, currently, the most market available PVT are water- or air-based flat plate collectors. The most used applications of the flat-plate PVT collectors are domestic hot water, space heating, industrial processes and air conditioning.

A concentrator, such as a parabolic trough or Fresnel lens, can be used to increase the efficiency of solar energy conversion and solar irradiation density received by the PVT collector.

As a result of solar concentration, a higher operating temperature is reached, which leads to better thermal performance between 40 % to 60 % and electrical efficiency of 8 %-11 % [24].

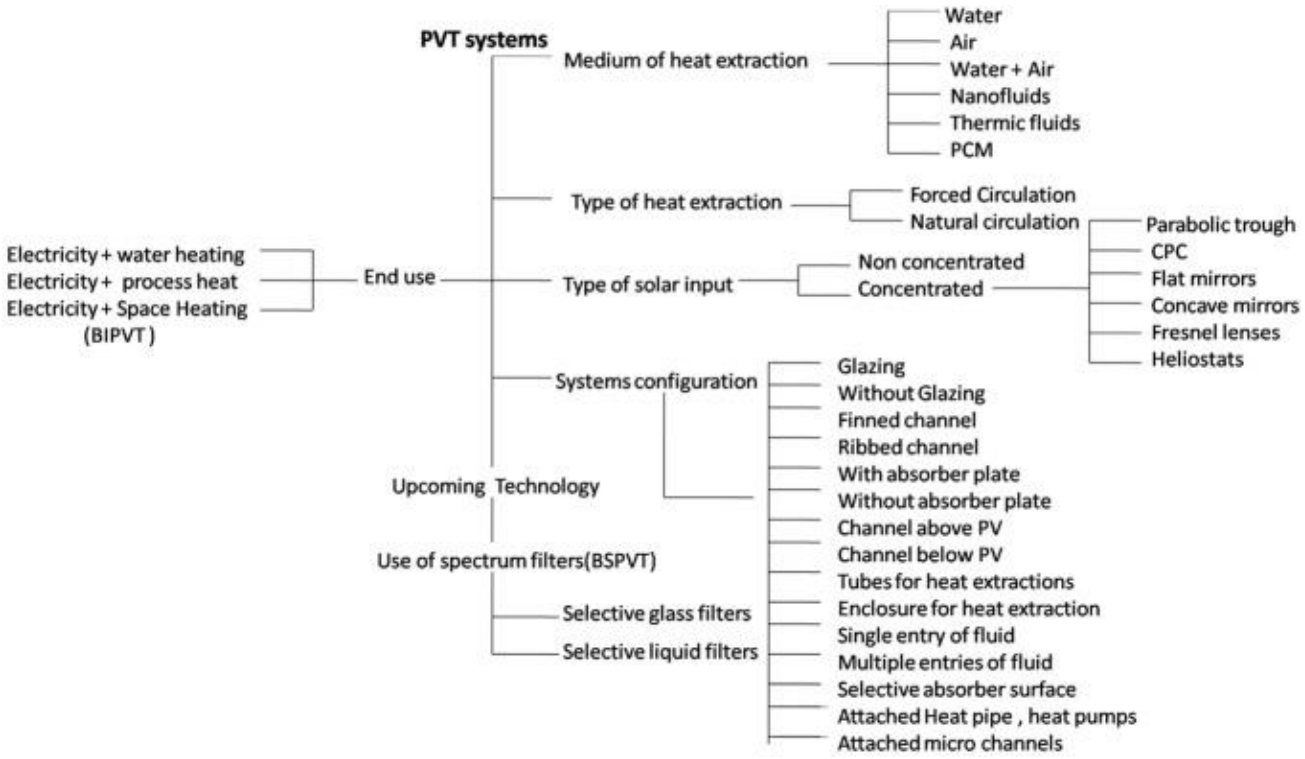

Figure 1-11: *The map of the PVT classification [31]*.

3. Fuel-fired micro-cogeneration systems

Fluctuating solar energy generation requires thermal and electrical storage technologies to facilitate energy management in the highly fluctuating energy demand environment of residential and commercial buildings. Additionally, solar energy production depends highly on the seasonal variation in the availability of solar radiation. Due to this, a hybridization of solar technologies with fuel-fired micro combined heat and power (CHP) units can come over the problem of the fluctuating solar energy production in terms of daily, weekly and seasonal variation. The fuel-fired micro-CHP units normally benefit from continuous running with low ON/OFF frequency. Due to this, the hybridization can allow running the fuel-fired micro-CHP during the colder season with high space heating demand and the use of solar heat and electricity production during the lower heating demand period. Thermally activated cooling devices would extend the running hours of the fuel-fired micro-CHP.

In the fuel-fired micro-CHP units, a prime mover is used to convert fuel energy to mechanical work and heat is recovered as a by-product from the prime mover cooling. In the literature, the micro-CHP prime movers are divided into the following groups: external, internal and no combustion-based [13]. The external combustion-based units, such as organic Rankine cycle (ORC) and Stirling engine, have good fuel flexibility compared to the internal combustion engine (ICE) based units. These units can use a wide variety of renewable sources as a fuel, such as solar energy, solid biomass and waste heat [13]. However, the ICE-powered units are, at the moment, the most developed and used technology in terms of micro-CHP systems [33]. As a prime mover, fuel cells are no combustion-based units in which a chemical reaction with oxygen is used in the conversion process.

The ICE and fuel cells based micro-CHP units are commonly used to convert natural gas into heat and power [18]. However, these technologies can use solid biomass as fuel, but further conversion technologies, such as gasification of biomass is required [12]. The ICE can use also bioliquids, such as biodiesel, as fuel [18]. In Table 1-1 is presented a comparative assessment of different prime movers that can be adapted to use solid or gaseous biomass as a fuel and are suitable for residential building use.

Table 1-1: Comparative assessment of the different prime mover technologies

Prime mover	Fuel cells	ICE	Stirling engine	ORC
Advantages	Electricity/heat ratio suitable for residential use [18]	High electrical efficiency and durability [18]	Simple design [34]	Low-grade heat use starting from 50°C [33, 35]
	High electrical efficiency [13]	Fast response to load [33]	Low maintenance, noise, vibration and emissions [12]	Fuel flexibility [12]
	Extremely low emissions, quiet operation and low maintenance [18, 36]	Low maintenance costs and space requirements [18]	Fuel flexibility [13, 34]	Easy to retrofit the existing heating device [14]
	High reliability [36]	Low investment cost [18, 33]	Noise level and electricity/heat ratio suitable for residential use [13, 37]	High partial load efficiency [33]
			High thermal efficiency [34]	
			Good partial load	

			performance [33]	
Disadvantages	Very high investment costs [18, 33]	Short maintenance intervals [33]	Low electrical efficiency [18, 37]	High investment costs [33]
	Short lifetime [18, 38]	Low fuel flexibility [33]	High investment costs [12, 33]	Relatively low electrical efficiency and waste heat recovery [14, 33]
	CO_2 emissions and energy use of hydrogen production [36]			Challenges in efficient downscaling [12]
Main fuel type in micro-CHP applications	Natural gas, hydrogen [13, 18, 39]	Natural gas [13, 18]	Biomass, natural gas, solar radiation [27]	Waste heat, geothermal, biomass, solar radiation [12, 14, 39]
Stage of technology	R&D and some commercially available [18, 39]	Commercially available [39]	Commercially available [39, 40]	R&D and some commercially available [39, 40]
Company	Vaillant, Viessmann	Honda Ecowill, Senertec Dachs, Vaillant	ÖkoFen, Whispergen, BAXI, Sunmachine, Genoastirling S.r.l.	Rank®, Kaymacor ORChidea, Viking Development Group

Next, state-of-art different commercially available renewable energy-based micro-cogeneration systems for buildings are presented. These systems include fuel-fired micro-CHP unit hybridized with solar technologies.

3.1 Fuel cells

Considering micro-CHP in residential applications, an electrochemical fuel cell (FC) system has great potential due to its high electrical efficiency, low emissions and quiet operation [18]. The fuel cells differ from the other prime movers significantly because of their non-combustive process to generate heat and power from hydrogen, natural or biogas. Due to the conversion process, fuel cells have only a few moving parts, which leads to higher reliability than the combustion-based prime movers [36]. In the fuel cells, fuel is converted into electricity through a chemical reaction with oxygen. The conversion process produces only heat and water

as a by-product which makes it the cleanest prime mover in terms of energy conversion [36]. However, the production of oxygen and hydrogen for fuel cells requires a high amount of energy and produces CO_2 emissions [33, 36]. As for disadvantages, the fuel cells have very high investment costs and a shorter lifetime [18, 33, 38]. Additionally, to use solid biomass as a fuel in the FC micro-CHP system, a gasification system is required to further produce biogas at a high fuel purity level [33].

The fuel cells are classified into different categories by the following used electrolyte types: phosphoric acid FC (PAFC), proton exchange membrane FC (PEMFC), molten carbonate FC (MCFC) and solid oxide FC (SOFC). The operating temperature of the fuel cells differs from 80°C to 1000°C based on the category [24, 41]. The PAFC and MCFC types are used only in large-scale power plants and are not suitable for residential-scale applications [41]. However, the PEMFC and SOFC are the most suitable for the residential micro-CHP application and are gaining more attention in the building sector [41, 42]. The PEMFC can be divided into low- and high-temperature PEM fuel cells depending on the operating temperature ranging from 60-80°C to 100°C -200°C, while the SOFC operating range is 700°C-1000°C [41].

The PEMFC and SOFC are considered in this review because they have high potential in the residential micro-CHP applications, and they can be fed by biogas. Table 2 shows the list of fuel cell micro-CHP systems with and without solar support.

Table 1-2: The fuel cell micro-CHP systems hybridized by solar energy

Fuel cell	Power outputs	Fuel	Solar hybridization	Methods	Evaluation	Key findings	Ref.
SOFC	P_{el} = 1kW	H_2, natural gas	- PV -Electricity to H_2 production	- TRNSYS, HOMER - Life cycle analysis -Sensitivity analysis -Single-family house - Comparison H_2- and NG-fired units	LCA, CO_2, energy demand	-PV reduces CO_2 emissions with H_2 as fuel - NG-fuelled better performance -PV integration gives the best results	[43]
SOFC	P_{el} = 1kW	Biogas	-	- Residential - Comparison of 3 different biogas processing methods - Sensitivity analysis	η_{el}, η_{CHP}, exergy	- Biogas suitable fuel for residential SOFC - Electrical efficiencies: 42.4%, 41.7%	[44]

				-Exergy, energy		and 33.9% -The highest CHP efficiency of 80.5%.	
PEMFC with ORC for DHW production	$P_{el,PEMFC}$ = 5kW $P_{el,max,ORC}$ = 5.33kW	H_2	-PTC -Produce superheated vapor for ORC expander	-EES -residential building -energy analysis -micro-CCHP system -impact of the key operation factors	$\eta_{overall}$	-the max. CCHP efficiency of 85% - Increasing ambient temperature decreases overall efficiency in summer and opposite in winter -CCHP efficiency stays constant if less than 550 W/m^2 solar radiation	[45]
SOFC	P_{el} = 95kW	H_2	CPTC	-TRNSYS -MATLAB -University building,Italy -polygeneration -thermoeconomic optimization of system design parameters	-energy -economics	-highly energy efficient -economic barrier -high temperature cogeneration crucial to optimize the system balance -public funding policies important	[46]
PEMFC	P_{el} = 4kW P_{th} = 6.5kW	Biogas, H_2	-PV -to produce H_2 or building use	-MATLAB Simulink -Experimental data	η_{el}, $\eta_{overall,}$ economic parameters	-simulation period 1 month	[47]

3.2 Internal combustion engine

The piston-driven internal combustion engines are the most developed and proven technology of the fuel-fired prime mover technologies due to their utilization in vehicles and low investment costs [33]. However, it is used in electricity generation and CHP applications as well. In terms of micro-cogeneration, the spark-ignited Otto engine is applied and gaseous or liquid fuels are combusted in the internal combustion chamber [48]. Due to the internal combustion process, the ICE-based micro-cogeneration systems cannot use directly solid fuels, such as

biomass, but the gasification can be used to produce suitable syngas from biomass [48]. However, the ICE is highly sensitive to the purity of the fuel gas in terms of efficiency reduction [33]. As a micro-cogeneration system, the waste heat from the ICE is recovered from the exhaust gas and jacket water to cool the engine. The electricity is generated by the piston displacement. The micro-scale ICE cogeneration systems can reach higher electrical efficiency than the other prime mover technologies resulting in 30 %-35 %, which makes it attractive [33]. However, in terms of building applications, the thermal energy demand is significant, and the thermal losses of the ICE are higher compared to the other prime movers [33].

Table 1-3 presents the ICE-based micro-CHP systems hybridized by solar energy.

Table 1-3: The ICE micro-CHP systems with solar hybridization.

Power outputs	Fuel	Solar support	Methods	Evaluation	Key findings	Ref.
P_{el} = 5.5 kW	Natural gas	PV and SHC	- TRNSYS model - Different configurations of solar support - system optimization - Sensitivity analysis - Different climate conditions	- PE consumption - CO_2 emissions -LCC analysis	- Hybridization decreases PE use and CO_2 emissions but has the highest LCC -The component costs and administrative barriers should be reduced	[49]
P_{el} = 1.2 kW	Natural gas	PV	- Comparison of different system configurations - system sizing	- Technical evaluation	-Hybridization increase significantly PV penetration - Battery storage is not required - Energy waste was reduced	[50]
P_{el} = 1 kW	Natural gas	PV	- A new method to calculate the LCOE of the hybrid system - Case study of the residential building	-LCOE -Sensitivity analysis	- The hybrid system can enable profitable off-grid operation - The LCOE for the off-grid hybrid system	[51]
P_{el} = 4 kW	Natural Gas	PVT	-Design and operation optimization - Linear programming	- Saving through the operation optimization -Comparison of savings	- Operation optimization increases the profit - Larger battery does not lead always to the higher savings	[52]

3.3 Stirling engine

The Stirling engine operates on a closed and regenerative thermodynamic cycle, whereas the cyclic expansion and compression of the working fluid, (i.e air, helium or hydrogen) are used

to move the piston and generate electricity. The pressure variation is created by heating and cooling the engine's hot and cold ends. This prime mover technology is based on the exterior heat source allowing a wide range of renewable fuels to be used, such as biomass, biogas and solar. In terms of building applications, the Stirling engines have the quietest operation potential compared to other engines, suitable power-to-heat ratio and low maintenance requirements [13, 33]. In Figure 1-12 is presented the domestic ÖkoFEN micro-CHP unit with its Stirling engine.

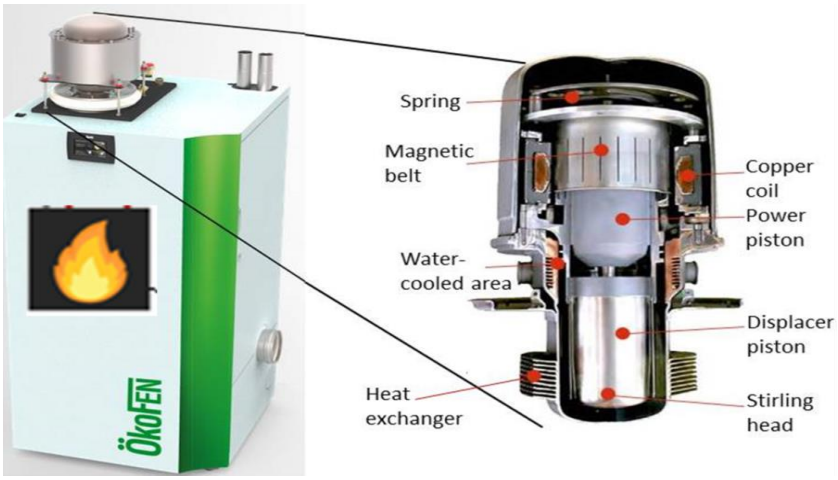

Figure 1-12: *A dynamic type free piston engine of the ÖkoFEN biomass-fueled micro-CHP unit [53].*

Ferreira et al. [27] assessed the Stirling engine performance comparing solar energy and biomass as primary energy source. Based on the simulations, the biomass-fueled alpha-Stirling engine provided 87.5% more power output and significantly higher operation temperatures compared to solar powered engine. Finally, the levelized costs of energy for the solar powered system were 52% higher than biomass-fueled system. Additionally, the biomass-fueled system overcomes the fluctuating nature of solar energy. In Table 1-4 is presented Stirling engine micro-CHP systems hybridized by solar energy.

Table 1-4: The Stirling engine micro-CHP systems with solar hybridization

Power outputs	Fuel	Solar support	Methods	Evaluation	Key findings	Ref.
P_{el} = 1kW P_{th} = 7kW	Natural gas	-PV -flat plate solar thermal - to	-Experimental study - Operation data of 36 days in Spain - Matlab -Comparison to a	η_{el}, η_{th}, CO_2 emissions	-Higher performance is expected if heat demand is extended to space heating and cooling -The system reliability	[54]

		produce heat and electricity	reference system including electric grid and diesel oil boiler -Typical residential domestic hot water and electricity demand profiles		increased with thermal and electrical storages, and micro-CHP unit - CO_2 emissions reduced by 36% - 76% of total energy demand is covered -Biomass use proposed for further CO_2 reduction	
P_{el} = 1kW P_{th} = 26 kW	Natural gas	-PV -to produce electricity	-Comparison of different PV powers and battery capacities with Stirling micro-CHP -Experimental data of PV and micro-CHP installation	-demand self-coverage index -sold share index -energy stored share -self-consumption -net present value	-The system enables significant improvement in self-sufficiency -High investment costs -High ecological effect	[55]
P_{el} = 1-5 kW_{el} P_{th} = 3-17.5 kW_{th}	Solar energy	-parabolic solar collector - powering a Stirling engine	-Matlab numerical simulation -Generalized Pattern Search optimization algorithm -Optimal design -Residential building	Economic analysis	-Payback time of 10 years -The best configuration: 3.65 kW_{el}, 11.06 kW_{th} to fulfill base heating demanf of residential building - the most drawbacks of renewable micro-CHP is still in the investment costs - energy storage required	[28]
P_{el} = 6 kW	Wood pellets	-PV -to produce electricity	-HOMER, Matlab Simulink -System comparison of PV/diesel generator/battery to PV/Stirling/battery	-energy efficiency -economic feasibility -CO_2 emissions	-PV/Stirling/battery resulted in the higher performance -69% CO_2 savings -11% annual cost savings -5% fuel savings	[34]

3.4 Organic Rankine cycle

The organic Rankine cycle (ORC) is based on the conventional Rankine cycle and organic fluids, such as toluene, n-pentane or hydrocarbons, as a working fluid instead of pure water. Using the organic fluids enables the utilization of the lower vaporization temperatures and low-heating value fuels, such as geothermal, solar or biomass [48]. The main principle of the Rankine cycle (RC) is to produce mechanical work by vaporizing high-pressure working fluid which expands in a turbine to lower pressure. Thus, the main components to enable the ORC are the feed water pump, evaporator, expander and condenser. The good development of the RC has

its roots in the 1980s, and it has been utilized in the industrial-scale power plant applications [13]. The ORC-based micro-cogeneration systems are also widely studied by research centers and companies, but the market availability of the systems is still limited [14]. The main difference between the building-related ORC applications to the industrial ORC is the dynamic energy demand profile and non-steady operation conditions with a requirement of a short response time. Due to this, the main development requirements should be focused on the evaporator of the ORC to enhance the delivery of the primary energy to the cycle [14].

In Table 1-5 is presented the ORC-based micro-CHP systems hybridized by solar energy.

Table 1-5: The ORC micro-CHP systems with solar hybridization

Power outputs	Fuel	Solar support	Methods	Evaluation	Key findings	Ref.
P_{el} = 40 kW P_{th} = 310 kW	Biomass	-PVT - to produce heat and electricity for demand	- Matlab -Transient techno-economic modelling -Design optimization - Sport center in Bari, Italy	Techno-economic analysis	-Payback time 11.5 year - 100% renewable energy supply with hybrid system - Electricity production capability increased significantly	[56]
P_{el} = 14 kW P_{th} = 70 kW	Biomass	-PV - to produce electricity for demand	-System modelling and analysis -Residential building block - Electricity, space heating and domestic hot water	- Energy analysis -Self-consumption - Fuel savings	- Yearly electrical self-consumption 84.9% with hybrid system, 32.5% with PV only. 54.9% of thermal energy demand covered - Significant natural gas savings - ORC overcomes the fluctuation of solar energy source	[57]
P_{el} = 5 kW	Biomass	-SHC	- to model the solar assisted ORC cycle with 3 operating temperature ranges - comparison with and without heat storage	-energy analysis -economic analysis -different working fluids - 3 different locations	- Cyclohexane performed well as a working fluid - integration of heat storage extend the running periods	[58]

4. Exergy approach

4.1 Introduction

Thermodynamics is a field of science considering energy with four laws and the following terms: heat Q, work W, pressure p, temperature T, entropy S and internal energy U

[59]. The first law of thermodynamics considers the quantity and conservation of energy. It quantifies the amount of energy which can change its form, but the total amount remains constant in the system. The second law of thermodynamics states that, in addition to the quantity, the quality of energy exists. As opposed to the quantity, the quality of energy is always destroyed in an energy conversion process. The amount of destroyed quality can be used as a second efficiency measure for energy conversion processes.

The exergy concept has its fundamentals back in 1824 when Sadi Carnot stated that the temperature difference defines the available work of a heat engine [60]. This was the beginning of the second law of thermodynamics on which, in addition to the first law of thermodynamics, the exergy approach is based. In the 1870s, Josiah Willard Gibbs introduced the term "available energy" of a system, and he developed the concept of Gibbs free energy [60, 61]. Until the end of the 1960s, the theory of exergy was contributed by multiple scientists from many countries, such as Germany, France, the US and Russia, and completed in a big picture [60]. However, the penetration of the exergy analysis within the practical applications was still low.

In the 1970s, humankind faced its first oil-crisis 1973, and the energy efficiency improvements became a focus of industries and governmental agencies [60]. This was the beginning of applying the exergy method in significantly growing number of applications to improve the hidden inefficiencies of the energy conversion processes. The engineers started to adopt the exergy analysis more and more as a useful concept to analyze energy systems after 1977 [59].

Sciubba and Wall [60] presented the modern definition of exergy based on the work of Gibbs: "*The exergy is the maximum theoretical useful work obtained if a system S is brought into thermodynamic equilibrium with the environment by means of processes in which the S interacts only with this environment."*. Dincer and Rosen [62] defined the exergy to be *"the maximum shaft work that can be done by the composite of the system and a specified reference environment"*. Moran and Sciubba [63] defined the exergy as follows: *"the maximum theoretical work that can be extracted from a combined system of system and environment as the system passes from a given state to equilibrium with the environment".* On the other hand, Evola et al. [64] gave a following definition for the exergy: "*the maximum amount of work that can be produced by exploiting a system or an energy flow available at a certain temperature, through an ideal reversible process evolving until the dead state is reached*". As can be said, a beloved

child has many names, the following terms have been used for exergy through its history of development: availability, essergy, useful energy, available energy, work potential, thermodynamic potential and technical working capacity [59, 60, 62].

The first law of thermodynamics-based energy analysis is used to quantify the amount of energy which can only change the form in the conversion process and not be created or destroyed. However, it does not count how well the quality of the fuel energy is preserved in the energy conversion process. In contrast to the energy analysis, the exergy analysis quantifies the quality of energy which is destroyed in each irreversible energy conversion process. The quality of energy is measured as a work potential of a heat engine to the specified environment or system equilibrium. The exergy analysis is used to reveal more information about the energy system efficiency than quantity-based energy analysis which does not take into account the work potential or quality of different energy levels.

The energy flows in the building environment mainly consist of space heating, cooling, domestic hot water and electricity of which electricity is seen as pure exergy. However, the thermal products are required at a low-temperature level which indicates low quality. To have an efficient energy system in the building, the target is to produce the required low-quality energy from low-quality energy sources. However, often high-quality energy sources, such as electricity and fossil fuels, are used as an energy source. This inefficient use of energy sources is not seen by the energy analysis but revealed by the exergy analysis.

Next, the most important issues according to the exergy method are presented and discussed. Additionally, a great number of research studies on the exergy method applied to micro-cogeneration and hybrid renewable energy systems are reviewed and discussed in the following sections.

4.2 Reference environment

The amount of the system's energy is independent of its environmental state. However, the reference environment or dead state is always mentioned in the definition of exergy, and the exergy is calculated as a work between the system and its environment or dead state. Due to this, two states are required to be defined when using the exergy analysis. The first state is the actual state of the system, and the second state is the reference state, equilibrium or dead state. Selecting a suitable reference environment was stated as a problem already in the early years of

exergy analysis [60]. Once the reference environment is specified, the value of exergy can be fixed depending on the state of the system [63]. Due to this, the exergy value as a result of the system analysis is highly sensitive to the defined reference environment and its properties should be defined carefully.

The total exergy of a system includes the following four components with different property associations: chemical exergy associated with the chemical composition, physical exergy associated with the system pressure and temperature, kinetic exergy associated with the velocity of the system and potential exergy associated with the system height [65]. The physical exergy has two components: thermal and mechanical exergy. In terms of thermal exergy, the reference environment is described by the temperature. The greater the difference between the state and its environment, the greater the amount of exergy and the useful work.

In terms of micro-cogeneration and hybrid renewable energy systems in buildings, a restricted dead state, defined by Moran and Sciubba [63], can be considered. At this state, only the physical exergy in terms of mechanical and thermal equilibrium is taken into account and the difference to the environment in the velocity and elevation properties are set to zero [63]. At the restricted dead state, the reference temperature and pressure can be set to be ambient and atmospheric values of T_0 = 25 °C and p_0 = 1 atm, respectively. However, in this thesis, only the thermal exergy component of the physical exergy is used in the analysis. Additionally, the electrical energy flow produced by the energy systems is considered. Electrical work is seen as pure exergy and can be fully converted into useful exergy.

Typically, the reference environment is defined to be the natural surroundings of the system with constant properties of pressure, temperature and chemical composition. When the system reaches the properties of the reference environment, it has reached the dead state, and there is no possibility to extract useful work anymore. Rosen and Dincer [66] presented that the reference temperature T_0 is the main property which has an impact on the results of the exergy analysis. Additionally, they showed that if the temperature difference between the system and environment is large, the amount of exergy is less sensitive to the variation of the reference temperature. However, if the system temperature is close to the reference temperature, which is the case in micro-cogeneration systems and buildings, the values of exergy are highly sensitive to the variation of the reference temperature [66]. Due to this, in terms of low-temperature

applications, the reference temperature should be selected carefully to obtain the most realistic and comparable exergy analysis results.

In terms of the micro-cogeneration systems for buildings, the selected reference temperature in the literature is the ambient temperature of the surroundings [67–69]. However, the ambient temperature fluctuates strongly over time which would result in a dynamic reference temperature. The variable reference temperature has been adopted for the exergy analysis by some authors in the literature. However, Pons et al. [70] studied exergy with fluctuating ambient conditions. They stated that the reference temperature T_0 must be fixed and constant because a variable reference temperature would lead to the thermodynamic contradictions. In the literature, there is no agreement of the value of the constant reference temperature, and some authors adopt values such as 20°C or 25°C. However, if the yearly analysis is conducted, the ambient temperature varies strongly in many locations depending on the season of the year. Selecting the reference temperature of 25°C for a winter month leads to misleading results. Due to this, Fujisawa and Tani [71] adopted the average monthly ambient temperature and Evola and Marletta [72] selected the monthly minimum ambient temperature to be a constant reference temperature in the exergy analysis of the solar micro-cogeneration system.

In a conclusion, the selection of the reference environment has a high impact on the results of the exergy analysis, and there is still a lack of a common reference environment definition in the scientific community. The common definition would make different exergy analyses comparable and facilitate the standardized use of exergy analysis in energy systems and buildings.

In this thesis, the monthly average ambient temperature is selected to be the reference environment in the yearly exergy analyses to compare fairly exergy values in the different locations.

4.3 Exergy in energy systems

Several books about thermodynamics and the exergy method have shown that the performance of any energy conversion process cannot be measured properly using the analysis based only on the first law of thermodynamics [60]. Due to this, the energy flows in the system should be expressed by the exergy indicators. In the scope of this thesis, the thermal exergy has

the highest impact on the exergy analysis due to the fact that electrical energy is seen as pure exergy.

4.3.1 Thermal exergy

As discussed earlier, exergy is seen as an extracted work caused by the temperature difference between two states. Heat can be transferred by convection, radiation and mass flows. When heat is transferred by convection from temperature T to the environment T_0, the thermal power Q is recognized. The exergy of the thermal power Q transferred by convection under steady-state conditions is calculated as follows [64]:

$$Ex = Q\left(1 - \frac{T_0}{T}\right) \tag{1}$$

The term in parentheses defines the quality of the thermal power Q and is called "exergetic temperature factor", "quality factor", or "Carnot factor" [64, 73].

For the radiative heat transfer in which a certain body absorbs radiation from air to convert it into available work or exergy, the following definitions occur [64]:

$$Q = \varepsilon\sigma A(T^4 - T_0^4) \tag{2}$$

$$Ex = Q\left[1 - \frac{4}{3}T_0\frac{(T^3 - T_0^3)}{(T^4 - T_0^4)}\right] \tag{3}$$

In Eq. (3) the quality factor exists in parentheses as in Eq. (1) but it takes also into account the exergy destruction generated by the absorption of the radiation.

The thermal power Q can be transferred also by a mass flow ṁ in temperature T which is greater than the reference temperature T_0. When taking into account the physical component of exergy, the exergy of the mass flow ṁ can be written [63, 64]:

$$Ex = \dot{m}[(h - h_0) - T_0(s - s_0)] = \dot{m}c_p\left[(T - T_0) - T_0 ln\left(\frac{T}{T_0}\right)\right] \tag{4}$$

$$= \dot{m}c_p(T - T_0)\left[1 - \frac{T_0}{(T - T_0)}ln\left(\frac{T}{T_0}\right)\right]$$

where h and s are the specific enthalpy and entropy, respectively and the quality factor is in the last square brackets. This quality factor can be applied in the case of varying states of the system [74]. In terms of micro-cogeneration and hybrid renewable energy systems in buildings, the thermal exergy of the mass flow is highly important parameter because the mass flow is used to transfer heat from the energy conversion system to the building or thermal storage.

The quality factor f_q was defined above using the temperature difference between the system and the reference environment. This factor shows a share of useful work extracted from an energy conversion process which has reached its reference environment. Concerning this, the quality factor can be defined also as a ratio between the available exergy and energy as follows [74]:

$$f_q = \frac{Ex}{En} \tag{5}$$

4.3.2 Solar irradiation as exergy source

In terms of solar-based micro-cogeneration systems, the exergy of solar irradiation is used as fuel exergy for the system and converted into heat and electricity. According to the common opinion in the literature, solar radiation is not seen as a pure exergy source, but a conversion coefficient, or quality factor, is used to define the exergy of solar irradiation. However, several opinions occur about defining the magnitude of the conversion coefficient. Jeter (1981) [75] proposed to use the Carnot Factor as a conversion coefficient as follows:

$$\psi = 1 - \frac{T_0}{T_{sol}} \tag{6}$$

where T_{sol} is the solar temperature of 5777 K. Using the Carnot Factor approach, it leads to an assumption of the direct contact between the Earth and Sun, and the reversible thermal engine receives the all available solar irradiation as an input. However, this approach does not take into account the quality reduction taken place when solar radiation is converted into useable heat utilized by the ideal heat engine [64].

According to [76, 77], Petela gave a different approach to defining the coefficient. In his study, he compared non-atmospheric solar irradiation to irradiation from an undiluted blackbody. Next, he used the heat equal to solar irradiation absorbed by the blackbody as an input for an ideal piston cylinder with the initial state presented by (V_1, T_1). Petela stated that the maximum

work of the irradiation is defined by this piston cylinder when it settles into the reference temperature (dead-state) T_0 [77]. Finally, he presented the following coefficient to calculate the maximum available work from the solar irradiation [77]:

$$\psi = 1 - \frac{4}{3}\frac{T_0}{T_{sol}} + \frac{1}{3}\left(\frac{T_0}{T_{sol}}\right)^4 \tag{7}$$

The exergy of solar irradiation G_{irr} to a receiving surface A is presented as follows:

$$Ex_{sol} = AG_{irr}\psi \tag{8}$$

Eq. (6-7) result in the values of 0.948 and 0.931, respectively [75]. In terms of evaluating the available energy of solar irradiation, Pons [78] argued that, in addition to the radiative nature, the direct and diffuse irradiation of solar energy should be taken into account. Almost the same daily solar insolation can be observed with different direct/diffuse rations depending on the cloud coverage of the sky. This leads to a qualitative difference in the received solar energy input. Pons [78] showed that if the distinction between direct and diffuse radiation is taken into account, the quality factor on a cloudy day is between 0.68 and 0.7, and in clear sky conditions between 0.9-0.91. In this way, the varying quality of solar insolation is taken into account, which is missing from the approaches presented by Eq. (6-7). Despite the detailed and accurate approach of Pons, the conversion coefficient presented in Eq. (7) is used in this thesis to evaluate solar exergy.

4.3.3 Exergy indicators

To assess the energetic and exergetic performance of a micro-cogeneration system, certain indicators are introduced in the literature. When considering a control volume of an energy conversion system, the following energy and exergy balance equations can be written, respectively:

$$\sum E_{fuel} = \sum E_{product} + \sum E_{loss} \tag{9}$$

$$\sum Ex_{fuel} = \sum Ex_{product} + \sum Ex_d \tag{10}$$

where “fuel” indicates energy and exergy inputs to the system and “product” indicates energy and exergy outputs, such as thermal and electrical products in terms of micro-cogeneration. According to the first law of thermodynamics, a part of the fuel energy is converted into energy losses, E_{loss}, to the environment. However, according to the second law of thermodynamics, a part of fuel exergy is destroyed, Ex_d, in the energy conversion process. The exergy destruction Ex_d is called also exergy irreversibility of the process.

The energy and exergy efficiency are the main indicators to measure the effectiveness of converting the fuel energy and exergy into the products and are presented as follows, respectively:

$$\eta = \frac{\sum E_{product}}{\sum E_{fuel}} = 1 - \frac{\sum E_{loss}}{\sum E_{fuel}} \tag{10}$$

$$\zeta = \frac{\sum Ex_{product}}{\sum Ex_{fuel}} = 1 - \frac{\sum Ex_d}{\sum Ex_{fuel}} \tag{11}$$

Compared to the energy efficiency η, the exergy efficiency ζ gives a more detailed insight into the performance of the conversion process because it takes into account different values of heat and electricity. Due to this, the exergy analysis is extremely useful in terms of analyzing the cogeneration systems. It also gives a good understanding of how good is the thermodynamic rationality of the energy system [64]. While the exergy efficiency aims to improve the performance by reducing energy quality degradation, the energy efficiency intends to reduce emission [73]. For many energy systems, the energy losses to the environment are minimized effectively, and the energy efficiency can be high. However, the exergy destruction in the process can still be high and more difficult to reduce than energy losses. The exergy destruction rate is calculated as follows:

$$\Omega = \frac{\sum Ex_d}{\sum Ex_{fuel}} \tag{12}$$

The exergy destruction rate can be used to identify the system components that cause the majority of the exergy destruction. The exergy irreversibility rate, which causes the exergy consumption, can be calculated based on the exergy efficiency as follows [79]:

$$Ir = (1 - \zeta) Ex_{fuel} \tag{13}$$

The micro-cogeneration systems produce heat and electricity simultaneously from a single fuel source. Due to this, the performance of the cogeneration system is useful to be evaluated by comparing it to the separated production of heat and electricity. The energetic comparison indicator is the Primary Energy Savings (PES) which reveals the savings relative to the reference system of the separated production. The PES is presented as follows [15]:

$$PES = \left(1 - \frac{1}{\frac{\eta_{el}}{\eta_g} + \frac{\eta_{th}}{\eta_b}} \right) \times 100\% \tag{14}$$

where η_g and η_b are the electrical and thermal efficiency of power grid and thermal boiler, respectively, and η_{el} and η_{th} are electrical and thermal efficiency of the cogeneration system.

Alongside the PES indicator, Ertesvåg (2007) [79] introduced an exergetic comparison indicator called the Relative Avoided Irreversibility (RAI) which takes into account also the thermodynamic value difference between heat and electricity. The RAI is expressed by the irreversibility rate generated in the cogeneration and separated production as follows:

$$RAI = 1 - \frac{Ir_{CHP}}{Ir_g + Ir_b} \tag{15}$$

The introduced comparison indicators are used to evaluate the novel hybrid renewable energy system based on micro-cogeneration to the reference system in this thesis.

4.4 From steady state to dynamic exergy analysis

The exergy analysis can be conducted as a steady-state, quasi-steady state or dynamic analysis [74]. Compared to high-temperature energy conversion processes, such as centralized thermal power plants, the micro-cogeneration systems operate close to the outdoor conditions. Due to this, the exergy flows in the micro-cogeneration systems are highly sensitive to variations in the conditions of the reference environment as discussed in section 3.1. As consequence, the dynamic exergy analysis is required to conduct an accurate performance analysis of the micro-cogeneration systems and a steady-state analysis is recommended to be used only for the first estimations of the system exergy performance [64].

The quasi-steady analysis is a simplification of the dynamic analysis and can be a reasonable solution if conducting the fully dynamic exergy analysis is demanding. The error between the analyzing methods depends on the climate conditions and is expected to be larger for the milder conditions [74].

Blanco (2012) [74] concluded that when comparing different energy systems, such as solar micro-cogeneration systems, the quasi-steady or dynamic exergy analysis is the best choice to evaluate the performance in terms of minimizing the error in the analysis.

In this thesis, the energy systems are compared under different climate conditions, which led to a decision of using the dynamic exergy analysis for a fair comparison between the selected locations.

4.5 Exergy of different technology types

The different technology types for building energy systems can be evaluated based on their energy performance. However, the exergy performance gives better insight into energy quality degradation in the conversion process by revealing the real thermodynamic performance of the system. Energy efficiency concerns only the quantity aspects related to energy production neglecting the quality aspect. For this reason, the exergy method, which is based on the second law of thermodynamics, is used to complete the energy assessment of the system.

Depending on the energy conversion technology, different amounts of exergy is destroyed to get electricity and useful heat. Figure 1-13 shows the energy and exergy efficiencies of different technology types and caused exergy destruction during the conversion process under the same environmental conditions.

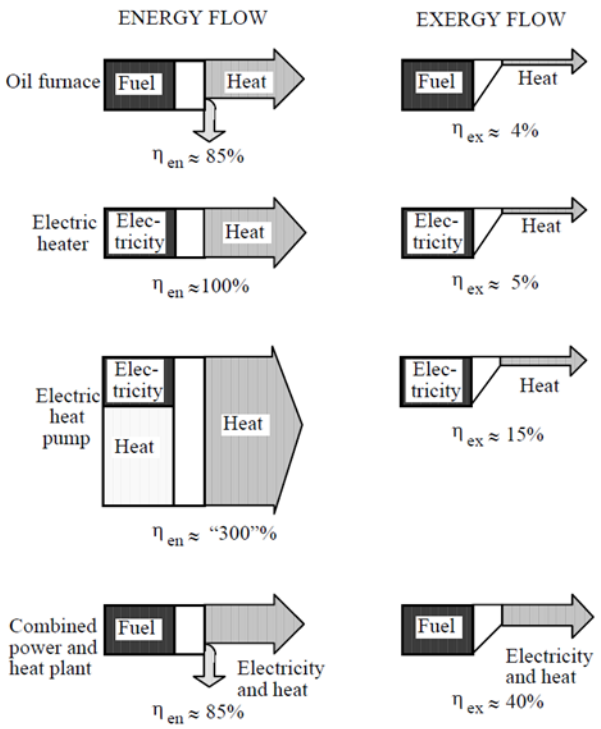

Figure 1-13: *Energy and exergy efficiency of different energy conversion devices [80]*.

Figure 1-13 reveals that the conventional oil furnace heating system has an energy efficiency of 85 %, but the exergy efficiency is only 4 % because of high exergy degradation in the conversion process. The oil furnace can burn a thousand-degree flame resulting in hot water at only 60°C temperature. The heat pump can reach an energy efficiency of 300 % because it takes "free" energy from the environment. However, from the exergy point of view, the environment is taken into account, and only the electricity used in the heat pump has quality as an input in the energy conversion process. Figure 1-13 shows that a combined heat and power system has the highest exergy efficiency of 40 %. Its energy efficiency is the same as the oil furnace, but the high quality of the electricity production increases the exergy efficiency significantly. Based on the exergy efficiency, the use of cogeneration is highly recommended [80, 81].

Electricity is seen as pure exergy, and the exergy content of heat depends on the temperature difference between heat and the environment or the reference state. Solar radiation has high exergy content and has a quality factor of around 0.93 [82]. Figure 1-14 presents the energy and exergy efficiencies and flows of solar PV, solar thermal and PVT technologies.

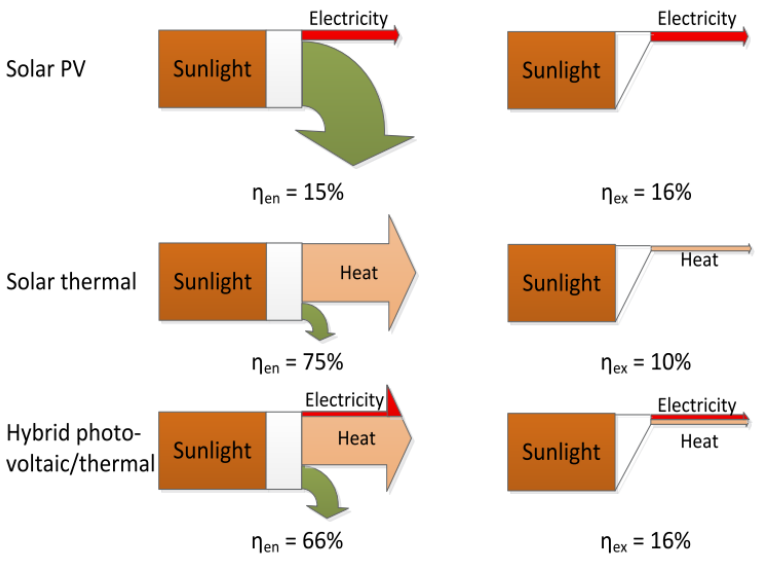

Figure 1-14: *Energy and exergy efficiency of different solar energy conversion devices [82].*

The energy and exergy efficiency of solar PV is 15 % and 16 %, respectively. The exergy efficiency is higher because electricity is seen as pure exergy, but solar radiation is not. The energy efficiency of the solar PV is mainly limited due to the physical limitations in the photoelectric conversion and heat losses to the environment are caused by the conversion process. Solar heat generation reaches the energy conversion efficiency of 75 %, but the exergy efficiency is only 10 % due to the low-temperature level of the generated heat, which is close to the ambient temperature. The solar cogeneration technology can reach an energy efficiency of over 66 %, but the exergy efficiency is the same as the solar PV because the temperature of the generated low-grade heat is even closer to the ambient temperature than in the solar thermal technology [82].

However, the electrical efficiency of the PVT should be higher than solar PV because of the cooling effect, which increases the electrical energy and exergy efficiency. This should be taken into account when comparing solar PV and PVT technologies [83]. Additionally, high-temperature PVT technologies have been developed, and those can reach the same temperature levels as solar thermal [84]. Due to this, the exergy efficiency of solar cogeneration increases significantly.

Torio and Schmidt (2011) [3] introduced, in the Annex 49 Final Report, the low exergy approach for buildings and their energy systems. They presented that the most efficient and

sustainable way to produce energy is to have a good match between the supply and demand in terms of their quality levels. The high-quality fuel should be used to satisfy high-quality demand and vice versa. Figure 1-15 presents the energy quality flows in the building environment to match the quality levels of the supply and demand sides.

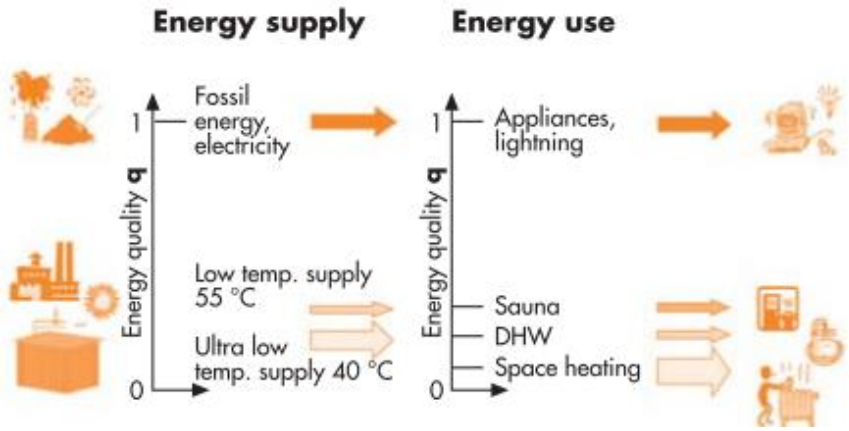

Figure 1-15: *Optimal matching of the supply and demand quality levels in the building environment [3]*.

The heat demand in buildings has typically low-quality demands, as shown in Figure 1-15, the domestic hot water is required at 55°C to 60°C, and the room temperature is maintained at around 20°C. For these purposes, the low-quality energy sources are ground source, solar and waste heat [3]. As discussed earlier, solar irradiation has a quality factor of 0.93, which is almost as high as natural gas of 1.03. However, the exergy approach does not separate non-renewable and renewable energy sources, which should be always evaluated in addition to the exergy analysis [74]. Due to this, in the case of solar energy, it has to be taken into account that it is free of charge and of CO_2 emissions which makes it highly sustainable. Generally, the high-quality fuels, such as fossil fuels or biomass, are required to produce electricity (f_q = 1) for the household appliances. In this case, biomass fuel is the most sustainable way to produce electricity due to its renewable nature and low CO_2 emissions. However, biomass is a limited renewable source which should be used in the high efficient systems [3]. The external combustion engine-based cogeneration systems are well suitable for high efficient biomass use.

In a conclusion, when evaluating the energy technology types for buildings, the usage of the exergy approach is highly recommended. This approach reveals the thermodynamic reality of efficiency and takes into account the environment where we live. Completing the energy

assessment with the exergy approach reveals that the micro-cogeneration systems can have significantly higher exergy efficiency (40%) than the boiler (4%). Additionally, Torio and Schmidt [3] stated that the cogeneration systems should be used for heating instead of the high-energy efficient boilers. Based on the given review of the exergy in the different technology types, the solar and fuel-fired cogeneration systems can have a renewable nature and the highest exergy efficiencies. Due to this, in this thesis, micro-cogeneration systems are studied, and a novel hybrid renewable energy system is proposed and analyzed to improve energy production efficiency in buildings.

4.6 Exergo-economics

Decades later, after the concept of the exergy was introduced, a need to link thermodynamics and costing aspects arose. In 1932, J. H. Keenan [85] proposed a costing method which used exergy to allocate costs properly to different energy products. He studied a cogeneration plant and concluded that exergy, instead of energy, gives the proper measure for the economic value of the produced electricity and steam. J.H. Keenan was followed by M. Benedict, who presented the use of exergy costing method in the optimal system design in 1949 [85].

Energy economics is a field which combines energy and economics to define monetary values for different energy commodities, such as fuel, electricity and heat. However, the fact is that energy is a quantity and not of value, and, due to this, there is no relation between the costs and value (Rosen [4]). However, exergy represents the value of energy and combining economics with exergy is a rational costing method (Rosen [4]).

The term “exergo-economics” was first introduced by Tsatsaronis in 1983 [85]. He wanted clearly to describe a thermo-economic analysis which integrates exergy and economics with exergy costing. Thermo-economics consider any thermodynamic analysis conducted with or next to any economic analysis of the same system, and the analyses do not have to be merged [85]. In this case, the thermodynamic analysis can take into account both the first and/or second law of thermodynamics. Thermo-economics has the following two separate quantifiers: energy/exergy and money of which the first assess the technical performance of a system and the second the profitability of the energy products [86]. However, in exergo-economics the exergy-based thermodynamic analysis is integrated with the economic analysis assigning monetary values for the exergy flows through exergy costing [85].

4.6.1 Principles of exergo-economics

The exergo-economics are based on the exergy flows, exergetic and non-exergetic costs. In terms of cogeneration systems, a certain input exergy flow is experienced by the system and generated into two different exergy products, heat and electricity. Additionally, valueless exergy destruction flow occurs due to irreversibility in the conversion process. On the component level, an input flow can be a product of a previous system component, and the product can be an output of the system or input for the next component in the system [87].

In addition to exergy flows, each component has cost flows that can be divided into exergetic and non-exergetic cost flows. The exergetic cost flow depends on the exergy flow entering and leaving the component and refers to the money used to produce a certain exergy flow. The non-exergetic cost does not depend on the magnitude of the exergy flows in the component but refers to the initial investment cost and operation and maintenance cost of the component [87]. Figure 1-16 shows the exergy, exergetic cost and non-exergetic cost flows of the k^{th} component. The exergy input cost flow is seen as a fuel "F", and the exergy product cost flows are seen as product "P". In terms of cogeneration, Product 1 is electricity, and Product 2 is heat, and the related exergy product costs are $\dot{C}_{P1}$ and $\dot{C}_{P2}$.

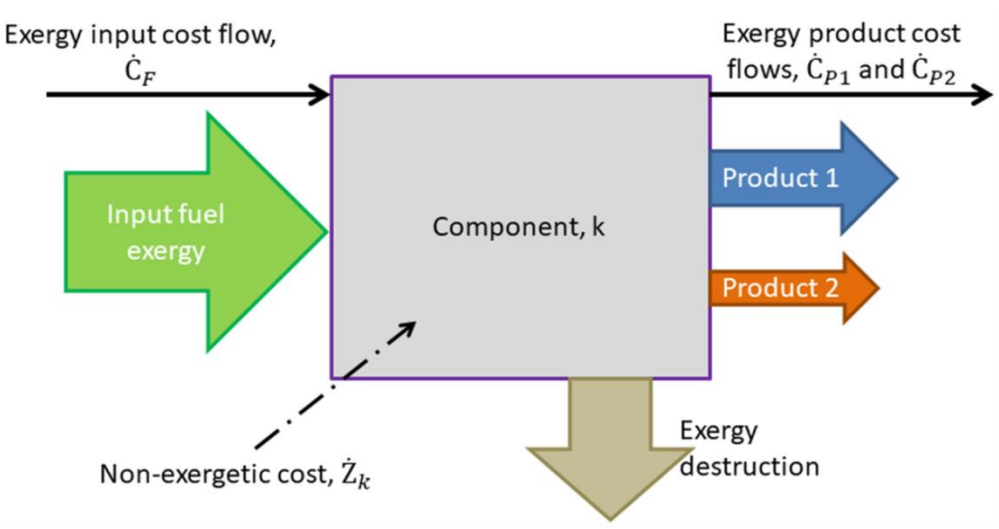

Figure 1-16: *The exergo-economic balance of k^{th} component.*

In the exergo-economic cost balance of the component, the exergy product cost flows equal to the sum of the component's non-exergetic cost and the exergy input cost. Generally, the costs in the exergo-economic analysis are presented as rates in 1/s or 1/h, and the analysis is

conducted in a steady state with the constant rates of the costs. The non-exergetic cost of the component k is as follows [87]:

$$\dot{Z}_k = \dot{Z}_I + \dot{Z}_{OM} \tag{16}$$

where $\dot{Z}_I$ is the initial investment costs and $\dot{Z}_{OM}$ is the operation and maintenance cost of the component. Generally, the exergy cost associated with a certain exergy flow is calculated as follows [85]:

$$\dot{C}_i = c_i \dot{Ex}_i \tag{17}$$

where $\dot{Ex}_i$ is the exergy rate of the considered flow and c_i is the specific cost of exergy unit in the flow i. The exergy destruction flow defines the irreversible loss of exergy within the component. The monetary value of the destruction flow can be set to zero if the analysis aims to calculate the costs of the final products [85]. In this case, the exergy destruction cost rates $\dot{C}_d$ are directly transferred to the final exergy products, such as heat and electricity in a cogeneration system [85]. Finally, the exergo-economic cost balance for the component k in Figure 1-16 is presented as follows [85]:

$$\dot{C}_{P1} + \dot{C}_{P2} = \dot{C}_F + \dot{Z}_k - \dot{C}_d \tag{18}$$

$$c_{P1}\dot{Ex}_{P1} + c_{P2}\dot{Ex}_{P2} = c_F\dot{Ex}_F + \dot{Z}_k \tag{19}$$

Equation 19 shows that the exergo-economic analysis can be used to calculate the specific monetary value for the final products of the system by taking into account costly exergy destruction of the fuel exergy and the non-exergetic costs. These specific costs of the final product can be used for pricing and recovered by selling the products. On the other hand, these costs can be compared to a reference system and recovered by generating savings by onsite use of the products.

4.6.2 Exergo-economic analysis methods

In cost accounting, the costs should represent value, and exergy shows the real value of energy which makes it rational to associate the costs with exergy instead of energy [88]. As stated by Tsatsaronis (1993) [89], the exergy and exergo-economic analysis can be considered methods for cost accounting and optimization. Exergo-economics can be used to evaluate multi-

product energy systems and their designs, and to optimize the operation and the design of the system or individual component. In the literature, the exergo-economic analysis has been proved to be a rational method for cost accounting and optimization to increase the efficiency of the energy systems. However, there is still an urgent requirement to simplify and standardize the exergo-economic method to be adopted by the engineers and decision-makers as was already in 1993 according to Tsatsaronis [89].

The above-discussed fundamentals of exergo-economics have led to different methods to combine exergy and economics. All these methods have the following common characteristics: they use exergy as a commodity of value, define the costs and prices of the exergy products of the system, evaluate economic profitability and feasibility and aim to optimize the operation and design of energy systems by minimizing costs [88]. Rosen (2008) [88] reviewed different methods to conduct the exergo-economic analysis. He distinguished the following most common methods: loss-cost ratio analysis, EXCEM analysis, exergy cost accounting, and exergy and environmental economics.

The loss-cost ratio analysis recognizes the correlations between exergy destruction and capital costs to improve system design in terms of efficiency or capital costs reduction [90]. The EXCEM analysis was developed by M.A. Rosen and I. Dincer (2003) [90] to enhance the process simulator software Aspen Plus by the exergy approach. The analysis is used to assess process and system and is based on the four quantities, as indicated in the name: exergy, cost, energy and mass [90]. The main principle of the EXCEM analysis is that mass and energy flows are conserved and exergy and cost flows decrease and increase, respectively, or remain constant [90].

The widely used and general methodology of exergy cost accounting is the SPECO analysis proposed by Lazzaretto and Tsatsaronis [91]. The name of the analysis indicates the Specific Exergy Costing, and it is used systematically to determine exergy efficiencies and costs per exergy unit in energy systems [91]. The main principle of the SPECO is to define exergy fuel(s) and product(s) of each system component. Afterwards, the fundamentals from business administration are used to form the cost balances and auxiliary costing equations to calculate the exergy-related costs for each exergy input and output flow of the system components [91].

The SPECO analysis uses the fuel-product (F-P) principle to determine the costs of the exergy flows. In contrast to exergy analysis, the exergy costing based on the F-P principle does

not distinguish between costs of high- and low-value products. According to Lazzaretto and Tsatsaronis [91], the P principle concludes that supplying any exergy unit to any product stream happens at the same average cost. This leads to the fact that the P principle is against the principle of high quality and high price, for example, electricity should have a higher price due to the higher energy level than low-grade waste heat. To solve this contradiction, Wang et al. [92] proposed a modified exergo-economic analysis method to allocate the multi-product cost consistently according to the principle of high quality and high price. They considered different energy levels of different exergy products by applying a principle stating the direct proportionality of the specific cost of any flow to its energy level. The energy level of electricity equals 1 and is defined as follows for thermal products [92]:

$$EL = \frac{\Delta Ex}{\Delta H} = 1 - T_0 \frac{\Delta S}{\Delta H} \tag{20}$$

where T_0, ΔEx, ΔS and ΔH are the reference temperature, exergy, entropy and enthalpy changes, respectively.

The environmental aspects are added to the analysis in exergy and environmental economics. Sciubba [93] proposed a method called Extended Exergy Accounting (EEA) which integrates exergy accounting and thermos-economics with environmental factors. The main benefit of the EEA is that it enables a direct quantitative comparison of non-exergetic parameters, such as labor and environmental impact. This is conducted by calculating the exergetic equivalents for non-exergetic parameters.

4.7 Exergy and exergo-economics applied to micro-cogeneration systems

Micro-cogeneration, or combined heat and power (CHP), systems have been seen as a key technology to reduce primary energy use and CO_2 emissions in the building sector. These systems have been modelled and analyzed by several authors in the literature. The International Energy Agency published Annex 42 [94], in which the fuel-fired micro-cogeneration systems for residential buildings were studied in terms of model development and experimental testing. Bouvenot et al. [95] developed a dynamic model of a biomass-fired steam engine-based micro-cogeneration. The model was validated by experimental results and built into the TRNSYS environment. Bouvenot et al. [96] investigated experimentally also a gas-fired Stirling engine

micro-cogeneration system, and a simulation model was developed. Uchman et al. [97] studied gas-fired free-piston Stirling engine coupled with thermal storage and built up a data-driven model. González-Pino et al. [98] investigated a gas-fired Stirling micro-cogeneration as well. They built up an experimental set-up and modelled the detailed behavior of the unit in terms of start-up and cool-down periods and partial load performance. Martinez et al. [99] investigated the performance of a solar micro-cogeneration system integrated into a residential building. The parabolic trough collectors were used to produce steam for a steam engine prime mover. The PVT collectors can be seen as micro-cogeneration systems. Brottier and Bennacer (2020) [100] investigated experimentally the thermal performance of 28 PVT installations in the residential building environment. The modelling and energy performance of the PVT collectors in the residential building sector has been studied widely in the literature [30, 101–108].

The above-mentioned studies considered only the performance analysis based on the first law of thermodynamics. However, the second law of thermodynamics is required to complete the energy assessment of the micro-cogeneration systems. In terms of fuel-fired micro-cogeneration, the exergy analysis has been conducted in steady-state conditions without building or environmental-related dynamic behavior. Gonçalves et al. [109] conducted an energy and exergy analysis on the steady-state experimental data of the ICE-based micro-cogeneration system and compared the performance to a reference system. Taie et al. [110] studied the energy and exergy performance of the ICE-based cogeneration system on the device and component level to identify the main areas of inefficiency. They conducted the analysis on the steady-state experimental data. Their results revealed that the largest exergy destruction occurred in heat transfer. However, these both steady-state exergy analyses used a different definition of the reference environment. Gonçalves et al. [109] selected to use as a reference temperature the cooling water temperature of 10°C, and Taie et al. [110] used the environmental temperature of 20°C. Due to the dependence on the constant fuel feed, the steady-state analysis of the fuel-fired micro-cogeneration units using the constant reference temperature in the exergy analysis is reasonable. However, the exergy performance of the solar-based micro-cogeneration systems is highly dependent on fluctuating environmental conditions, such as solar irradiation and ambient temperature. Due to this, a more dynamic analysis is reasonable to analyze the exergy performance of the PVT collectors over a certain time horizon. Several authors have conducted the exergy analysis of the PVT collectors [67, 83, 111, 112]. However, some of the authors have

not stated clearly the conditions used in the exergy analysis. Evola and Marletta [72] conducted a dynamic exergy analysis of the PVT collector and operation optimization. The reference temperature was changed dynamically, and the monthly minimum temperature was used as a reference temperature in their analysis. Finally, they conducted exergo-economic costing method for the PVT thermal and electrical output. Abdul-Ganiyu et al. [113] used exergy analysis to analyze experimentally the technical and economic performance of the PVT collector in comparison to the PV panel. Finally, the PVT resulted in a lower levelized cost of exergy than the PV system, especially, if the battery storage was connected to the system. In their exergy analysis, the yearly average daily ambient temperature was used as a reference temperature. Based on the literature review, the exergy analysis is widely applied to different micro-cogeneration systems. However, there is a lack of a common approach to selecting the reference temperature, which has a significant impact on the results of the exergy analysis, especially in low-temperature applications.

The micro-cogeneration systems rarely operate as a single unit but are integrated with the whole building system including highly dynamic energy demand. The cogeneration systems are typically integrated with thermal and/or electrical storage and can be hybridized with other energy production systems. Mahian et al. [114] presented a review on exergy analysis in the cogeneration systems with different prime movers. Their results revealed that more exergy-based investigations are recommended on small-scale systems in the residential sector. Additionally, more research should be focused on hybrid cogeneration systems with renewable energy sources. The exergy analysis of a single micro-cogeneration unit can be extended to consider an exergo-economic analysis of a hybrid renewable energy system based on cogeneration. Wang et al. conducted the exergy and exergo-economic analysis of the hybrid energy system based on the ICE micro-cogeneration with solar heat collectors in [115] and concentrated PVT collectors in [116]. The analysis of the system was done in steady-state conditions for cooling and heating periods. However, a constant reference temperature of 25°C was used throughout the analysis. In their exergo-economic analysis, the energy levels of the different energy products were taken into account to handle the fact that the higher quality energy product should have a higher specific cost of exergy. Chen et al. (2021) [117] presented the exergy and exergo-economic analysis of the solar-driven combined cooling, heating and power system based on the organic Rankine cycle and absorption heat pump for residential energy production. In their analysis, the

energy levels of the products were taken into account, and the steady-state analysis was separated into three seasons: heating, cooling and transition. Additionally, the analysis was conducted under conditions of four different climatic regions in China. The reference temperature of the analysis was selected to be the average ambient temperature of each season and specific for each location.

The above-mentioned exergo-economic studies considered only the steady-state operation conditions. This approach has been more used in the large power plant applications where the exergy flows stay constant over a certain period. However, when including solar technologies and highly dynamic residential energy demand profiles in the analyzed system, dynamic system analysis is more recommended than a steady state. Calise et al. (2015) [118] presented dynamic exergy and exergo-economic analysis of a renewable polygeneration system which provided heating, cooling and electricity for small isolated communities. They were able to present exergy flows and efficiencies of each system component on the hourly level. Additionally, they presented the exergo-economic costs of the energy products on weekly and seasonal levels. However, in their analysis, the energy levels of different energy products were not taken into account and the reference temperature of 25°C was selected to be constant over a year. As discussed in Section 3.1, the reference temperature has a higher influence on the exergy generation if the system is operating close to the ambient conditions. This would lead to a recommendation of using changing reference temperature.

Based on the given literature review on the exergy and exergo-economics, more accurate and dynamic analysis of hybrid renewable energy systems is required including different weather conditions, seasonally adaptable reference temperature and the consideration of energy levels of the cogenerated energy products. In this thesis, different dynamic models from a single micro-cogeneration unit to a hybrid renewable energy system are developed to conduct advanced and detailed energy, exergy and exergo-economic analyses and optimization.

5. Conclusion

In this Chapter, the state-of-art of exergy method in the micro-cogeneration systems was presented. First, the definition and benefits of micro-cogeneration were discussed followed by the technologies for solar and fuel-fired micro-cogeneration systems. The literature review on the hybridization of solar technologies with different fuel-fired micro-cogeneration systems was

conducted, and the main studies were presented in Section 3. The review showed that hybridization has been studied on the micro-scale but in many cases fossil fuels have been used to run the micro-CHP unit. Additionally, the utilized solar technology was often either photovoltaic or solar heat but rarely photovoltaic-thermal collector, which is the most efficient way to utilize solar energy in buildings. Due to this, in this thesis, the PVT collector and biomass-fueled Stirling engine micro-CHP unit are further studied and coupled to form a hybrid renewable energy system.

The exergy approach was presented in this Chapter including the exergy and exergo-economic analysis. This approach has been widely used in the industrial sector to increase the efficiency of power plants and processes. However, due to the high primary energy consumption and CO_2 emissions of the building sector, applying the exergy approach to the building energy systems is becoming more interesting and necessary.

The main studies applying the energy, exergy and exergo-economic analyses on the solar and fuel-fired micro-cogeneration systems were selected for comparison in Table 1-6. In the first row, the subjects included in this thesis are presented. There are several studies that include the PVT collectors or fuel-fired micro-CHP units analyzed by considering only the first law of thermodynamics. If the second law of thermodynamics was taken into account, only a few studies used varying reference temperatures, such as monthly values. It was also rare to compare different climate conditions in the context of both energy and exergy analysis of micro-cogeneration. The analysis of a single micro-cogeneration system was more common than the hybrid renewable energy system (HRES). Most of the studies used dynamic analysis instead of steady-state analysis. Based on Table 1-6, the main contributions of this thesis to the literature are to apply dynamic exergy and exergo-economic analysis with varying reference temperatures to the HRES including the hybridization of solar and biomass-fueled micro-cogeneration systems. Additionally, the different European climate conditions are compared, and multi-objective design optimization is performed. The Matlab/Simulink is used as a simulation tool which was rarely used in the literature.

Table 1-6: Overview of the main studies considering energy, exergy and exergo-economic analyses applied to micro-cogeneration systems in the building sector.

Author	PVT collectors	Renewable micro-CHP	Non-renewable micro-CHP	HRES	Energy analysis	Exergy analysis	Exergo-economics	Varying reference temperature	Different climate conditions	Dynamic analysis	Multi-objective optimization	Matlab/ Simulink
Thesis	x	x		x	x	x	x	x	x	x	x	x
Bouvenot et al. [95]		x			x					x		
Bouvenot et al. [96]			x			x				x		
Uchman et al. [97]			x		x					x		
Martinez et al. [99]		x			x							
Brottier et al. [100]	x				x							
Gonçalves et al. [109]			x		x	x						
Taie et al. [110]			x		x	x						
Da Silva et al. [103]	x				x					x		x
Tamayo Vera et al. [30]	x				x					x	x	
Barbu et al. [101]	x			x	x				x	x		
Chow et al. [67]	x				x	x				x		
Evola et al. [72]	x				x	x	x	x		x		
Abdul-Ganiyu et al. [113]	x			x	x	x	x			x		
Wang et al. [116]	x		x	x	x	x	x					
Chen et al. [117]		x		x	x	x	x	x	x			
Calise et al. [118]	x			x	x	x	x			x		

CHAPTER 2. Energy analysis and exergy optimization of photovoltaic thermal collector under different climate condition

Sonja Kallio and Monica Siroux

INSA Strasbourg ICUBE, University of Strasbourg

This article is published in *Energies*

doi.org/10.3390/en13195106

Abstract

A photovoltaic-thermal (PVT) collector is a solar-based micro-cogeneration system which generates simultaneously heat and power for buildings. The novelty of this paper is to conduct energy and exergy analysis on PVT collector performance under two different European climate conditions. The performance of the PVT collector is compared to a PV panel. Finally, the PVT design is optimized in terms of thermal and electrical exergy efficiencies. The optimized PVT designs are compared to the PV panel performance as well. The main focus is to find out if the PVT is still competitive with the PV panel electrical output, after maximizing its thermal exergy efficiency. The PVT collector is modelled into Matlab/Simulink to evaluate its performance under varying weather conditions. The PV panel is modelled with the CARNOT toolbox library. The optimization is conducted using Matlab gamultiobj-function based on Non-Dominated Sorting Genetic Algorithm-II (NSGA-II). The results indicated 7.7% higher annual energy production in Strasbourg. However, the exergy analysis revealed a better quality of thermal energy in Tampere with 72.9% higher thermal exergy production. The electrical output of the PVT is higher than from the PV during the summer months. The thermal exergy- driven PVT design is still competitive compared to the PV panel electrical output.

1. Introduction

Micro combined heat and power (μ-CHP) systems are operating in the building sector in order to produce heat and electricity simultaneously. The European Parliament has defined the micro-cogeneration to be the units up to an electrical output of 50 kW [99]. Solar energy can be counted to be an inexhaustible source of energy, and it is mostly deployed in the building sector in terms of photovoltaic (PV) panels and thermal collectors [30]. This separated production of electricity and heat can be combined by the technology called photovoltaic-thermal (PVT). The

PVT collector is a renewable solar-based micro-cogeneration unit which produces electricity by the PV module and useful heat by cooling the PV module with a coolant circulation. This leads to increased overall system efficiency but also to increased electrical efficiency of the PV cell due to the decreased operating temperature of the PV module [30].

Different kind of PVT configurations has been developed and modelled in the literature. Zhang et al. [119] presented different practical applications of PVT technologies. They presented that the air-based PVT is the most commonly used and installed PVT technology, achieving the maximum thermal efficiency of 39% and electrical efficiency of 8%. The second very popular technology is the water-based PVT of which popularity is increasing due to its ability to increase the electrical efficiency and better thermal energy utilization. Next to these two popular technologies, they brought a refrigerant-based PVT which has the potential to replace air- and water-based technologies because it can significantly improve the solar utilization rate compared to air- and water-based technologies. The fourth interesting technology is a heat-pipe-based PVT which is seen as a next-generation technology in terms of heat removing from the PV panel and effectively to use it. For the future technology, they also marked the integration of the phase change material to the PVT in order to increase energy efficiency. To increase the efficiency of the PVT collector using nanofluids as heat transfer fluid have been investigated in [29, 120].

The above-described PVT technologies have a challenge in that the electrical efficiency decreases as the operating temperature increases. On the other hand, higher operating temperature increases thermal efficiency. The novel PVT technologies are investigated and developed in [121, 122] to solve this problem by thermally decouple the electrical and thermal units of the collector. These PVT systems use spectral liquid beam splitter which divides the solar spectrum into different wavelength bands in front of the PV panel. These bands are then used separately by electrical and thermal units, and the liquid operates as cooling fluid [121].

The performance of the PVT system can be analyzed in terms of energy and exergy analysis. The latter is based on the Second Law of thermodynamics, and it takes into account also the quality of various kinds of energies. The exergy method helps to understand how useful the produced heat is in terms of mechanical work at the temperature in which the heat is available [123].

In the literature, several papers about the exergy analysis on CHP-systems and PVT collectors have been published. For example, Feidt et al. [124, 125] used the exergy analysis to

analyze the performance of different CHP-systems and proposed it to be essential for the optimization of the systems. Evola and Marletta [72] studied the energy and exergy performance of the glazed PVT collector. They conducted the analyses based on the simulations for a water-based PVT collector. They optimized the coolant inlet temperature to maximize the overall exergy efficiency of the collector. They found that low inlet temperature leads to very high overall energy efficiency but in terms of exergy analysis, this is not recommended. The optimized inlet temperature and overall exergy efficiency varied between 30-42 °C and 14-15%, respectively, depending on the mass flow rate and the weather conditions.

The operation of the PVT collector is highly dynamic and influenced on the time-varying weather conditions. Due to this steady-state analysis of the PVT performance is not sufficient, but a dynamic model has to be implemented to evaluate the performance of the collector. In the literature, a range of theoretical PVT models has been introduced and validated based on the experimental data and literature [107, 126, 127]. Da Silva and Fernandes [103] conducted the dynamic simulations of the PVT collector combined with thermal storage. They implemented a dynamic model of the PVT system into the modular environment of Simulink in Matlab. The model was validated based on the literature and showed good agreement.

The PVT collector performance is highly depending on the weather. Because of that, it is important to study the PVT performance in different locations with different climate conditions. In terms of energy analysis, the energy yield of the PVT collector is strongly depending on the solar irradiation of the considered location. However, in terms of exergy analysis, also the ambient temperature around the PVT collector has a big role. Barbu et al. [101] studied the energy performance of the residential PVT system under two similar climate conditions Bucharest, Romania and Strasbourg, France. Despite the similar climate conditions, their results indicated 10-12% better energy performance in Bucharest compared to Strasbourg. The study showed that the performance of the PVT is highly dependent on the local weather conditions and estimations of the performance are difficult to make before studying it locally. The PVT performance in different locations was studied in [106, 128] as well.

Due to cooling underneath the PV module, the higher electrical output could be expected from the PVT collector than the PV panel. However, the PVT collector is not always fully packed with the PV, which may lead to lower electrical output despite higher cell efficiency. Abdul-Ganiyu et al. [129] made an experimental comparison of the water-based PVT collector

and PV panel performance in Ghana. Their results indicated that the annual electrical output from the PVT was 149.92 kWh/m^2 and from the PV 194.79 kWh/m^2. The PV cell operating temperatures were lower in the PVT over a year. In their study, the PV panel had a higher rated power than the PVT collector. However, a numerical comparison between the PVT and PV is required to find out the impact of different PVT variables, such as the mass flow rate, packing factor and inlet temperature, on the comparison.

The multi-objective optimization techniques are used to solve optimization problems where the objectives are conflicting between each other. In terms of the PVT collector performance, the electrical efficiency suffers if the thermal efficiency is maximized and the other way round. Due to this, the PVT collector optimization should be done with the multi-objective optimization techniques that take into account the conflicting nature of the PVT operation. Tamayo Vera et al. [30, 130] studied the multi-objective optimization of the water-based PVT collector performance parameters with the Non-Dominated Sorting Genetic Algorithm-II (NSGA-II). They derived a Pareto optimal set, which illustrates the trade-off between solutions. The decision variables for multi-objective optimization problems of the PVT collector were the mass flow rate, packing factor and air gap thickness. They found that the solutions that simultaneously maximize both electrical and thermal efficiencies had a mass flow rate of 0.008 kg/s, packing factor of 0.6 and air gap of 8 cm. The air-based PVT collector was optimized using NSGA-II in [131]. Conti et al. [132] used the multi-objective optimization to minimize the total costs and non-renewable primary energy consumption of a hybrid energy system, including PVT collectors in a nearly zero-energy building. The exergy efficiency of the PVT collector was optimized using the genetic algorithm in [133]. However, to the best of author's knowledge, there is no work focusing on the multi-objective optimization of the PVT collector's thermal and electrical exergy efficiencies to maximize the quality of the produced energy. In the literature, there is also a lack of work to compare the optimized PVT designs with the PV panel performance.

In this given framework, a research contribution is provided by this paper by analyzing the water-based PVT collector's energy and exergy performance under two different climate conditions. Compared to the previous work in the literature [101, 106, 128], this paper takes into account the northern location of Europe to be an opportunity for the PVT market by making a comparative analysis between the northern location of Tampere, Finland and southern location of

Strasbourg, France. In France, the PVT technology is more commonly in use than in Finland. Additionally, the PVT performance is compared to the PV panel in terms of the PV cell operating temperature and electrical output in both locations. The impact of different variables, such as the PVT packing factor, mass flow rate and inlet temperature, on the comparison, is investigated. The further contribution of this paper is to study the multi-objective optimization method of the PVT collector design with the genetic algorithm to optimize electrical and thermal exergy efficiencies and to understand how different PVT variables behave in the optimized design configurations. The Pareto optimal set of design solutions is derived The contribution is extended to compare selected optimized PVT design configurations with the PV panel performance and to find out if the PVT is still competitive with the PV panel electrical output, after maximizing its thermal exergy efficiency.

First, the PVT collector and considered climate conditions are described. Next, the mathematical model of the PVT collector is presented. The covering equations of the model are implemented in Matlab/Simulink, which is a programming environment for numerical computation and data analysis. The PV panel is modelled to Simulink as a PV Generator- block using the CARNOT Toolbox Version 7.0 developed by Solar-Institute Jülich of the FH Aachen, Jülich, Germany [134]. The energy and exergy analyses are conducted for the described PVT collector under two different climate conditions, and results are discussed. The PVT collector and PV panel performance are compared. The multi-objective optimization of the PVT collector is conducted, and the Pareto optimal set is derived. Finally, the performance of the selected optimized PVT design configurations are compared to the PV panel.

2. Methodology

2.1 Description of Photovoltaic-Thermal (PVT) collector

A water-cooled PVT collector with a sheet and tube heat exchanger is simulated and analyzed in this study. Figure 2-1 shows the geometry and cross-section of the PVT collector [101]. The collector consists of glazing, air gap, PV panel, absorber plate with tubes, working fluid and insulation. The cover glass limits the heat losses to the environment and the air gap of 2 cm between the glass and PV panel enhances the heat transfer. The PV layer consists of PV glass, EVA (ethylene vinyl acetate) films, silicon PV cells, protective Tedlar and bonding adhesive. The thermal absorber is a coper plate with the boned parallel water tubes [107]. The

last layer is few centimeters thick insulation which prevents the heat losses to the environment. The water-based PVT collector is investigated because they achieve higher overall efficiency than air-based collectors due to the higher heat capacity of water [32]. High efficient PV cells are still relatively expensive, and in this study, the PVT collector has a polycrystalline silicon PV cell with a reference electrical efficiency (η_{STC}) of 17.3% at the reference operating temperature (T_{ref}) of 25 °C. The packing factor (r_c) and the temperature coefficient (β_T) are 0.804 and 0.405%/K, respectively. The diameter of the tubes is 9 mm, and the number is 10. The tilt angle of the PVT collector is 30°, which is only used to estimate transmittance of the cover glass in this study. Regarding to [127] the influence of the tilt angle on the transmittance is irrelevant. The inlet temperature of the water-glycol coolant fluid is 20 °C. Table 2-1 summarizes the main geometrical, thermo-physical, optical properties and the parameters of the PVT collector used in the simulation and analyses.

Table 2-1: The geometrical, thermo-physical and optical properties of the PVT collector.

Property	**Glass**	**Air gap**	**PV**	**Thermal absorber**	**Fluid**	**Insulation**	**Unit**
Emissivity (ε)	0.88	-	0.96	-	-	-	-
Absorbance (α)	0.1	-	0.9	-	-	-	-
Transmittance (τ)	0.93	-	-	-	-	-	-
Thickness (H)	0.004	0.02	0.0002	0.0002	-	0.015	m
Area (A)	2	2	1.6	2	-	2	m^2
Mass flow	-	-	-	-	0.044	-	kg/s
Density (ρ)	2200	-	2330	2702	1050	20	kg/m^3
Specific heat (c)	670	-	900	800	3605	670	J/(kgK)
Thermal conductivity (k)	1.1	-	140	310	0.615	0.034	W/(mK)

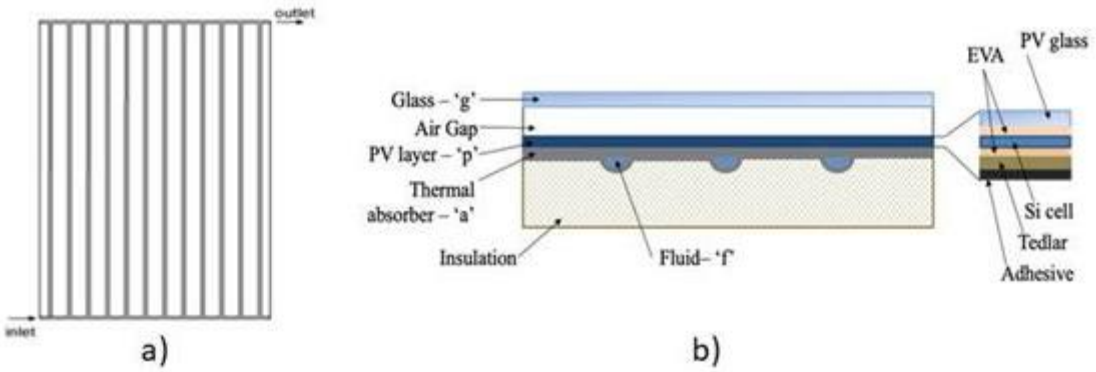

Figure 2-1: *The PVT collector: (a) Direct flow collector geometry; (b) Cross section of the PVT collector [101].*

The following assumptions are taken into account in the mathematical modelling:

- The temperature distribution is uniform in the layers.
- It is assumed that there are no heat losses through the edges.
- The optical and thermal properties of the materials and fluids are constant.
- No surrounding shading or dust is taken into account.
- The thermal resistance between the layers is negligible.
- The ambient temperature is equal around the PVT collector.

2.2 Meteorological Data

The behavior of the PVT collector depends strongly on the meteorological conditions. The main influence weather parameters are the solar irradiation, ambient temperature and wind speed. The solar irradiation influences strongly on the electrical output of the PVT and it heats up the material layers of the collector through radiative heat transfer. The ambient temperature and wind speed influence on the temperatures of the PVT layers through the convective and conductive heat transfer. The wind speed influences strongly the heat losses through the surface and back of the PVT collector. In this paper, two different climate conditions are compared, and the behavior of the PVT collector and PV panel under these conditions is investigated.

The selected meteorological conditions are at Tampere, Finland, and Strasbourg, France. Tampere is the second largest city of Finland and the largest inland city in the Nordic countries. It is located 180 km to the north from the capital city Helsinki. According to Köppen climate classification Tampere has a typical subarctic climate border, which means that the ambient

temperature is above 10 °C only 3 months in a year. Tampere also borders on an isolated warm-summer humid continental climate, which means that the winters are cold and summers are cool to warm.

Strasbourg is located in the Central Europe in Northern France at the border with Germany. It is the largest city of the Grand Est region of France. According to Köppen climate classification Strasbourg has oceanic and semi-continental climate. This means warm and relatively sunny summers and cool winters.

The hourly yearly meteorological data of Tampere is obtained from the experimental measuring center of Tampere University. The similar data for Strasbourg is obtained from the Meteonorm Database.

The following figures present samples of the hourly climate data of Tampere and Strasbourg. Figure 2-2 shows the solar irradiation, ambient temperature and wind speed, respectively, during a summer week in Tampere and Strasbourg.

In Figure 2-2a can be seen that during the summer period the solar irradiation in Tampere can reach the same maximum values around 800 W/m2 than in Strasbourg.

Figure 2-2b presents the ambient temperature, and it can be seen again that in Tampere temperatures as high as in Strasbourg can be reached.

Figure 2-2c shows that the wind speed is more stable in Tampere and stays the most of the time between 2.5 m/s to 5 m/s. In Strasbourg the wind speed is really low the most of the week with values below 2.5 m/s but also really high values, over 5 m/s, during some periods of the week.

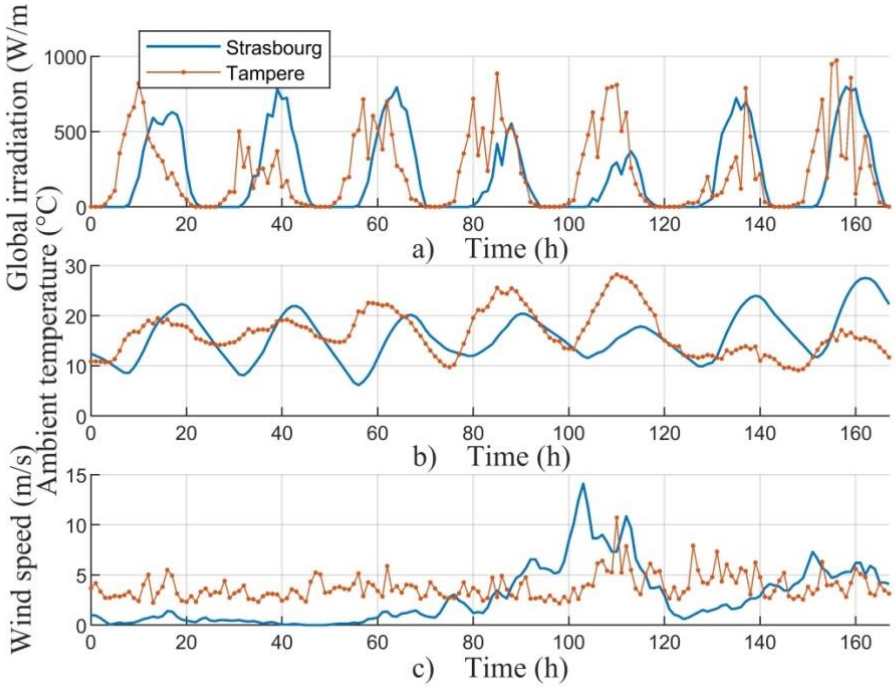

Figure 2-2: *Climate conditions during the summer week in Tampere and Strasbourg: a) solar irradiation; b) ambient temperature; c) wind speed.*

Figure 2-3 shows the solar irradiation, ambient temperature and wind speed, respectively, during a winter week in Tampere and Strasbourg.

Figure 2-3a shows the solar radiation at the end of December, which is the darkest time of the year. It can be seen that the solar irradiation in Tampere is almost non-existent and the PVT collector can produce neither electricity nor heat.

Figure 2-3b presents the ambient temperature, which reaches negative values in both Tampere and Strasbourg.

Figure 2-3c presents the wind speed, which is slightly slower in Tampere during the winter period than the summer period. On the other hand, in Strasbourg the wind speed is higher in winter than in summer period. The wind speed influences on the convective heat losses of the PVT collector. The slow wind speed during the summer period can be seen as a benefit in terms of the heat production due to reduced convective heat losses.

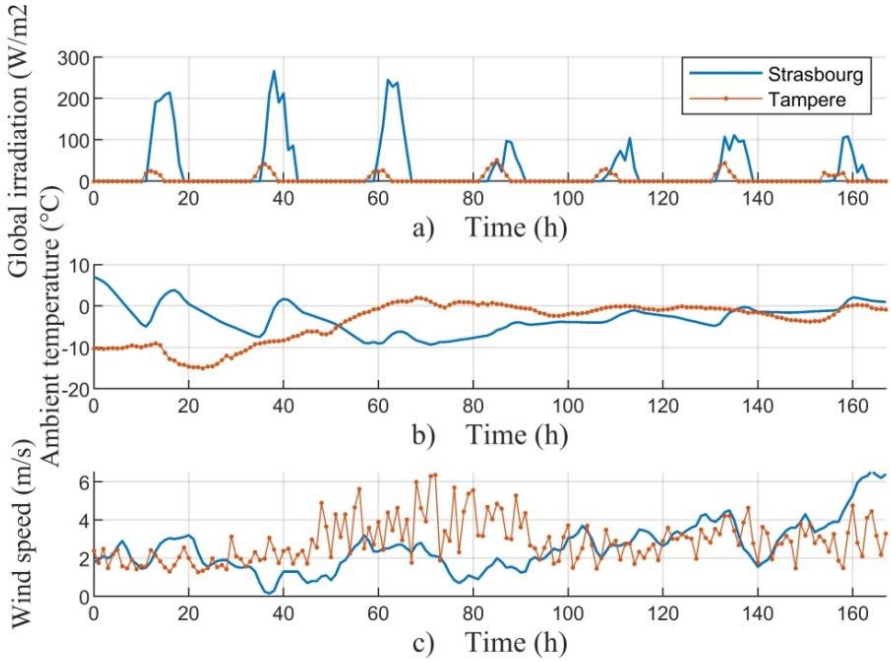

Figure 2-3: *Climate conditions during the winter week in Tampere and Strasbourg: a) solar irradiation; b) ambient temperature; c) wind speed.*

Table 2-2: The monthly average outdoor temperatures used in the exergy analysis.

Month	Tampere, average temperature[°C]	Strasbourg, average temperature[°C]
January	-6.4	2.3
February	-6.9	3.3
March	-2.8	7.0
April	3.3	11.5
May	9.7	15.7
June	14.1	19.4
July	16.9	20.6
August	15	19.8
September	9.8	15.8
October	4.6	11.3
November	-0.6	6.5
December	-4.5	3.3

2.3 Mathematical Model

A dynamic numerical model of the glazed flat-plate water-cooled PVT collector is presented in this paper. The model is used to assess the energy and exergy performance of the PVT collector under different climate conditions.

The PVT collector is modelled a layer by layer in order to see the temperatures of each layer and the coolant fluid outlet temperature. In this paper the study of the energy and exergy performance is conducted by looking at the control volume in Figure 2-4. The considered control volume composed of a glass layer, PV panel, absorber plate, a grid of tubes for the coolant fluid flow and insulation.

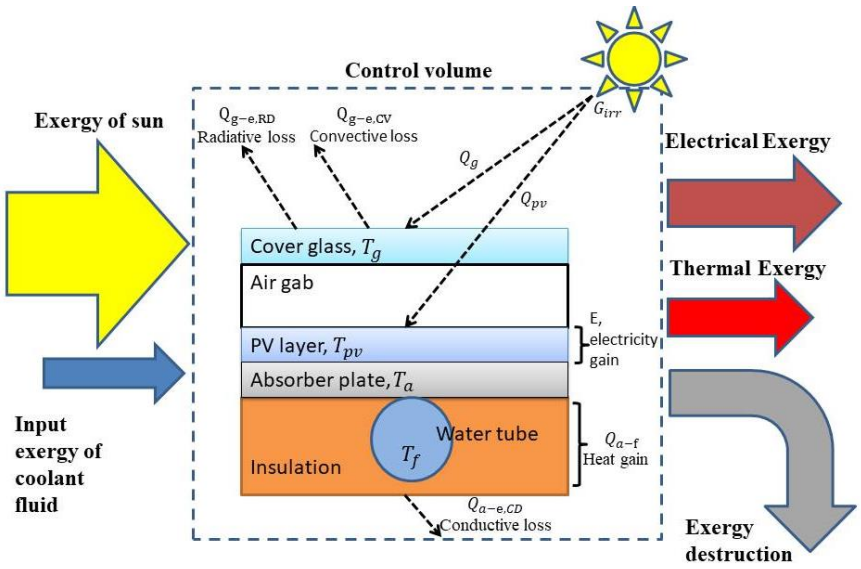

Figure 2-4: *The control volume and exergy flows of the PVT collector model.*

2.3.1 Numerical Model of PVT for Energy Analysis

The energy analysis of the PVT collector is based on the First law of thermodynamics and energy performance of the system can be evaluated based on the analysis. The analysis takes into account the thermal and electrical efficiency of the PVT collector and thermal and electrical energy produced by the collector during a certain time period.

The energy balance equations are developed and solved for each layer and the coolant fluid, and for dynamic energy analysis [107].

The governing equations are based on the variation of internal energy in a physical body.

$$mc\frac{dT}{dt} = \frac{dU}{dt} \tag{1}$$

The energy balance for the glass layer "g" considers on the right hand side the heat losses to the environment consisting of the forced convective heat transfer due to wind ($Q_{g\text{-}e,CV}$) and radiative losses ($Q_{g\text{-}e,RD}$). On the other hand, there is the convective and radiative heat transfer from the glass to the PV layer in the air gap ($Q_{g\text{-}pv,CV}$ and $Q_{g\text{-}pv,RD}$) and heat absorbed by the glass Q_g [107].

$$\begin{aligned} m_g c_g \frac{dT_g}{dt} &= Q_{g-e,CV} + Q_{g-e,RD} + Q_{g-pv,CV} + Q_{g-pv,RD} + Q_g \\ &= h_{g-e,CV}A\left(T_e - T_g\right) + h_{g-e,RD}A\left(T_{sky} - T_g\right) \\ &+ h_{g-pv,CV}A\left(T_{pv} - T_g\right) + h_{g-pv,RD}A\left(T_{pv} - T_g\right) \\ &+ A\alpha_g G_{irr} \end{aligned} \tag{2}$$

The heat transfer coefficient of forced convection ($h_{g\text{-}e,CV}$) is expressed through the correlation proposed by [135] and is widely used for numerical PVT models. The correlation covers the wind speed from 0 to 10 m/s.

$$h_{g-e,CV} = \begin{cases} 5.7 + 3.8v_w & \text{for } v_w < 5\frac{m}{s} \\ 6.47 + {v_w}^{0.78} & \text{for } v_w > 5\frac{m}{s} \end{cases} \tag{3}$$

The heat transfer coefficient of the radiative heat loss ($h_{g\text{-}e,RD}$) is calculated based on the emissivity of glass (ε_g), the Stefan-Boltzmann constant (σ= 5.67×10−8 W/m^2/K^4) and the equivalent radiative temperature of the sky (T_{sky}). The temperature of the sky can be calculated as a linear function of the ambient temperature and the sky cloud coverage in octaves (N) [32]. If clear sky conditions are assumed or there is no data available on the cloud coverage, Equation (5) can be further simplified to Equation (6), with less than 1% effect on the thermal and electrical output of the system [136, 137].

$$h_{g-e,RD} = \varepsilon_g \sigma\left({T_g}^2 + {T_{sky}}^2\right)\left(T_g + T_{sky}\right) \tag{4}$$

$$T_{sky} = 0.0552{T_e}^{1.5} + 2.652N \tag{5}$$

$$T_{sky} = 0.0552{T_e}^{1.5} \tag{6}$$

The thermal coefficient of the gap ($h_{g\text{-}pv,CV}$) takes into account the convective heat transfer in the air gap.

$$h_{g-pv,CV} = \frac{Nu_{air}k_{air}}{H_{gap}} \tag{7}$$

The Nusselt number correlation for inclined plates, tilt angles from 0 to 60, is given by [138]. H_{gap} and k_{air} are the thickness of the air gap between glazing and PV layer and thermal conductivity of air, respectively. The radiative coefficient between the glass and the PV panel ($h_{g\text{-}pv,RD}$) is expressed below:

$$h_{g-pv,RD} = \frac{1}{\frac{1}{\varepsilon_{pv}} + \frac{1}{\varepsilon_g} - 1}\sigma\left({T_g}^2 + {T_{pv}}^2\right)\left(T_g + T_{pv}\right) \tag{8}$$

The thermal balance of the PV layer "pv" considers the convective and radiative heat transfer to the PV layer ($Q_{pv-g,CV}$ and $Q_{pv-g,RD}$) from the glass layer, the conductive heat transfer to the absorber layer ($Q_{pv-a,CD}$) through the adhesive layer and the conductive heat transfer through the adhesive layer to the tube at the tube bonding position, the heat absorbed by the PV layer (Q_{pv}) and electricity production (E).

$$\begin{aligned} m_{pv}c_{pv}\frac{dT_{pv}}{dt} &= Q_{pv-g,CV} + Q_{pv-g,RD} + Q_{pv-a,CD} + Q_{pv-t,CD} + Q_{pv} - E = \\ &= h_{g-pv,CV}A\left(T_g - T_{pv}\right) + h_{pv-g,RD}A\left(T_g - T_{pv}\right) + h_{pv-a,CD}A_{pv-a}\left(T_a - T_{pv}\right) + \\ &\quad h_{pv-t,CD}A_{pv-t}\left(T_t - T_{pv}\right) + G_{irr}(\alpha\tau)_{pv} - G_{irr}r_c\eta_{EL(T)} \end{aligned} \tag{9}$$

The heat transfer coefficient in the air gap and the radiation coefficient are calculated in Equations (7-8). $(\alpha\tau)_{pv}$ is the effective absorbance. In Equation (9):

$$h_{pv-a,CD} = \frac{k_{adh}}{H_{adh}} \tag{10}$$

$$A_{pv-a} = A\left(1 - \frac{D_o}{W}\right) \tag{11}$$

$$h_{pv-t,CD}A_{pv-t} = \frac{H_{pv}L}{\frac{x_{pv}}{2k_{pv}} + \frac{H_{adh}}{k_{adh}}\frac{H_{pv}}{D_o}} \tag{12}$$

$$x_{pv} = \frac{W}{4} \tag{13}$$

The PV converts a fraction of the solar radiation into the electricity. However, this also increases the operation temperature T_{pv}, which causes a reduction of the electrical efficiency of the PV cell. Due to this the electrical efficiency of the PV depends linearly on the temperature T_{pv}, the temperature coefficient β_{PV} and on the efficiency at standard conditions T_{ref}. The efficiency is calculated according to the following relation:

$$\eta_{EL(T)} = \eta_{STC}\left[1 - \beta_{PV}\left(T_{pv} - T_{ref}\right)\right] \tag{14}$$

The thermal balance of the absorber layer "a" considers the conductive heat transfer to the PV layer ($Q_{a-pv,CD}$), the heat transfer to the fluid (Q_{a-f}) and the heat loss to the exterior through the insulation ($Q_{a-e,CD}$).

$$m_a c_a \frac{dT_a}{dt} = Q_{a-pv,CD} + Q_{a-t} + Q_{a-i,CD} = \\ = h_{a-pv,CD}A_a\left(T_{pv} - T_a\right) + h_{a-t}A_{a-t}(T_t - T_a) + h_{a-i,CD}A_{a-i}(T_i - T_a) \tag{15}$$

Where

$$A_{a-i} = A\left(\frac{W - D_o}{W}\right) \tag{16}$$

$$A_{a-t} = H_a L \tag{17}$$

$$h_{a-t} = \frac{2k_i}{x_a} \tag{18}$$

$$h_{a-i} = \frac{2k_i}{H_i} \tag{19}$$

$$x_a = \frac{(W - D_o)}{4} \tag{20}$$

The heat transfer coefficient to the PV layer ($h_{a-pv,CD}$) is the same as in Equation (10). The energy balance for the tube bonding "t" considers the conductive heat transfer between the absorber plate ($Q_{t-a,CD}$), PV layer ($Q_{t-pv,CD}$), insulation ($Q_{t-i,CD}$) and the coolant fluid (Q_{t-f}).

$$m_t c_t \frac{dT_t}{dt} = Q_{t-pv,CD} + Q_{t-a,CD} + Q_{t-i,CD} + Q_{t-f} =$$
$$= h_{t-pv,CD} A_{pv-t}(T_{pv} - T_t) + h_{t-a} A_{a-t}(T_a - T_t) + h_{t-i,CD} A_{t-i}(T_i - T_t) \quad (21)$$
$$+ h_{t-f} A_{t-f}(T_f - T_t)$$

Where

$$A_{t-f} = \pi D_i L \quad (22)$$

$$A_{t-i} = \left(\frac{\pi}{2} + 1\right) D_o L \quad (23)$$

The heat transfer coefficient of the fluid depends on the type of flow (laminar or turbulent) [139].

$$h_{t-f} = \begin{cases} 4.36 \frac{k_f}{D_H} & \text{for } Re < 2300 \\ 0.023 \frac{k_f}{D_H} Re^{0.8} Pr^{0.4} & \text{for } Re > 2300 \\ 2 \frac{k_f}{D_H} & \text{for } \dot{m} = 0 \text{ kg/s} \end{cases} \quad (24)$$

The energy balance for the insulation "i" considers the heat transfer from the absorber plate, tube and to the environment due to conductive and convective heat loss.

$$m_i c_i \frac{dT_i}{dt} = Q_{i-a,CD} + Q_{i-t,CD} + Q_{t-e,CD+CV} =$$
$$= h_{a-i,CD} A_{a-i}(T_a - T_i) + h_{t-i,CD} A_{t-i}(T_t - T_i) \quad (25)$$
$$+ h_{i-e,CD+CV} A(T_e - T_i)$$

The energy balance for the coolant fluid "f" considers the thermal energy coming from the tube (Q_{f-t}) and the heat accumulated by the fluid (Q_f) as follows:

$$m_f c_f \frac{dT_f}{dt} = Q_{f-a} + Q_f = \; h_{t-f} A_{t-f}(T_a - T_f) + \dot{m} c_f (T_{f,in} - T_{f,out}) \quad (26)$$

The heat transfer coefficient of the coolant fluid (h_{t-f}) is calculated in Equation (24). T_f is the mean temperature of the fluid. The mass flow rate of the fluid in the channels is (kg/s) and $T_{f,in}$ and $T_{f,out}$ are the inlet and outlet temperatures of the fluid, respectively.

$$T_f = 0.5 T_{f,in} + 0.5 T_{f,out} \quad (27)$$

The full derivation of the governing equations is presented by Chow [107]. The Equations (2, 9, 15, 21, 25, 26) are implemented to assess the energy performance of the PVT collector. The following thermal, electrical and overall efficiencies can be calculated:

$$\eta_{el} = \frac{E}{AG_{irr}} \tag{28}$$

$$\eta_{th} = \frac{\dot{m}c_f(T_{fout} - T_{fin})}{AG_{irr}} \tag{29}$$

$$\eta_{overall} = \frac{\dot{m}c_f(T_{fout} - T_{fin}) + E}{AG_{irr}} \tag{30}$$

2.3.2 Numerical Model for Exergy Analysis

Compared to energy analysis the exergy analysis is based on the Second Law of Thermodynamics and takes into account the quality of energy. The exergy balance of the system can be expressed as follows:

$$\sum Ex_{in} - \sum (Ex_{th} + Ex_{el}) = \sum Ex_d, \tag{31}$$

In the case of PVT collector the exergy flow to the system (Ex_{in}) comes from solar irradiation. However, solar irradiation is not seen as pure exergy and due to this a conversation coefficient is included in the calculation of the PVT incoming exergy [10]:

$$Ex_{in} = AN_cG_{irr}\left(1 - \frac{4}{3}\frac{T_0}{T_{sol}} + \frac{1}{3}\left(\frac{T_0}{T_{sol}}\right)^4\right) \tag{32}$$

In Equation (32) T_{sol} is the solar temperature and T0 is the reference temperature which according to the literature should be a constant, for example, T_0 = 20 °C, T_0 = 25 °C or the average temperature of the month. In this study the monthly average outdoor temperatures, presented in Section 2.2., were used in the exergy analysis as reference temperatures. N_c is the number of the collectors.

Electric energy is seen as pure exergy, but the exergy content of thermal energy depends on the temperature at which the heat is made available. In the model, the exergy of thermal (Ex_{th}) and electric (Ex_{el}) energy are respectively calculated as follows [29]:

$$\mathrm{Ex_{th}} = \dot{m}\mathrm{c_f}\left[(\mathrm{T_{out}} - \mathrm{T_{in}}) - \mathrm{T_0}\ln\frac{\mathrm{T_{out}}}{\mathrm{T_{in}}}\right] \quad (33)$$

$$\mathrm{Ex_{el}} = \eta_{\mathrm{pv}}\mathrm{G_{irr}}\mathrm{rA} \quad (34)$$

Where η_{pv} presents the PV cell efficiency and r is a packing factor which is a ratio of PV cell area to the collector area. By Equations (32, 33, 34) both thermal (ξ_{th}) and electrical exergy (ξ_{el}) efficiencies and the overall exergy efficiency (ξ) of the PVT collector can be calculated as follows:

$$\xi_{th} = \frac{Ex_{th}}{Ex_{in}} \quad (35)$$

$$\xi_{el} = \frac{Ex_{el}}{Ex_{in}} \quad (36)$$

$$\xi_{el} = \frac{Ex_{el} + Ex_{th}}{Ex_{in}} \quad (37)$$

2.3.3 Model Validation

In order to conduct the energy and exergy analysis and design optimization of the PVT, the implemented numerical model was validated by comparing the model results to the experimental data shown in [127] in the same steady-state condition: solar radiation 800 W/m^2, ambient temperature 30 °C and wind speed 1 m/s, and is presented in Figure 2-5. The model is in good agreement with the experimental data of the reference.

The numerical PVT model was used to plot the variation of the electrical and thermal efficiencies against the reduced temperature in Equation (38).

$$T^* = \frac{T_{in} - T_e}{G_{irr}}, \quad (38)$$

The reduced temperature takes into account that the thermal efficiency depends on inlet and environment temperature and global solar irradiation.

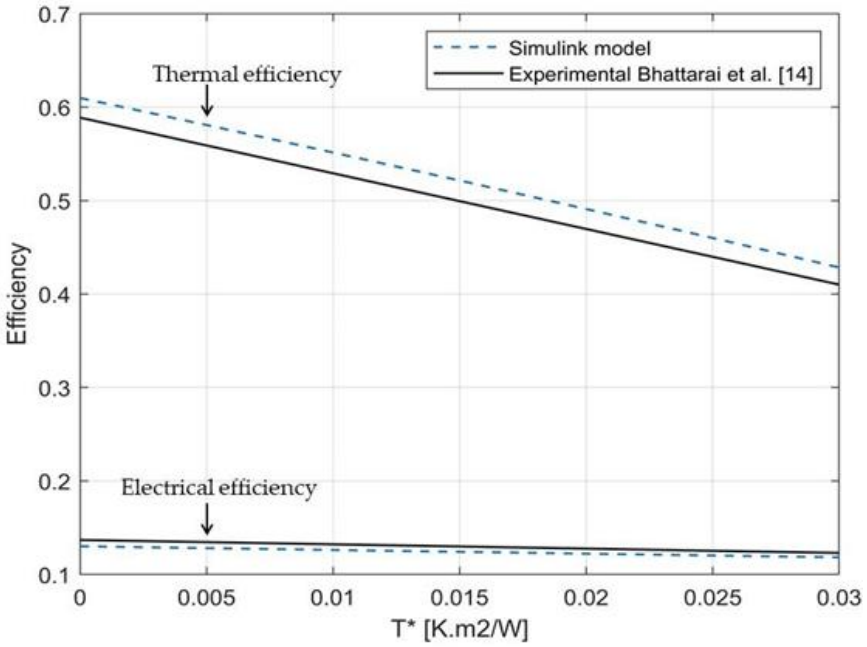

Figure 2-5: *Simulated thermal and electrical efficiencies as a function of the reduced temperature.*

The PVT thermal efficiency of 58.87% and electrical efficiency of 13.69% under zero reduced temperature conditions were reported in [127]. In Figure 2-5, the corresponding values from the Simulink model are 60.97% and 13.01%. The good agreement with the experimental data allows the model to be used for the energy and exergy analysis and optimization in this study.

3. Multi-Objective Optimization of PVT collector

The energy and exergy performance analyses based on the simulations of the PVT model show a conflict between performance parameters, such as thermal and electrical energy and exergy efficiencies, as functions of various decision variables. The electrical efficiency of the PV panel decreases when the operating temperature of the collector increases. On the other hand, increased operating temperature leads to the higher thermal energy and exergy efficiency. This means that both efficiencies cannot be directly maximized at the same time, but a solution has to be found, which satisfies both trade-off objectives (electrical and thermal exergy efficiencies in this study) at the same time. The thermal simulations of the PVT system alone do not provide a set of optimal solutions of decision variables in terms of thermal and electrical exergy

efficiencies. This set can be found by using the multi-objective optimization (MOO) technic with an evolutionary algorithm.

3.1 Multi-objective optimization using gamultiobj-function

In this study, the Matlab function called gamultiobj of the Global Optimization Toolbox is used to run the multi-objective optimization of the PVT collector design. The gamultiobj-function creates a set of optimal solutions in the space of decision variables on the Pareto front. The function uses a controlled, elitist genetic algorithm, which is a variant of NSGA-II [140]. Generally, the multi-objective optimization problem of two or more conflicting objectives is described mathematically as follows [30]:

$$\begin{gathered}\text{Minimized/Maximized } f_m(x),\ m = 1,2,\ldots,M;\\ \text{Subject to } g_j(x) \geq 0,\ j = 1,2,\ldots,J;\\ h_k(x) = 0,\ k = 1,2,\ldots,K;\\ x_i^{(L)} \leq x \leq x_i^{(U)},\ i = 1,2,\ldots,n;\end{gathered}$$

In this formulation, the objective functions are minimized or maximized subject to certain constraints.

In this work, the overall electrical and thermal exergy efficiencies are two objectives to be optimized. Due to the fact that the NSGA-II is a minimization tool the objective functions are multiplied by (-1) in order to get the maximum values [30]. The 2-dimensional optimization problem of the exergy efficiencies is formulated as follows:

To minimize:

$$f_1(\mathbf{x}) = -\frac{Ex_{el}}{Ex_{in}} = -\frac{\eta_{STC}\left[1-\beta_{PV}\left(T_{pv}-T_{ref}\right)\right]G_{irr}A_{pv}}{AN_cG_{irr}\left(1-\frac{4}{3}\frac{T_0}{T_{sol}}+\frac{1}{3}\left(\frac{T_0}{T_{sol}}\right)^4\right)} = -\xi_{el} \tag{39}$$

$$f_2(\mathbf{x}) = -\frac{Ex_{th}}{Ex_{in}} = -\frac{\dot{m}c_f\left[\left(T_{out}-T_{in}\right)-T_0\ln\frac{T_{out}}{T_{in}}\right]}{AN_cG_{irr}\left(1-\frac{4}{3}\frac{T_0}{T_{sol}}+\frac{1}{3}\left(\frac{T_0}{T_{sol}}\right)^4\right)} = -\xi_{th} \tag{40}$$

where ξ_{el} and ξ_{th} are the electrical and thermal exergy efficiencies, respectively.

The optimization decision variables were selected based on the sensitivity analyze, which has shown the most sensible parameters of the PVT collector operation in terms of exergy

efficiencies. These parameters are the cooling-water mass flow, inlet temperature, air gap thickness between the cover glass and PV module and insulation thickness. Table 2-3 presents the decision variables to be optimized and their upper and lower bounds to be used in the optimization.

Table 2-3: Decision variables for multi-objective optimization problem.

Symbol	Decision variable	Bounds	Unit
$\dot{m}$	Fluid mass flow rate	$0.0083 \leq x(1) \leq 0.044$	kg/s
T_{in}	Inlet temperature	$15 \leq x(2) \leq 45$	°C
H_{gap}	Air gap thickness	$0.02 \leq x(3) \leq 0.25$	m
H_i	Insulation thickness	$0.015 \leq x(4) \leq 0.09$	m

4. Results and Discussion

First, the dynamic model is used to evaluate annual energy and exergy performance of the PVT collector under two different climate conditions described in Section 2. The main performance differences between two selected climate conditions are revealed and assessed. Additionally, the comparison between the PVT and PV panel performance under the described climate conditions is conducted. The main focus of the comparison is on the electrical output, operating temperature and on the impact of the PVT packing factor. Secondly, the results of the multi-objective optimization are presented and discussed. The selected optimized PVT designs are compared to the PV panel performance.

4.1 Simulation Results

Hourly simulations were conducted with the dynamic PVT model. The electrical power output of the PVT collector was illustrated during the summer and winter weeks. The summer week was selected to present a good summer week in Tampere and Strasbourg. Because of the northern location of Tampere, the selected summer week in Tampere was at the end of June, and in Strasbourg in the beginning of August. The winter week was in both cases at the end of December.

Figure 2-6 presents generated electrical power, which reached the same maximum level, around 200 W, in the northern and southern locations during the summer week. However, during the winter week, solar irradiation is almost non-existent in the northern location because of the polar night and the electrical power generation is zero. In the southern location, there is still the possibility for electric power generation during the winter week.

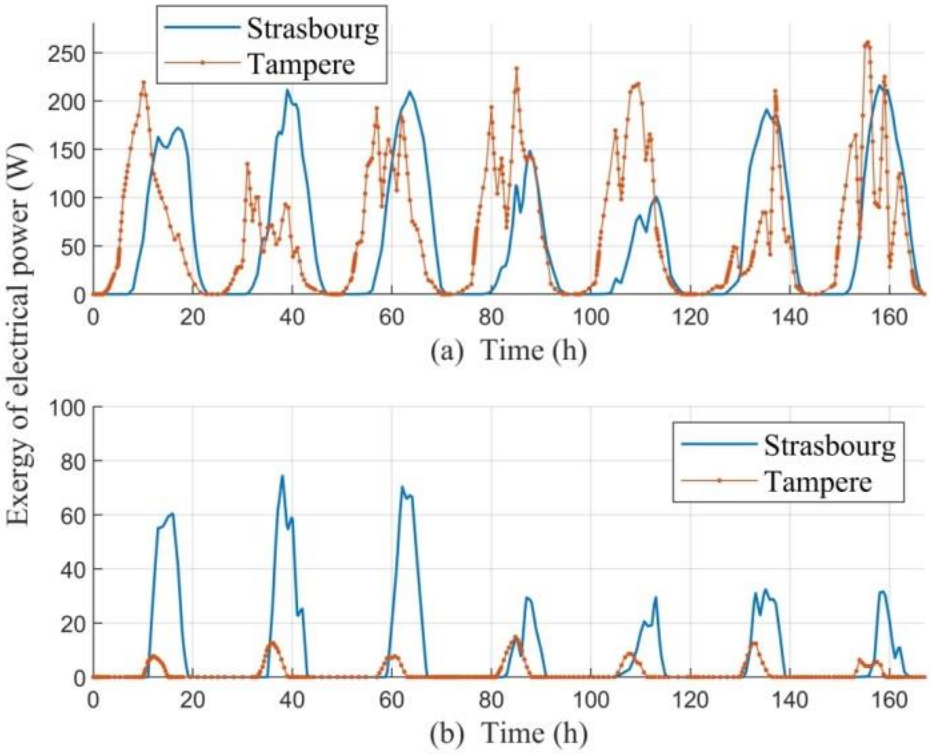

Figure 2-6: *Exergy of electrical power during: (a) summer week; (b) winter week.*

The PV cell efficiency is influenced by its operating temperature. The electrical exergy efficiency is always slightly higher than the electrical energy efficiency because solar irradiation is not seen as pure exergy but is reduced by the factor in Equation (32). Figure 2-7 shows the simulation of the PVT layer temperatures over a day and how the electrical efficiency decreased when ambient, collector surface and coolant fluid outlet temperatures increased, and vice versa. On the other hand, an increase in the collector temperature results in the higher thermal efficiency due to the better heat transfer to the coolant fluid. In other words, when operating a PVT collector, both electrical and thermal efficiencies cannot be maximized at the same time.

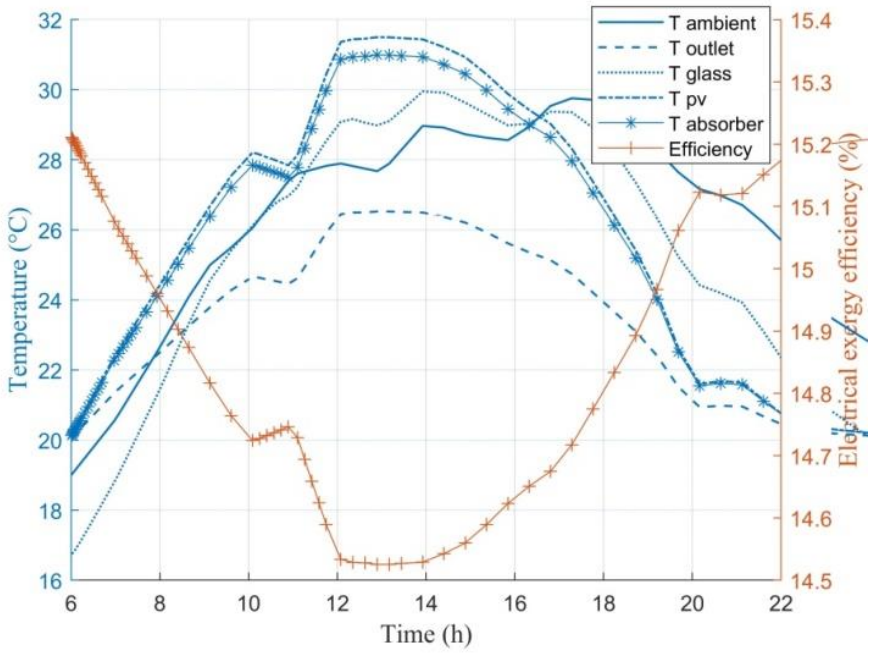

Figure 2-7: *The electrical exergy efficiency, PVT surface, fluid outlet and ambient temperature during a summer day.*

Next, the annual energy and exergy production and efficiencies were simulated and analyzed monthly. The thermal exergy generation and efficiency are influenced by the ambient temperature. To evaluate these parameters fairly under the different climate conditions, the reference temperature for the exergy analysis was selected to be an average outdoor temperature of the considered month based on the statistics. The monthly average temperatures for Tampere were taken from [141] and Strasbourg from [142].

Figure 2-8 shows the monthly thermal and electrical efficiencies in Tampere and Strasbourg over a year. It reveals that the monthly electrical efficiency reached 0.4-6.8% higher values in the northern location due to the cooler climate conditions and lower PV operating temperature. However, during the summer months, the efficiency was 13.8% in both locations. The thermal efficiency did not get zero values in Strasbourg, but in Tampere, the thermal energy production was zero during January, November and December. The thermal efficiency varied the most between two locations in mid-summer. In June the thermal efficiency suffered due to the rainy summer weather of the northern location. In the southern location, the summer weather was more stable, and there was no sign of a significant drop in efficiency.

The energy performance results show that there was no significant difference between the northern and southern location in terms of maximum thermal and electrical efficiencies. Next, the analysis of the exergy efficiencies is conducted to reveal the quality of the produced energy in the northern and southern location.

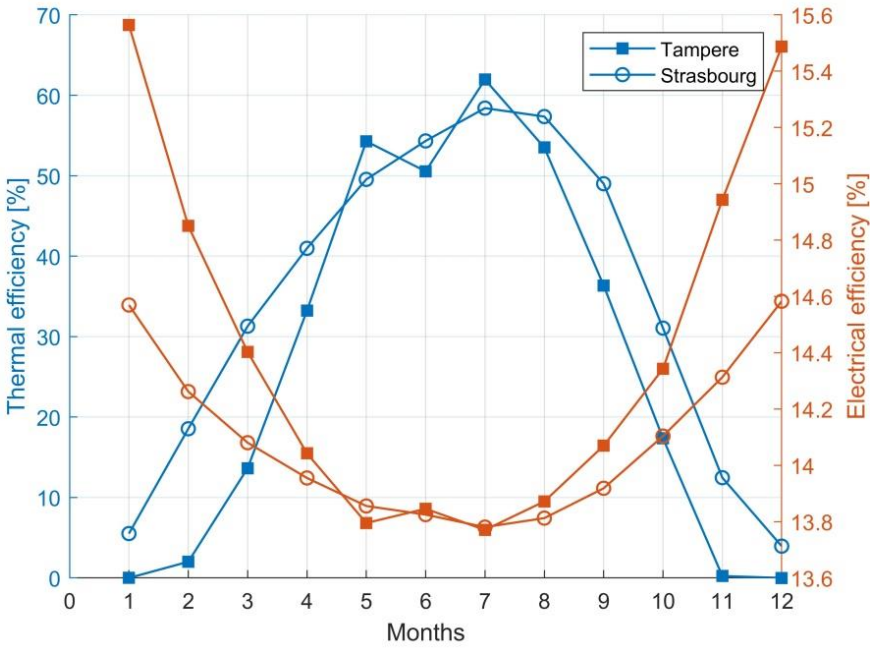

Figure 2-8: *Monthly electrical and thermal efficiencies over year in Tampere and Strasbourg.*

The monthly thermal and electrical exergy efficiencies in Tampere and Strasbourg are shown in Figure 2-9. The results show that although the thermal efficiency in Tampere and Strasbourg followed a similar shape over the year, the thermal exergy efficiency did not show the same trend between the locations. The comparison of Figure 2-9 a) and b) reveals that the highest thermal exergy efficiency of 2.47% was reached in Tampere in May and in Strasbourg already in March 1.62% although the highest thermal efficiencies of 62% and 58.4%, respectively, were reached in both locations in July. The thermal exergy efficiencies were significantly lower than the thermal energy efficiencies. That means the PVT collector can convert the available solar energy well into useful heat, but it happens close to the reference ambient temperature. The useful heat has low quality in terms of its ability to do mechanical work.

After reaching the highest point, the thermal exergy efficiency decreased in both locations due to increased ambient temperature of the summer weather conditions. After the

summer months June, July and August, the thermal exergy efficiency increased to the same level than before the summer months in the southern location but in the northern location the efficiency did not increase after summer months due to decreasing ambient temperature and amount of solar irradiation.

The thermal exergy efficiency was 44-255% higher in Tampere between April and September than in Strasbourg due to good solar irradiation level but relatively lower monthly average outdoor temperatures presented in Table 2-2. The study of the thermal exergy efficiency revealed that produced thermal energy has higher quality in the northern location than the southern.

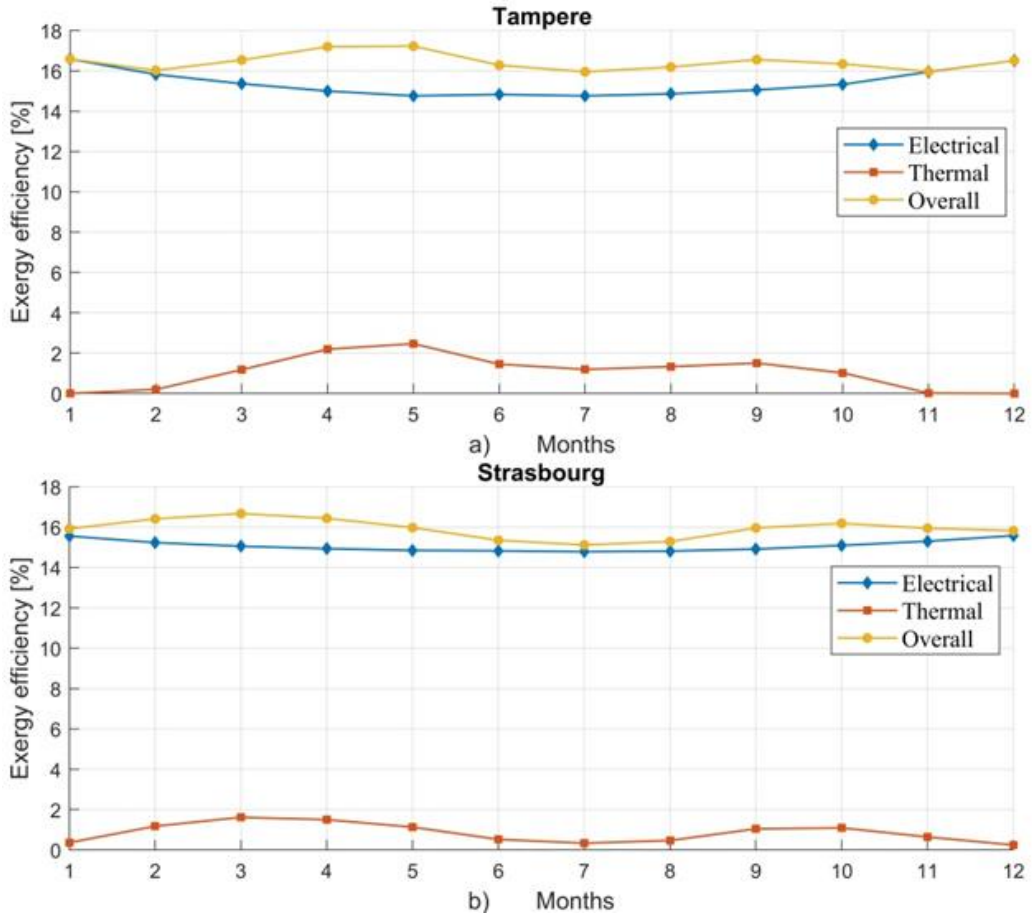

Figure 2-9: *Thermal, electrical and overall monthly exergy efficiencies in a) Tampere and b) Strasbourg.*

The electrical exergy efficiency behaved similarly to the electrical energy efficiency and got slightly higher values in the northern location than the southern due to the lower ambient

temperature and lower PV cell operating temperature. However, during the summer months, the electrical exergy efficiency reached same values in both locations.

Table 2-4 summarizes the annual energy and exergy production in Tampere and Strasbourg. The thermal energy production and solar gain in Strasbourg were 8.4% and 6.2%, respectively, higher than in Tampere. However, the produced thermal energy in the northern location was of "higher quality" because the thermal exergy production in Tampere was 72.9% higher than in Strasbourg.

Although the results showed that the electrical energy and exergy efficiencies were slightly higher in Tampere most of the year, the yearly produced electrical energy and exergy were 5.8% higher in Strasbourg than in Tampere due to the 6.2% higher solar irradiation to the collector area in Strasbourg.

The total annual energy production was 7.8% higher in Strasbourg than in Tampere. However, the results show that the total exergy production was only 1.27% higher in Strasbourg than in Tampere, although the solar exergy gain was 6% higher.

Table 2-4: Simulation results of the energy and exergy analysis

Production	**Strasbourg [kWh/year]**	**Tampere [kWh/year]**
E_{th}	992.1	915.5
E_{el}	305.5	288.8
E_{in}	2191.8	2064.8
Ex_{th}	17.4	30.1
Ex_{el}	305.5	288.8
Ex_{in}	2046.2	1930

4.2 Comparison between PVT Collector and Photovoltaic (PV) panel

A comparison between the PVT collector and PV panel was conducted using simulation models. The PV panel was simulated with the PV generator-block of the open-source CARNOT Toolbox [24]. The PV panel and PVT collector had the same area of 2 m^2 and the same reference cell efficiency of 17.3%.

Implementing a water-based cooling system underneath the PV layer of the PVT collector reduces the PV cell operating temperature and enhances its efficiency. Figure 10 presents the PV cell operating temperatures and efficiencies during three selected summer days

in Tampere and Strasbourg. The corresponding weather conditions are presented in Figure 2 in Section 2.

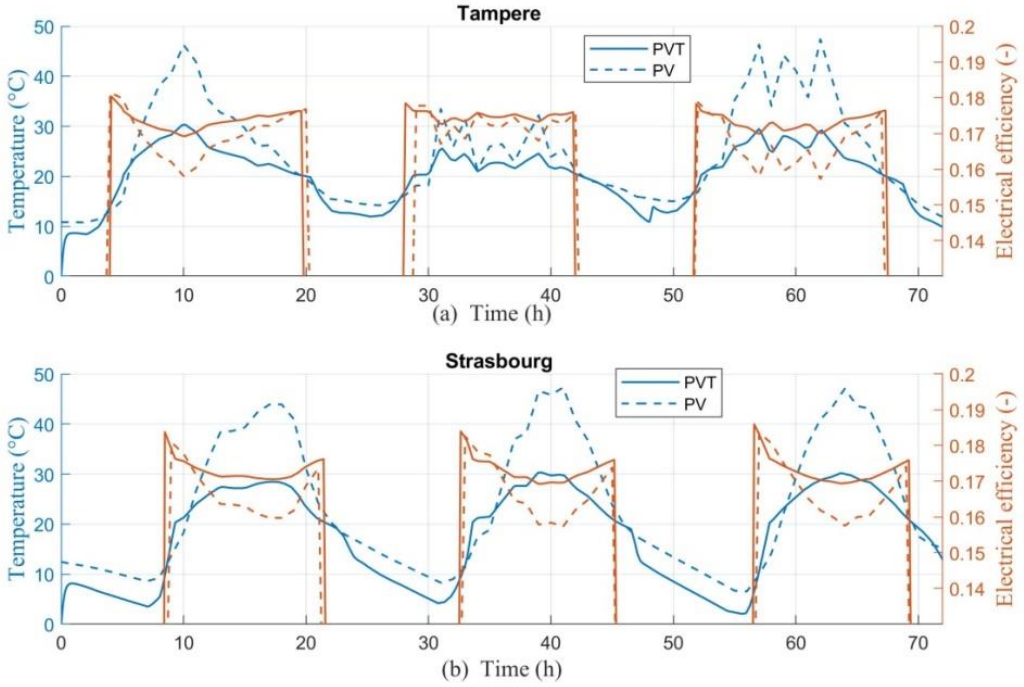

Figure 2-10: *The PV cell operating temperatures and electrical efficiency (a) in Tampere and (b) in Strasbourg during the three summer days.*

Over the summer days in Figure 2-10, the PV cell operating temperatures were significantly higher within the PV panel than in the PVT collector. In both locations, the maximum operating temperature of the PV was around 48 °C and of the PVT collector 30 °C. Due to the cooling effect of the water mass flow underneath the PV layer in the PVT collector, the maximum increase in the electrical efficiency was around 1.1 percentage point during the second summer day in Strasbourg.

Despite the same PVT collector and PV panel area, the electrical energy production of the PVT collector is influenced by the packing factor (r_c) of the collector. However, this is not a case in the PV panels that are fully covered with the PV cells. Because of the packing factor, the better cell efficiency in the PVT collector does not always lead to higher electricity production compared to the PV panel.

The impact of the packing factor on the PV cell operating temperature and electrical energy production of the PVT collector was studied in comparison to the PV panel. Figure 2-11

presents the monthly maximum temperatures of the PV panel and PVT collector with the different packing factors of 0.6, 0.8 (base case) and 1 in Tampere and Strasbourg.

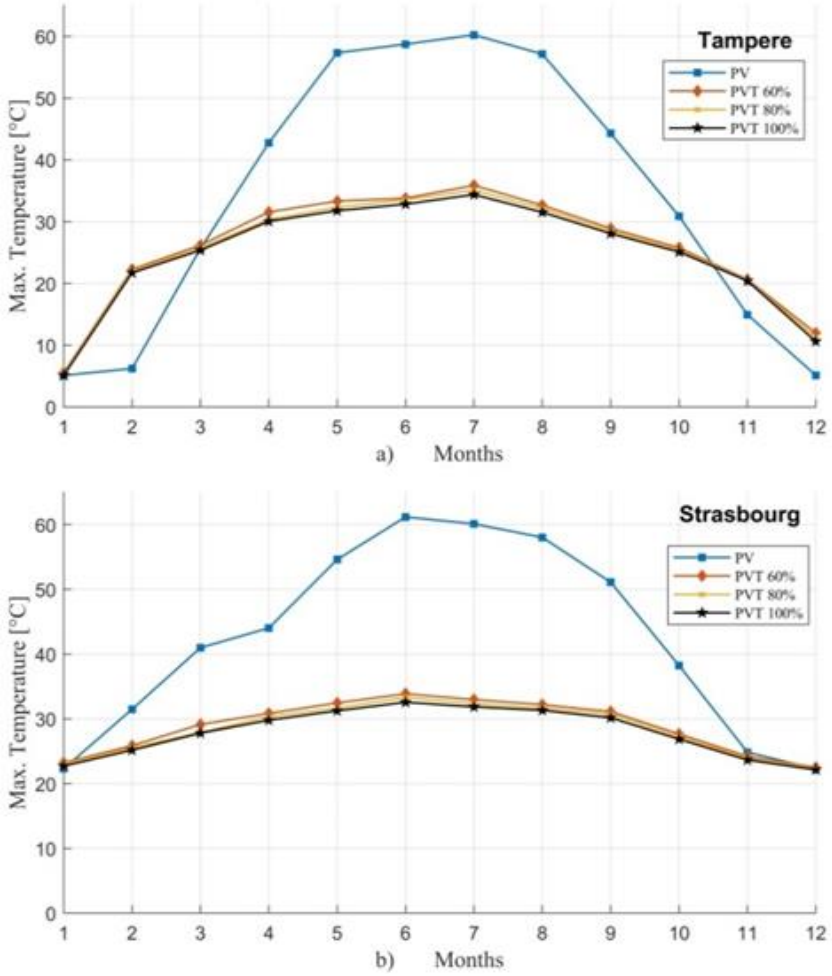

Figure 2-11: *Monthly maximum PV cell operating temperatures of the PV panel and PVT collector with different packing factors in (**a**) Tampere and (**b**) Strasbourg.*

The results in Figure 2-11 indicate that the packing factor had only a slight influence on the PV cell operating temperature of the PVT collector. The PVT with the packing factor of 0.6 had 1% to 5% higher maximum operating temperatures over year than the fully packed collector. In both locations, the monthly maximum PV cell operating temperatures of the PV panel were significantly higher, from 11 to 27 °C, from April to September/October than in the PVT collector. The maximum operating temperature of the PV panel in both locations was around 60 °C and 35 °C for the PVT collector.

Figure 2-12 and Figure 2-13 present the monthly electrical output of the PV panel and the PVT collector with different packing factors in Tampere and Strasbourg, respectively.

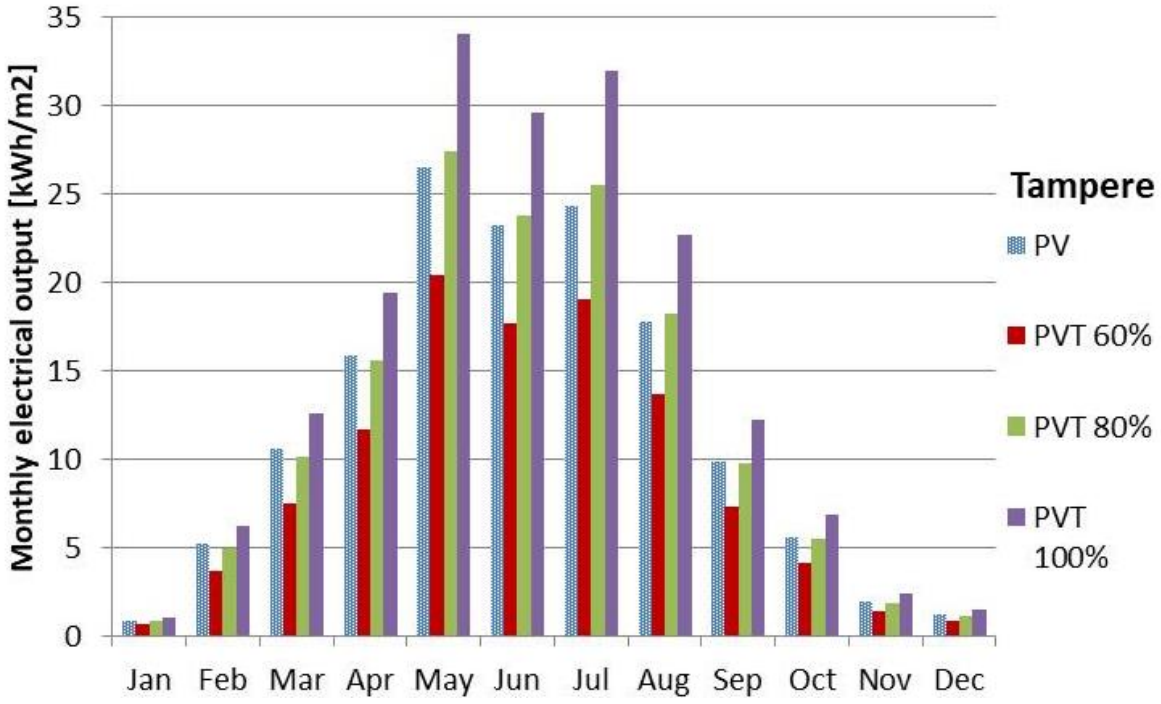

Figure 2-12: *Monthly electrical output of the PV panel and PVT collector with different packing factors in Tampere, Finland.*

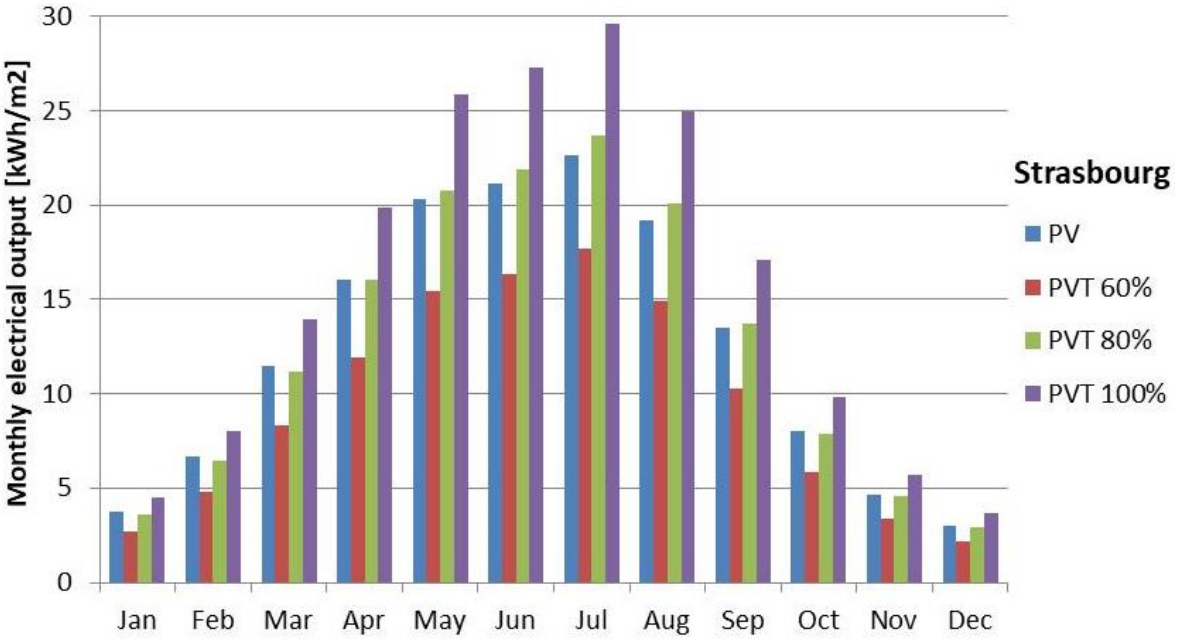

Figure 2-13: *Monthly electrical output of the PV panel and PVT collector with different packing factors in Strasbourg, France.*

A typical PVT collector has a packing factor of 0.8, and that is used as a base case in this study. With this typical design, the monthly electrical output of the PV and PVT were only slightly different in both locations. The PV panel had higher electrical output during winter and spring months from January to April and October to December because of the lower ambient temperatures. However, during the warmer months from May to September, the electrical output of the PVT was higher than PV due to higher ambient temperatures, solar radiation and the cooling effect of the PVT.

In Tampere, the maximum PVT electrical output was 34 kWh/m^2 in May and in Strasbourg 29.5 kWh/m^2 in July. The annual electrical output of the PV panel and base case PVT collector was 142.7 kWh/m^2 and 144.4 kWh/m^2, respectively, in Tampere. This result indicates that although the packing factor of the PVT was 80%, 1.2% higher electrical output was reached because of the cooling effect underneath the PV cells. In Strasbourg, the annual electrical output of the base case PVT collector was 1.5% higher than from the PV panel resulting in 152.8 kWh/m^2 and 150.5 kWh/m^2 electrical energy yield, respectively. In Strasbourg, the annual electrical output of the fully packed PVT collector was 190.2 kWh/m^2, which is 26.4% more electrical output than from the PV panel. In Tampere, the fully packed PVT produced annually 180.1 kWh/m^2, which is 26.2% more electrical output than from the PV panel.

4.3 Multi-Objective Optimization

The simulation-based multi-objective optimization process was conducted. The main objective was to find different optimal design solutions for the PVT collector depending on its operational purpose, which can be defined by the user. Additionally, the objective was to study the impact of the decision variables, such as water mass flow rate and inlet temperature, on the comparison between the PV panel and PVT collector electrical output and PV cell operating temperature.

First, the selected decision variables were varied and the initial population and score matrixes for the genetic algorithm were generated by the simulation model. These matrices were given for the gamultiobj-function, which started the iterative process by evaluating the fitness function with the simulation model and making selection, crossover and mutation of the population. Based on this process, a new population or generation was created. The new

generations were created as long as a stopping criterion was met. The criterion was the number of generations. The multi-objective optimization process is described in Figure 2-14.

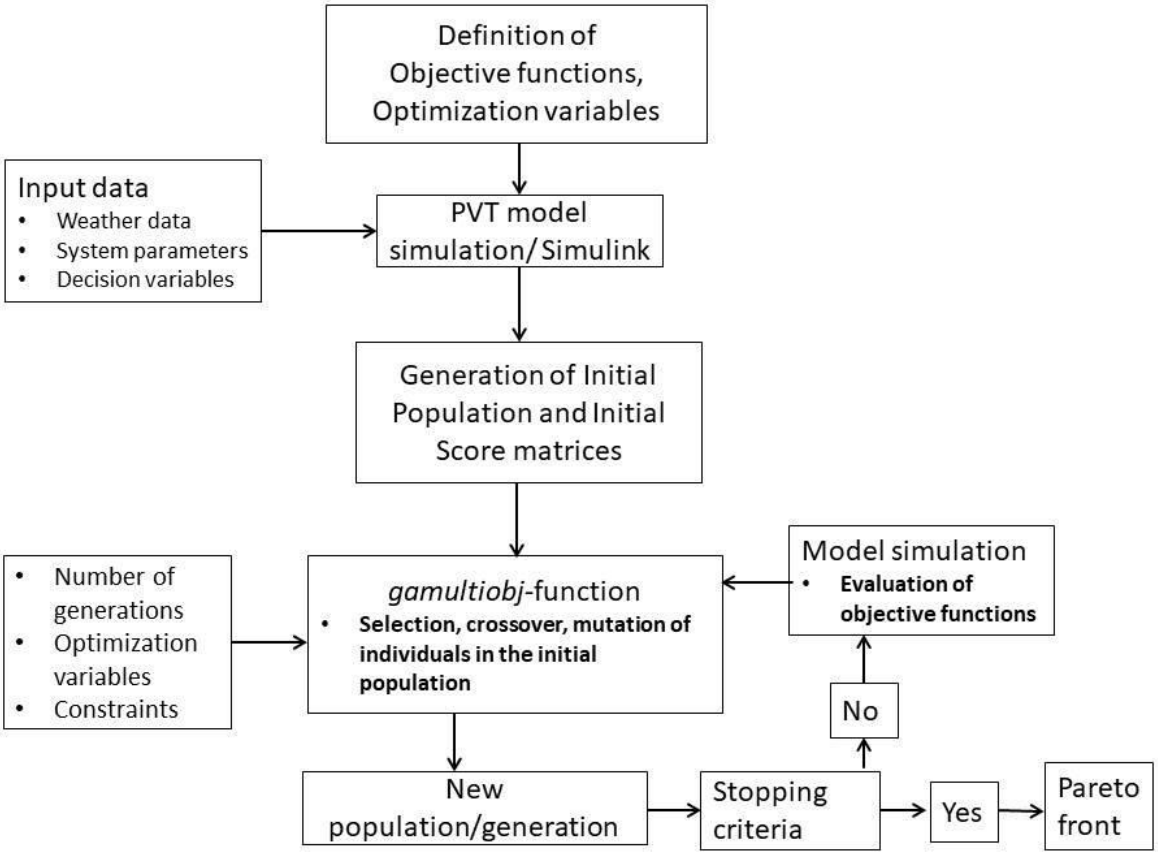

Figure 2-14: *The simulation based multi-objective optimization process.*

The optimization was conducted with steady-state weather conditions that were defined to be the following: solar irradiation of 500 W/m^2, ambient temperature of 16 °C and wind speed of 2 m/s. These conditions present average weather conditions in Tampere and Strasbourg during the best PVT operation months. The selected decision variables of the optimization are discussed in Section 4. The other parameters are presented in Section 2. The relation of the variables to the electrical and thermal exergy efficiencies are shown in Figure 2-15.

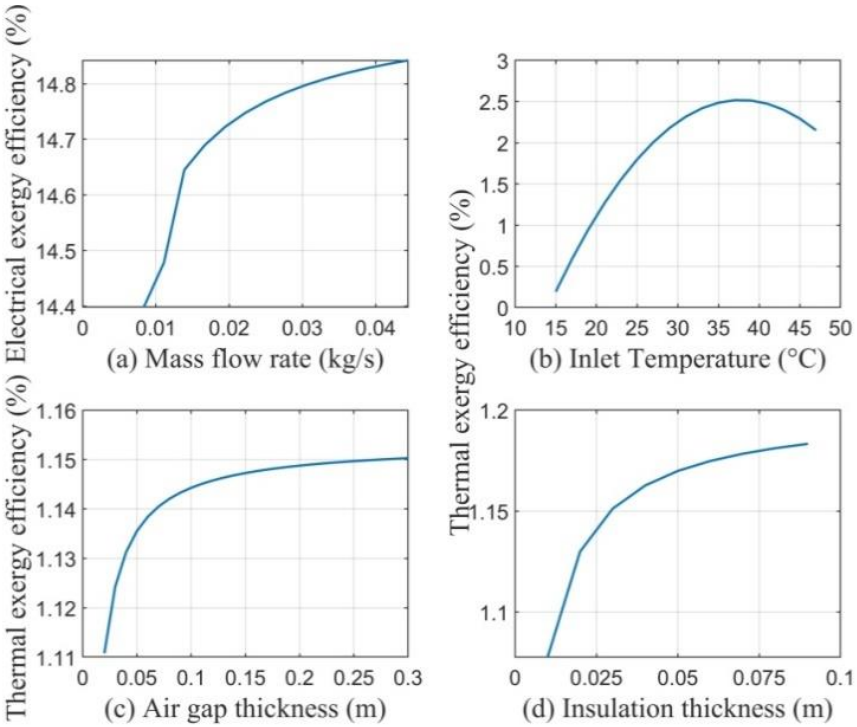

Figure 2-15: *The sensitivity of the decision variables to electrical and thermal exergy efficiencies: (a) mass flow rate, (b) inlet temperature, (c) air gap thickness and (d) insulation thickness.*

Figure 2-15 presents the sensitivity of the decision variables to the electrical and thermal exergy efficiencies. The main findings of the sensitivity analysis are following. Increasing the mass flow rate of the coolant fluid increases the electrical exergy efficiency due to increasing cooling effect. First, the electrical exergy efficiency increases strongly. On the other hand, if the coolant mass flow is increased too much, the thermal efficiency is decreased. Increasing the inlet temperature of the coolant fluid increases the thermal exergy efficiency at a certain point. However, the electrical efficiency suffers when increasing the inlet temperature due to the higher operating temperature. The insulation and air gap thickness have a strong influence on the thermal exergy efficiency until 10 cm.

Figure 2-15 shows that all decisions variables can reach an optimal value at certain point but they are also depending on each other. Conducting a multi-objective optimization takes into account the relation between these variables and the optimal solution may be different than when investigating a single variable.

After studying the sensitivity of the selected decision variables, the thermal and electrical exergy efficiencies were selected to be objective functions and the optimization problem was

solved using the gamultiobj function of Matlab Global Optimization Toolbox. The function is based on NSGA-II algorithm. In this study, the set of the optimal solutions called Pareto front is obtained with the generation number of 160 and the population size of 192.

Figure 16 shows the obtained Pareto front of the solutions derived with the defined weather conditions. The decision variables are also shown for three selected solution points. The values of the variables showed the same behavior as in Figure 2-15a–d. From the Pareto front three solution levels were derived depending on the priority of the PVT operation:

- Electric-driven: the priority is to maximize electricity production within the Pareto optimal;
- Thermal exergy-driven: the priority is to maximize thermal exergy production within the Pareto optimal;
- Trade-off solution: the priority is to produce optimally electricity and thermal exergy within the Pareto optimal front.

Based on the Pareto front in Figure 16, the electric-driven solution was characterized by the high mass flow rate of 158.4 kg/h, thinner air gap thickness of 13 cm, low inlet temperature of 15.1 °C and insulation thickness of 3 cm. The thermal exergy-driven solution was characterized by the low mass flow rate of 44.6 kg/h, high inlet temperature of 30.8 °C, thick air gap thickness of 19.3 cm and thicker insulation thickness of 9 cm. The trade-off solution was similarly characterized than thermal exergy solution, but the mass flow rate was higher, resulting as 86.4 kg/h, and lower inlet temperature of 23 °C was allowed.

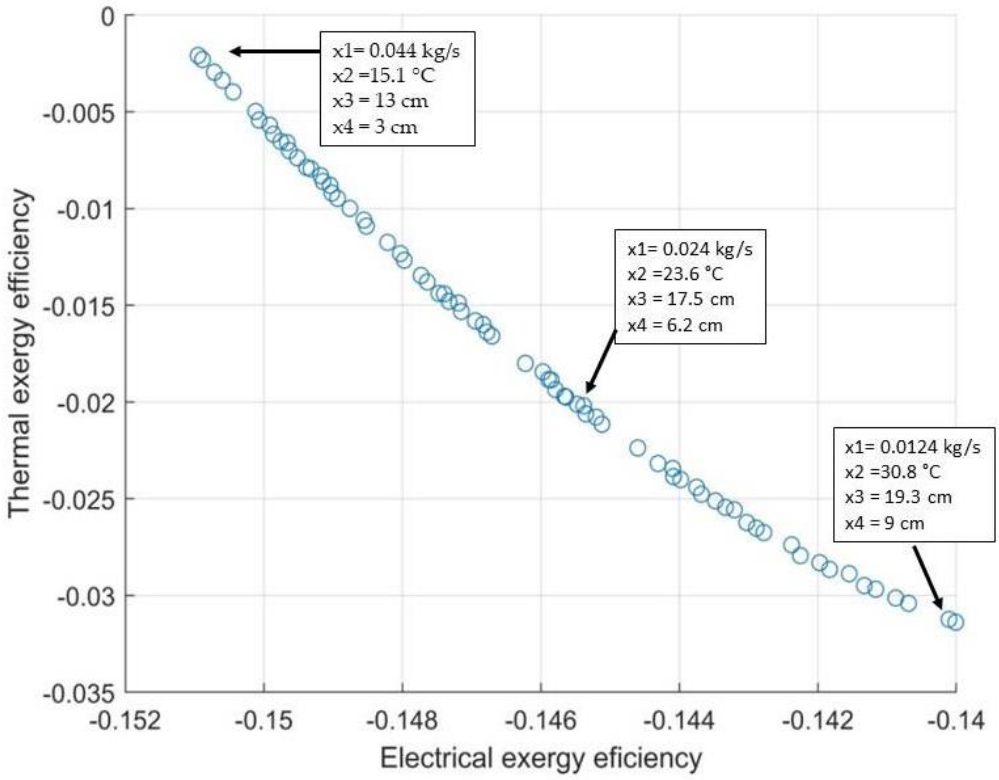

Figure 2-16: *The Pareto optimal front in the objective space of the electrical and thermal exergy efficiencies.*

To see how the decision variables, such as mass flow and inlet temperature, influence the comparison between PVT collector and PV panel, three different optimal PVT designs, shown in Figure 2-16, were simulated under the climate conditions of Strasbourg. The results were compared with the PV panel performance. Figure 2-17 shows the monthly maximum PV cell operating temperatures in the PVT collectors and the PV panel.

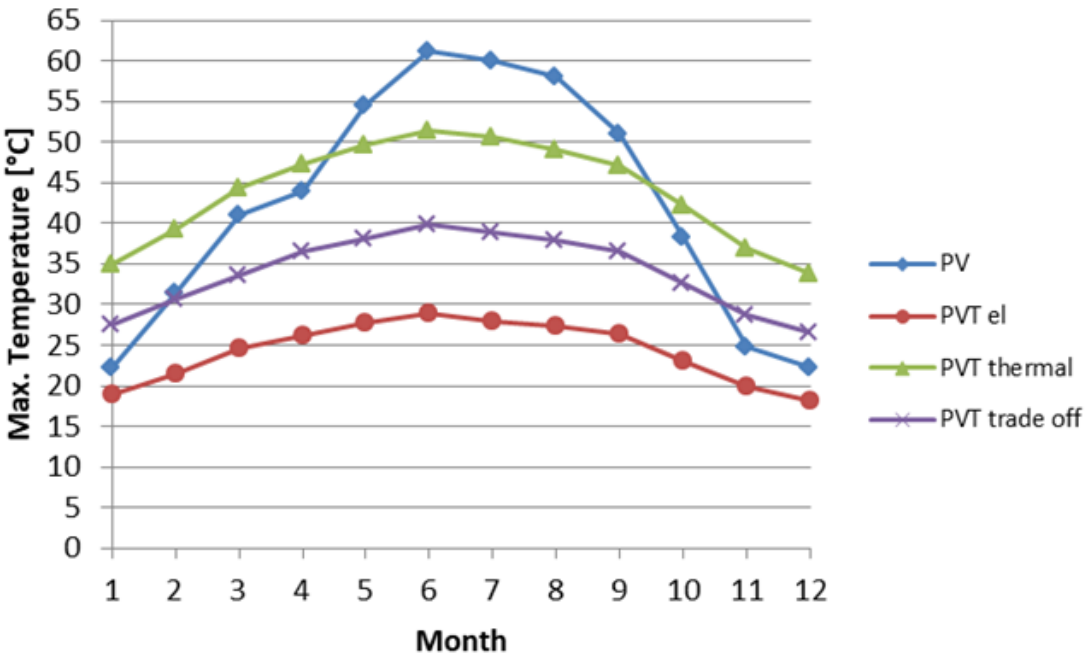

Figure 2-17: *Monthly maximum PV cell operating temperatures in the PV panel and optimal PVT designs.*

Figure 2-17 shows that the lowest maximum PV cell temperatures were reached if the electric- driven design was selected. The maximum temperature was only 29 °C during the summer period. At the same time, the PV panel reached its maximum temperature of 61.2 °C. The lowest maximum PV cell temperatures were reached due to the high mass flow of 158.4 kg/h and low inlet temperature of 15.1 °C. On the other hand, if the mass flow was decreased, and the inlet temperature increased to maximize thermal exergy production, the significantly higher PV cell operating temperatures with a maximum of 51 °C resulted. That is shown in Figure 17 with the thermal exergy-driven PVT design. However, the maximum cell temperatures were still around 10 °C lower during the summer period than in the PV panel. During the beginning and end of the year, the PV cell operating temperatures were higher in the PVT than in PV because of the heat production in the lower ambient temperature.

Figure 2-18 shows how different decision variables influence the electricity production of the PVT collector compared to the PV panel.

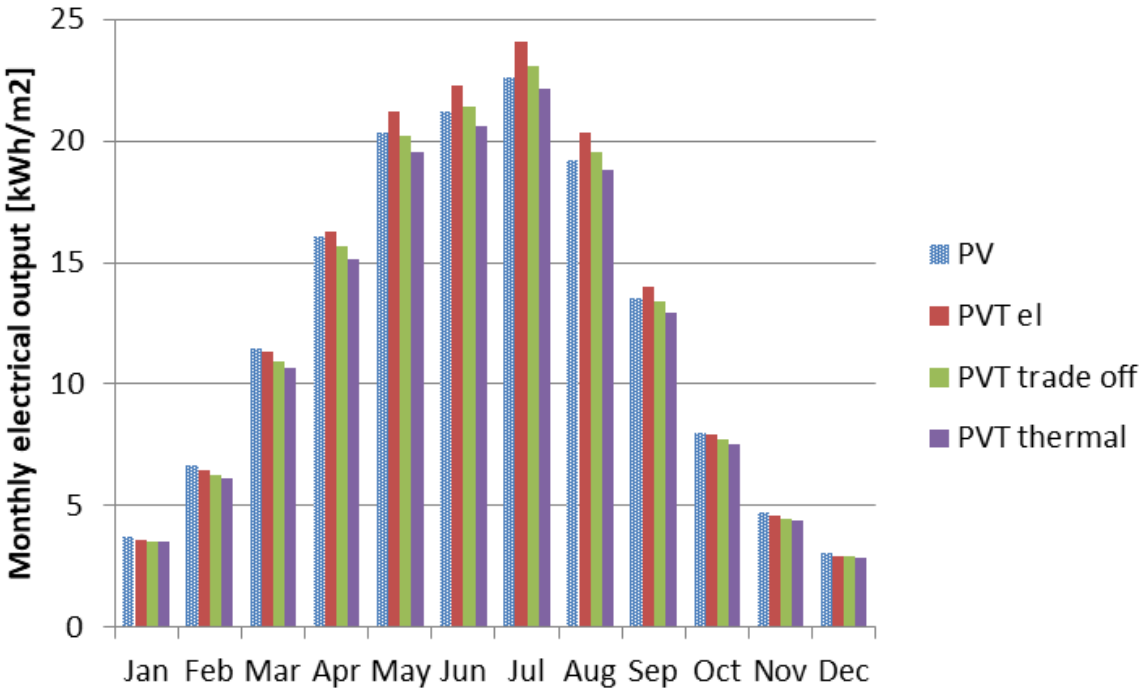

Figure 2-18: *Monthly electrical output of the PV panel and three optimal PVT designs.*

The results show that the high mass flow rate and low inlet temperature resulted in the higher electrical output during the warmest months from April to September compared to the PV panel electrical output. The annual electricity production of the PV panel was 150.5 kWh/m^2, and the electric-driven PVT design produced 155.1 kWh/m^2, which is 3% more, although the packing factor was 0.8. The annual electrical output of the trade-off design was 149.1 kWh/m^2, which is only 1% less than from the PV panel.

If the mass flow was reduced and the inlet temperature increased significantly, the electrical output was lower than in the PV panel during each month. The annual production was 144.2 kWh/m^2, which is 4.2% less than from the PV panel. However, the production was not significantly lower than from the PV output if taking into account the beneficial thermal output of the PVT collector as well. Based on the simulation results in Section 5.2., it could be assumed that the fully packed thermal exergy-driven PVT design could produce higher electrical output than the PV panel.

Figure 2-19 presents the produced thermal exergy of the base case PVT and three optimal PVT designs of the Pareto front.

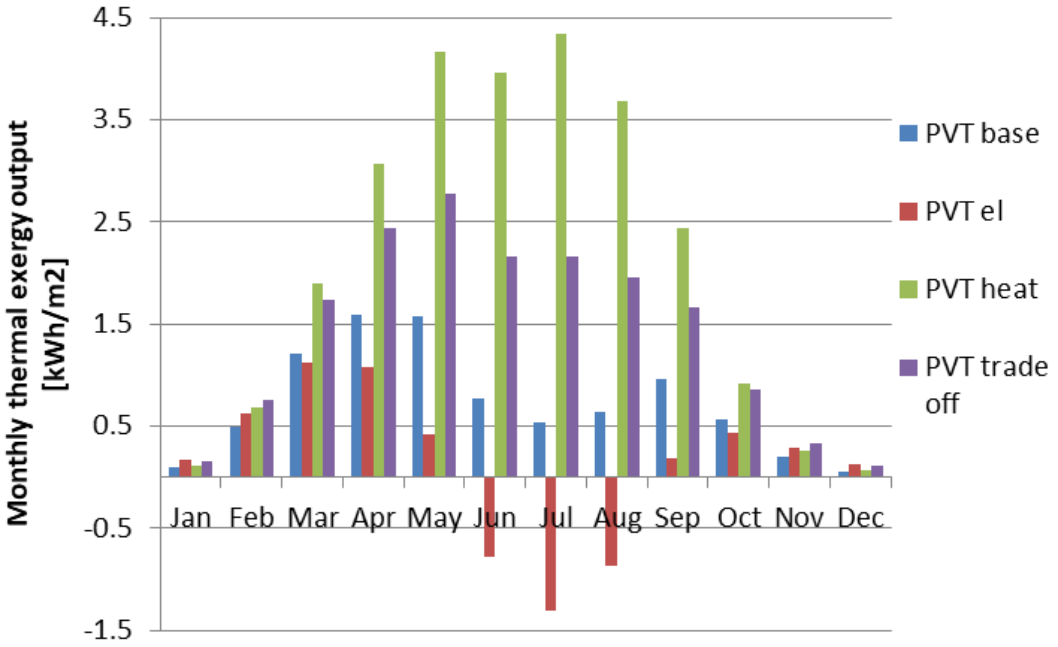

Figure 2-19: *Monthly thermal exergy of different PVT designs.*

Produced thermal exergy indicates the quality of the produced thermal energy and its ability to do mechanical work at the reference ambient temperature. Figure 2-19 shows that the produced thermal exergy was even negative in the case of the electric-driven PVT design in which the mass flow rate was high, inlet temperature low and the insulation thinner. This means that the thermal energy was produced really close to or even below the reference ambient temperature and that leads to poor quality of the produced thermal energy.

As a conclusion, the optimization results indicated that maximizing the thermal exergy efficiency of the PVT collector results in the high inlet temperature, low mass flow rate and thicker insulation. These variables resulted in increasing PV cell operating temperatures that were, however, still lower than in the PV panel during the warmest months. The electricity yield was 4.2% lower, but as a fully packed PVT collector, the electrical output would be higher than from the PV panel. For a PVT building application, these results show that optimizing the high-quality energy output of the PVT collector allows the higher inlet temperature and low mass flow rate from heat storage and still the electrical output is competitive compared to the PV panel.

5. Conclusion

The objective and novelty of this study were to conduct energy and exergy analysis of the PVT performance under two different European climate conditions in Tampere, Finland and Strasbourg, France. The dynamic model of the water-cooled PVT collector was implemented in Matlab/Simulink to assess the collector performance under varying weather conditions. Additionally, the objective was to conduct a numerical comparison between the PVT collector and PV panel in terms of the PV cell operating temperature, efficiency and electrical output. In the first comparison, the packing factor of the PVT collector was varying, and its influence on the operating temperature and electrical output was investigated.

The main findings of the energy and exergy analyses were:

- Despite the northern location of Tampere, the similar electric power generation conditions were reached during the summer period than in Strasbourg.
- The monthly electrical efficiency reached 0.4–6.8% higher values in the northern location due to the cooler ambient conditions and lower PV cell operating temperature. However, during the summer months, the electrical efficiency was 13.8% in both locations.
- The annual thermal and electrical energy production and solar gain were 8.4%, 5.8% and 6.2%, respectively, higher in Strasbourg than Tampere. The total annual energy production was 7.7% higher in Strasbourg.
- Based on the exergy analysis, the thermal energy produced in the northern location of Tampere was of “higher quality” because the thermal exergy production in Tampere was 72.9% higher than Strasbourg. However, the total exergy production was 1.27% higher in Strasbourg than Tampere because of 5.8% higher electrical exergy production.
- The climate conditions with high solar irradiation but relatively low temperatures are favorable for thermal exergy production.

The results of the analyses lead to the conclusion that in terms of exergy efficiency, the PVT collector should be considered in thermal energy production, especially in the northern locations, such as Finland. In the southern locations with higher average outdoor temperatures, the low-grade thermal energy production is less efficient due to the smaller temperature difference between the produced heat and ambient temperature.

The comparison between the PVT and PV performance resulted in the following main findings:

- In both locations, the monthly maximum PVT operating temperatures were lower than in the PV panel. The maximum operating temperature of the PVT was around 32–35 °C and of the PV 60–61 °C. The lower operating temperatures resulted in around 1%-unit higher cell efficiency in the PVT compared to the PV panel.
- The electrical output was significantly influenced by the PVT packing factor. The fully packed PVT collector resulted in the 26% higher annual electrical output than the PV panel.
- The PVT collector had a higher electrical output during the summer months compared to the PV panel.
- The annual PVT electrical output is competitive with the PV panel.

The other contribution of this paper was to propose an approach to derive optimized designs for different operational purposes of the PVT collector. The multi-objective optimization approach, based on the genetic algorithm, suitable for the PVT collector design optimization, was demonstrated in this paper. The Pareto front was derived for the defined optimization problem and used to define the optimal design solutions for three different operational purposes. The derived PVT design solutions were compared to the PV panel. The main focus was to find out if the PVT was still competitive with the PV panel electrical output, after maximizing its thermal exergy efficiency within the Pareto front.

Maximizing the thermal exergy efficiency resulted in the low mass flow rate, high inlet temperature and thicker insulation. These variables also increased the PV cell operating temperature, which reduces the PV cell efficiency. However, the results indicated that the yearly PVT electrical output was only 4.2% lower than from the PV panel. In this case, the PVT collector was 80% covered. Based on the simulation results with the different packing factors, the fully packed PVT collector can result in higher electrical output than from the PV panel. This fact makes the thermal exergy- driven PVT collector competitive compared to the PV panel in the building applications that require high-quality electrical and thermal output.

In the literature, Evola and Marletta [72] found that the optimal PVT inlet temperature was around 40 °C in terms of the thermal exergy efficiency. However, the multi-objective optimization results of this study showed that the inlet temperature can be lower than 40 °C to

optimize thermal exergy efficiency if the design parameters, such as air gap thickness and insulation were adjusted as well. In the Pareto front, the maximum inlet temperature was 30 °C. The results showed that compared to the typical PVT configuration, used in the energy and exergy analysis of this study, the optimization gave a new collector configuration with much lower mass flow rate, and thicker air gap and insulation. The use of a lower mass flow rate has a benefit of required lower pumping power in a building application with heat storage.

The optimization results revealed that the multi-objective optimization with the genetic algorithm can be used to define the optimal design of the PVT collector for different operational purposes.

In future work, an investigation of using the design optimization approach with the genetic algorithm to the dynamic hybrid system model including PVT collectors, energy storage and demand-side with an electric car will be conducted. A 3E (energy, exergy, economic) analysis of a hybrid system should be conducted based on yearly simulations.

Author Contributions: Conceptualization, S.K. and M.S.; methodology, S.K.; software, S.K.; validation, M.S.; formal analysis, S.K.; investigation, S.K.; resources, S.K. and M.S.; data curation, S.K.; writing—original draft preparation, S.K.; writing—review and editing, S.K. and M.S.; visualization, S.K.; supervision, M.S.; project administration, M.S.; funding acquisition, M.S. All authors have read and agreed to the published version of the manuscript.

Funding: This research was funded by Interreg V Rhin supérieur ACA-MODES project.

Acknowledgments: The authors would like to thank Interreg V Rhin supérieur ACA-MODES project for their support and funding of this research.

Conflicts of Interest: The authors declare no conflict of interest.

Nomenclature

A	area, m^2
c	specific heat, J/(kg K)
D	diameter, m
E	DC power, energy, W
Ex	exergy, W
G	solar irradiation density, W/m^2
H	thickness, m
h	heat transfer coefficient, $W/(m^2 K)$
k	thermal conductivity, W/(mK)
L	length, m
M	number of objectives
m	mass, kg
$\dot{m}$	mass flow rate, kg/s
N	number of collectors
Nu	Nusselt number
P	power, W
Pr	Prandlt number
Q	heat flux, W

Re	Reynolds number
r	packing factor
T	temperature, °C, K
T*	reduced temperature, K m^2/W
U	internal energy, J
v	wind speed, m/s
W	tube spacing, m

Greek symbols

η	efficiency
α	absorbance
(ατ)	effective absorbance
β	temperature coefficient, %/K
ε	emissivity
ξ	exergy efficiency
τ	transmittance
ρ	density, kg/m^3
σ	Stefan–Boltzmann constant, W/m^2/K^4

Subscripts

a	absorber
adh	adhesive layer
c	collector
CD	conduction
CV	convection
d	destruction
e	environment
el	electrical
f	fluid
f_{in}	fluid inlet
f_{out}	fluid outlet
g	glass cover
gap	air gap
irr	irradiation
o	outer
pv	photovoltaic
PV_g	photovoltaic glass
RD	radiation
sol	solar
ted	tedlar layer
th	thermal
tot	total
0	reference

CHAPTER 3. Exergy optimization of a multi-stage solar micro-cogeneration system

Sonja Kallio and Monica Siroux
INSA Strasbourg ICUBE, University of Strasbourg
This article is published in *IET Renewable Power Generation*
doi.org/10.1049/rpg2.12372

Abstract

This paper proposes a dynamic model of a solar-based micro-cogeneration system called photovoltaic-thermal (PVT) collector to perform a design optimization of the multi-stage PVT system. The parametric study reveals the most important design parameters influencing the water-based flat-plate PVT system performance. The analysis also shows an existing trade-off between thermal and electrical efficiencies during the PVT operation. A novel exergy-based multi-objective design optimization method is demonstrated to find a trade-off design solution of the multi-stage PVT collector which compromises between the electrical and thermal exergy efficiencies under different weather conditions. The electrical and thermal exergy efficiencies are defined to be the objective functions of the Matlab gamultiobj-function, which is a multi-objective evolutionary algorithm using non- dominated sorting genetic algorithm-II (NSGA-II). As a result of the algorithm, the Pareto optimal sets were derived that revealed the optimal solutions taking into account the trade- off nature of the optimization problem. The decision-making method called an ideal point method was used in the decision-making process to find the final optimal solutions for different weather conditions. The results revealed that the optimal number of the PVT collectors in series depended on the weather conditions and decreased from 3 to 2 if the conditions got cooler.

1. Introduction

The building sector has a high impact on greenhouse gas emissions and final energy consumption in the European Union (EU) by being the largest energy end-use sector with a share of 41% [143]. Renewable energy production is getting a stronger role in energy production. Micro combined heat and power (micro-CHP), or co-generation, systems are operating in the building sector to produce simultaneously from a single fuel source heat and power at high efficiency and close to the consumption point. The systems are used to produce on-site energy

for space heating, domestic hot water (DHW) and electricity demand. The European Parliament has defined the micro-cogeneration to be the units up to an electrical output of 50 kW [99]. However, micro-CHP commonly refers to units up to 15 kW of electrical power [20]. The renewable energy-based micro-CHP systems are in a key role in reaching the primary energy and pollutant emissions reduction targets of the EU [98].

Solar energy can be counted to be an inexhaustible source of energy, and its use does not depend on the energy markets. At the moment, solar energy is mostly deployed in the building sector in terms of photovoltaic (PV) panels and thermal collectors [30]. This separated production of electricity and heat can be combined by the technology called photovoltaic-thermal (PVT). The PVT collector is a renewable solar-based micro-cogeneration system that produces electricity by the PV module and useful heat by cooling the PV module with a coolant circulation. That leads to increased overall system efficiency but also an increasing electrical efficiency due to the decreased operation temperature of the PV module [30]. Zhang et. Al [119] argued that the most commonly used and installed PVT technologies are air- and water-based collectors. The popularity of the water-based PVT collector is increasing due to its ability to increase the electrical efficiency and better thermal energy utilization in DHW and space heating. The highly dynamic and weather dependent operation of a single PVT collector is widely studied in the literature, and a range of theoretical PVT models has been introduced and validated in [30, 83, 107, 126, 127, 144]. However, the N number of the PVT collectors can be connected in series to increase the coolant outlet temperature and produce more thermal energy at a higher quality than from a single collector. This kind of multi-stage PVT collector can be used in several applications. In the building sector, the multi-stage PVT collector can be integrated with energy storages, such as thermal storage, battery systems and electrical vehicles (EV). On the other hand, the multi-stage PVT collector is useful for other applications as well. Sahota and Tiwari [145] conducted a review on N series-connected PVT systems. They explored different PVT applications, such as flat plate PVT collectors with solar still and greenhouse dryer. Liang et al. [146] studied the performance of PVT collectors connected in series. They performed a numerical and experimental study, in which six PVT collectors were connected in series resulting in a total amount of 36 collectors. They analyzed coolant fluid outlet temperature, PV module temperature, and electrical and thermal efficiencies. Dubey and Tiwari [128] studied flat plate water PVT collectors in series and calculated energy and exergy yield by varying the

number of collectors under four different weather conditions in India. They discovered that increasing the mass flow and the number of collectors increased thermal energy gain but only until a certain point.

The performance of the multi-stage PVT system can be analyzed in terms of energy and exergy analysis. The energy analysis concerns only the quantity aspects related to the energy production of the system neglecting the quality aspect. For this reason, the exergy method is used to complete the energy assessment of the system. The exergy method takes into account the quality of the produced energy as an ability to work at the temperature, at which a certain energy flow is available. Evola and Marletta [72] performed an exergy-based optimization of a flat plate water-based PVT system. They concentrated on optimizing the coolant inlet temperature in order to maximize the overall exergy efficiency of the system at any operating condition. They discovered that low inlet temperature resulted in very high overall energy efficiency, but in terms of exergy, this is not recommended. The optimized inlet temperature and overall exergy efficiency varied between 30–42 °C and 14–15%, respectively, depending on the mass flow rate and the weather conditions. Tiwari et al. [147] conducted an overall exergy analysis of the N-PVT compound parabolic concentrator collector for constant collection temperature. The system was applicable to the absorption refrigeration system. They concluded that using an exergy approach in design optimization is highly recommended.

In recent years, the conventional correlation- and simulation-based design optimization methods have got alongside new design methods using nature-inspired artificial intelligence methods, such as genetic algorithm (GA), evolutionary algorithm and particle swarm optimization (PSO). The multi-objective optimization techniques are used to solve optimization problems where the objectives have a trade-off with each other. In terms of the PVT collector performance, the electrical efficiency suffers if the thermal efficiency is maximized and the other way round. The energy-based multi-objective optimization of the water-based PVT collector performance parameters with the non-dominated sorting genetic algorithm (NSGA-II) was performed in [30, 130]. The Pareto front was obtained for different optimization problems to illustrate the trade-off between solutions. The multi-objective optimization of the air-based PVT system with the NSGA-II algorithm was investigated in [131]. The single objective optimization of the PVT collector with the genetic algorithm was performed in [133] to maximize the overall exergy efficiency.

Within the given framework, there is a lack of studies considering the multi-objective optimization of the number of collectors in a PVT series based on the genetic algorithm and exergy approach. Additionally, there is a research question if the optimal number of the PVT collectors varies according to the weather conditions.

This paper proposes a dynamic model of a PVT collector with a crystalline silicon roll-bond collector in Matlab/Simulink. The model is extended to describe a multi-stage PVT collector. Energy and exergy analysis is conducted with the simulation model, and the most influencing design variables are identified and evaluated with a parametric study. Due to fact that the optimal design of the multi-stage PVT system cannot be defined with the simulations alone, the multi-objective optimization of the electrical and thermal exergy efficiencies with the non-dominated sorting genetic algorithm (NSGA-II) is conducted and the Pareto optimal set is derived in order to show the set of the optimal solutions taking into account the trade-off between exergy efficiencies.

The rest of the paper is organized as follows. In the second section, the description of a single PVT collector is presented with the geometrical, thermos-physical and optical properties followed by the modelling approach of a single collector. The main governing equations of the model are presented. Additionally, the exergy approach is introduced. The multi-objective optimization method is presented in the third section with the objective functions. In the fourth section, the results of the parametric study and optimization are presented and discussed. Finally, the main conclusion is drawn in the fifth section.

1.1 Literature review

In this section, more background on research of the PVT collectors is provided. The current water-based PVT technologies face a challenge in which the electrical efficiency decreases as the operating temperature increases. On the other hand, higher operating temperature increases thermal efficiency. In [121, 122], novel PVT technologies were investigated to overcome this problem. The solution was to decouple thermally the electrical and thermal units of the collector using an optical coolant fluid layer above the PV modules. This layer worked simultaneously as a spectrum splitter of solar radiation and as a coolant fluid of the system, and its spectral properties were modified using nanofluids. The layer absorbed ultraviolet radiation and part of infrared radiation and transmitted to the PV modules only the useful

infrared and visible radiation for electricity production. The results were promising, and the spectrum splitting increased the efficiency of the PVT collector.

The multi-stage PVT collector is useful for multiple applications where distributed micro-scale energy production is required, such as desalination. Giwa et al. [148] reviewed comprehensively the polygeneration in different desalination approaches using flat plate and concentrated PVT systems. The integration of the PVT systems with desalination showed increased efficiency. From the economical point of view, the installation costs were higher than PV systems. However, the PVT systems provided cost reduction and reduced environmental impacts in the long term. Anand et al. [149] presented as well a review on PVT integrated desalination technologies. They concluded that the overall performance of the PVT coupled desalination system is better than coupling with separated energy production by PV and solar thermal collectors.

In terms of serial connection, an interesting approach is to connect a flat plate PVT collector in series with another type of solar technology, such as a flat plate solar thermal collector or concentrated PVT to increase thermal and electrical output. Ma et al. [150] studied a novel series connection of a PVT and solar thermal collector (PVT-ST) to produce electricity and heat at an even higher quality level. They compared the serial connection to a glazed and unglazed PVT and a PV panel. As a result, the PVT-ST system was competitive in terms of electrical efficiency and had significantly higher thermal and primary energy savings efficiency. Kazemian et al. [151] conducted a similar study of the PVT-ST system compared to other solar technologies and used the multi-objective Taguchi method to optimize operation variables. They generated 3D-models of each system by SolidWorks software to conduct the study. The results indicated 19% higher daily thermal power of PVT-ST compared to a PVT system but the electrical power was equal.

The exergy analysis is an effective way to investigate the true potential of an energy system. In terms of PVT application, Sarhaddi [152] conducted an exergy analysis of a PVT connected solar still system. The results of the study showed that two PVT collectors in series improved the most the overall exergy efficiency of the PVT-solar still system.

2. Methodology

2.1 Description of the PVT collector

A water-based PVT collector with a direct flow geometry and roll bond channels is simulated, analyzed and optimized in this study. Figure 3-1 shows the geometry and cross-section of the PVT collector [101]. The water-based PVT collector is investigated because they achieve higher overall efficiency than air-based collectors due to the higher heat capacity of water [32]. High efficient PV cells are still relatively expensive and in this study, the PVT collector has a crystalline silicon PV cell with a reference electrical efficiency (η_{STC}) of 18.7% at the reference operating temperature (T_{ref}) of 25°C. The temperature coefficient (β_T) and packing factor (r_c) are 0.5%/K and 0.95, respectively. The diameter of the tubes is 8 mm and for the initial simulation conditions, the number of tubes is 11. The initial inlet temperature of the coolant fluid is 20°C and the coolant mass flow 0.017 kg/s (60 kg/h). Table 3-1 summarizes the main geometrical, thermo-physical, optical properties and the parameters of the single PVT collector used in the simulation and optimization.

Table 3-1: The main geometrical, thermo-physical and optical properties of the single PVT collector.

Property	Glass	Air gap	PV	Thermal absorber	Unit
Emissivity (ε)	0.9	-	0.96	-	-
Absorbance (α)	0.1	-	0.9	-	-
Transmittance (τ)	0.93	-	-	-	-
Thickness (H)	0.004	0.02	0.006	0.001	m
Area (A)	2	-	1.9	2	m^2
Density (ρ)	2200	-	2330	2699	kg/m^3
Specific heat (c)	670	-	900	800	J/(kgK)
Thermal conductivity (k)	1.1	-	140	237	W/(mK)

Property	Fluid	Insulation	Unit
Thickness (H)	-	0.04	m
Area (A)	-	2	m^2
Density (ρ)	1050	16	kg/m^3
Specific heat (c)	3605	1120	J/(kgK)
Thermal conductivity (k)	0.615	0.035	W/(mK)

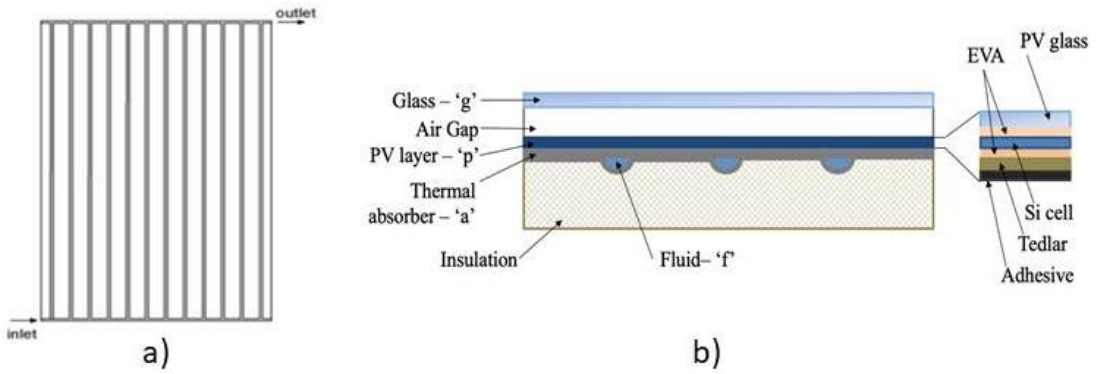

Figure 3-1: *The single PVT collector: (a) Direct flow collector geometry, (b) Cross section of the PVT collector [27].*

The described single PVT collector is multiplied to present a multi-stage PVT collector, in which N number of collectors is connected in series in order to solve a problem of low-temperature heat production of a single PVT collector. The working principle of the multi-stage collector is shown in Figure 3-2. The coolant mass flow is fed into the first PVT collector, and heat is recovered. The outlet temperature of the first collector is the inlet temperature of the second collector. The coolant temperature is increased by each collector in series, and the thermal exergy efficiency is increased until a certain point.

In reality, the electrical efficiency would be the highest in the collectors at the beginning of the series and the lowest at the end of the series because the temperature of the coolant flow increases towards the end of the series. However, due to simplicity, a global model of the multi-stage PVT collector is used to solve the optimization problem of this study. The model does not calculate the coolant temperature after each PVT or the collector specific electrical efficiency. However, the area, thermal mass and the tube length of the collector array are always increased or decreased by the geometry of the single collector described above.

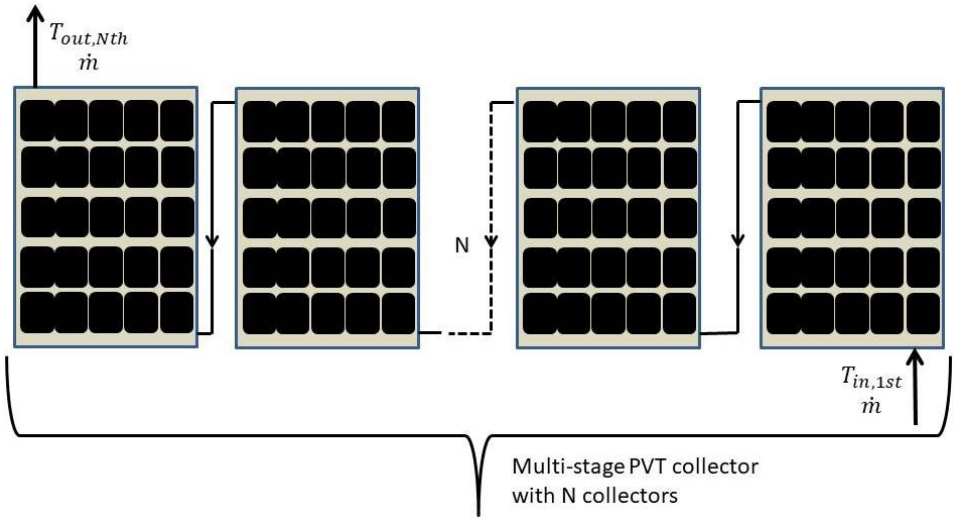

Figure 3-2: *The working principle of the multi-stage PVT collector.*

2.2 Modelling approach for energy and exergy analysis

The numerical modelling of a single water-based PVT collector is based on the following main governing equations of the energy balance in the various layers of the collector. The more detailed derivation of the governing equations and the validation of the model is presented in [83] where the used heat transfer coefficient are defined as well.

The glass cover (g):

$$m_g \times c_g \times \frac{dT_g}{dt} = h_{g-e,CV} \times A \times \left(T_e - T_g\right) + h_{g-e,RD} \times A \times \left(T_{sky} - T_g\right) + h_{g-pv,CV} \times A \times \left(T_{pv} - T_g\right) + h_{g-pv,RD} \times A \times \left(T_{pv} - T_g\right) + A \times \alpha_g \times G_{irr} \quad (1)$$

The photovoltaic layer (pv):

$$m_{pv} \times c_{pv} \times \frac{dT_{pv}}{dt} = h_{g-pv,CV} \times A \times \left(T_g - T_{pv}\right) + h_{pv-g,RD} \times A \times \left(T_g - T_{pv}\right) + h_{pv-a,CD} \times A_{pv-a} \times \left(T_a - T_{pv}\right) + h_{pv-t,CD} \times A_{pv-t} \times \left(T_t - T_{pv}\right) + G_{irr} \times A \times (\alpha\tau)_{pv} - G_{irr} \times A \times r_c \times \eta_{pv(T)} \quad (2)$$

In which r_c is the ration of the cell area to the PVT collector area, in the other words, packing factor. The electrical efficiency $\eta_{pv(T)}$ depends on the photovoltaic layer temperature T_{pv}. Due to this, the electrical efficiency of the PV depends linearly on the temperature T_{pv}, the

temperature coefficient β_{pv} and on the efficiency at standard conditions T_{ref}. The efficiency is calculated according to the following relation:

$$\eta_{pv(T)} = \eta_{STC} \times \left[1 - \beta_{pv} \times \left(T_{pv} - T_{ref}\right)\right] \tag{3}$$

Additionally, the photovoltaic layer temperature T_{pv} depends on the following parameters based on the geometry of the collector [83, 107]:

$$A_{pv-a} = A\left(1 - \frac{D_o}{W}\right) \tag{4}$$

$$h_{pv-t,CD} \times A_{pv-t} = \frac{H_{pv} \times L}{\frac{W \times k_{pv}}{2} + \frac{H_{adh}}{k_{adh}} \times \frac{H_{pv}}{D_o}} \tag{5}$$

$$m_{pv} = \rho_{pv} \times H_{pv} \times A \times r_c \tag{6}$$

The absorber layer (a):

$$m_a \times c_a \times \frac{dT_a}{dt} = h_{a-pv,CD} \times A_a \times \left(T_{pv} - T_a\right) + h_{a-t} \times A_{a-t} \times (T_t - T_a) + h_{a-i,CD} \times A_{a-i} \times (T_i - T_a) \tag{7}$$

The tube bonding (t):

$$m_t \times c_t \times \frac{dT_t}{dt} = h_{t-pv,CD} \times A_{pv-t} \times \left(T_{pv} - T_t\right) + h_{t-a} \times A_{a-t} \times (T_a - T_t) + h_{t-i,CD} \times A_{t-i} \times (T_i - T_t) + h_{t-f} \times A_{t-f} \times (T_f - T_t) \tag{8}$$

The insulation layer (i):

$$m_i \times c_i \times \frac{dT_i}{dt} = h_{a-i,CD} \times A_{a-i} \times (T_a - T_i) + h_{t-i,CD} \times A_{t-i} \times (T_t - T_i) + h_{i-e,CD+CV} \times A \times (T_e - T_i) \tag{9}$$

The coolant fluid (f):

$$m_f \times c_f \times \frac{dT_f}{dt} = h_{t-f} \times A_{t-f} \times \left(T_a - T_f\right) + \dot{m} \times c_f \times \left(T_{f,in} - T_{f,out}\right) \tag{10}$$

The Equations (1-10) are implemented into Matlab/Simulink with details to assess the energy and exergy performance of the PVT collector. In the case of multiple PVT collectors, the area, thermal mass of each layer and the tube length of a single panel are multiplied by the number of the collectors in order to assess the performance of the PVT series.

Compared to energy analysis, the exergy analysis is based on the Second Law of Thermodynamics and takes into account the quality of the produced energy.

The exergy balance of the system can be expressed as follows:

$$\sum Ex_{in} - \sum (Ex_{th} + Ex_{el}) = \sum Ex_d \tag{11}$$

In the case of the PVT collector, the exergy flow to the system Ex_{in} comes from the solar irradiation. However, solar irradiation is not seen as pure exergy and due to this a conversation coefficient is included in the calculation of the PVT incoming exergy [29]:

$$Ex_{in} = A \times N_c \times G_{irr} \times \left(1 - \frac{4}{3}\frac{T_0}{T_{sol}} + \frac{1}{3}\left(\frac{T_0}{T_{sol}}\right)^4\right) \tag{12}$$

In Eq. (9) T_{sol} is the solar temperature and T_0 is the reference temperature, which according to the literature, should be a constant, for example, T_0 = 20°C, T_0 = 25°C or the minimum temperature of the month. In this study, T_0 = 20°C is selected. N_c is the number of collectors.

Electrical energy is seen as pure exergy, but the exergy content of thermal energy depends on the temperature at which the heat is made available. In the model, the exergy of thermal (Ex_{th}) and electrical (Ex_{el}) energy are calculated as follows, respectively [29]:

$$Ex_{th} = \dot{m} \times c_f \times \left[(T_{out} - T_{in}) - T_0 \times ln\frac{T_{out}}{T_{in}}\right] \tag{13}$$

$$Ex_{el} = \eta_{pv} \times G_{irr} \times r_c \times A \times N_c \tag{14}$$

By Equations (12-14) the both thermal (ξ_{th}) and electrical exergy (ξ_{el}) efficiencies and the overall exergy efficiency (ξ) of the PVT collector can be calculated as follows:

$$\xi_{th} = \frac{Ex_{th}}{Ex_{in}} \tag{15}$$

$$\xi_{el} = \frac{Ex_{el}}{Ex_{in}} \tag{16}$$

$$\xi = \frac{Ex_{el} + Ex_{th}}{Ex_{in}} \tag{17}$$

The following assumptions are taken into account in the modelling:

- The temperature distribution is uniform in the layers and in the PVT collectors in series.
- It is assumed that there are no heat losses through the edges.
- The optical and thermal properties of the materials and fluids are constant.
- No surrounding shading or dust is taken into account.
- The thermal resistance between the layers is negligible.

3. Multi-objective optimization of the PVT collector

The energetic and exergetic performance analyses based on the simulations of the thermal PVT model show a trade-off between performance parameters, such as thermal and electrical energy and exergy efficiencies as functions of various decision variables. The simulation results have shown a trade-off between thermal and electrical exergy efficiencies of the PVT collector. The electrical efficiency of the PV panel decreases when the operating temperature of the collector increases. On the other hand, increased operating temperature leads to higher thermal exergy efficiency. This means that both efficiencies cannot be directly maximized at the same time but a solution has to be found, which satisfies both trade-off objectives (electrical and thermal exergy efficiencies) at the same time. The thermal simulations of the PVT system alone don't provide a set of optimal solutions of decision variables in terms of thermal and electrical exergy efficiencies. Instead of simulations alone, the set of optimal solutions can be found by using the multi-objective optimization (MOO) technic using an evolutionary algorithm.

3.1 Multi-objective optimization using gamultiobj-function

In this paper, the Matlab function called gamultiobj of Global Optimization Toolbox is used to run the multi-objective optimization of the multi-stage PVT collector. The gamultiobj-function creates a set of optimal solutions in the space of decision variables on the Pareto front. The function uses a controlled, elitist genetic algorithm, which is a variant of NSGA-II [140].

Generally, the multi-objective optimization problem of two or more trade-off objectives is described mathematically as follows [30]:

$$\begin{gathered}\text{Minimized/Maximized } f_m(x),\ m = 1,2,\ldots,\mathrm{M};\\ \text{Subject to } g_j(x) \geq 0,\ j = 1,2,\ldots,\mathrm{J};\\ h_k(x) = 0,\ k = 1,2,\ldots,\mathrm{K};\\ x_i^{(L)} \leq x \leq x_i^{(U)},\ i = 1,2,\ldots,\mathrm{n};\end{gathered}$$

In this formulation, the objective functions are minimized or maximized subject to certain constraints.

In this work, the overall electrical and thermal exergy efficiencies are two objectives to be optimized. Due to the fact that the NSGA-II is a minimization tool the objective functions are multiplied by (-1) in order to get the maximum values [30]. The 2-dimensional optimization problem of the exergy efficiencies is formulated as follows:

To minimize:

$$\mathrm{f}_1(\mathbf{x}) = -\frac{\mathrm{Ex_{el}}}{\mathrm{Ex_{in}}} = -\frac{\eta_{\mathrm{STC}} \times \left[1 - \beta_{\mathrm{PV}} \times \left(\mathrm{T_{pv}} - \mathrm{T_{ref}}\right)\right] \times \mathrm{G_{irr}} \times \mathrm{A_{pv}} \times N_c}{\mathrm{A} \times N_c \times \mathrm{G_{irr}} \times \left(1 - \frac{4}{3}\frac{\mathrm{T_0}}{\mathrm{T_{sol}}} + \frac{1}{3}\left(\frac{\mathrm{T_0}}{\mathrm{T_{sol}}}\right)^4\right)} = -\xi_{el} \tag{18}$$

$$\mathrm{f}_2(\mathbf{x}) = -\frac{\mathrm{Ex_{th}}}{\mathrm{Ex_{in}}} = -\frac{\dot{\mathrm{m}} \times \mathrm{c_f} \times \left[\left(\mathrm{T_{out}} - \mathrm{T_{in}}\right) - \mathrm{T_0} \times \ln\frac{\mathrm{T_{out}}}{\mathrm{T_{in}}}\right]}{\mathrm{A} \times N_c \times \mathrm{G_{irr}} \left(1 - \frac{4}{3}\frac{\mathrm{T_0}}{\mathrm{T_{sol}}} + \frac{1}{3}\left(\frac{\mathrm{T_0}}{\mathrm{T_{sol}}}\right)^4\right)} = -\xi_{th} \tag{19}$$

where ξ_{el} and ξ_{th} are the electrical and thermal exergy efficiencies, respectively. The electrical exergy efficiency is influenced by the number of the PVT collectors in terms of the thermal mass and tube length according to Eq. (2-6).

In terms of exergy efficiency, the sensitivity analysis has shown that the most sensible variables of the multi-stage PVT collector operation are the cooling-water mass flow, inlet temperature and number of collectors. Table 3-2 presents the decision variables to be optimized and their upper and lower bounds to be used in the optimization.

Table 3-2: Decision variables for multi-objective optimization problem.

Symbol	Decision variable	Bounds	Unit

$\dot{m}$	Mass flow rate	$0.008 \leq x(1) \leq 0.042$	kg/s
N_c	No. of collectors	$1 \leq x(2) \leq 10$	
T_{in}	Inlet temperature	$15 \leq x(3) \leq 40$	°C

4. Results and discussion

The simulation-based multi-objective optimization process was conducted with the PVT model in Matlab/Simulink. The main objective of the optimization was to find an optimal number of PVT collectors in series to satisfy the operational purpose of the multi-stage PVT collector. First, the decision variables were varied, and the initial population and score matrixes for the genetic algorithm were generated by the simulation model. These matrices were given for the gamultiobj-function of Global Optimization Toolbox, which started the iterative process by evaluating the fitness functions with the simulation model and making selection, crossover and mutation of the population. Based on this process, a new population or generation was created. The new generations were created as long as a stopping criterion was met. The criterion was selected to be the number of generations and set to be 100 generations. The population size was 50. The multi-objective optimization process is described in Figure 3-3.

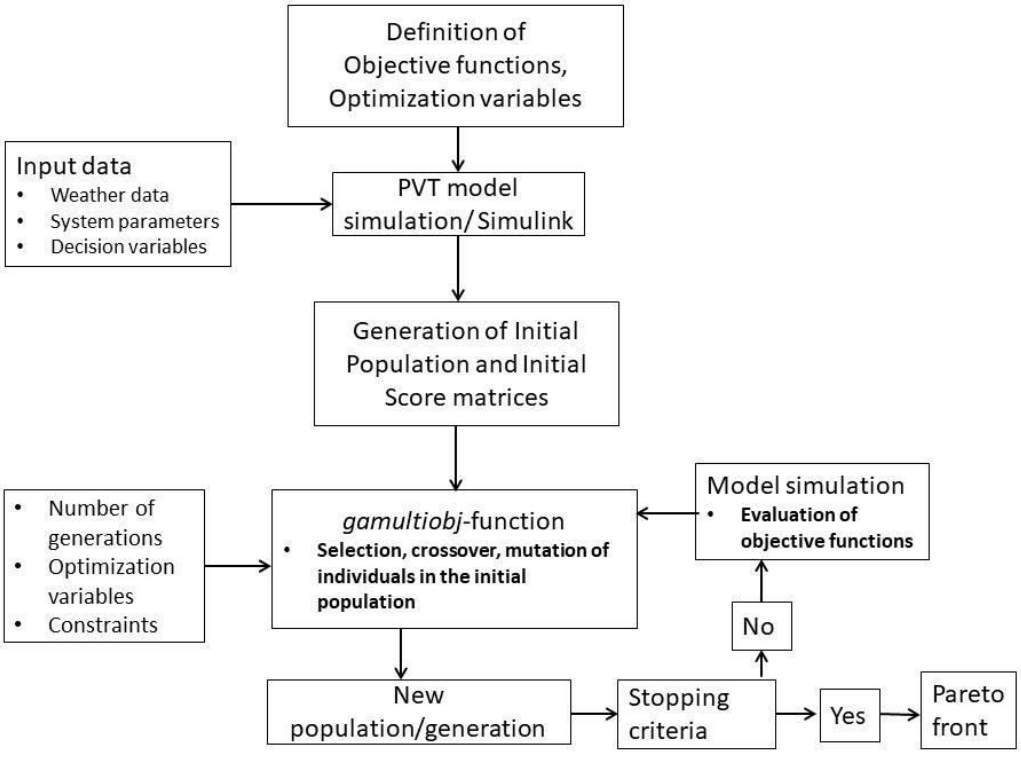

Figure 3-3: *The simulation-based multi-objective optimization process.*

The optimization was conducted with the weather data concerning three steady-state climate conditions: hot summer day conditions, of which solar irradiation was 1000 W/m^2, ambient temperature 30°C and wind speed 1 m/s; medium conditions with 800 W/m^2, 25°C and 1 m/s; and cooler summer conditions with 600 W/m^2, 18°C and 5 m/s. According to [153], these weather conditions can be addressed for different European locations, such as the southern Mediterranean, central and northern Europe, respectively.

Figure 3-4 presents the simulated temperatures of the different PVT collector layers, ambient temperature and solar irradiation over a summer day.

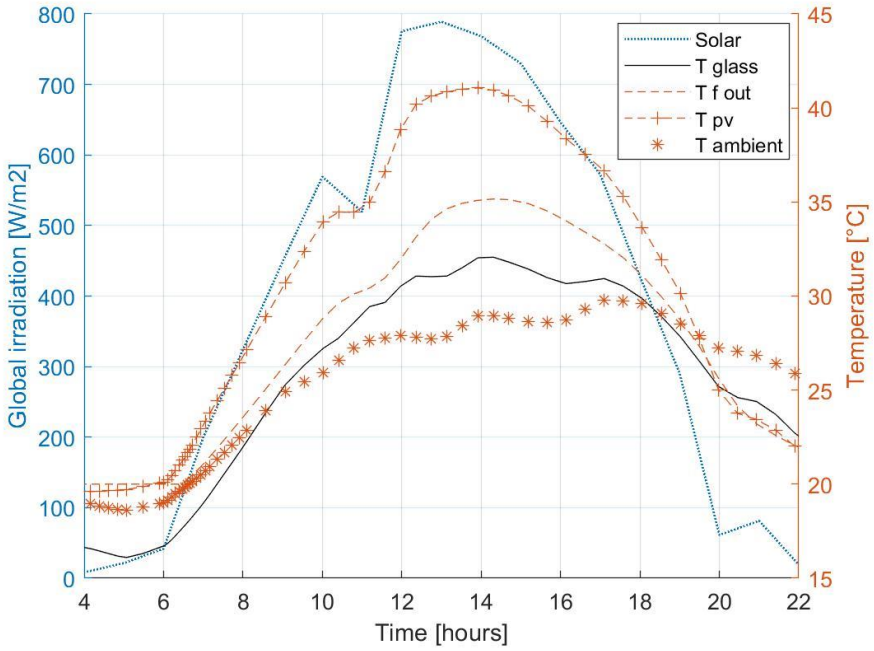

Figure 3-4: *The temperatures of the PVT layers, the solar irradiation and ambient temperature.*

The parametric study was conducted. The PVT collector was investigated under steady-state medium weather conditions of G_{irr} = 800 W/m^2, T_e = 25°C and v = 1 m/s. The used simulation parameters of the PVT were presented in Section 2. Additionally, when the number of PVT collectors was increased, the coolant inlet temperature of 30°C was used in the simulation. The relation of the decision variables to the energy and exergy efficiencies are shown in Figure 3-5 and Figure 3-6. The relation of the PVT collectors in series to the efficiencies and outlet water temperature is presented in Figure 3-7, Figure 3-8 and Figure 3-9. The mass flow rate had a similar relation to the thermal energy and exergy efficiencies. Both efficiencies decreased when the mass flow increased. However, if the number of the collectors and coolant inlet temperature

were increased, the thermal energy and exergy efficiencies behaved differently. This is shown in Figure 3-8.

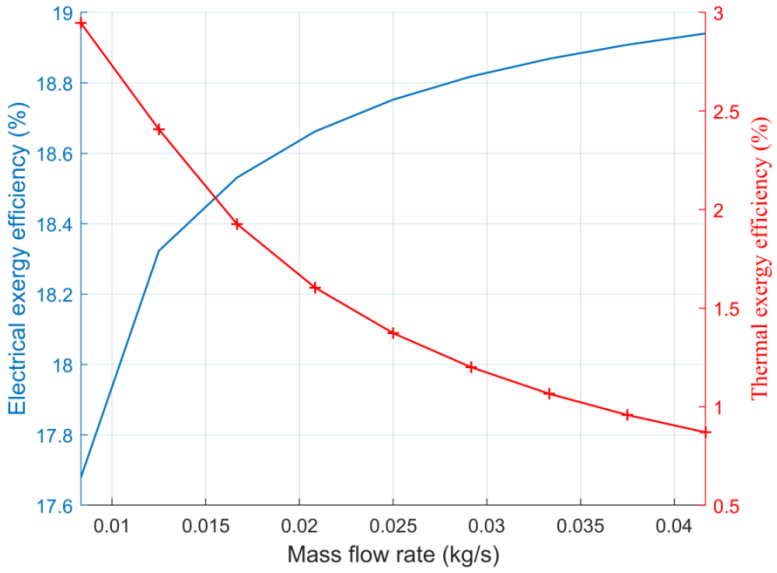

Figure 3-5: *The variation of electrical and thermal exergy efficiency with the coolant mass flow rate.*

Figure 3-5 shows the trade-off nature of the PVT collector operation. Increasing the mass flow rate of the coolant fluid, increased the electrical exergy efficiency due to the stronger cooling effect. However, at the same time, thermal exergy efficiency was decreased. Due to this relation, a multi-objective optimization was used to optimize the design of the multi-stage PVT collector. Table 3-2 presents the selected decision variables of the optimization problem.

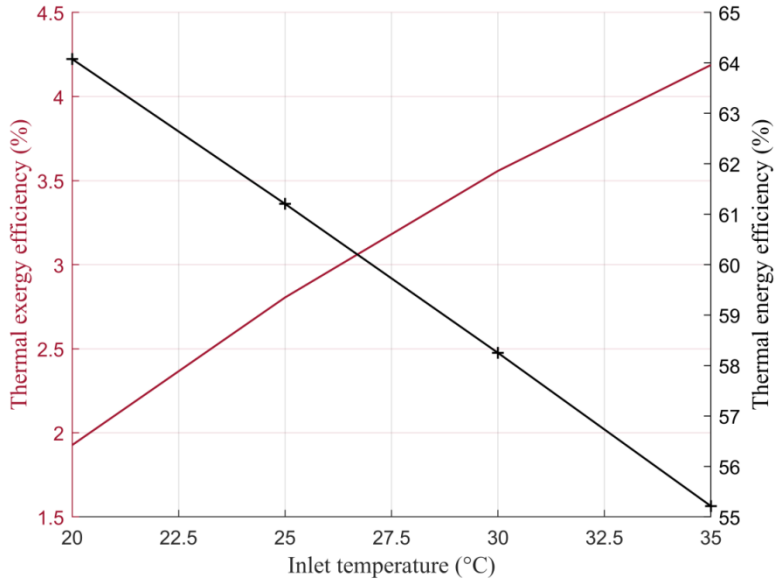

Figure 3-6: *The variation of thermal exergy and energy efficiency with coolant inlet temperature.*

Figure 3-6 reveals that increasing the inlet temperature of the coolant fluid increased the thermal exergy efficiency but decreased thermal energy efficiency. Additionally, the electrical efficiency suffers when increasing the inlet temperature because of the higher operating temperature.

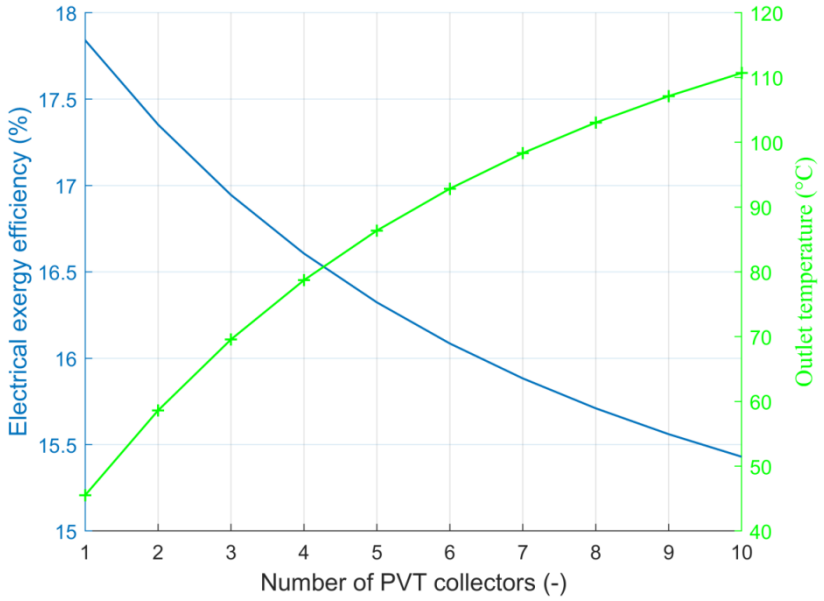

Figure 3-7: *The variation of electrical exergy efficiency and the coolant outlet temperature with the number of the PVT collectors.*

Figure 3-7 presents the increasing coolant outlet temperature and decreasing electrical efficiency when the number of PVT collectors in series was increased. The electrical efficiency was decreased because of the higher operating temperature of the multi-stage PVT collector. Increasing the temperature level of the coolant outlet flow with additional PVT collectors leads to the higher quality of the produced thermal energy. However, there is a certain optimal point to increase the number of collectors although the outlet temperature increases. Figure 3-8 presents the thermal exergy and energy efficiencies with the additional PVT collectors.

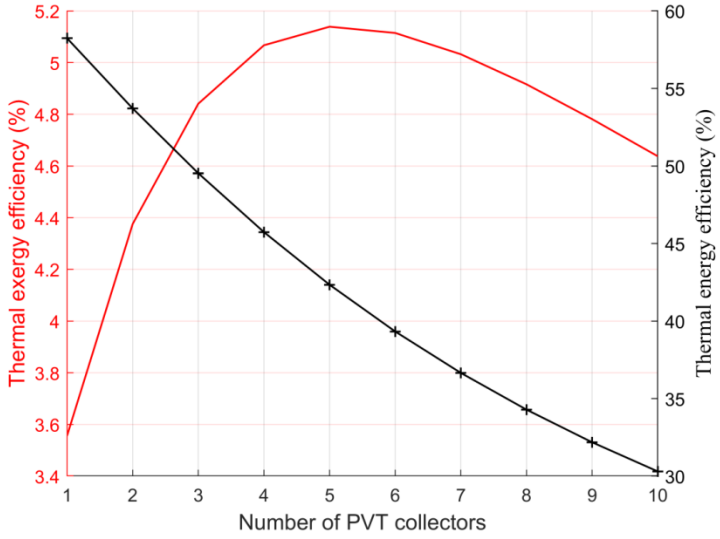

Figure 3-8: *The variation of thermal exergy and energy efficiency with the number of the PVT collectors in series.*

The thermal energy efficiency decreased if the number of collectors was increased due to the increased total collector area and its relation to the gained outlet temperature. However, the exergy approach takes into account the quality of the produced energy and the additional collectors increased the thermal exergy efficiency until a certain point. This point was also influenced by the coolant inlet temperature. Figure 3-9 presents the thermal exergy efficiency in terms of the inlet temperature and the number of collectors in series.

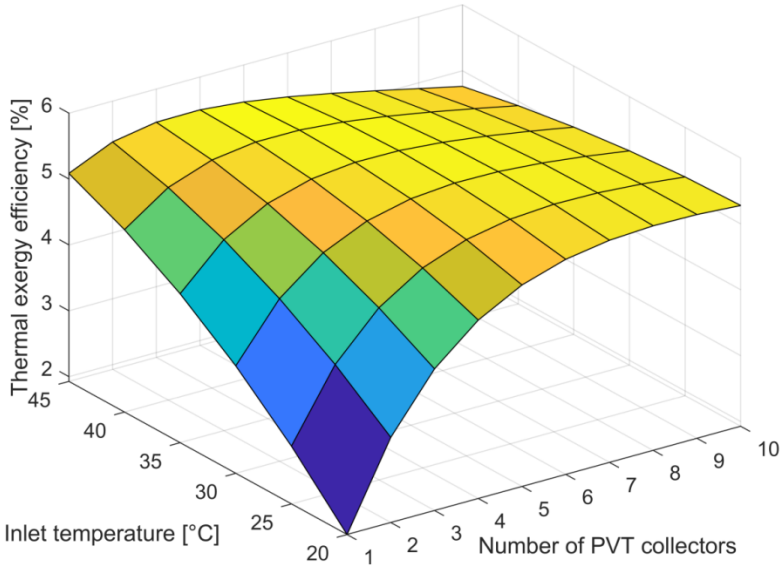

Figure 3-9: *The variation of the thermal exergy efficiency in terms of the coolant inlet temperature and the number of the PVT collectors.*

Figure 3-9 reveals that the lower coolant inlet temperature required more PVT collectors in series to achieve higher thermal exergy efficiency. If the inlet temperature was increased, the relatively smaller number of the collectors led to higher thermal exergy efficiency.

The parametric study revealed the relations of the decision variables to the performance of the multi-stage PVT system. It revealed the trade-off nature of the PVT operation in terms of thermal and electrical performance. The design of the multi-stage PVT collector was optimized in terms of the thermal and electrical exergy efficiencies as objective functions in order to maximize the quality of the produced energy. The optimization was performed by using gamultiobj-function of Matlab Global Optimization Toolbox. The function is based on NSGA-II algorithm. The set of optimal solutions called Pareto front was obtained with the generation number of 100 and the population size of 50. Figure 3-10 presents the obtained Pareto front of the optimal solutions under the medium weather conditions of 800 W/m^2, 25°C and 1 m/s.

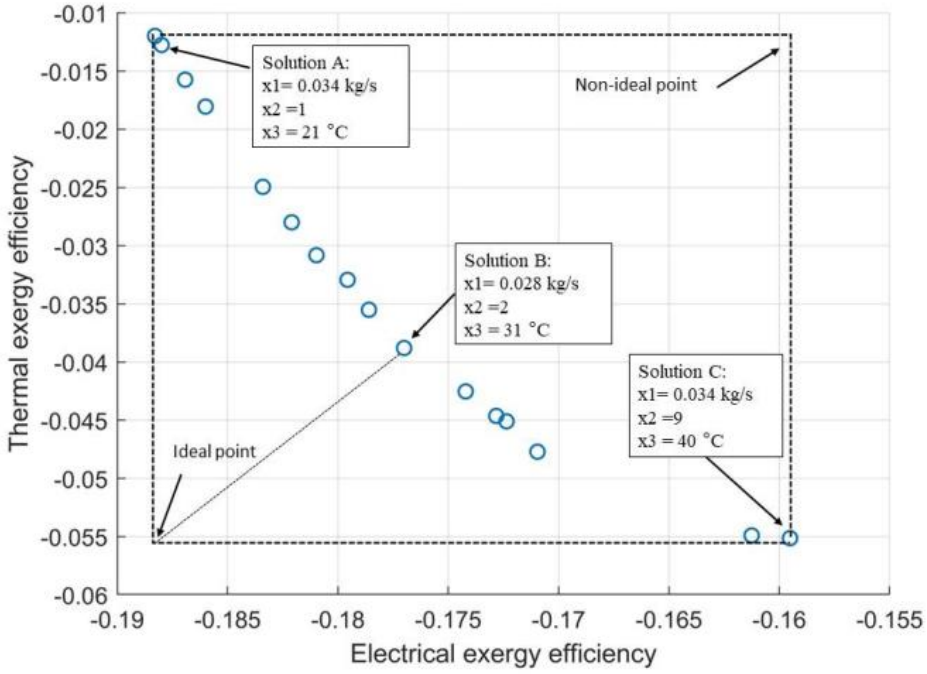

Figure 3-10: *The Pareto optimal front in the objective space of the electrical and thermal exergy efficiencies.*

The decision variable values are shown for three selected solutions. The values of each solution are presented in Table 3-3. The values of the decision variables show the same behavior as in the parametric study. This can be seen in Figure 3-11 and Figure 3-12 where each optimal solution of Table 3-3 is presented in terms of electrical and thermal exergy efficiency.

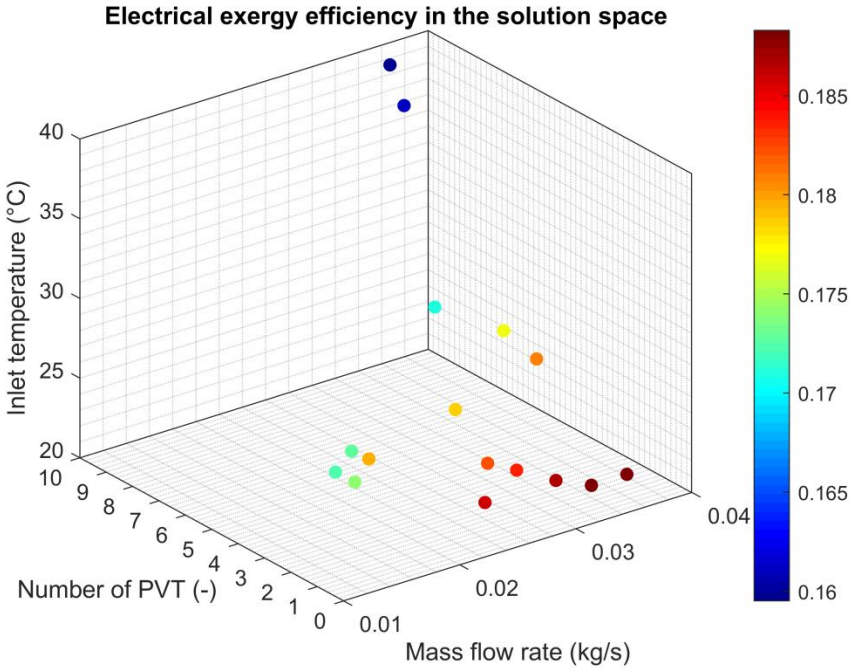

Figure 3-11: *The set of optimal solutions from Table 3-3 in terms of the electrical exergy efficiency*

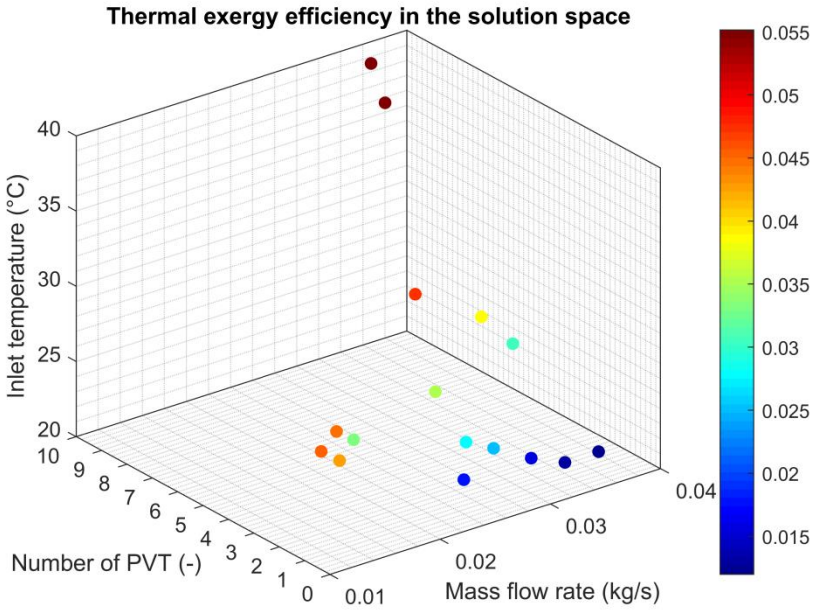

Figure 3-12: *The set of optimal solutions from Table 3-3 in terms of the thermal exergy efficiency.*

In Figure 3-11 the electrical exergy efficiency was the highest in the optimal solutions with the high coolant flow and low number of the PVT collectors. The solutions with the high inlet temperature resulted in the lowest electrical exergy efficiency.

In Figure 3-12 the thermal exergy efficiency was the highest if the optimal solution had the high inlet temperature and high number of the PVT collectors in series.

The results revealed that the number of collectors in the set of optimal solutions varied from 1 to 9. The higher number of the collectors resulted in the higher thermal exergy efficiency and the lower number to the higher electrical efficiency. The Pareto front showed a trade-off of the different solutions in which the electrical exergy efficiency varied from 15.95% to 18.8% and the thermal exergy efficiency from 1.2% to 5.5%. If electricity production is the priority of operating the multi-stage PVT system, the decision-maker can select the solution with the higher electrical exergy efficiency by increasing the coolant mass flow rate and decreasing the inlet temperature. On the other hand, the higher thermal exergy efficiency can be achieved by increasing the number of the PVT collectors and increasing the inlet temperature. The Pareto front does not show a single optimal solution but a set of solutions presented in Figure 3-10 - Figure 3-13 that can be used to help decision-makers to design the optimal multi-stage PVT system depending on the purpose.

Figure 3-13 presents the overall exergy efficiency of each solution in Table 3-3 according to Eq. 17.

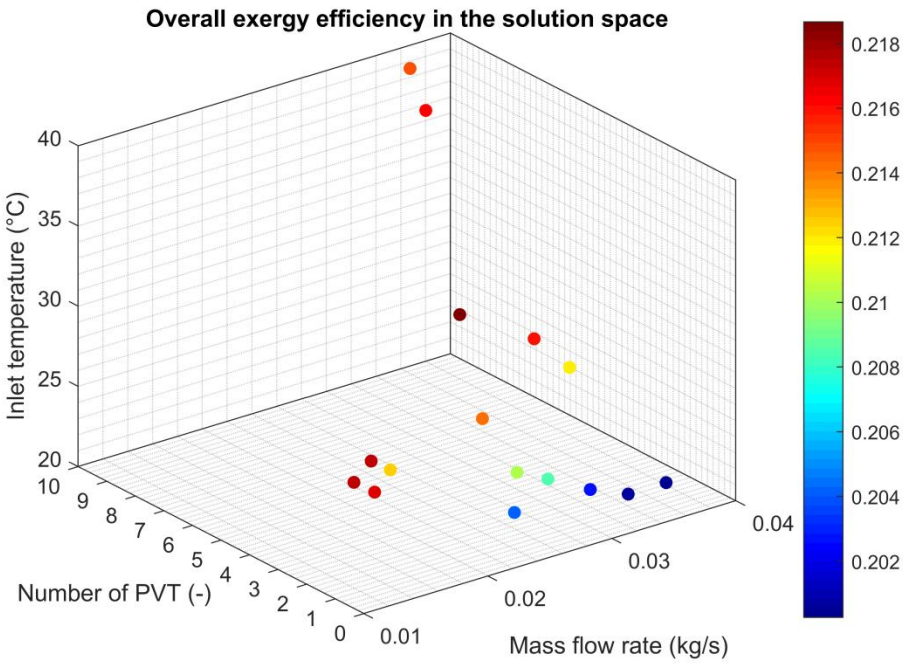

Figure 3-13: *The set of optimal solutions from Table 3-3 in terms of the overall exergy efficiency.*

The overall exergy efficiency varied from 20.03% to 21.87% between the solutions. The results revealed a solution which maximizes the overall exergy efficiency by having the inlet temperature of 31 °C, 4 collectors in series and the mass flow rate of 0.0269 kg/s. This solution results to electrical, thermal and overall exergy efficiencies of 17.1%, 4.77% and 21.87%, respectively.

The decision-making process is required to select the final optimal solution from the set of optimal solutions. A hypothetical point called an ideal point can be used to help the decision-makers [154]. At this point, marked in Figure 3-10, both objectives have their independent optimal values, but it is not a feasible solution in the multi-objective optimization and not located on the Pareto front. However, the final optimal solution might be the closest point of the Pareto front to the ideal point. In this case, Solution B in Figure 3-10 would be the final optimal solution if the decision-maker does not have any particular desire to maximize electrical or thermal exergy efficiency within the Pareto front optimal solutions. On the other hand, in the case of PVT collectors, the decision makers can select the final solution which maximizes the overall exergy efficiency showed in Figure 3-13. However, in this case, the ideal point method in Figure

3-10 did not result in the same solution but to the solution with only 0.3% lower overall exergy efficiency.

The optimization was performed under three different weather conditions cold, medium and hot to see an impact of the conditions on the Pareto optimal solutions. In Figure 3-14 are presented three Pareto fronts under different weather conditions.

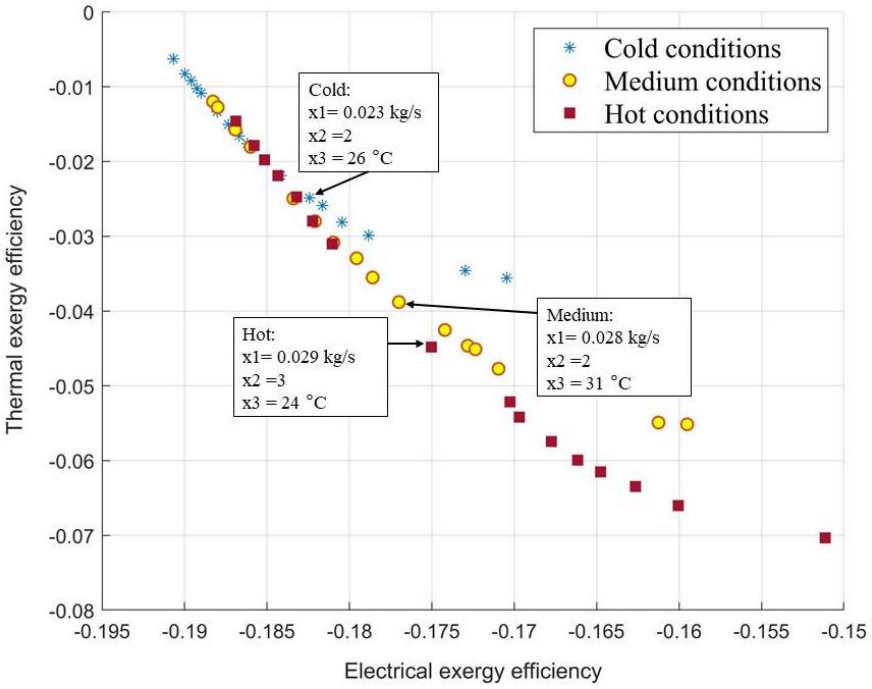

Figure 3-14: *The Pareto optimal front for the electrical and thermal exergy efficiencies under three different steady-state weather conditions.*

Figure 3-14 shows that the set of optimal solutions was different depending on the weather conditions. In terms of exergy efficiency, it seems to be beneficial to select the number of PVT collectors in series depending on the weather conditions of the system location. However, the different Pareto fronts had also an area where they overlap each other. This combined area of the Pareto front rather maximizes the electrical exergy efficiency than thermal exergy efficiency within the objective space. The highest electrical exergy efficiency of 19.1% was reached under cold conditions and the highest thermal exergy efficiency of 7% was reached under hot conditions. The weather conditions had an impact on the range of optimal solutions in the objective space. The cold conditions resulted in the smallest range while the hot conditions had the widest range.

By using the ideal point method of the decision making, the three final optimal solutions of each weather condition were selected and marked in Figure 3-14. The inlet temperature varied from 24°C to 31°C. The number of PVT collectors was decreased from 3 to 2 if the weather conditions were changed from hot to cold. The selected optimal solutions revealed that under the colder weather conditions the multi-stage PVT collector had better electrical performance compared to the optimal solution under medium and hot conditions. In this case, it can be reasonable to couple the multi-stage PVT collector with electric storage and use heat as a by-product. On the other hand, under hotter weather conditions the reasonable coupling application can be a heat-driven desalination system.

5. Conclusion

In this paper, solar cogeneration based hybrid energy system was modelled into Matlab/Simulink environment. The parametric study was conducted and the optimal sizing problem was solved using NSGA-II algorithm. The ideal point method was used in the decision-making process to select the final optimal solution from the Pareto front for three different weather conditions.

The dynamic model of the water-based multi-stage PVT system was optimized using gamultiobj-function of Matlab Global Optimization Toolbox which is based on the fast elitist multi-objective optimization algorithm NSGA-II. The electrical and thermal exergy efficiencies were used as objective functions because of their trade-off nature in the PVT operation which leads to difficulties for decision-makers to select the electrical and thermal efficiencies and the design variables. In this study, the selected decision variables were the coolant mass flow rate, number of PVT collectors and coolant inlet temperature to the system. The results showed that multi-objective optimization based on the genetic algorithm has a high potential when designing the multi-stage PVT system. The used multi-objective optimization approach finds the Pareto front which is a set of optimal solutions in the objective space. This set can be used by decision-makers to find the final optimal solution.

The main findings of the parametric study and multi-objective optimization were:

- Increasing the inlet temperature of the coolant fluid increased the thermal exergy efficiency but decreased thermal energy efficiency. The exergy approach revealed the hidden efficiency although the energy efficiency indicated inefficiency.

- Increasing the coolant mass flow rate increased the cooling effect and electrical exergy efficiency but decreased thermal exergy efficiency.
- Increasing the number of PVT collectors decreased the electrical exergy efficiency and thermal energy efficiency. However, the thermal exergy efficiency indicated the efficiency of the collectors in series by increasing until a certain point.
- Electrical and thermal exergy efficiencies of the PVT operation cannot be maximized at the same time. The multi-objective optimization based on NSGA-II is a suitable method to optimize PVT and multi-stage PVT system design.
- The Pareto optimal front can be used by the decision-makers to select a suitable optimal design of the multi-stage PVT system depending on the purpose and the weather conditions.
- The higher number of the PVT collectors in series resulted in the higher thermal exergy efficiency and the lower number to the higher electrical efficiency.
- The climate conditions had an impact on the optimal number of the PVT collectors in series. Under the cooler weather conditions, a smaller amount of the PVT collectors is recommended compared to warmer conditions.

In future work, the investigation of using the multi-objective optimization approach to the dynamic hybrid energy system including multi-stage PVT collector, thermal and electrical storage, electrical vehicle and demand-side will be conducted. The multi-stage PVT collector model will be developed to show the outlet temperature of each collector in series. Additionally, analysis and optimization of the flat plate multi-stage PVT collector coupled with concentrated PVT collectors would be interesting for future work.

Table 3-3: Decision variables for the multi-objective optimization problem in the Pareto front.

$\dot{m}$ [kg/s]	N	T_{in} [°C]	ξ_{el}	ξ_{th}
0.0344	9	40	-0.1595	-0.0551
0.0367	1	21	-0.1883	-0.0120
0.0367	1	21	-0.1883	-0.0120
0.0306	1	22	-0.1869	-0.0157
0.0175	3	25	-0.1728	-0.0446
0.0294	2	22	-0.1834	-0.0249
0.0283	2	31	-0.1770	-0.0388
0.0242	2	27	-0.1786	-0.0355

0.0344	9	40	-0.1595	-0.0551
0.0144	1	27	-0.1796	-0.0329
0.0244	1	22	-0.1860	-0.0180
0.0269	4	31	-0.1710	-0.0477
0.0178	3	23	-0.1742	-0.0425
0.0336	1	21	-0.1880	-0.0127
0.0269	2	23	-0.1821	-0.0280
0.0289	1	30	-0.1810	-0.0308
0.0161	3	24	-0.1724	-0.0451
0.0311	7	40	-0.1613	-0.0549
0.0344	9	40	-0.1595	-0.0551
0.0367	1	21	-0.1883	-0.0120

Acknowledgements

The authors would like to thank Interreg V Rhin supérieur ACA-MODES project for their support and funding of this research.

Author Contributions: Conceptualization, S.K. and M.S.; data curation, S.K; formal analysis, S.K.; funding acquisition, M.S.; investigation, S.K.; methodology, S.K.; project administration, M.S.; resources, S.K. and M.S.; software, S.K.; supervision, M.S.; validation, M.S.; visualization, S.K.; writing – original draft, S.K.; writing – review and editing, S.K. and M.S. All authors have read and agreed to the published version of the manuscript.

Conflict of Interest: The authors declare no conflict of interest.

Nomenclature

A	PVT collector area (m^2)
c	specific heat (J/kg K)
D	diameter (m)
Ex	exergy rate (W)
G	solar irradiation density (W/m^2)
H	thickness (m)
h	heat transfer coefficient (W/m^2K)
k	thermal conductivity (W/mK)
L	tube length
m	mass, (kg)
$\dot{m}$	mass flow rate (kg/s)
N	number of collectors
r	packing factor
T	temperature (K, °C)
W	tube spacing

Greek symbols

α	absorbance
$(\alpha\tau)$	effective absorbance
ε	emissivity
η	efficiency
τ	transmittance
ζ	exergy efficiency
ρ	density (kg/m^3)

Subscripts

a	absorber
adh	adhesive layer
c	collector
CD	conduction
CV	convection

d	destruction
e	environment
el	electrical
f	fluid
g	glass cover
in	inlet
irr	irradiation
o	outer
out	outlet
pv	photovoltaic
ref	reference
sol	solar
STC	standard test conditions
t	tube
th	thermal
0	reference

CHAPTER 4. Energy and exergy analysis of biomass-fueled micro-CHP unit

Sonja Kallio, Monica Siroux and Stefan-Dominic Voronca
INSA Strasbourg ICUBE, University of Strasbourg
This article is published in ECOS 2021
34th International Conference on Efficiency, Cost, Optimization, Simulation and Environmental Impact of Energy Systems (ECOS 2021)
doi.org/10.52202/062738-0008

Abstract

To reduce primary energy consumption and CO2 emissions, more efficient and environmentally friendly energy production is required in the building sector. Micro combined heat and power (micro-CHP), or co-generation, units produce simultaneously heat and electricity from a single fuel source at high efficiency and close to the consumption point. These units offer significant benefits: reduced primary energy consumption and CO2 emissions, and avoidance of distribution losses due to central plant and network construction. The objective of this paper is to conduct energy and exergy analysis of a biomass-fueled Stirling engine micro-CHP system through modelling of the system. Additionally, a comparison to a reference system with separate production of heat and power is conducted. The energy analysis concerns only the quantity aspects related to the energy production of the system neglecting the quality aspect. For this reason, the exergy method is used to complete the energy assessment of the system. The exergy method takes into account the quality of the produced energy as an ability to work at the temperature, at which a certain energy flow is available. A dynamic model of the Stirling engine micro-CHP system is implemented in Matlab/Simulink environment including the exergy method and the experimental data on the micro-CHP operation is used to characterize the model. The Primary Energy Savings (PES) and Relative Avoided Irreversibility (RAI) are used as the main comparison indicators in the energy and exergy analysis, respectively. The results indicated overall energy and exergy efficiencies of 105% and 14%, respectively, for the micro-CHP operation in the laboratory. The cooling water inlet temperature has a strong impact on the exergy efficiency. The comparative results revealed that the utilization of the micro-CHP unit saves primary energy and can avoid exergy destruction compared to the reference system.

Keywords: Exergy; micro-CHP; cogeneration; Stirling engine; biomass; relative avoided irreversibility; exergetic efficiency.

1. Introduction

The building sector has a high impact on greenhouse gas emissions and final energy consumption in the European Union (EU) by being the largest energy end-use sector with a share of 41% [143]. The micro combined heat and power (micro-CHP), or co-generation, units produce simultaneously heat and electricity from a single fuel source at high efficiency and close to the consumption point [12]. Micro-CHP systems are operating in the building sector to produce on-site energy for space heating, domestic hot water and electricity demand. Due to the efficient decentralized production of heat and electricity, the overall system efficiency of up to 85-90 % can be reached with the micro-CHP units [13, 155]. The micro-CHP systems can respond to the intrinsic requirements of the residential building sector, such as highly variable thermal and electrical demand loads. The highly variable loads require a short response time which can be provided by micro-CHP systems [14]. The European Parliament has defined micro-cogeneration to be the units up to an electrical output of 50 kW [99]. However, micro-CHP commonly refers to units up to 15 kW of electrical power [20]. The renewable energy-based micro-CHP systems are in a key role in reaching the primary energy and pollutant emissions reduction targets of the EU [98].

The micro-CHP system can be based on different conversion devices, such as internal and external combustion engines or non-combustion devices, such as fuel cells and photovoltaic-thermal. Figure 4-1 presents the classification of the CHP technologies.

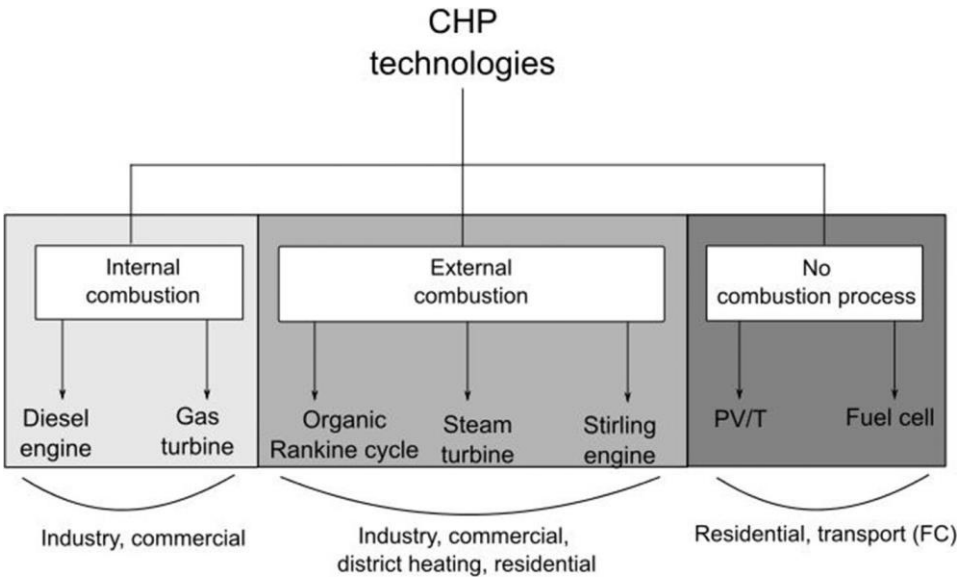

Figure 4-1: *The main conversion technologies of the micro-CHP systems [13]*.

In 2017, Martinez et al. [13] published a review article on the micro-CHP systems based on renewable energy sources. The work presented different micro-CHP conversion technologies and fuels. Finally, they focused on the solar energy-based technologies and presented shortly the main micro-CHP systems that were coupled with renewable energy sources. This study is focused on modelling and analyzing biomass-fueled micro-CHP powered by the Stirling engine conversion device.

In the literature, several modelling approaches for micro-CHP systems have been studied. In 2020, Cheekatamarla et al. [156] presented a review article on the modelling of the micro-CHP system with a focus on the combustion engine as a prime mover. They found out that Annex 42 [94] model was the most used modelling approach. Annex 42 proposes a grey-box model for micro-CHP steady-state and transient operation including four phases: stand-by, warm-up, steady-state, and cool-down phases. Bouvenot et al. [95] developed a dynamic model of the biomass micro-CHP based on the steam engine prime mover. The model was based on experimental studies and used to predict energy performance and emissions of the system. TRNSYS was used as a modelling environment. González-Pino et al. [98] presented a dynamic semi-empirical grey box model for a natural gas-fueled micro-CHP system based on a Stirling engine. The model was validated with the experimental data. The model took into account the start-up and cool-down dynamics of the micro-CHP system. Additionally, different partial loads were studied. The study aimed to improve the existing Stirling engine based micro-CHP models.

Uchman et al. [97] developed a data-driven model of a natural gas-fueled free-piston Stirling engine micro-CHP system with thermal storage into MATLAB/Simulink environment. The model enabled the time-domain simulation of the system behavior. The laboratory setup was developed to collect long-term operation with a variable thermal load and to validate the data-driven model. However, due to the data-driven nature of the model, it is limited to be used only within the laboratory experiment.

The studies in the literature, considering the performance of the micro-CHP system, focus mainly on the First Law of Thermodynamics and analyze the energy efficiency of the operation. Based on the First Law of Thermodynamics, energy cannot be created or destroyed but is always converted into different forms, such as electricity or heat losses. However, based on the Second Law of Thermodynamics the quality of the energy flow can be destroyed and deteriorates in the energy conversion device. Depending on the energy conversion technology, different amounts of exergy is destroyed to get electricity and useful heat. The exergy takes into account the quality of the produced energy as an ability to work at the temperature, at which a certain energy flow is available. The exergy method can be used to complete the energy assessment of the system [80, 83].

In the literature, several studies are conducted taken into account the exergy analysis to complete the energy assessment of the micro-CHP system. Mahian et al. [114] presented a review on exergy analysis in CHP systems with different prime movers. Their results revealed that more exergy-based investigations are recommended on small-scale CHPs in the residential sector. Additionally, more research should be focused on hybrid CHPs with renewable energy sources. In the previous work of the authors [83], the dynamic exergy analysis and optimization was conducted on the solar micro-cogeneration system called photovoltaic-thermal (PVT) collector. The system was analyzed under different weather conditions. The significantly low thermal exergy efficiency was reached due to the low-grade heat production of the PVT collector. Gonçalves et al. [109] studied energy- and exergy-based evaluation of the internal combustion engine-based micro-CHP system with the comparison to the reference system. The model was built into TRNSYS environment, and the exergy method was included. Their results revealed the importance of the exergy method to complete the energy assessment of the system. Taie et al. [110] presented a detailed thermodynamic investigation of an ICE-based micro-CHP system. First, they conducted energy and exergy analysis on the device level and afterwards on

the component level to identify the main areas of inefficiency. The exergy efficiency of 30% was reached, and the largest exergy destruction was identified in heat transfer. Ertesvåg [79] defined an exergy-based comparison indicator for combined heat and power systems called Relative Avoided Irreversibility (RAI). The indicator presents the exergy destruction that can be avoided by replacing separate heat and power generation with a CHP system. The RAI takes into account the thermodynamic value of heat.

Based on the conducted literature review, the research gap is revealed in studies involving exergy analysis of micro-CHP systems fueled by biomass and based on a Stirling engine prime mover. The objective of this study is to model a biomass-fueled Stirling engine micro-CHP system developed by ÖkoFEN and to conduct energy and exergy analysis of the system with a comparison to a reference system. The experimental data from the laboratory set-up is used to characterize the model, and different thermal power configurations are investigated. Primary Energy Savings (PES) and RAI comparison indicators are used to compare the considered micro-CHP to the reference system.

2. Method

In this section, a grey box model of the micro-CHP system is presented. The model includes parameters that are determined with the experimental data. The main objective of the model is to predict the energy and exergy performance of the system under different thermal power configurations. The model is based on Annex 42 [94] modelling approach of the external combustion engine and implemented into MATLAB/Simulink environment. Additionally, the comparison indicators used in the energy and exergy analysis are introduced to compare the cogeneration of heat and power to the separated production.

2.1 Description of the micro-CHP system

The studied biomass-fueled micro-CHP unit is powered by a Stirling engine. The unit is manufactured by Austrian company ÖkoFEN and the model is Pellematic Condens_e. The nominal electrical power of the unit is 1 kW. The thermal power varies between 10-14 kW. The unit uses condensing technology to increase the efficiency. The Stirling engine is a dynamic type free piston engine presented in Figure 4-2 with the whole micro-CHP unit.

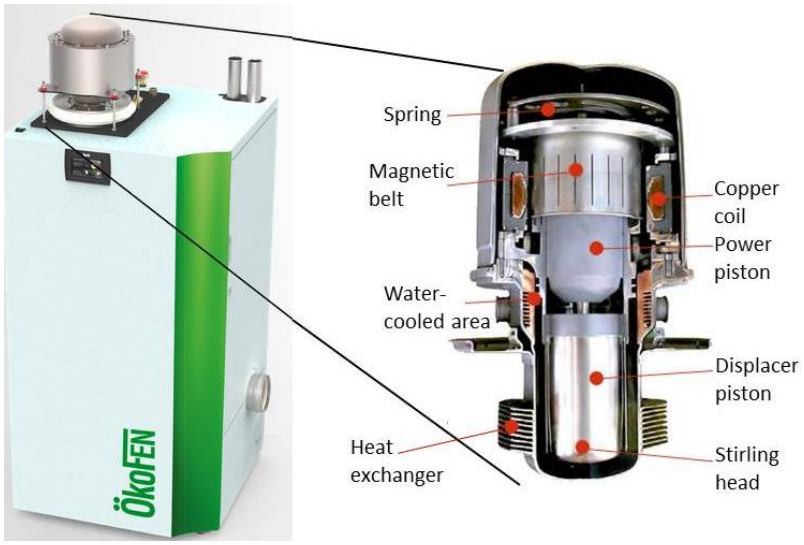

Figure 4-2: *ÖkoFEN biomass-fuelled micro-CHP unit powered by the Stirling engine [53]*.

As a working principle, the Stirling's head is heated up by the flame of the combustion furnace. The generated heat is removed to the working fluid (helium) by the hot end heat exchangers presented in Figure 4-2. Due to the expansion of the working fluid, the displacer piston pushes the fluid through the water-cooled area to the cooler end of the engine. The heating and cooling of the working fluid cause a pressure wave that moves the power piston up and down through a magnetic belt and copper coil. The movement of the power piston generates the alternating current and AC power at 50 Hz. The recovered heat from the water-cooled area is used for domestic hot water (DHW) and space heating demand.

The main components of the studied micro-CHP unit are presented in Figure 4-3. In addition to the Stirling engine, the unit consists of the combustion furnace and heat exchangers to recover the heat from flue gasses (regenerative preheater), engine cooling circuit (preheater) and combustion furnace.

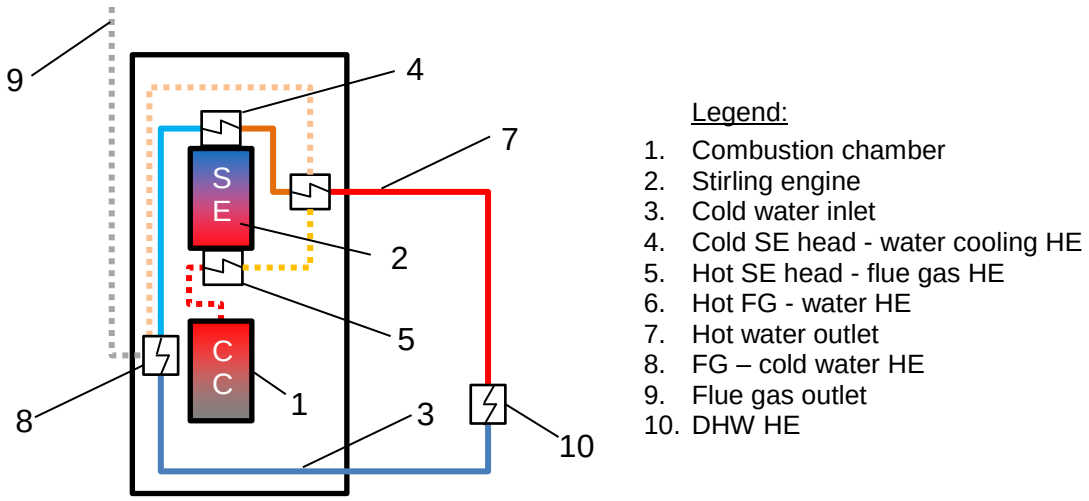

Figure 4-3: *The flow chart of the Stirling engine based micro-CHP unit.*

2.2 Mathematical model

In this section, the mathematical model of the micro-CHP is presented. The model is based on the mass and energy conversion principles, and the variation of the internal energy in a physical body. In Figure 4-4 is presented the control volumes of the model, and mass and energy flows.

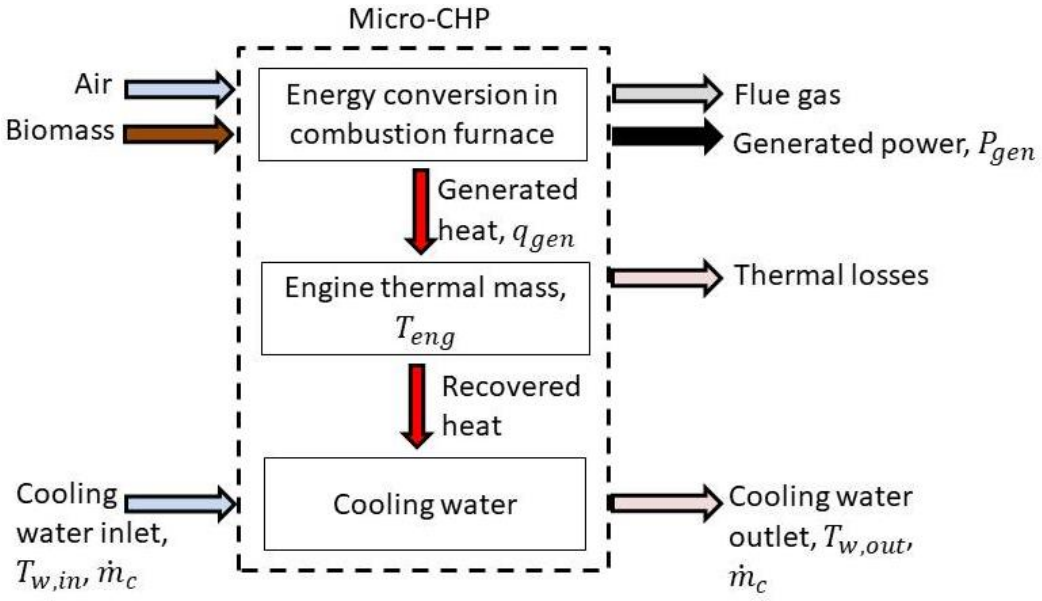

Figure 4-4: *The control volumes of the model, and energy and mass flows in the system.*

The chemical energy of biomass is converted into electric power and heat. The engine's thermal mass MC_{eng} is heated up to an average temperature T_{eng} and thermal losses are

transferred from the engine to the environmental temperature. The heat is recovered from the engine thermal mass to the cooling water of the thermal capacity MC_w. The thermal power of the unit depends on the temperature difference between the cooling water inlet $T_{w,in}$ and outlet $T_{w,out}$ temperature, and on the mass flow rate .

The energy balance governing equations of the micro-CHP system are implemented to model the unit [155].

The engine thermal mass:

$$MC_{eng}\frac{dT_{eng}}{dt} = UA_{HX}\left(T_{w,out} - T_{eng}\right) + UA_{loss}\left(T_{env} - T_{eng}\right) + q_{gen} \quad (1)$$

The cooling water control volume:

$$MC_{w}\frac{dT_{w,out}}{dt} = \dot{m}_{w}c_{p,w}\left(T_{w,in} - T_{w,out}\right) + UA_{HX}\left(T_{eng} - T_{w,out}\right) \quad (2)$$

The previously collected experimental data of the considered micro-CHP is used to identify the thermal capacity of the engine MC_{eng} and cooling water MC_w, and the engine specific heat transfer coefficients UA_{HX} and UA_{loss}. The identification is performed with Simulink Parameter Estimator Tool.

The fuel energy supplied to the engine Q_f is calculated with the fuel mass flow rate into the combustion and the lower heating value of the fuel LHV [34].

$$Q_f = \dot{m}_f LHV_{biomass} \quad (3)$$

Under steady-state conditions the heat generation transferred to the engine thermal mass and electrical power are calculated as follows [20].

$$q_{gen} = \eta_{th} Q_f \quad (4)$$

$$P_{el} = \eta_{el} Q_f \quad (5)$$

The recovered heat from the micro-CHP control volume QCHP is calculated from the measured data of cooling water mass flow rate and temperature difference between the inlet and outlet of the flow [157].

$$Q_{CHP} = \dot{m}_w c_{p,w}\left(T_{w,in} - T_{w,out}\right) \quad (6)$$

The overall energy efficiency of the micro-CHP operation is presented as a ratio of total useful energy output to the total fuel energy as follows [158]:

$$\eta_{CHP} = \frac{P_{el} + Q_{CHP}}{Q_f} \quad (7)$$

2.3 Exergy analysis

In addition to the first law energy analysis, the device-level exergy analysis of the micro-CHP operation is conducted. The first law analysis quantifies the amount of energy produced by the micro-CHP operation. However, it does not count how well the quality of the fuel energy is preserved in the energy conversion process. The exergy analysis is based on the second law of thermodynamic and quantifies the quality of the input and output energy in the conversion process. The quality of energy is measured as a work potential to the specified environment or dead state. Typically, the dead state is the environmental conditions of the energy conversion device, for example, atmospheric air and a temperature of 20 °C. The exergy of the system depends on the defined dead state and should be defined carefully. Through the energy conversion process, the exergy of the fuel is destroyed and exergy is never in balance. However, energy is never destroyed but changes the form, for example, to heat losses, and is always in balance [159].

The exergy of the micro-CHP system control volume can be described as follows:

$$\sum Ex_{in} - \sum (Ex_{th} + Ex_{el}) = \sum Ex_d \quad (8)$$

where Ex_{in} is the exergy content of biomass fuel, Ex_{th} and Ex_{el} are the thermal and electrical exergy product of the conversion process, and Ex_d is the exergy destruction in the process.

The following exergy assessment parameters are used in the exergy analysis of this study. The overall exergy efficiency is the ratio between exergy output or product and total exergy input of the micro-CHP operation, and is calculated as follows [158]:

$$\zeta_{CHP} = \frac{Ex_{pr}}{Ex_{in}} = \frac{(Ex_{th} + Ex_{el})}{Ex_{in}} = 1 - \frac{Ex_{d}}{Ex_{in}} \quad (9)$$

The exergy associated to the fuel and electrical power is defined as follows [109]:

$$Ex_{in} = f_{q,biomass} \dot{m}_f LHV_{biomass} \quad (10)$$

$$Ex_{el} = f_{q,el} P_{el} \quad (11)$$

where $f_{q,biomass}$ and $f_{q.el}$ are the quality factors of the wood pellet fuel and electrical energy. In this paper, $f_{q,biomass}$ = 1.13 and $f_{q,el}$ = 1 [159] are used in the exergy analysis.
The exergy associated to the produced heat depends on the specific enthalpy and entropy of the cooling water flow at the inlet and outlet of the micro-CHP [109].

$$Ex_{th} = \dot{m}_w [h_{out} - h_{in} - T_0(s_{out} - s_{in})] \quad (12)$$

where T_0 is the temperature at the dead state conditions of the flow and defined as 10 °C in this study.

2.4 Comparison of micro-CHP to separate production

The energy- and exergy-based comparison of the micro-CHP energy production to the separated heat and electricity production is conducted. In this study, the reference systems for the separated energy production are the electric grid based on the centralized nuclear power plant for electricity and a natural gas-fired boiler for heat. Two indicators are selected to compare cogeneration and separated generation of energy. The energy-based indicator is Primary Energy Savings (PES) which reveals the saved primary energy when using cogeneration relative to the reference system. The PES is given as follows [109].

$$PES = \left(1 - \frac{1}{\frac{\eta_{el}}{\eta_{eg}} + \frac{\eta_{th}}{\eta_{b}}} \right) \quad (13)$$

where the electrical and thermal efficiencies of the cogeneration are divided by the grid electrical and boiler thermal efficiencies.

However, the energy-based efficiencies and indicator do not take into account the thermodynamic value of produced heat and it qualifies the work and heat to be the same value. However, in terms of exergy, the work has much higher quality than heat and it is not reasonable to directly compare the different products. The exergy efficiency is calculated for the specific system and it does not consider a reference system. Thus, Ertesvåg [79] proposed an exergy-based comparison indicator called Relative Avoided Irreversibility (RAI) which considers the generated exergy destruction or irreversibility of the energy conversion process. The exergy irreversibility is expressed as follows [109]:

$$\mathrm{I} = (1 - \zeta)\mathrm{Ex_{in}} \tag{14}$$

where is the exergy efficiency of the considered system and $\mathrm{Ex_{in}}$ is the exergy input associated to the fuel. The RAI indicator is presented in Eq. (15) as a relative difference of the irreversibility generated by the micro-CHP unit, electric grid and boiler [109].

$$\mathrm{RAI} = \left(1 - \frac{I_{CHP}}{I_{eg} + I_b}\right) \tag{15}$$

The fuel exergy in the reference system can be calculated based on the quality factor of the considered fuel and exergy-to-heat ratio of the reference system. The exergy-to-heat ratio is a measure of the quality of delivered heat [79]. For the low-exergy heat source, such as hot water, the ratio can be 0.15-0.19 [79, 109]. The fuel exergy of the electric grid and exergy efficiency are presented as follows [79]:

$$Ex_{f,eg} = f_{q,eg}\frac{P_{el}}{\eta_{el,eg}} \tag{16}$$

$$\zeta_{eg} = \frac{P_{el}}{Ex_{f,eg}} \tag{17}$$

The fuel exergy of the boiler is calculated with the quality factor of the fuel and the exergy-to-heat ratio of the boiler [79]:

$$Ex_{f,b} = \frac{\alpha_{q,b}Q_{CHP}}{\zeta_b} \tag{18}$$

$$\zeta_b = \frac{\alpha_{q,b} Q_{CHP}}{f_{q,biomass} \frac{Q_{CHP}}{\eta_b}} \quad (19)$$

3. Results and discussion

The model of the discussed micro-CHP unit was implemented into Matlab/Simulink environment and the parameter estimator was used to estimate the engine and cooling water thermal masses, and specific heat transfer coefficients. The estimation was performed by using the micro-CHP operation data from the previously conducted laboratory experiment in which the unit was started, running at full-load for 50 min and shut down. Table 4-1 present the estimated parameters and other used parameters in the analysis.

Table 4-1: The micro-CHP system parameters.

Parameter	*Value*	*Unit*
MC_{eng}	1943	J/K
MC_w	19429	J/K
UA_{HX}	35	W/K
UA_{loss}	0.5	W/K
P_{nom}	1	kW
Q_{nom}	12	kW
$f_{q,biomass}$	1.13	-
LHV	4900	W/kg
$c_{p,w}$	4180	J/kgK
T_0	10	°C
$T_{w,in}$	15	°C
$T_{w,env}$	20	°C

The steady-state energy and exergy analysis was conducted at the maximum operation mode of the micro-CHP unit. Based on the experimental data, the full-load thermal and electrical efficiencies were 98% and 7%, respectively. The overall efficiency was 105% due to the applied condensing technology of the ÖkoFEN Pellematic Condens_e micro-CHP system. The technology recovers the residual heat of the flue gas by cooling it below condensation temperature in the flue gas heat exchanger presented in Figure 4-3. At the maximum operation mode, a thermal power rate of 13.5 kW and electrical power of 1 kW was produced. The cooling water inlet temperature was constant 15 °C. In Figure 4-5 is presented the energy and exergy

rates associated with thermal and electrical energy production, fuel input, destruction and losses to the environment.

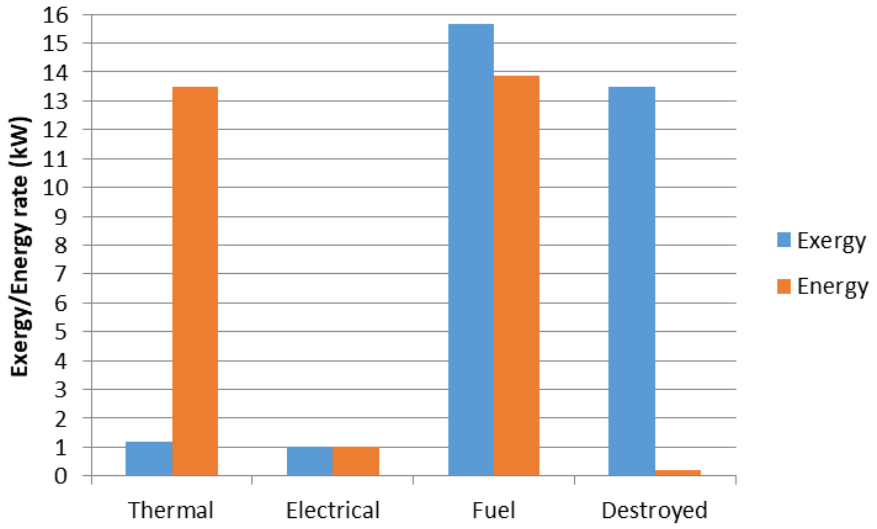

Figure 4-5: *The energy and exergy flows at maximum operation mode.*

Figure 4-5 shows that the fuel input of 13.9 kW was almost totally converted to useful heat due to the high thermal efficiency. However, the exergy input of 15.7 kW was almost destroyed in the conversion process due to the produced low-grade heat at the temperature of 64 °C. The thermal exergy rate was only 1.2 kW and thermal exergy efficiency was 7.6%. The electrical power rate was 1 kW in terms of energy and exergy because electrical energy is seen as pure exergy. However, the electrical exergy efficiency was 6.4%, which was lower than the electrical efficiency due to the high exergy factor of biomass ($f_{q,biomass}$ = 1.13). The overall exergy efficiency was 14% and 86% of the exergy input was destroyed in the energy conversion process. Compared to the energy losses of 1.5% to the environment, the exergy analysis revealed the inefficiency of the energy conversion process although the energy analysis indicated high efficiency of the process.

In Figure 4-6 is presented the total exergy in the system divided to the fuel, destruction and product exergy. The exergy input with fuel presented 50% of the total exergy and 43% destroyed exergy. The share of the usable product exergy was only 7% of which 4% was thermal exergy and 3% electrical exergy.

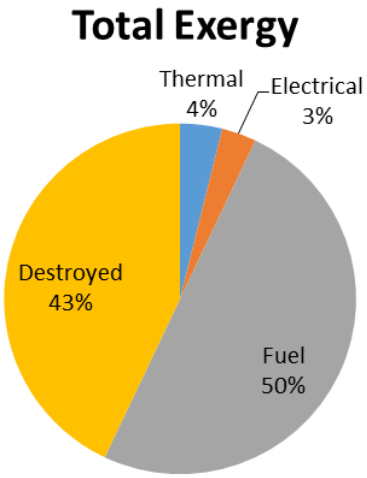

Figure 4-6: *The total exergy divided to the fuel, destruction and thermal and electrical product exergy.*

The thermal exergy rate is sensible to the cooling water inlet temperature. In the first analysis based on the experimental data, the constant inlet temperature of 15°C was used. However, the inlet temperature can vary over micro-CHP operation time. Figure 4-7 shows the electrical, thermal and overall exergy efficiencies at the inlet temperature of 40°C and 60°C as a function of thermal power configuration (10 kW, 12 kW and 14 kW) of the considered micro-CHP unit. The configuration was changed by increasing the cooling water mass flow from 3.4 to 4.1 l/min.

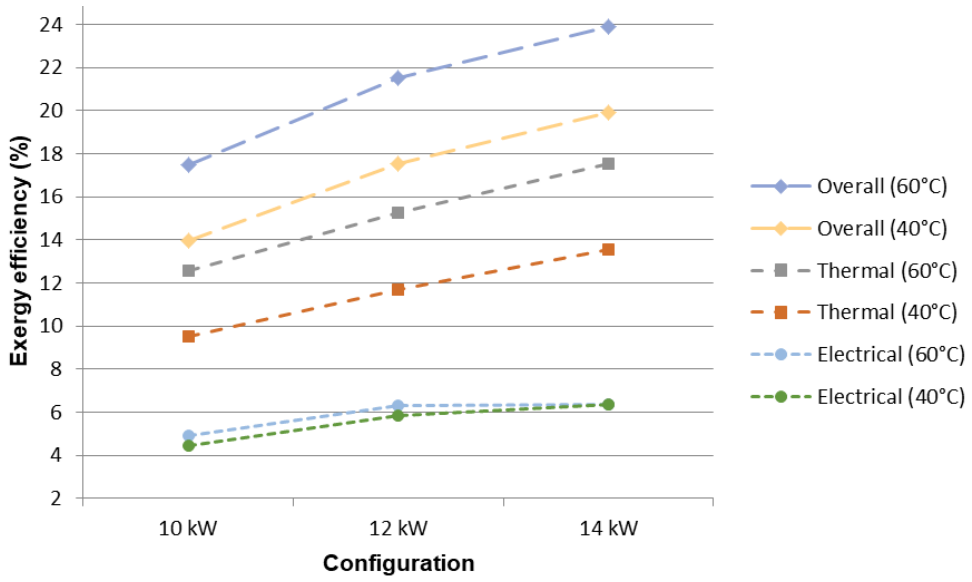

Figure 4-7: *Exergy efficiency at different inlet temperatures as a function of thermal power configuration.*

The inlet temperature was increased from 40°C to 60°C to see the impact on the exergetic value of the thermal energy. Figure 4-7 shows that the thermal exergy efficiency was higher at 60°C inlet temperature and varied from 12.5% to 17.5% depending on the thermal power configuration. At 40°C inlet temperature, the thermal exergy efficiency varied from 9.5% to 13.5%. The electrical exergy efficiency was slightly higher at 60°C inlet temperature due to the lower cooling effect to the engine and reached its maximum of 6.4% at the maximum operation mode. The overall exergy efficiency increased due to the increased thermal exergy efficiency, and varied from 13.9% to 23.9% depending on the inlet temperature and the power configuration.

3.1 Comparative results of cogeneration and reference system

The micro-CHP energy generation was compared with the separated production of heat and power. The PES and RAI indicators were introduced in Section 2 and used to assess primary energy and irreversibility savings if the separated production was changed to the studied biomass-fueled micro-CHP unit. In the reference system, the electricity is bought from the electric grid and heat is generated by a natural gas-fired boiler. For simplicity, the electric grid was assumed to be supplied by a nuclear power plant which is around 70% of the electricity mix in France. The energy efficiencies and exergy quality factors for the fuels and heat generation used in the calculation are presented in Table 4-2.

Table 4-2: The factors to calculate the PES and RAI indicators.

Parameter	*Value*	*Unit*	*Ref.*
$\eta_{el,eg}$	0.35	-	[160]
η_{b}	0.9	-	[109]
$\eta_{el,CHP}$	0.07	-	Experimental data
$\eta_{th,CHP}$	0.98	-	Experimental data
$f_{q,el}$	1	-	[159]
$f_{q,nuclear}$	0.95	-	[159]
$f_{q,biomass}$	1.13	-	[159]
$f_{q,gas}$	1.03	-	[159]
$\alpha_{q,b}$	0.19	-	[79]

First, the indicators were calculated at the maximum operation mode of the micro-CHP described at the beginning of Section 3. At the considered operation mode the cooling water inlet

temperature was 15°C. The efficiency of the electric grid was assumed to be 35% and the boiler 90%. The results above showed that the quality of the delivered heat was increased if the inlet temperature was increased. Next, the RAI indicator was calculated for the inlet temperatures of 40°C and 60°C as well. The results are shown in Table 4-3.

Table 4-3: The PES and RAI indicators at different cooling water inlet temperatures.

Parameter	$T_{w,in}$ = 15°C	$T_{w,in}$ = 40°C	$T_{w,in}$ = 60°C
PES	0.22	0.22	0.22
RAI	0.08	0.14	0.19

To produce 1 kW power and 13.5 kW thermal power rate, the primary energy savings were 22% compared to the separated production of heat and power. The relative avoided irreversibility of the laboratory experiment was 8%. In other words, 8% of exergy destruction was avoided if the reference system was replaced by the micro-CHP unit with the cooling water at 15°C temperature. However, if the inlet temperature was increased to 40°C and 60°C, 14% and 19% of exergy destruction were avoided, respectively.

The efficiency of the reference system influences both PES and RAI indicator. In Figure 4-8 is presented the contour or isolines for the PES and RAI indicators as a function of the varying efficiencies of the separated heat and power production. The efficiency of the power generation was varied from 30% to 45%, which is a typical efficiency range of centralized nuclear power plants. The boiler efficiency was varied from 80% to 100% which includes a typical efficiency range. In terms of the First Law of thermodynamic, the 100% efficiency is not realistic but is still included to evaluate the progress of the isolines. From the micro-CHP point of view, the laboratory experiment at the lowest cooling water inlet temperature was used as an operation mode.

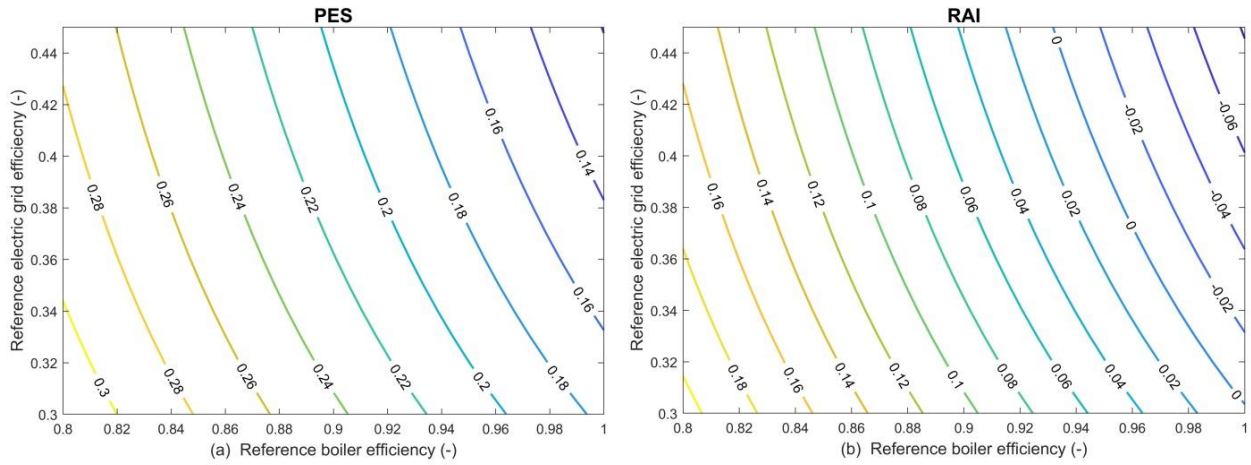

Figure 4-8: *The contour lines of a) PES and b) RAI as a function of the electric grid efficiency and the boiler thermal efficiency.*

Figure 4-8 shows that the primary energy savings were between 12-14%, with the highest efficiencies of the reference system. On the other hand, the savings were above 30%, with the lowest reference system efficiencies. However, in any case, the changing the reference system to the cogeneration system saved primary energy. Over the varying efficiencies, the RAI indicator was always lower than the PES. If the reference system got its highest efficiency, the RAI was negative, and the cogeneration was not an improvement from the reference system. The highest level of avoided exergy destruction was 20%.

The results revealed the significant influence of the cooling water inlet temperature on the thermal exergy efficiency and the RAI indicator. Before using the PES and RAI indicators in the decision making, the inlet water temperature should be carefully defined. Figure 4-9 presents the RAI contour lines with the cooling water inlet temperature of 40°C.

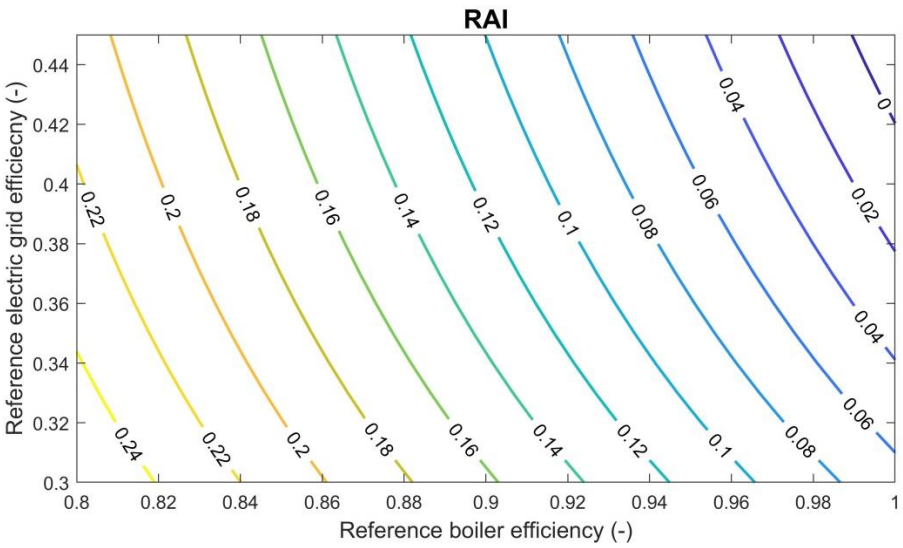

Figure 4-9: *The contour lines of RAI with the micro-CHP inlet temperature of 40°C.*

The results in Figure 4-9 reveal that the micro-CHP unit was an improvement from the reference system with a wider range of the reference system efficiencies if the cooling water inlet temperature was increased. Additionally, the highest level of avoided exergy destruction was above 24% instead of 20%.

As conclusion, to conduct a complete energy assessment, the PES and RAI are suitable indicators to compare the micro-CHP utilization to the reference system from the energetic and exergetic point of view. However, the exergy-to-heat ratio should be carefully defined to result in a realistic assessment of the RAI indicator. The results showed that the studied biomass Stirling engine micro-CHP unit saved primary energy and avoided exergy destruction compared to the considered reference system.

4. Conclusion

The objective and novelty of this study were to conduct a specific energy and exergy analysis of the ÖkoFEN biomass-fuelled Stirling engine micro-CHP unit. The study was based on the experimental data, and the analysis was completed with an energetic and exergetic comparison of the micro-CHP to a separate production of heat and power. A dynamic model of the micro-CHP unit was implemented into Matlab/Simulink environment, and it was characterised by the experimental data. The model included also the calculation of the Primary Energy Saving (PES) and Relative Avoided Irreversibility (RAI) indicators.

The main findings of the energy and exergy analysis were:

- The exergy analysis revealed the inefficiency of the energy conversion process in the micro-CHP although the energy analysis indicated the high efficiency of the process. The thermal and electrical efficiencies of the micro-CHP in the laboratory test were 98% and 7%, respectively. At the same time, the thermal exergy efficiency was only 7.6% and electrical exergy efficiency 6.4%. The overall energy and exergy efficiencies were 105% and 14%, respectively.
- The share of the usable product exergy was only 7% of the total exergy in the system.
- The thermal exergy production of the micro-CHP unit was highly dependent on the cooling water inlet temperature. If the inlet temperature was increased from 15°C to 60°C, the thermal exergy efficiency was increased from 7% to 17.5%.

In addition to the energy and exergy analysis of the micro-CHP operation, the comparative analysis was conducted in terms of energy and exergy. The results revealed that the cogeneration with the ÖkoFEN unit saved 22% of the primary energy use and avoided 8% of the exergy destruction compared to the reference system, including electricity from the grid and conventional natural gas boiler for heat production with the efficiencies of 35% and 90%, respectively. However, the exergy-based RAI indicator revealed that the micro-CHP unit was not an improvement from the reference system with the high-efficiency reference system. On the other hand, the cooling water inlet temperature had a high impact on the thermal exergy production and the increased inlet temperature resulted in the micro-CHP unit being an improvement from the reference system also with the high-efficiency reference system.

The ÖkoFEN micro-CHP unit is a reasonable technology for heat and power generation from an energetic and exergetic point of view. The role of the exergy method in comprehensive energy analysis has high importance to reveal the real value of the heat in the energy conversion process.

In future work, a comparison of the cogeneration with the ÖkoFEN unit with different reference systems, including renewable energies, such as solar technologies, would be reasonable to conduct. Additionally, the micro-CHP model will be extended to take into account start-up and cool-down operation phases and to include a thermal storage and demand side to perform a dynamic energy and exergy analysis of the yearly operation. The laboratory experiment with varying cooling water inlet temperature and thermal storage integration should be conducted.

Acknowledgements

The authors would like to thank Interreg V Rhin supérieur for their support and funding of this research.

Nomenclature

$c_{p,w}$	specific heat, J/(kg K)
Ex	exergy rate, W
f	quality factor
h	specific enthalpy, J/kg
I	irreversibility rate, W
LHV	lower heating value, W/kg
$\dot{m}$	mass flow rate, kg/s
MC	thermal mass, J/K
Q	thermal energy rate, W
P	electrical energy rate, W
PES	Primary Energy Savings
RAI	Relative Avoided Irreversibility
s	specific entropy, J/kgK
UA	heat transfer coefficient, W/K
T	temperature, K,°C

Greek symbols

α	exergy-to-heat ratio
η	efficiency
ζ	exergy efficiency

Subscripts and superscripts

b	boiler
d	destruction
eg	electric grid
eng	engine
env	environment
el	electrical
f	fuel
gen	generated
HX	heat exchanger
in	inlet
loss	Energy losses
nom	nominal power
out	outlet
pr	product
q	quality factor
th	thermal
w	water

CHAPTER 5. Hybrid renewable energy systems based on cogeneration

Sonja Kallio and Monica Siroux
INSA Strasbourg ICUBE, University of Strasbourg
This article is published in *Energy Reports*
doi.org/10.1016/j.egyr.2021.11.158

Abstract

Hybrid renewable energy systems (HRES) are seeing as a solution to overcome the fluctuation and randomness of certain renewable energy sources, such as solar and wind power. Coupling the fluctuating renewable energy sources with the controllable sources, such as biomass-fueled micro-cogeneration, constitute an HRES that significantly reduces CO_2 emissions and primary energy consumption. The purpose of this work is to review research works on hybrid renewable energy systems based on micro-cogeneration and to present a case study of optimizing a solar-based micro-cogeneration system. First, renewable energy-fueled micro-cogeneration systems are presented according to the prime mover technology: Stirling engine, organic Rankine cycle and photovoltaic-thermal (PVT). The different prime movers are assessed according to their advantages, disadvantages and market availability. Next, several research works on hybrid renewable energy systems including solar and micro-cogeneration technologies are summarized and key findings are highlighted. Finally, the results of the case study are presented for reasoning the necessity of system hybridization. The results indicated that more experimental data on HRES and research effort on energy management strategies and stochastic optimization models are required. The results of the case study showed maximum thermal and electrical reliability of 68% and 70%, respectively. The optimized PVT/battery/thermal storage system was not able to cover all energy demand of the case study but supporting heat and electricity sources are required.

Keywords: Renewable energy sources; Energy conversion; Solar energy; Hybrid renewable energy systems; Micro-cogeneration; Microgrid energy management

1. Introduction

The building sector has a high impact on greenhouse gas emissions and final energy consumption in the European Union (EU) by being the largest energy end-use sector with a share of 41% [143].

The micro combined heat and power (micro-CHP), or cogeneration, units produce simultaneously decentralized heat and power from a single fuel source at high efficiency. The building integrated micro-cogeneration systems are in the key role in reaching the primary energy and pollutant emissions reduction targets of the EU [98].

Hybrid renewable energy systems integrate two or more renewable energy sources with or without conventional energy source to produce heat and electricity to satisfy a certain end-use demand [161]. The common features for these systems are decentralized set-up, high renewable energy share, flexible operation to follow local energy demand and small- or micro-scale system components.

Due to the multitude of possible combinations, hybrid energy systems can deliver highly efficient solutions for energy generation. The targets of using hybrid energy systems are to increase reliability, to support fluctuating renewable energy sources, to improve overall efficiency and fuel flexibility. Additionally, these systems reduce costs, fossil fuels, primary energy use and CO2 emissions. HRES can operate as a grid-connected system or stand-alone system in rural areas without an existing power grid.

The HRES are widely studied in the literature. Shivarama et al. [162] presented a comprehensive review on hybrid renewable energy systems. They considered modelling, analysis, optimal sizing, energy management and control aspects of the HRES. If the technology types of the HRES are selected appropriately, the system can be used to produce cooling, heating and power, simultaneously. Applying combined cooling, heating and power (CCHP) systems can reach an overall efficiency even more than 90% compared to a conventional centralized power plant, which has an efficiency of 30-45% [163]. Gu et al. [163] presented the review of modeling, planning and optimal energy management of CCHP micro-grids. They defined that a typical CCHP system consists of four main elements: the renewable energy source, prime mover, energy storage and load. Wang et al. (2020) reviewed current research of small-scale hybrid solar-assisted CCHP systems. They highlighted that more research is required on system integration evaluation and advanced energy management strategies. Wegener et al. [33]

presented a review on small-scale CCHP systems covering biomass-fired systems and solar extensions. The results indicated the high energetic and environmental potential of biomass-fired CHP systems with solar extensions. However, they pointed out that more experimental data on the system operation is required.

In this given framework, a research gap has been indicated and more research effort is required in biomass-fired micro-scale CHP systems with solar support to enable highly efficient and 100% renewable energy systems in the building sector as well. The present work provides a research contribution by summarizing possible renewable energy-based micro-cogeneration prime movers and by reviewing research works on HRES based on micro-cogeneration and solar technologies. Finally, a case study of solar-based micro-cogeneration system with energy storages is presented for reasoning the necessity of system hybridization.

2. Renewable energy based micro-cogeneration

Prime movers are used to transform fuel energy to mechanical work and heat as a by-product. The prime movers of the micro-CHP systems can be divided into the following three categories: internal, external and no combustion process [13]. The most developed, used and researched technology is internal combustion engine (ICE) based micro-CHP systems [33]. However, the external combustion-based systems, such as Stirling and organic Rankine cycle (ORC) have better fuel adaptability to use different renewable sources, such as solid biomass, waste heat and solar energy [13]. Fuel cells and photovoltaic-thermal (PVT) collectors are based on the no combustion process. In the fuel cells, the chemical energy of a fuel is converted to electricity through a chemical reaction with oxygen. The PVT collectors convert solar radiation into heat and electricity simultaneously from the same installed area. An assessment of different micro-CHP prime movers presented in this review is shown in Table 5-1. The selection of the considered prime movers was based on their adaptability to use solid biomass and solar as fuel and market penetration in the building sector. The assessment is based on the literature findings.

Table 5-1: Assessment of renewable energy based micro-CHP prime mover technologies

Prime mover	Stirling engine	ORC	PVT
Advantages	Low maintenance, noise, vibration and emissions [12]	Low-grade heat use starting from 50°C [33, 35]	Well developed as flat plate collector [31]

	High fuel flexibility [13, 34] Noise level and electricity/heat ratio suitable for residential use [13, 37] High thermal efficiency [34] Good partial load performance [33]	High fuel flexibility [12] Easy to retrofit the existing heating device [14] High partial load efficiency [33]	Simple operation without moving parts [31] Wide range of possible applications [31]
Disadvantages	Low electrical efficiency [18, 37] High investment costs [12, 33]	High investment costs [33] Relatively low electrical efficiency and waste heat recovery [14, 33] Challenges in efficient downscaling [12]	Difficulty of sun tracking with flat plate [31]
Fuel types	Biomass, natural gas, solar radiation [27]	Waste heat, geothermal, biomass, solar radiation [12, 14, 39]	Solar energy
State of technology	Commercially available [39, 40]	R&D and some commercially available [39, 40]	R&D and commercially available [31]
Market availability	ÖkoFEN, Whispergen, BAXI, Sunmachine, Genoastirling S.r.l.	Rank®, Kaymacor ORChidea, Viking Development Group	DualSun, Abora Solar, Naked Energy, Solarus

3. Hybrid renewable energy system

Various technology types are identified in the literature for the planning and design of hybrid energy systems. Their suitability depends on available fuel sources on the generation side, the availability of a grid connection or a heating network, and the considered application scenario. Within the scope of the HRES, the utilization of the following technologies can be considered: solar technologies: photovoltaic (PV), solar thermal and PVT systems, mini-wind turbines, micro combined heat and power (micro-CHP) systems, heat pumps and thermal chillers.

The following storage technologies are often deployed in the HRES to facilitate energy management in the system: sensible and latent heat storages, electric battery storages, thermally activated building systems and electric vehicles as flexible electric storages.

The above-listed components can form different configurations for the HRES depending on the considered application and load demand. As an example, photovoltaic electricity production can be used to support the electricity consumption of the heat pump. On the other hand, the combustion-based micro-CHP can support fluctuating solar energy production and activate thermal chiller during the cooling period. Different configurations for the HRES have been studied in the literature. Zabalaga et al. [34] presented the performance analysis of the HRES including photovoltaic (PV), biomass Stirling engine and battery system. They compared the HRES with the PV/diesel engine/battery hybrid system and performed the analysis in terms of energy efficiency, environmental sustainability and economic feasibility. Their results revealed that the HRES performed better in terms of each indicator in the analysis. Calise et al. [164] studied a novel solar-assisted CCHP system, which coupled PVT collectors with a reversible heat pump and adsorption chiller. The aim was to design, dynamic simulation and analyzing the energetic, environmental and economic performance of the system.

In this study, the solid biomass-fueled micro-CHP systems supported by solar technologies are considered as components to form a hybrid renewable energy system with energy storages. The selection is based on the exergy approach which indicates the highest overall exergy efficiency for the HRES components based on the combined heat and power production [80, 82]. Additionally, the literature review has shown that coupling the micro-CHP system with solar technologies can overcome the intermittency issues of solar energy production, increase self-consumption and reduce primary energy use and fuel costs. Table 5-2 summarizes the cases of the hybrid solar supported micro-CHP systems in the literature.

Table 5-2: The cases in the literature of the hybrid renewable energy systems based on micro-CHP and solar support

Prime mover	Solar support	Methods	Evaluation	Key findings	Ref.
Power output					
Fuel					

Stirling engine P_{el} = 1 kW, P_{th} = 7 kW Natural gas Biomass possibility	PV Flat plate solar thermal To produce heat and electricity	Experimental study Operation data of 36 days in Spain Matlab Comparison to a reference system including electric grid and diesel oil boiler Typical residential domestic hot water and electricity demand profiles	η_{el} η_{th} CO_2 emissions	Higher performance is expected if heat demand is extended to space heating and cooling The system reliability increased with thermal and electrical storages, and micro-CHP unit CO_2 emissions reduced by 36% 76% of total energy demand is covered Biomass use proposed for further CO_2 reduction	[54]
Stirling engine P_{el} = 1 kW, P_{th} = 26 kW Natural gas Biomass possibility	PV To produce electricity	Comparison of different PV powers and battery capacities with Stirling micro-CHP Experimental data of PV and micro-CHP installation	Demand self-coverage index Sold share index Energy stored share Self-consumption index Net present value	The system enables significant improvement in self-sufficiency High investment costs High ecological effect Research on energy management and control required	[55]
ORC P_{el} = 40 kW, P_{th} =310 kW Biomass	PVT To produce heat and electricity	Matlab Transient techno-economic modelling Design optimization Sport center in Bari, Italy	Thermo-economic analysis	Payback time 11.5 years 100% renewable energy supply with hybrid system Electricity production capability increased significantly	[56]
ORC P_{el} = 14 kW, P_{th} =70 kW Biomass	PV To produce electricity	System modelling and analysis Residential building block Electricity, space heating and domestic hot water	Energy analysis Self-consumption Fuel savings	Yearly electrical self-consumption 84.9% with hybrid system, 32.5% with PV only. 54.9% of thermal energy demand covered Significant natural gas savings ORC overcomes the fluctuation of solar energy source	[57]

PVT Natural gas boiler as back-up	Dynamic simulation in TRNSYS Optimization of the system configuration Hotel in Naples, Italy	Energy, economic and environmental analysis Sensitivity analysis	Primary energy savings 57.66% CO_2 emissions reduction of 51.63% Simple payback time 11.64 years	[165]

4. Case study

The preliminary study was conducted considering residential electricity and domestic hot water production by a photovoltaic-thermal system integrated with thermal and electrical storages. The hourly demand profiles with daily average demands of 24.6 kWh and 7.5 kWh for electricity and thermal energy, respectively, were used. The study was conducted under meteorological conditions of Strasbourg, France. To this purpose, the dynamic system model was built into Matlab/Simulink environment and a multi-objective optimization with genetic algorithm was performed. The aim of the optimization was to find a Pareto optimal set of system designs to maximize self-consumption and autonomy of the system over year with the minimum initial investment costs. The considered system is presented in Figure 5-1.

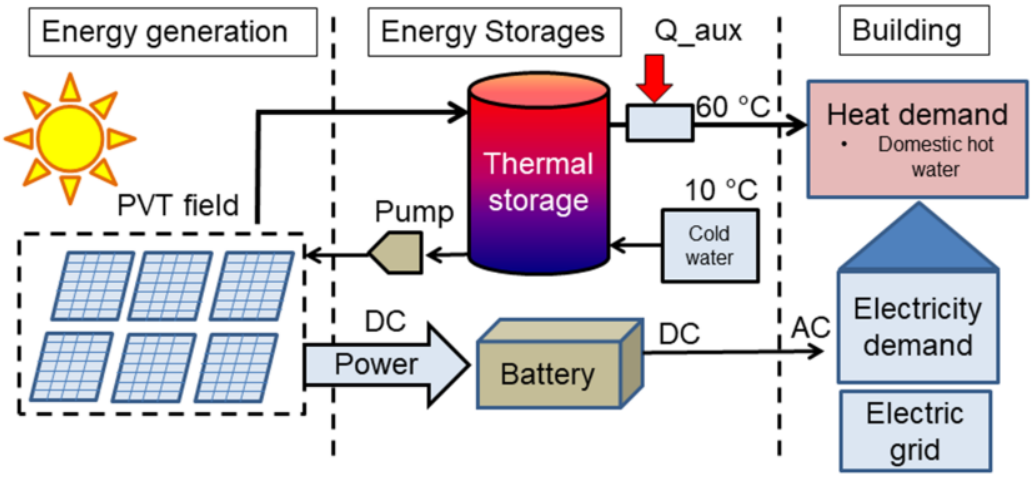

Figure 5-1: *The system layout of the case study.*

The dynamic model of the PVT collector have been presented in the literature [30, 83, 103, 107, 127] and used to evaluate the thermal and electrical performance of the collector. In this case study, glazed water cooled PVT collectors with sheet-and-tube thermal absorbers were

used and modelled with the main heat transfer mechanisms between the PVT layers. The key governing equations of the PVT collector and thermal storage are presented as follows.

$$m_g * c_g * dT_g/dt = Q_{g,s} + Q_{g-e,CV} + Q_{g-sky,RD} + Q_{g-pv,CV} + Q_{g-pv,RD} \quad (1)$$

$$m_{pv} * c_{pv} * dT_{pv}/dt = Q_{pv,s} + Q_{pv-g,CV} + Q_{pv-g,RD} + Q_{pv-f,CV} - E \quad (2)$$

$$m_f * c_f * dT_f/dt = Q_{f-pv,CV} + Q_f \quad (3)$$

$$m_{TS} * c_w * dT_{TS}/dt = Q_{f-TS} + Q_{aux} + Q_{DHW} + Q_{TS,loss} \quad (4)$$

In Equations (1-4) m, c, T, Q and E indicate mass, specific heat capacity, temperature, heat transfer rate and electricity production, respectively. The following subscripts: “g”, “s”, “e”, “CV”, “sky”, “RD”, “pv”, “f”, “TS”, “w”, “aux”, “DHW” and “loss” refer to glass cover, solar energy, environment, convection, sky, radiation, PV module, fluid, thermal storage, water, auxiliary, domestic hot water and heat losses. The more detailed description of the PVT governing equations and model validation are presented in the Authors’ previous work [83].

The PV converts a fraction of the solar radiation into the electricity. The electrical efficiency of the PV depends linearly on the PV temperature T_{pv}, the temperature coefficient β_{PV} and on the efficiency η_{STC} at standard conditions T_{ref}. The electrical efficiency η_{el} is calculated according to the following relation:

$$\eta_{el(T)} = \eta_{STC}\left[1 - \beta_{PV}\left(T_{pv} - T_{ref}\right)\right] \quad (5)$$

The battery model was based on the load balance between the electricity production and demand. If the electricity production was higher than demand, the battery was charged and discharged if the demand was higher. The surplus electricity was sold to the grid. However, selling and buying from the grid was aimed to be minimized in order to maximize self-consumption and autonomy of the system. The battery state of charge SOC_B is presented as follows:

$$SOC_B(t) = SOC_B(t - \Delta t) + \eta_{ch} P_{ch}(t)\Delta t/C_B - \eta_{dis} P_{dis}(t)\Delta t/C_B \quad (6)$$

where P_{ch}, P_{dis}, C_B, η_{ch} and η_{dis} are charging power, discharging power, battery capacity, charging and discharging efficiency, respectively.

The multi-objective design optimization problem was formulated to maximize the thermal and electrical reliability $R_{thermal}$ and $R_{electric}$, respectively, and minimize the initial investment costs of the considered system, simultaneously. The inflation was not considered in the case study. The Matlab function called gamultiobj of the Global Optimization Toolbox was applied to create a set of optimal solutions in the space of decision variables on the Pareto front. The function uses a controlled, elitist genetic algorithm, which is a variant of non-dominated sorting genetic algorithm-II (NSGA-II). The detailed description of the algorithm is presented by Deb in [140]. Table 5-3 presents the selected decision variables to be optimized by minimizing the objective functions with NSGA-II optimization algorithm. The bounds of the variables were selected based on the previous research on the PVT collectors [83] and on the market availability of the components for residential buildings. Table 5-4 present the estimated prices of the system components used in the optimization.

Table 5-3: The decision variables for the multi-objective optimization problem

Decision variable	Bounds	Unit
Coolant mass flow rate, $\dot{m}$	$60 \leq x(1) \leq 130$	kg/h
Nr. of PVT in series, N	$1 \leq x(2) \leq 6$	-
Nr. of PVT rows, M	$1 \leq x(3) \leq 6$	-
Battery capacity, C_B	$4 \leq x(4) \leq 14$	kWh
Thermal storage volume	$0.1 \leq x(5) \leq 0.5$	m^3

Table 5-4: The component prices of the system

Component	Price	Ref.
PVT collector	325 €/m^2	DualSun company
Thermal storage	2.95 €/dm^3	[130]
Electrical storage	1143 €/kWh	Enphase company

As a result, the Pareto front was obtained for the optimization problem and is presented in Figure 5-2. The optimization algorithm found 18 non-dominating optimal solutions for the component sizing of the considered renewable energy system. The optimal solutions can be used

by the decision-makers to select the final optimal solution depending on the application and constraints, such as available roof area or budget. Three solutions were selected from Figure 5-2 based on the increasing investment costs. These solutions are presented in Table 5-5.

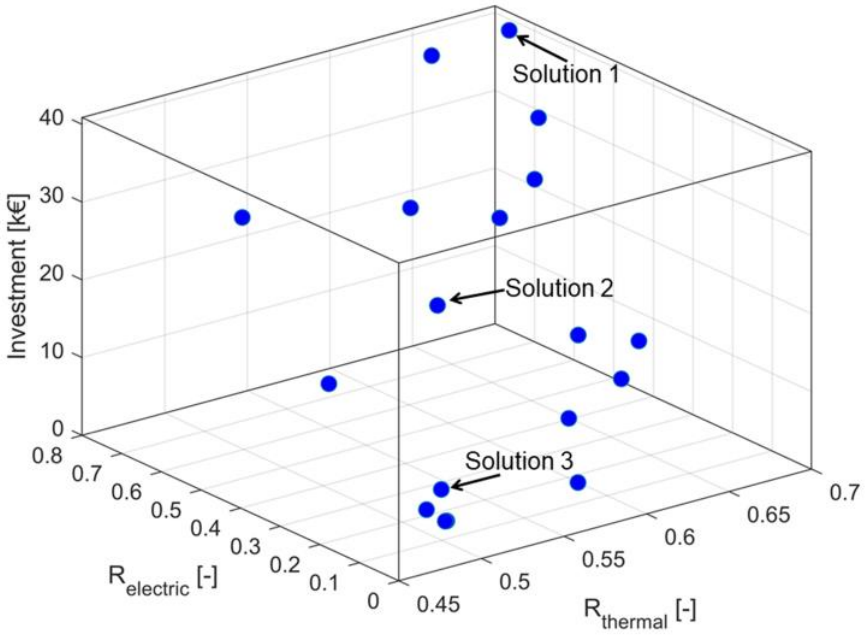

Figure 5-2: *The Pareto front of the optimal solutions in the objective space.*

Table 5-5: The selected optimal solutions from the Pareto front

Solution	ṁ (kg/h)	PVT in series	PVT rows	C_B (kWh)	V_{TS} (m^3)	$R_{thermal}$	$R_{electric}$	Inv. (€)
1	108	6	6	14	0.5	0.68	0.7	40877
2	64	6	2	9	0.2	0.57	0.41	18677
3	111	1	3	4	0.1	0.5	0.09	6817

Within the optimal solutions the investment costs varied from 8172 € to 40877 € while the thermal reliability increased from 0.48 to 0.68 and electrical reliability from 0.02 to 0.7.

The results show that the thermal and electrical energy demands of the considered case study under residential constraints, such as maximum available roof area, cannot be covered by the PVT system only. The results show also that the thermal and electrical storages increase the reliability of the system significantly. However, auxiliary heat and electricity sources are required to support fluctuating solar energy production and to cover the remaining part of the energy demand.

5. Conclusion

In the present work, the renewable energy-based micro-cogeneration prime movers (Stirling engine, ORC and PVT collector) were presented. The advantages and disadvantages of these technologies were assessed. Based on the assessment, the Stirling engine micro-CHP and PVT collectors have the highest potential for renewable cogeneration in the residential building sector.

The literature review on the HRES including micro-cogeneration and solar support on the building sector was conducted and the key findings were highlighted. It was seen that photovoltaic and solar thermal technologies were integrated with Stirling engine and ORC systems. In more advanced hybridization, the PVT was used as a solar extension. Based on the literature, the system reliability was increased with the hybridization and CO2 emissions were reduced. Additionally, the electricity production capability was increased significantly with PVT and the fuel-fired micro-CHP overcame the fluctuation of solar energy sources. However, more experimental data on hybridization and research on advanced energy management strategies are required.

The results of the case study including PVT/battery/thermal storage system revealed that hybridization with high efficient and fuel-fired heat and electricity generation is required. In this case, the coupling of the PVT system with the biomass-fueled Stirling engine micro-CHP system should be considered to cover residential electricity, space heating and domestic hot water demands. The Stirling micro-CHP can provide a stable baseload and support fluctuating solar energy production. The coupling of these technologies can form a hybrid renewable energy system that provides 100% renewable energy for buildings.

Acknowledgements

The authors would like to thank Interreg V Rhin supérieur ACA-MODES project for their support and funding of this research.

CHAPTER 6. Exergy and Exergo-economic analysis of a hybrid renewable energy system under different climate conditions

Sonja Kallio and Monica Siroux

INSA Strasbourg ICUBE, University of Strasbourg

This article is published in *Renewable Energy*

https://doi.org/10.1016/j.renene.2022.05.115

Abstract

The building sector has a great potential to accelerate the decarbonisation by using high efficient and 100% renewable energy production on-site. This allows also increased energy autonomy to protect building owners against increasing electricity prices. The key solution is to apply micro combined heat and power (micro-CHP) systems to form a domestic hybrid renewable energy system (HRES) which supports fluctuating solar energy production by the controllable biomass-fueled micro-CHP. However, despite the market availability of the technology, the initial investment of such a system is assumed to be a barrier to penetration. In this study, dynamic exergy and exergo-economic analyses of the HRES are conducted in Matlab/Simulink to define the specific costs of energy products when the market available system is applied to the European building stock under different climate and economic conditions. The overall exergy efficiency of the system is 13%-16%. The specific costs have high variation on a monthly and location basis. On a yearly basis, the lowest specific cost of electricity is 0.29 €/kWh in the southernmost location and of heat products 0.319 €/kWh$_{ex}$ (0.034 €/kWh). The comparative results show that the HRES is economically viable and reduces primary energy use and costly irreversibility up to 95%.

Keywords: Hybrid renewable energy systems; Climate conditions; Exergy analysis; Exergo-economics; Renewable micro-cogeneration

1. Introduction

The building sector is the largest energy end-use sector in the European Union (EU) with a share of 41% [143]. To reduce final energy use and greenhouse gas emissions in the building sector, the energy efficiency measures for buildings have been under strong focus in research and

in the content of the EU directives, such as the Energy Performance of Building Directive [166]. The EU has also set the energy efficiency targets for 2020 and 2030 by aiming to reduce energy consumption and emissions by 20% by the year 2020 and by at least 32.5% by the year 2030 compared to the 1990 level as a baseline [5]. However, despite the great energy-saving potential of the building sector, gaining the savings has proven challenging [167]. The EU Building Factsheets [167] present a breakdown of the residential buildings by the construction year, which show that the European building stock has a significant share of older buildings constructed before 1990. Due to this, the renovating and retrofitting measurements are required to implement to already existing buildings to gain the energy-saving potential of the building sector. These measures should not only be passive measures, such as building envelope enhancement [168], but also active measures to have decentralized high efficient solutions for electricity, space heating and domestic hot water (DHW) production in buildings. The active measures should aim to have 100% renewable energy production in the building sector, which is possible with the hybrid renewable energy systems combining different energy sources, such as biomass and solar energy [169].

The key solution for the active measures to accelerate the decarbonisation of the building sector is micro combined heat and power (micro-CHP), or co-generation, systems. Micro-CHP refers to the units that produce decentralized heat and power simultaneously from a single fuel source at high efficiency. Typically, these units operate in buildings or small communities to produce energy for on-site use. The micro-CHP units typically have an electrical power of up to 15 kW [20]. However, according to the definition of the EU in the energy efficiency directive [170], micro-cogeneration refers to units with electrical power below 50 kW.

The micro-CHP system can be powered by different prime movers, such as an internal and external combustion engine or non-combustion based prime mover. Such prime movers are internal combustion engine (ICE), organic Rankine cycle (ORC), fuel cells and Stirling engine. A photovoltaic-thermal (PVT) collector is a non-combustion based cogeneration unit that converts solar energy into heat and electricity simultaneously from the same installed area. The photovoltaic (PV) panel produces electricity which generates waste heat at the same time. In the PVT collector, the PV panel has a cooling circuit underneath the panel, and the waste heat is recovered to the coolant flow to produce thermal energy. This leads to the simultaneous production of heat and power at high efficiency. However, due to the fluctuating nature of solar

energy availability, the PVT collector cogenerates energy in an uncontrolled manner. On the other hand, a biomass-fueled Stirling engine micro-CHP is the external combustion based cogeneration unit that has high fuel flexibility and produces, in a controlled manner, heat and power, simultaneously. The Stirling engine can be fueled by renewable energy, such as biomass and solar energy. The performance of the biomass and solar energy-fueled Stirling engines were compared by Ferreira et al. [27]. They concluded that the biomass-fueled Stirling engine provided 87.5% more power output than the solar fueled, had 52% lower levelized costs of electricity production and had controlled energy output.

A hybrid renewable energy system (HRES) is a second key solution for the active measures. The HRES refers to the generation of multiple energy products from the integration of two or more renewable energy sources with or without conventional energy sources and storage [161]. These systems are especially appropriate for small- and micro-scale distributed generation applications [171]. The hybridization of the solar and engine-based cogeneration units enables the use of cost-free, clean and fluctuating solar energy, and as a base-load the controllable but paid fuel energy, such as biomass. Additionally, the energy storage can be used to facilitate the energy management between the production and highly varying energy demand of a building. The hybridization enables highly efficient energy generation, increased reliability and flexibility, support for fluctuating solar energy source and the reduction in costs, primary energy use and CO_2 emissions.

Numerous studies of the domestic HRES performance with different configurations of micro-CHP and solar technologies have been conducted in the literature. The ICE based micro-CHP unit was coupled with photovoltaic (PV) panels and solar thermal collectors in [49–51] and the ORC based prime mover was studied in [57, 58]. Kotowicz and Uchman studied a domestic HRES combining a natural gas-fuelled Stirling engine based micro-CHP with PV panels and electrical energy storage [55]. Aunón-Hidalgo et al. [54] presented an experimental study of a grid-connected HRES consisting of a natural gas-fueled Stirling engine micro-CHP combined with photovoltaic panels and solar thermal collectors for a domestic environment. The energy management between the system and the domestic user was facilitated by the electrical and thermal energy storages. They conducted an energy performance and CO_2 emissions assessment of the system. Their results showed that the system was able to cover 75.6% of the total energy demand and reached 36.2% reduction in CO_2 emissions. They concluded that biogas or biomass

should be used as a micro-CHP fuel instead of natural gas to achieve zero CO_2 emissions. A review on the domestic HRES based on cogeneration and solar support was presented in [172]. However, a research gap was indicated and there are no studies on a domestic HRES which combines the biomass-fueled Stirling engine micro-CHP with the PVT collectors.

The assessment of the HRES can be extended to exergy and exergo-economic performance. The latter is used to define the specific costs of energy products from the system with multiple products and the costs flows associated with exergy flows in the system. The exergo-economic method is useful when the considered system has multiple inputs and outputs with different exergies. Mouaky and Rachek [173] conducted a dynamic energy, exergy and exergo-economic assessment of a novel HRES driven by biomass and solar energy. The system was designed to be a polygeneration unit that, in addition to electricity cooling, heating and DHW, produced freshwater for a rural community of 40 residential buildings. Their results indicated that the system was able to cover fully the community's requirements except for cooling. The annual exergo-economic costs of the produced electricity DHW and space heating were 0.239 €/kWh, 0.043 €/kWh and 0.035 €/kWh, respectively. However, they concluded that the specific costs were competitive for remote communities but a significant reduction in the cost should be achieved to facilitate the implementation of such systems. Another dynamic exergy and exergo-economic analysis of a renewable solar-biomass HRES for polygeneration was studied by Calise et al. [118]. The system consisted of parabolic trough photovoltaic-thermal (cPVT) collectors, an absorption chiller, a biomass heater and a desalination unit. Based on their results, the cPVT collectors caused the highest exergy destruction followed by the biomass boiler in the system. The exergo-economic results revealed a high fluctuation over the year in the exergo-economic costs of the different products. Wang et al. [116] conducted an exergo-economic analysis and optimization of the HRES based on cogeneration units. The system consisted of cPVT collectors with a natural gas fired internal combustion engine (ICE) micro-CHP unit for a hotel building application to produce cooling, heating, DHW and electricity. The exergo-economic analysis was based on the energy level method. This method allows allocating the higher specific cost for the energy product with the higher energy level, such as electricity should be more expensive than low grade heat.

Within the given framework, this study aims to contribute to the existing literature through the dynamic energy, exergy and exergo-economic analysis of the cogeneration based

HRES under different European climate and economic conditions to satisfy residential building energy demand. The novel HRES configuration includes PVT collectors combined with the biomass fueled Stirling engine micro-CHP unit and thermal energy storage to facilitate the decarbonisation of the building sector.

The paper is structured as follows. In the second section, the detailed system description is provided with a modelling approach, building energy demand profiles and weather data. Additionally, the exergy and exergo-economic models are introduced with the performance indicators. In the third section, the results of the exergy and exergo-economic analysis are presented and discussed. Next, the comparative results of the HRES to the reference systems are presented and discussed. Finally, the main conclusion is drawn in the fourth section.

2. Methodology

2.1 System description

In the considered hybrid renewable energy system (HRES), the water-cooled flat plate PVT collectors are integrated with the biomass-fueled micro-CHP system and thermal energy storage (TES). The system layout with the energy and mass flows is presented in Figure 6-1. The HRES is used to produce domestic hot water, space heating and electricity for a residential building use. The cooling demand is not considered in this study. The biomass-fueled micro-CHP is a critical component of the HRES to satisfy, especially, the thermal energy demand and the PVT collectors are used as a support to reduce costly biomass use and CO_2 emissions. The same system configuration of the HRES is applied in each location to investigate how the utilization rates of the energy production units (the micro-CHP and PVT) vary under different climates and how they impact on the exergo-economic costs of the system. The system configuration is valid in each location because the winter conditions require the controllable energy production for the significant space heating and DHW demand but there is good solar availability in each location. The annual space heating demands are presented in Figure 6-3 and the annual solar availability and ambient temperatures in Figure 6-7.

The capacity of the micro-CHP was selected based on the market available domestic biomass-fueled micro-CHP technology called ÖkoFen Pellematic Condens_e powered by a Stirling engine. The unit has a nominal electrical power of 1 kW and thermal power of 12 kW. This micro-CHP unit has been experimentally tested in the laboratory of INSA Strasbourg

ICUBE in France and the aim of this study is to demonstrate the use of the unit in the existing residential sector. The ÖkoFen micro-CHP unit is fed by air (flow 1) and wood pellets (flow 2) to produce electricity (flow 3) and hot water (flow 4) as energy products. The coolant mass flow between the unit and TES is fixed to be 0.2 kg/s. The micro-CHP follows the heat-driven ON/OFF control strategy to satisfy the temperature levels of the thermal storage. The start-up and shut-down dynamics of the unit are neglected in this study. Additionally, the unit has internal control and is shut down if the coolant temperature reaches 75 °C.

The field of water-cooled flat plate PVT collectors is used to convert available solar radiation into heat (flow 11) and electricity (flow 12). The field consists of 9 collectors in a matrix of 3x3 to reach the higher outlet temperature from the field to the TES and to cover assumed available roof area of a typical residential building. The reference electrical efficiency of the collectors is 18.7%, and the coolant mass flow is 100 kg/h per row of the collectors. A differential temperature controller is used to control the coolant mass flow between the TES and PVT collectors. The controller compares the outlet temperature of the PVT to the temperature of the bottom of the thermal storage. The coolant mass flow is stopped or started gradually if the temperature difference is smaller or greater than 5 K to avoid cooling the storage.

The stratified 2 m^2 multi-port sensible heat storage is used to store the produced thermal energy from the micro-CHP and PVT collectors, simultaneously. Water is used as a storage medium. The volume of the storage was selected to be large to supply space heating and DHW, to enable more continues running of the micro-CHP and to store heat from two sources, simultaneously. The micro-CHP unit charges the TES to the top of the tank, and the return connection to the unit (flow 5) is at the bottom of the tank. The TES has an internal heat exchanger at the lower part of the tank to recover the heat from the PVT field. Both return connections are located at the bottom of the tank. The TES supplies heat for space heating (flow 8) of the reference building, and it has an internal heat exchanger to produce domestic hot water at 55 °C (flow 6).

The electricity flow from the micro-CHP (flow 3) and the PVT field (flow 12) are used to satisfy the power balance between the production and the electricity demand of the building presented in Figure 6-5. The surplus electricity is fed to the electric grid.

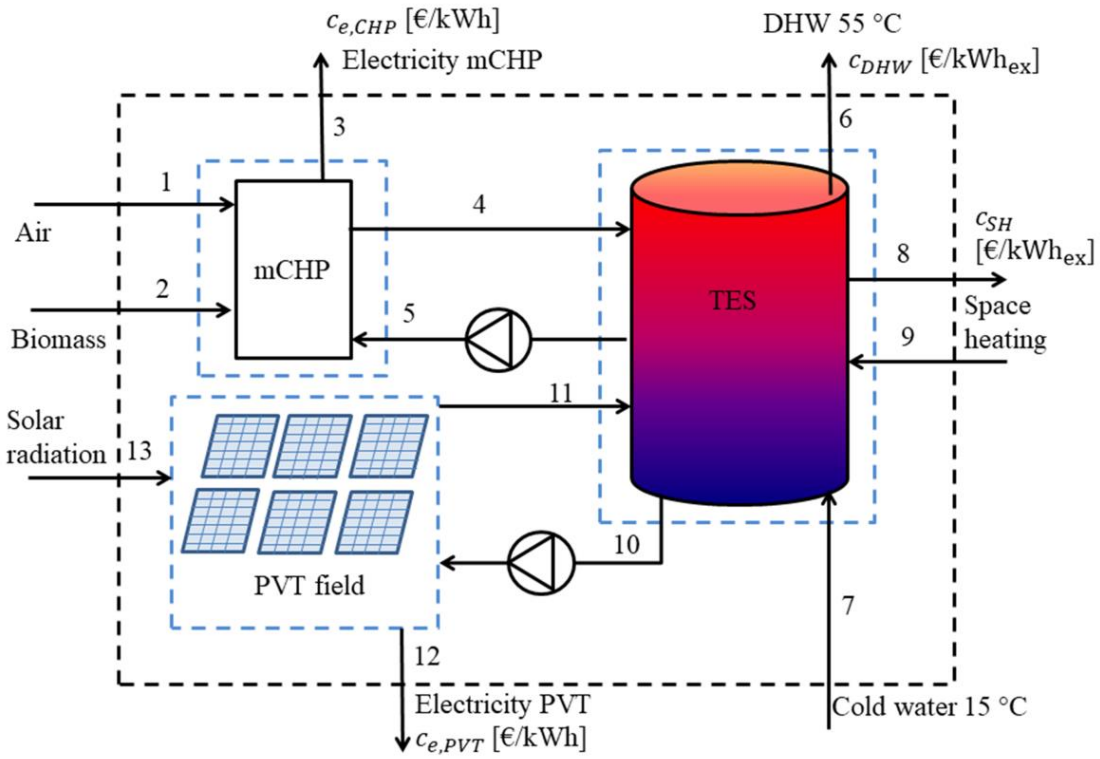

Figure 6-1: *The system layout and control volumes of the hybrid renewable energy system.*

The main characteristics of the described HRES are presented in Table 6-1.

Table 6-1: The main characteristics of the hybrid renewable energy system

Component	Parameter	Value	Unit
Micro-CHP	Thermal power	12	kW
	Electrical power	1	kW
	Fuel	Wood pellets	
PVT	Area single	2	m^2
	Ref. electrical efficiency	18.7	%
	PVT in series	3	-
	PVT in rows	3	-
TES	Volume	2	m^2
	Insulation	0.3	W/m^2K

2.2 Simulation models

A dynamic simulation model of the described HRES was built into Matlab/Simulink environment to analyze its yearly exergetic and exergo-economic performance.

The open-source CARNOT-Toolbox [134] was used to model the stratified multi-port thermal energy storage, pipe connections, thermostatic flow mixers for heat supply, valves and pumps. The validated tank model called "Storage_Type_5" was used in which the storage volume is divided into 6 nodes to present the stratification. For each node, the energy balance is calculated to find the current temperature of each node. The detailed tank model is presented in [174]. The thermostatic flow mixers were used to control the required heat supply temperatures of 40°C for space heating and 55°C for DHW.

In the authors' previous work [83], a single water-cooled flat plate PVT collector with glazing and sheet-and-tube heat exchanger was modelled into Matlab/Simulink and extended to present a field of the PVT collectors. The model considers the main heat transfer mechanisms between each PVT layer, such as the glass cover, PV module, absorber and coolant fluid. The electricity conversion efficiency of the PVT collector depends linearly on the PV module temperature T_{pv}, the temperature coefficient β_{PV} and the efficiency η_{STC} at standard conditions T_{ref}. The key governing equations of the PVT collector in terms of thermal and electrical energy are following:

$$m_g \times c_{p,g} \times dT_g/dt = Q_{g,sol} + Q_{g-e,CV} + Q_{g-sky,RD} + Q_{g-pv,CV} + Q_{g-pv,RD} \quad (1)$$

$$m_{pv} \times c_{p,pv} \times dT_{pv}/dt = Q_{pv,s} + Q_{pv-g,CV} + Q_{pv-g,RD} + Q_{pv-f,CV} - E \quad (2)$$

$$m_f \times c_{p,f} \times dT_f/dt = Q_{f-pv,CV} + Q_f \quad (3)$$

$$\eta_{el(T)} = \eta_{STC} \times \left[1 - \beta_{PV} \times \left(T_{pv} - T_{ref}\right)\right] \quad (4)$$

The detailed description of the used model and the validation can be found in [83].

The considered HRES includes the ÖkoFEN Pellematic Condens_e unit which is a biomass-fueled Stirling engine micro-CHP system and has been experimentally tested in the laboratory of INSA Strasbourg ICUBE in France. The mathematical model of the system is based on Annex 42 [94] modelling approach of the external combustion engine and the following energy balance governing equations are implemented to Simulink to model the heat transfer to the coolant fluid [155]:

$$MC_{eng}\, dT_{eng}/dt = UA_{HX} \times \left(T_{w,out} - T_{eng}\right) + UA_{loss} \times \left(T_{env} - T_{eng}\right) + q_{gen} \quad (5)$$

$$MC_{w} \times dT_{w,out}/dt = \dot{m}_{w} \times c_{p,w} \times \left(T_{w,in} - T_{w,out}\right) + UA_{HX} \times \left(T_{eng} - T_{w,out}\right) \quad (6)$$

The previously collected experimental data of the considered micro-CHP was used to validate and identify the thermal capacity of the engine MC_{eng} and cooling water MC_{w}, and the engine specific heat transfer coefficients UA_{HX} and UA_{loss}. The identification was performed with Simulink Parameter Estimator Tool.

The recovered heat from the micro-CHP control volume Q_{CHP} is calculated from the cooling water mass flow rate mw and temperature difference between the inlet and outlet of the flow [157].

$$Q_{CHP} = \dot{m}_{w} \times c_{w} \times \left(T_{w,in} - T_{w,out}\right) \quad (7)$$

2.3 Building energy demand

The considered HRES is installed in a single or multi-family house in different locations. As a reference building, a single-family house presented in Figure 6-2 was selected and simulated in the IDA ICE building simulation tool [175]. The building U-values were defined based on the building factsheets of the European Union [167], which represent the building stock characteristics in different European countries. Based on this average building performance data, the defined reference building was simulated under different climate conditions with the country-specific U-values of the building shell. The hourly heating demand profiles were obtained from the simulation in the different European locations and used in the exergo-economic analysis. The selected locations were Tampere, Finland; Strasbourg, France and Barcelona, Spain. The geometry of the reference building and building performance parameters in the different locations are presented in Table 6-2.

Figure 6-2: *The reference building used in the building simulation.*

Table 6-2: The main characteristics of the reference buildings and the climate classifications in each location [167].

Parameter	Building geometry	U-value [W/m^{2}K]		
		Finland	France	Spain
Windows	19 m^2	1.76	2.83	4.16
Walls	111 m^2	0.34	0.97	1.32
Floor	150 m^2	0.32	0.89	1.03
Roof	143 m^2	0.23	0.83	1.45
Windows to wall ratio	0.17			
Climate classification		Subarctic	Semi-continental	Dry-summer subtropical

The annual results of the hourly thermal load in three locations are presented in Figure 6-3. This Figure shows that space heating is required during the whole year in the northernmost location of Tampere resulting in the annual demand of 152 kWh/m^2. In Strasbourg, the annual demand is 160 kWh/m^2. The milder climate conditions of Strasbourg did not reduce the heating demand compared to Tampere, because of the higher U-values of the building envelope. However, during the summer period the heating demand was slightly lower in Strasbourg than in Tampere as shown in Figure 6-3. In Barcelona, the annual heating demand was significantly lower than in Tampere and Strasbourg due to the warmer climate resulting in 86 kWh/m^2. In Barcelona, there was no space heating demand during July, August and September.

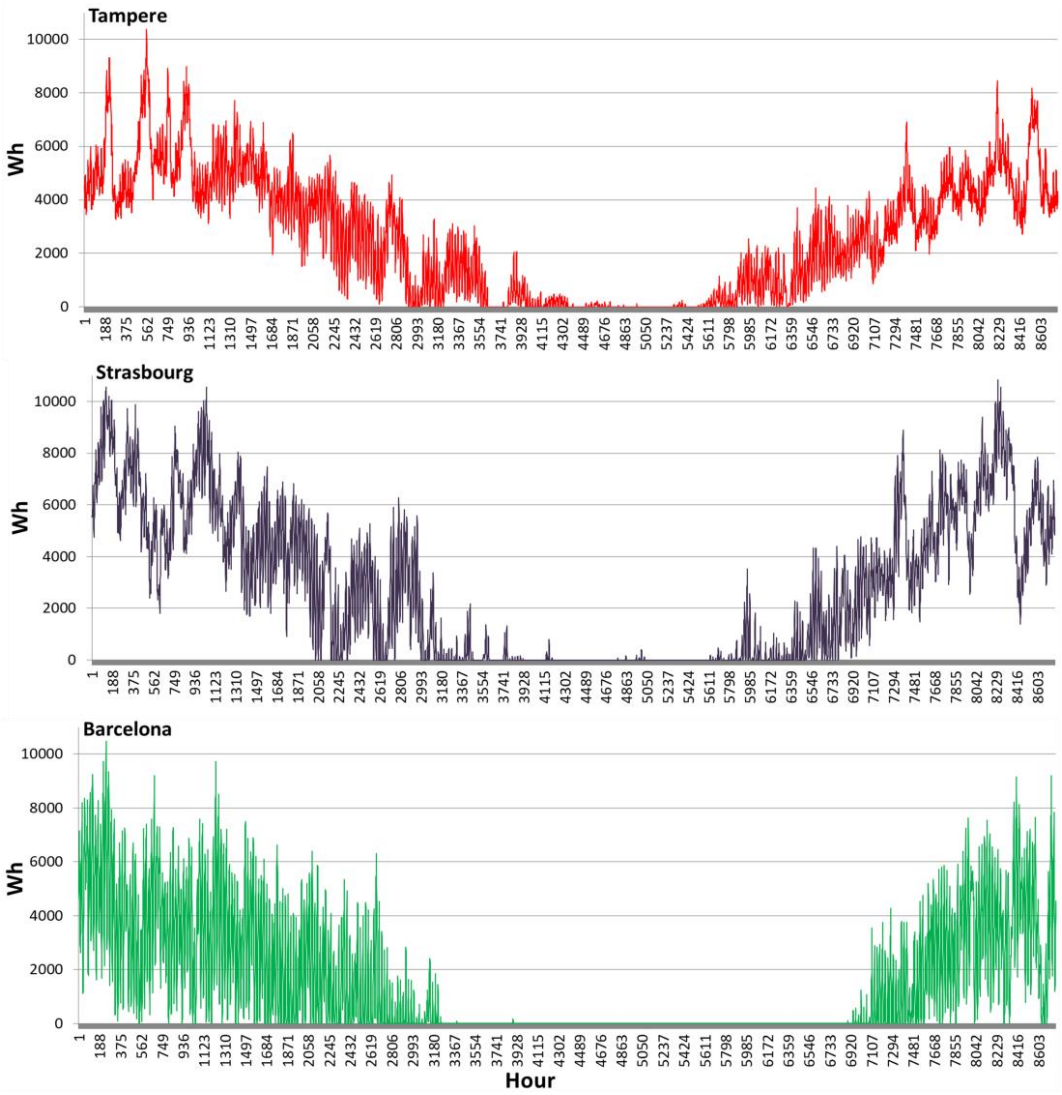

Figure 6-3: *The annual results of the hourly thermal load in each location.*

In addition to space heating, the HRES is used to produce domestic hot water (DHW). The reference building is assumed to include 4 inhabitants with 250 l/day average consumption. The hourly DHW demand profile based on probability distribution was generated using the DHW-calc tool developed for IEA-SHC Task 26 at the University of Kassel in Germany [176, 177]. The different parameters, such as the average daily consumption, flow rates and daily, weekly and monthly weighting of the consumption, were defined to generate a realistic DHW demand profile suitable for each location. An example of the demand profile is presented in Figure 6-4.

In the system simulations, the temperature of the cold water entering the system from the mains was assumed to be at 15 °C during the year in each location and the water was heated up to 55 °C.

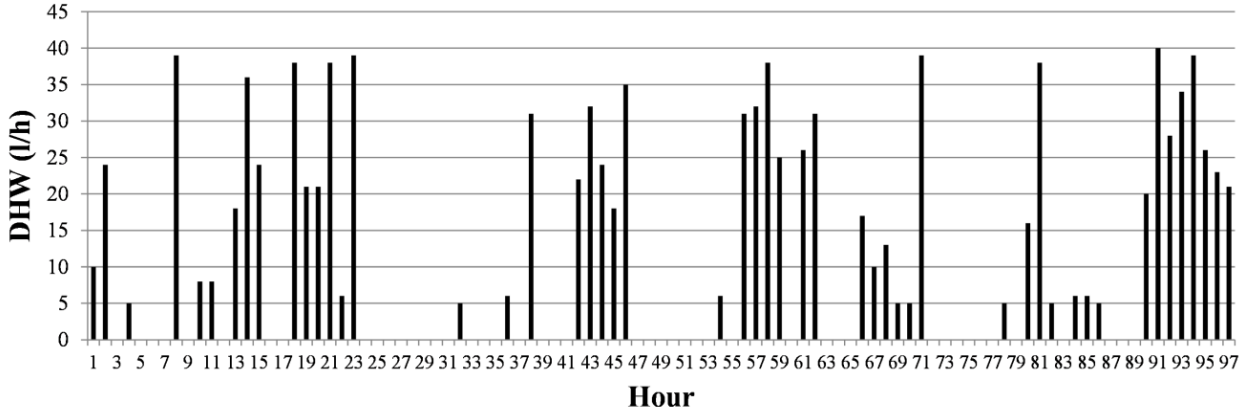

Figure 6-4: *The hourly DHW demand profile generated by the DHW-calc tool.*

The electricity demand profile was assumed to be the same in each location. The normalized standard electricity demand profiles for residential buildings generated by the German Association of Energy and Water Industries, BDEW (Bundesverband der Energie- und Wasserwirtschaft) [178] are used to simulate electricity demand every 15 min for certain yearly consumption. The profile takes into account electrical appliances excluding special applications, such as heat pumps and electrical storage heaters. The used electricity profile includes three different periods of the year: winter, summer and transition. Additionally, three different types of the day are presented: workday, Saturday and Sunday/holiday. Figure 6-5 shows the sample of the profile during a summer period. In the analysis, the yearly consumption of 6000 kWh was assumed for a single-family house in each location.

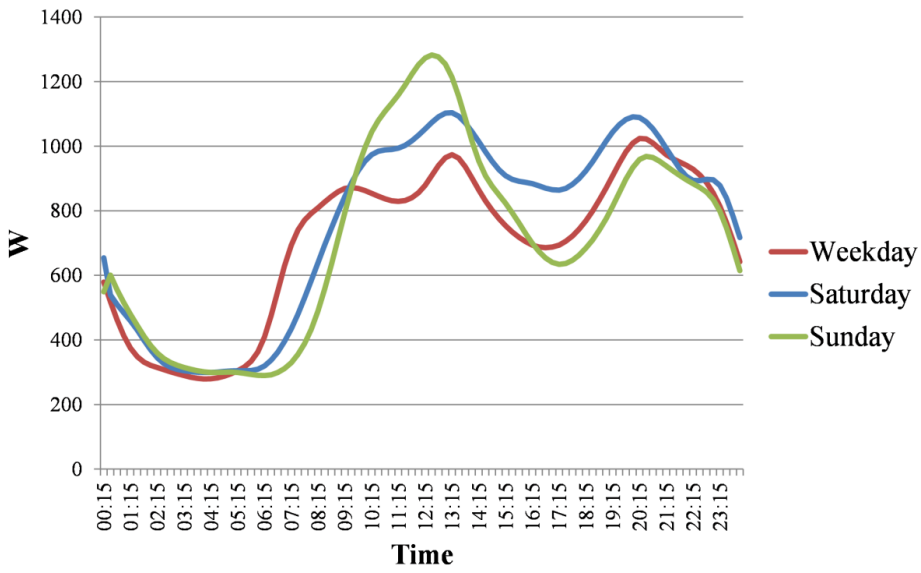

Figure 6-5: *The electricity profile for a day (weekday, Saturday and Sunday).*

2.4 Meteorological data

The proposed HRES is studied under three different European climate conditions because the energy yield of the PVT collectors depends strongly on the weather parameters, such as solar radiation, wind speed and ambient temperature. The performance of the PVT collectors has a direct impact on the available solar support in the hybrid energy system and on the fuel costs reduction.

The selected locations are Tampere, Finland; Strasbourg, France and Barcelona, Spain. According to the Köppen climate classification presented in Figure 6-6, Tampere represents Northern Europe with a subarctic climate border. This means that the ambient temperature reaches above 10 °C only 3 months in a year [83]. Strasbourg represents Central Europe, and according to the classification, it has a semi-continental climate with cool winters and relatively sunny summers. The Mediterranean location Barcelona represents South of Europe, and according to the classification, it has a dry-summer subtropical climate. This means hot and dry summer with a cooler and wetter wintertime.

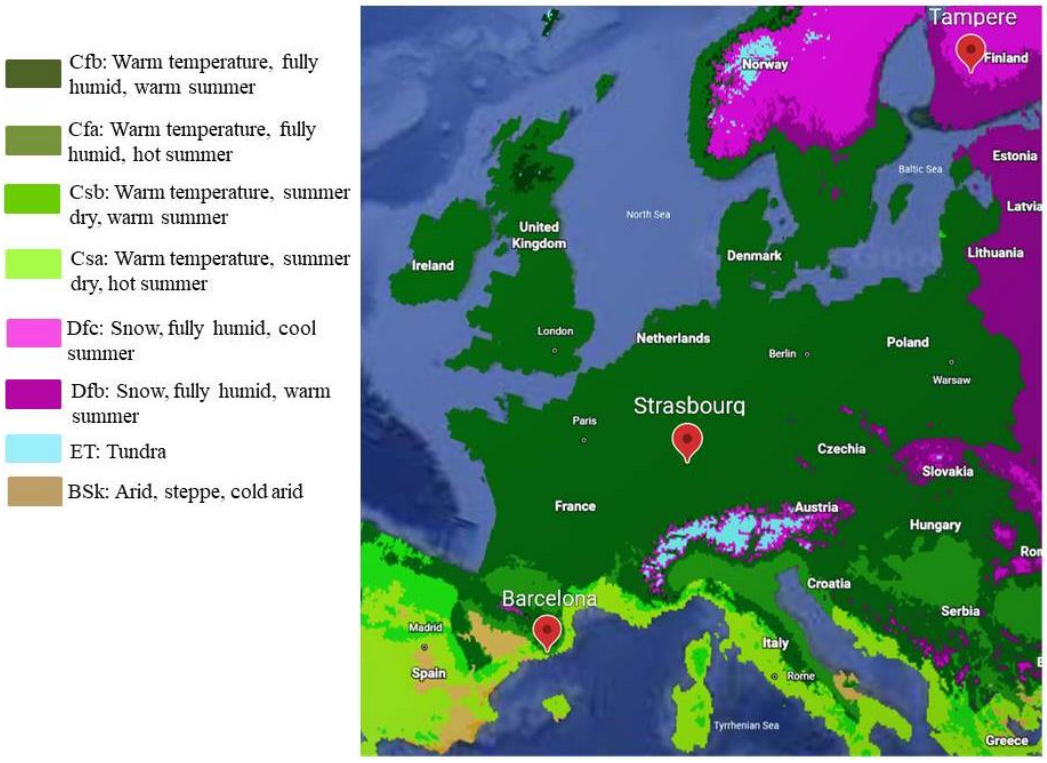

Figure 6-6: *The Köppen-Geiger Climate Classification map [179]*.

Figure 6-7 shows the global solar irradiation and ambient temperature over year in each location. The presented hourly weather data is obtained from the IDA ICE building simulation software and is based on the ASHRAE IWEC (International Weather for Energy Calculation) database [180]. In this database, the weather files for different locations are derived from the collected hourly weather data for up to 18 years [181]. These “typical” weather files for different locations smooth the yearly variation of the weather conditions.

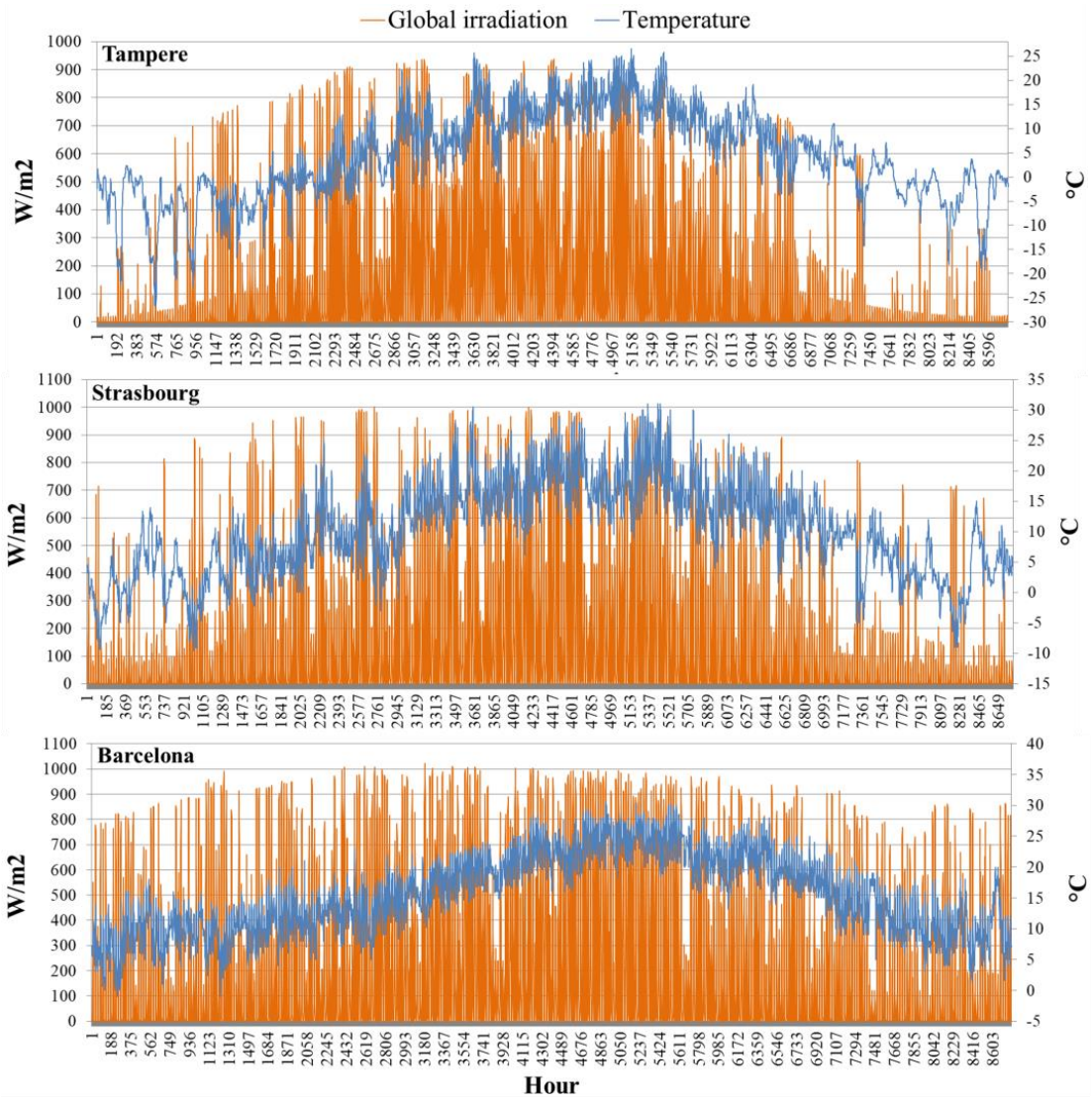

Figure 6-7: *The hourly solar radiation and ambient temperature based on the historical data in each location [180].*

The monthly average ambient temperatures are presented in Table 6-3. This data is used in the exergy and exergo-economic analysis as monthly reference temperatures in order to take into account the impact of the location to thermal exergy production.

Table 6-3: The monthly average temperatures in each location [180].

Month	Tampere, average temperature [°C]	Strasbourg, average temperature [°C]	Barcelona, average temperature [°C]
January	-6.3	2.3	8.2
February	-6.6	2.1	9.4

March	-2.5	6.0	11.2
April	3.3	9.9	13.2
May	9.6	14.7	17.1
June	13.5	17.4	21
July	16.6	18.9	23.6
August	15.1	19.0	24
September	9.2	14.7	21.5
October	4.6	10.5	17.2
November	-1.2	4.8	12
December	-4.2	2.7	9.7

2.5 Exergy analysis

The exergy analysis is based on the Second Law of Thermodynamics and it quantifies the quality of the input and output in the energy conversion process. It complements the First Law based energy analysis by counting how well the quality of the fuel energy is maintained in the conversion process while energy analysis quantifies only the amount of energy produced and lost in the process. Through the energy conversion process, exergy is always destroyed but energy changes its form and is never destroyed. The exergy analysis helps to reveal better inefficiencies in the conversion process. The quality of energy is counted as a work potential to the specific environment or reference temperature. Typically, this state is the environmental conditions of the energy conversion device. The selection of the reference temperature defines the exergy of the system and it should be selected carefully. In this study, the monthly exergy and exergo-economic analysis is conducted under different climate conditions and the monthly average ambient temperatures in Table 6-3 are used as reference temperatures.

The exergy balance of the cogeneration is generally presented as follows:

$$\sum Ex_{in} - \sum (Ex_{el} + Ex_{th}) = \sum Ex_{d} \qquad (8)$$

where Ex_d is the exergy destruction, Ex_{in} is the exergy content of the used fuel, and Ex_{el} and Ex_{th} represent the electrical and thermal exergy products, respectively. The exergy efficiency is calculated by dividing the sum of the exergy products by fuel exergy.

The considered system receives the fuel exergy from biomass and solar radiation. The PVT field absorbs exergy from solar radiation which is not seen as pure exergy but a following conversion conversation coefficient is used to calculate incoming exergy [103]:

$$Ex_{in,PVT} = A_c \times G_{irr} \times (1 - 4/3 \times T_0/T_{sol} + 1/3 \times (T_0/T_{sol})^4) \quad (9)$$

In Equation (9) T_0 is the monthly reference temperature in Kelvin and T_{sol} is the solar temperature (5777 K). The fuel exergy of biomass is defined as follows [109]:

$$Ex_{in,CHP} = f_{q,biomass} \times \dot{m}_f \times LHV_{biomass} \quad (10)$$

where $f_{q,biomass}$ is a quality factor of wood pellets and $LHV_{biomass}$ is the lower heating value of 4900 Wh/kg. In this study, the quality factor of 1.13 is used for wood pellets [159].
As an energy product, electricity is seen as pure exergy which can be totally transformed into work. However, the exergy content of thermal energy flow from the micro-CHP, PVT field and thermal energy storage depends on the specific enthalpy (h) and entropy (s) of the water flow at the inlet and outlet of the certain component. The specific enthalpy and entropy of the certain flow depends on the temperature at which the flow is made available. The thermal exergy of water flows in the system is presented as follows [29, 109]:

$$\begin{aligned} Ex_{th} &= \dot{m} \times [h_{out} - h_{in} - T_0 \times (s_{out} - s_{in})] \\ &= \dot{m} \times c_{p,f} \times [(T_{out} - T_{in}) - T_0 \times ln(T_{out}/T_{in})] \end{aligned} \quad (11)$$

where ṁ is the mass flow rate, $c_{p,f}$ is the fluid specific heat.

2.6 Performance indicators

The considered HRES has highly dynamic behavior due to dependence on the fluctuating solar radiation and energy demand. Due to this cumulative energy and exergy flows are used to calculate the performance indicators over defined periods:

$$Ex_j = \int_{period} \dot{E}x_j \, dt \quad (12)$$

The period is defined to be a month to see the difference in the performance indicators during a year.

The exergy efficiency of the whole HRES is presented as follows:

$$\zeta_{overall} = \frac{(Ex_8 - Ex_9) + (Ex_6 - Ex_7) + Ex_3 + Ex_{12}}{Ex_{in,CHP} + Ex_{in,PVT}} \quad (13)$$

where the exergy products are space heating, domestic hot water and electricity produced by the PVT field and micro-CHP unit.

The operation of the considered hybrid energy system including cogeneration units can be compared to separated production of heat and electricity. The defined reference system for separated energy production includes the electric grid based on the centralized nuclear power plant and a natural gas-fueled boiler. The energy based comparison indicator is Primary Energy Savings (PES) [109]:

$$PES = \left(1 - \frac{1}{\frac{\eta_{el}}{\eta_{eg}} + \frac{\eta_{th}}{\eta_b}}\right) \times 100 \quad (14)$$

The PES indicator shows the saved primary energy when cogeneration is used instead of the separated energy production. However, this indicator qualifies electricity and heat to be the same value but, in terms of exergy, heat has lower quality than electricity. This leads to a fact that it is not reasonable to directly compare the different energy products of the system. Thus, an exergy-based comparison indicator called Relative Avoided Irreversibility (RAI) [79, 109] is used and presented as follows:

$$RAI = \left(1 - \frac{Ir_{CHP}}{Ir_{eg} + Ir_b}\right) \times 100 \quad (15)$$

$$Ir = (1 - \zeta) \times Ex_{in} \quad (16)$$

where Ir is the generated exergy irreversibility or destruction of the certain energy conversion process.

2.7. Economic and Exergo-economic assessment based on energy level and varying reference temperatures

In this study, the considered HRES is economically assessed by the economic indicators called Simple Payback-Time (SPT) and Net Present Value (NPV) and by an exergo-economic analysis which specifies the costs of the energy products from the HRES.

2.7.1 Economic indicators

The SPT gives a rough estimation of the economic viability of the considered system by dividing the initial investment costs (Z_{sys}) by all counted revenues/savings that the system can generate during yearly operation. However, it does not take into account the time value of cost which results in the rough estimation of the payback-time in years. This indicator is calculated as follows [182]:

$$SPT = Z_{sys}/SV_{sys,year} \tag{17}$$

where $SV_{sys,year}$ is the yearly savings compared to a reference system and calculated as follows [182].

$$\begin{aligned} SV_{sys,year} = & \left(E_{el,load} \times c_{el,fromGrid} + \frac{\left(Q_{th,SH} + Q_{th,DHW}\right) \times c_{NG}}{LHV_{NG}\eta_b} \right)_{RS} \\ & - \left(m_{biomass} \times c_{biomass} + E_{el,fromGrid} \times c_{el,fromGrid} \right. \\ & \left. - E_{el,toGrid} \times c_{el,toGrid} + OM_{CHP} \right)_{HRES} \end{aligned} \tag{18}$$

where RS indicates the reference system and HRES the considered hybrid system.

Another useful economic indicator to evaluate the economic viability is the NPV, which takes into account time by discounting future savings to the present value over the lifetime of the HRES. A positive NPV indicates economically acceptable investment and a negative indicates unviable investment under considered circumstances.

$$NPV = -Z_{sys} + \sum_{n} \left(a \times SV_{sys,year} \right) \tag{19}$$

$$\mathrm{a} = 1/(1+r)^n \tag{20}$$

where a is the annuity factor, r is the discount rate and n is the lifetime of the system.

2.7.2 Exergo-economic analysis

The exergo-economic analysis combines exergy with economic analysis and is used to allocate the initial investment and operating and maintenance (O&M) costs for the energy products of the. In this study, the Specific Exergy Costing (SPECO) approach proposed by Lazzaretto and Tsatsaronis [91] is used. Based on that method, a cost value can be assigned to exergy unit of each energy flow in Figure 6-1 coming and leaving a certain system component. The exergy costing method reveals the prices for the produced electricity and heat that should be returned or saved to cover the initial investment and O&M costs of the HRES. According to the SPECO, the exergy cost balance equation of the kth component in steady operating conditions can be written as follows:

$$\dot{C} = c \times \dot{E}x \tag{21}$$

$$\sum_{\text{fuel}} \left(c_f \times \dot{E}x_f\right)_k + \dot{Z}_k = \sum_{\text{product}} \left(c_p \times \dot{E}x_p\right)_k \tag{22}$$

where $\dot{C}$ is exergy cost rate in €, c is the specific cost of exergy in €/kWh$_{ex}$ and $\dot{E}x$ is the exergy rate in kW. Due to the fluctuating nature of solar energy production, the cumulative exergy flows over defined period based on Eq. (12) are taken into account and the exergy rates in Eq. (22) are replaced by the cumulative values. In Eq. (22), $\dot{Z}$ represents non-exergetic costs including initial investment costs and O&M costs of the component with the Capital Recovery Factor (CRF). The cumulative non-exergetic costs are presented as follows:

$$\begin{aligned} \tilde{Z}_k &= I_k \times CRF \times t_{period}/8760 + OM_k \\ &= I_k \times \frac{i(1+i)^n}{(1+i)^n - 1} \times t_{period}/8760 + OM_k \end{aligned} \tag{23}$$

where t_{period} is the length of considered period, i is the interest rate, n is the lifetime of the component and OM is the O&M costs over the considered period. It is assumed to be 1.5% of the levelized investment cost of the period for the micro-CHP unit.

The considered HRES has multiple outputs and it includes cogeneration components that have multiple products. Due to this, auxiliary costing equations are required to define the specific cost of the multiple products. Additionally, the energy levels of different energy products are

taken into account in the costing method according to [183]. The energy level reveals the quality of the energy flow and its ability to work to the reference temperature [183]. By considering the energy level, the specific cost of any flow is directly proportional to its energy level and gives the higher price for the higher quality flow. This leads to more realistic evaluation of the exergo-economic performance of different energy product.

The energy level of electricity is 1 but the level of heat depends on the following formula [183]:

$$EL = 1 - T_0\,\Delta S/\Delta H \tag{24}$$

where T_0, ΔS and ΔH are the reference temperature, entropy change and enthalpy change, respectively.

In addition to the energy levels, the location and period specific reference temperatures in Table 6-3 were taken into account in the monthly exergo-economic analysis in order to have a fair comparison between different locations of the HRES.

Next, the exergo-economic model of the HRES in Figure 6-1 is presented. The model includes a number of cost balances and n-1 auxiliary costing equations for three main components: micro-CHP, PVT field and thermal energy storage. Table 6-4 presents the economic parameters used in the exergo-economic analysis. The initial investment costs are presented without the country specific Value Added Tax (VAT) which is taken into account in the calculations. The VAT is 24% for Finland, 20% for France and 21% for Spain.

Table 6-4: The economic parameters of the exergo-economic analysis.

Parameter	Description	Value	Unit	Ref.
I_{CHP}	Initial investment costs of micro-CHP	17600	€	ÖkoFEN company
OM_{CHP}	O&M costs of micro-CHP	1.5	%	
I_{PVT}	Initial investment costs of PVT	295	€/m^2	DualSun company
I_{inv}	Initial investment costs of inverters	100	€/piece	Enphase company
I_{TES}	Initial investment costs of TES	2300	€/m^3	Sailer company
c_{DHW}	Specific costs of tap water	0.00083	€/kg	[184]
$LHV_{biomass}$	Biomass lower heating value	4900	Wh/kg	
LHV_{NG}	Natural gas lower heating value	9.6	kWh/Sm^3	[182]

$\eta_{el,heater}$	Efficiency of electric heater	95	%
η_b	Efficiency of natural gas boiler	80	%
r	Discount rate	2	%
N	Lifetime	25	years

Micro-CHP

The biomass-fueled micro-CHP unit uses air, which is free of charge, biomass and the non-exergetic cost $\tilde{Z}_{CHP}$ to produce electricity (flow 3) and heat (flow 4), simultaneously. This leads to a following cost balance and auxiliary equations:

$$\dot{C}_1 + \dot{C}_2 + \tilde{Z}_{CHP} = \dot{C}_3 + \left(\dot{C}_4 - \dot{C}_5\right) \tag{25}$$

$$\dot{C}_1 = 0 \tag{26}$$

$$\dot{C}_2 = \dot{m}_{biomass} \times c_{biomass} \tag{27}$$

where $\dot{m}_{biomass}$ is the mass flow of wood pellets (kg/h) and $c_{biomass}$ is the specific cost of wood pellets in €/kg.

Based on the fuel and product rule of the SPECO [91] and on the fact that the specific costs of electricity and heat produced by the micro-CHP unit are directly proportional to their energy levels, the following auxiliary equation are written:

$$c_3/EL_3 = \ (c_4 - c_5)/EL_{4-5} \tag{28}$$

$$\frac{\dot{C}_3 \times \left(\dot{Ex}_4 - \dot{Ex}_5\right)}{\dot{Ex}_3 \times \left(\dot{C}_4 - \dot{C}_5\right)} = EL_3/EL_{4-5} \tag{29}$$

Finally, the specific costs of electricity from the micro-CHP unit are formulated as follows:

$$c_{el,CHP} = \frac{\dot{C}_2 + \tilde{Z}_{CHP}}{\left(1 + \frac{\left(\dot{Ex}_4 - \dot{Ex}_5\right) \times EL_{4-5}}{\dot{Ex}_3 \times EL_3}\right)\dot{Ex}_3} \tag{30}$$

PVT

The PVT field consumes solar energy (flow 13), which is free of charge, and the non-exergetic costs $\tilde{Z}_{PVT}$ to produce electricity (flow 12) and heat (flow 11), simultaneously. This leads to a following cost balance and auxiliary equations:

$$\dot{C}_3 + \tilde{Z}_{PVT} = \dot{C}_{12} + \left(\dot{C}_{11} - \dot{C}_{10}\right) \tag{31}$$

$$\dot{C}_3 = 0 \tag{32}$$

$$c_{12}/EL_{12} = \ (c_{11} - c_{10})/EL_{11-10} \tag{33}$$

$$\frac{\dot{\mathrm{C}}_{12}\left(\dot{\mathrm{Ex}}_{11} - \dot{\mathrm{Ex}}_{10}\right)}{\dot{\mathrm{Ex}}_{12}\left(\dot{\mathrm{C}}_{11} - \dot{\mathrm{C}}_{10}\right)} = \ \frac{\mathrm{EL}_{12}}{\mathrm{EL}} \tag{34}$$

Finally, the specific costs of electricity from the PVT field are formulated as follows:

$$\mathrm{c}_{\mathrm{el,PVT}} = \frac{\tilde{\mathrm{Z}}_{\mathrm{PVT}}}{\left(1 + \frac{\left(\dot{\mathrm{Ex}}_{11} - \dot{\mathrm{Ex}}_{10}\right)\mathrm{EL}_{11-10}}{\dot{\mathrm{Ex}}_{12}\mathrm{EL}_{12}}\right)\dot{\mathrm{Ex}}_{12}} \tag{35}$$

Thermal energy storage

The thermal storage receives heat "fuel" from the micro-CHP and PVT field and uses the non-exergetic costs $\dot{Z}_{TES}$ to store and exchange the heat to feed DHW and space heating circuits when necessary. The following cost balances are written for the TES:

$$\left(\dot{C}_4 - \dot{C}_5\right) + \left(\dot{C}_{11} - \dot{C}_{10}\right) + \dot{Z}_{TES} = \left(\dot{C}_8 - \dot{C}_9\right) + \left(\dot{C}_6 - \dot{C}_7\right) \tag{36}$$

$$\dot{C}_7 = \dot{m}_7 \times c_{DHW} \tag{37}$$

$$(c_8 - c_9)/EL_{8-9} = (c_6 - c_7)/EL_{6-7} \tag{38}$$

$$\frac{\left(\dot{C}_8 - \dot{C}_9\right)\left(\dot{E}x_6 - \dot{E}x_7\right)}{\left(\dot{E}x_8 - \dot{E}x_9\right)\left(\dot{C}_6 - \dot{C}_7\right)} = \frac{EL_{8-9}}{EL_{6-7}} \tag{39}$$

where $\dot{m}_7$ is the domestic hot water demand and c_{DHW} is the specific cost of tap water in €/kg.

Hybrid renewable energy system

Finally, the specific costs of electricity ($c_{el,sys}$), domestic hot water (c_{DHW}) and space heating (c_{SH}) are calculated as follows:

$$c_{el,sys} = \frac{\dot{C}_3 + \dot{C}_{12}}{\dot{E}x_3 + \dot{E}x_{12}} = \frac{c_{el,CHP} \times \dot{E}x_3 + c_{el,PVT} \times \dot{E}x_{12}}{\dot{E}x_3 + \dot{E}x_{12}} \quad (40)$$

$$c_{DHW} = \dot{C}_6 / \dot{E}x_6 \quad (41)$$

$$c_{SH} = \left(\dot{C}_8 - \dot{C}_9\right) / \left(\dot{E}x_8 - \dot{E}x_9\right) \quad (42)$$

3. Results and discussion

The simulation tool was built into Matlab/Simulink to evaluate the exergetic and exergo-economic performance of the HRES in Figure 6-1 under three different European climate conditions described in Section 2.4. The tool allows calculating exergy production, destruction and efficiency on the component and system level over a certain period. Additionally, the calculations of the exergo-economic specific costs of electricity, domestic hot water and space heating produced by the HRES can be conducted on the monthly basis.

3.1 Exergy analysis

Next, the results of the exergy analysis of the system in each location are presented and discussed. The aim of the considered HRES was to support energy production of the biomass micro-CHP with solar cogeneration in order to reduce biomass consumption and costly exergy destruction. Solar energy as a fuel has lower quality than biomass, and it is free of charge.

In Figure 6-8 are presented the exergy fuel, product and destruction flows over three representative days from spring, summer and winter periods in Strasbourg.

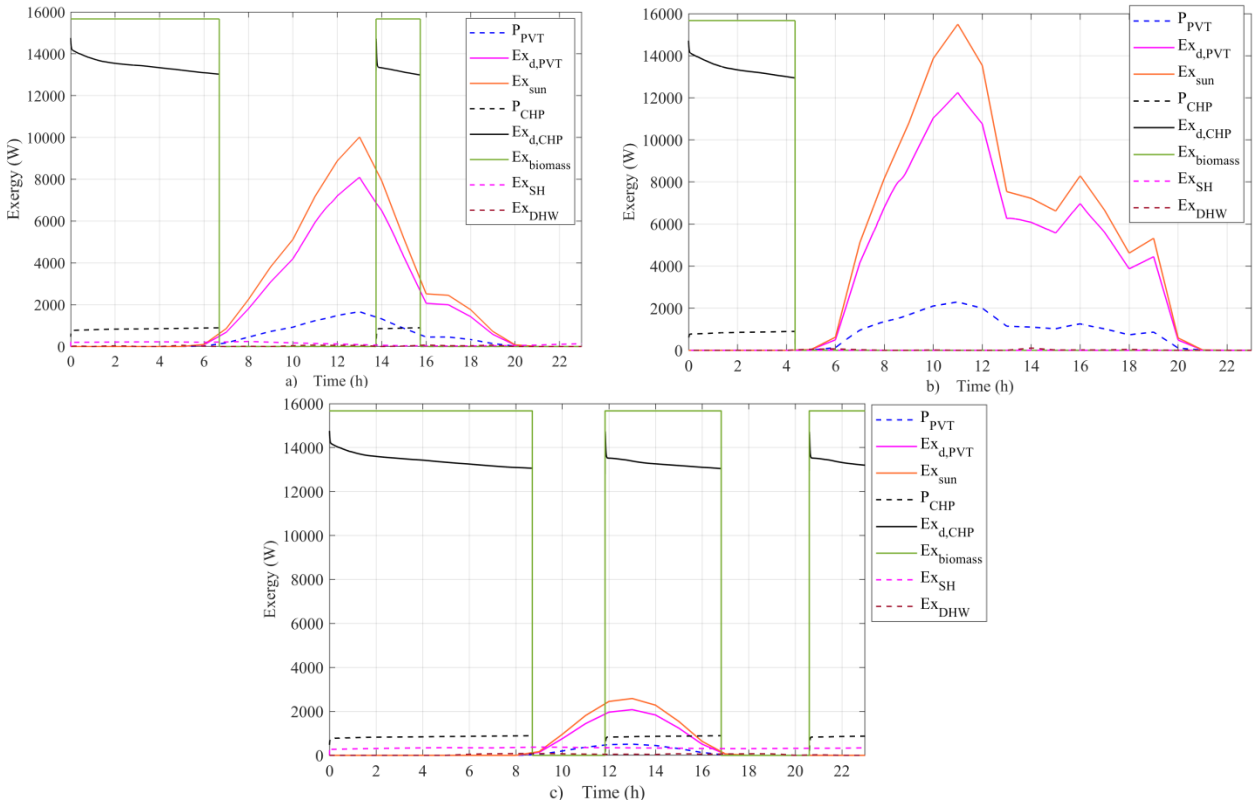

Figure 6-8: *The fuel, product and destruction exergy flows during three different days in Strasbourg a) in spring, b) in summer and c) in winter.*

Figure 6-8 shows the variation of the utilized solar and biomass exergies over time. On each day, the micro-CHP run during the night hours to satisfy the space heating and to maintain the temperature of the TES. The reduced solar availability during the spring and winter day forced to use biomass exergy also during the day hours. During the winter day, the main fuel exergy came from biomass use. The exergy destruction in both micro-CHP and PVT was significantly higher compared to the exergy products that are space heating, DHW and electricity. The magnitude of the space heating and DHW exergy products was low due to the low temperature levels. The highest exergy product was the electricity produced by PVT during the spring and summer days and the electricity produced by the micro-CHP during the winter day.

The exergy analysis in Figure 6-8 revealed a big difference between the magnitudes of the used fuel exergy fed to the system and the gained exergy products. The costly exergy destruction in the Stirling engine micro-CHP unit could be reduced by improving the electrical power output of the unit.

In Figure 6-9 is presented the used fuel exergy in each location. The higher availability of solar radiation during the summer months increased the solar share of the total fuel exergy. However, the solar share was also increased due to decreased energy demand of the building. Figure 6-9 clearly shows that in the southernmost location of Barcelona, the solar share of the fuel exergy was significant also during the winter months from November to March covering at worst 26% of fuel exergy in January. At the same time, the solar share was below 10% in Strasbourg and Tampere. This trend was seen in November and December as well.

Figure 6-9 reveals that despite the northern location of Tampere, the solar share of the fuel exergy was close to one in Strasbourg. However, in September the solar share was only 52% while it was still 78% and 97% in Strasbourg and Barcelona, respectively.

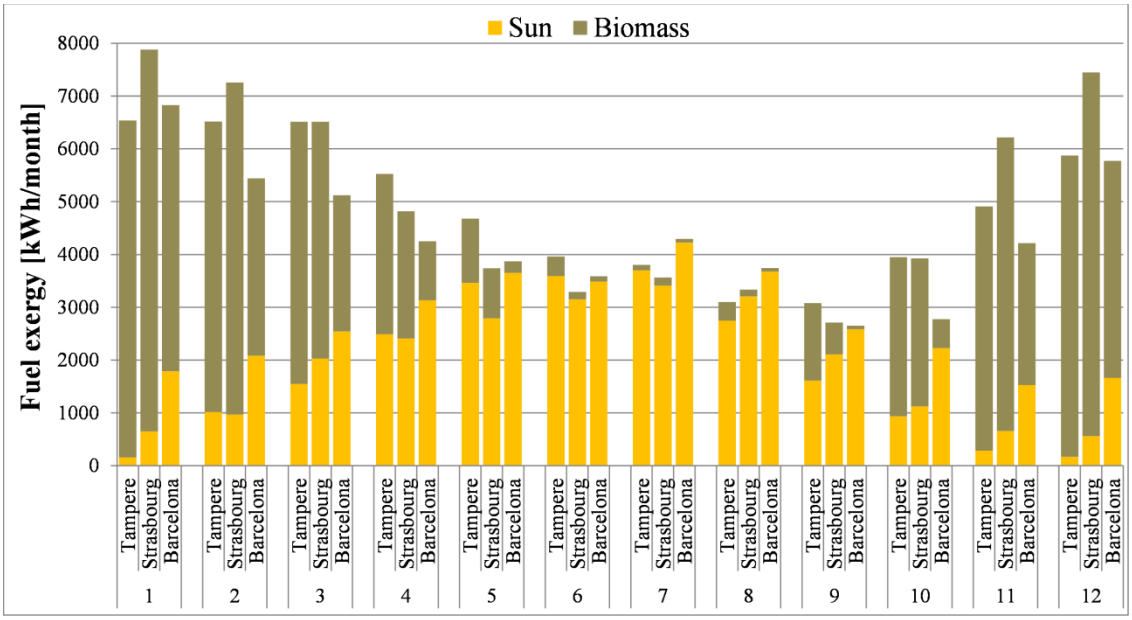

Figure 6-9: *The monthly fuel exergy flows in each location.*

Figure 6-10 shows the total exergy destruction divided for each system component (PVT, micro-CHP and TES) in each location. The exergy destruction was higher during the winter months from November to March because of the high demand for low-grade heat production for space heating. During these months, the micro-CHP caused most of the destruction in the system while the PVT dominated the destruction during the summer months. The TES was used to manage thermal exergy flows in the system and counted the smallest part of the total exergy destruction. However, the exergy destruction of the TES was significantly higher during the winter months. This was caused by using high thermal exergy flow from the micro-CHP to

produce a high amount of space heating which had low exergy content. On the other hand, during the summer months, while the space heating was almost zero, the low thermal exergy flow from the PVT field was used to produce domestic hot water which had high exergy content resulting in lower exergy destruction.

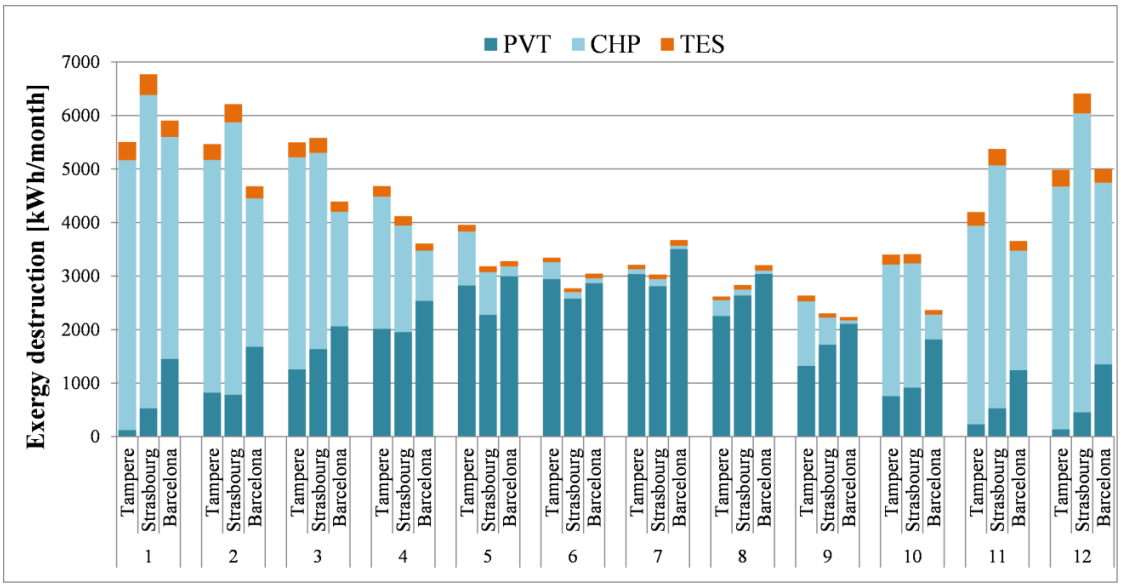

Figure 6-10: *The monthly exergy destruction in each location divided for each component.*

The exergy products from the HRES were space heating, domestic hot water and electricity produced by the micro-CHP unit and PVT field. These exergetic products are presented on monthly basis in Figure 6-11.

Figure 6-11 reveals that the exergy products were dominated by the electrical exergy produced by the PVT field. In the sunny location of Barcelona, the proportion of the PVT electricity was already higher than the one of the micro-CHP in January although the operation of the micro-CHP was high due to higher space heating demand. The same happened in Tampere and Strasbourg in March. This result show that the hybridization of the units increased significantly the free-fuel based electricity production capacity of the HRES. Additionally, the solar support helped to reduce biomass use and costly exergy destruction during the whole year.

In Tampere and Strasbourg, the space heating was a significant exergy product during the cooler months from November to February. However, the quality of the space heating as an exergy product depended on the reference temperature of the considered location. Due to this, the exergy of the heat products was the lowest in the warmest location of Barcelona.

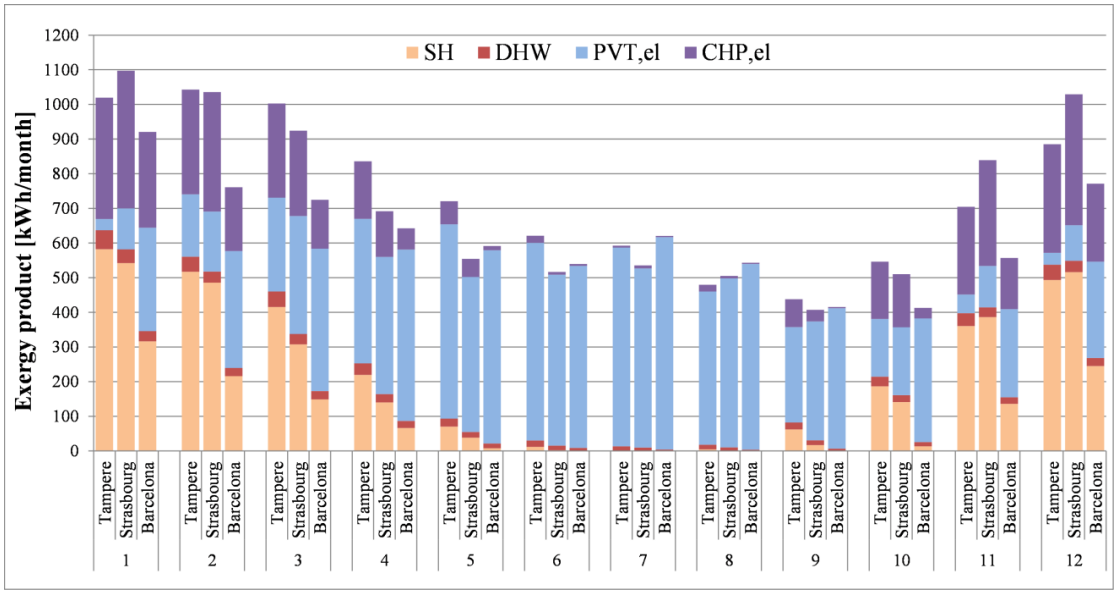

Figure 6-11: *The monthly exergy products from the hybrid renewable energy system in each location divided for each energy product of the system.*

Figure 6-12 shows the monthly overall exergy efficiency of the HRES in the selected locations. The exergy efficiency varied from 13% to 16% reaching the maximum value in Tampere already in February, in Strasbourg in June and in Barcelona in September. Due to the significantly cooler monthly reference temperatures, the efficiency was the highest in Tampere during the winter months. In Strasbourg and Barcelona, the exergy efficiency increased slowly from January to June and to May, respectively, while the solar irradiation increased and heating demand decreased. In each location, the exergy efficiency decreased strongly at the end of the year due to strongly reduced solar irradiation and increased use of the micro-CHP system for space heating demand. The decrease was strongest in Strasbourg from September to October by 2% percentage points. In Tampere and Barcelona, the fall in efficiency was slower and took place from August to October and from September to November, respectively.

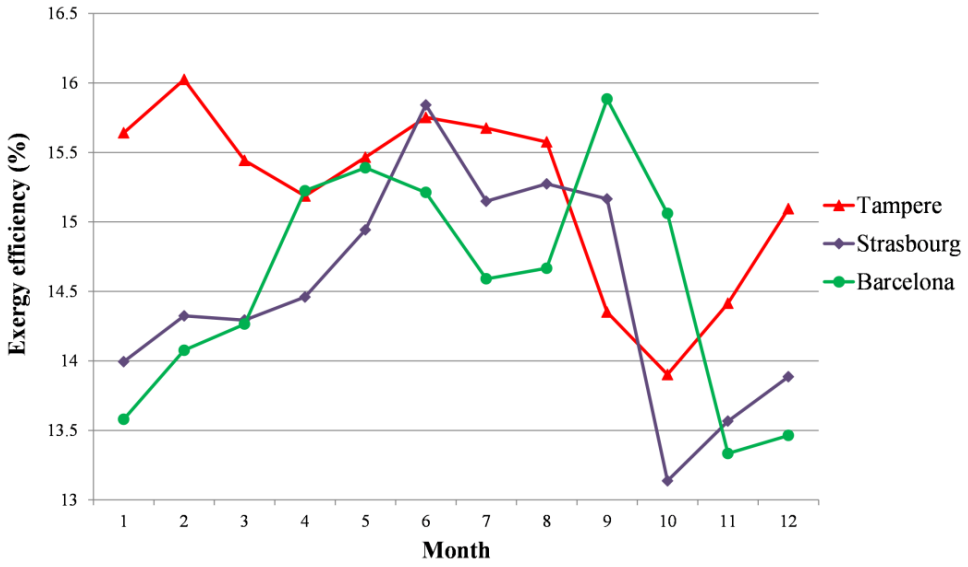

Figure 6-12: *The monthly exergy efficiency of the whole system in each location.*

The yearly overall exergy efficiency, given by Eq. (13), was the highest in Tampere resulting in 15.3% followed by Strasbourg and Barcelona with the same result of 14.3%. The efficiency was the highest in Tampere due to the coolest monthly reference temperatures which led to the higher exergy of the heat products. This increased relatively the amount of the total exergy products compared to the other locations. Barcelona and Strasbourg resulted in the same annual overall exergy efficiency. This was possible due to the different utilization rates of the energy production units of the system. Due to the higher heating demand, the micro-CHP unit produced more electricity and heat in Strasbourg. However, this led to the higher biomass fuel use in Strasbourg but, as compensation, the received solar energy fuel was lower than in Barcelona. In Barcelona, this was the other way around. Additionally, the amount of the PVT electricity product was higher but the amount of the heat exergy products was lower due to the lower heating demand and the higher monthly reference temperatures.

The overall exergy efficiency of the same HRES in different locations can be close to each other because of the different component utilization rates and varying exergy of the heat products depending on the reference temperature. In terms of the PVT collectors, the decreased value of the heat products is compensated by the increased amount of PVT electricity production due to the higher solar radiation.

Next, the results of the exergo-economic analysis will be presented and discussed.

3.2 Exergo-economic analysis

The exergo-economic costs of the electricity produced by the HRES in each location are presented in Figure 6-13. The specific cost of the system electricity takes into account the specific costs of the PVT and micro-CHP electricity according to Eq. (40). Figure 6-11 shows the specific cost of electricity cumulated on a monthly and yearly basis. The specific costs varied strongly in each location over the year with the minimum value as low as 0.189 €/kWh (or kWh_{ex} as electricity is seen as pure exergy) in each location during the summer and as high as 0.798 €/kWh in Tampere, Finland in November. In each location, the costs were lowest during the summer months when the PVT field produced most of the electricity. During the winter months, the costs increased in each location due to a greater share of the electricity produced by the micro-CHP, which had the higher initial investment cost, existing fuel costs and lower nominal electrical power. However, in Barcelona, the monthly specific costs were 15 to 30 c€/kWh lower during the winter months than in Strasbourg and France due to the better availability of solar energy.

Figure 6-13 shows that the specific cost of electricity was surprisingly close to each other in Strasbourg and Tampere when taking into account the physical distance between the locations. However, from November to January, the solar share of the electricity production was lower in Tampere resulting in over 10c€/kWh higher specific cost of electricity. The specific costs in Tampere and Strasbourg were close to Barcelona only during the best months of solar radiation, and during the rest of the year, the costs were 16% to 43% lower in Barcelona than in two other locations.

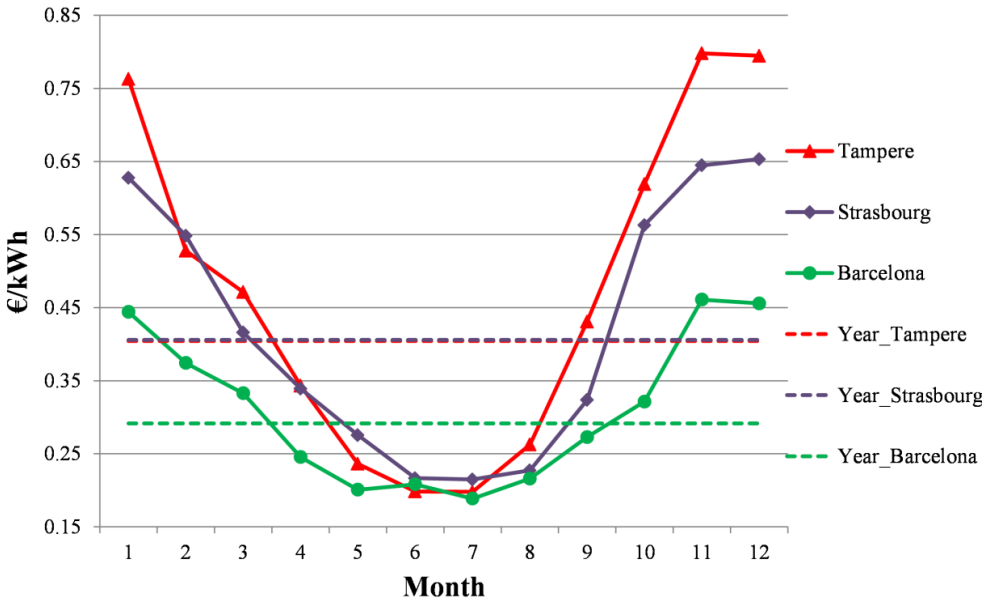

Figure 6-13: *The monthly and yearly exergo-economic costs of electricity produced by the hybrid energy system in Tampere, Strasbourg and Barcelona.*

The results in Figure 6-13 reveal that the available solar support from the PVT field decreased the specific cost of electricity significantly compared to the months, such as January and February, when the micro-CHP run almost at full requirements due to low solar irradiation and high space heating demand. In Tampere, the specific cost was reduced by 75%, by 66% in Strasbourg and by 59% in Barcelona due to increased solar support between the winter and summer. The impact of the solar support on the costs was also seen in the annual specific cost of electricity presented in Figure 6-11. These costs were the lowest in sunny Barcelona resulting in 0.292 €/kWh and the highest in Strasbourg with 0.406 €/kWh. The annual specific cost was only slightly lower in Tampere than in Strasbourg with 0.404 €/kWh although the highest monthly specific cost were resulted in Tampere.

In Figure 6-14 is presented the exergo-economic specific cost of space heating in each location on monthly and early basis.

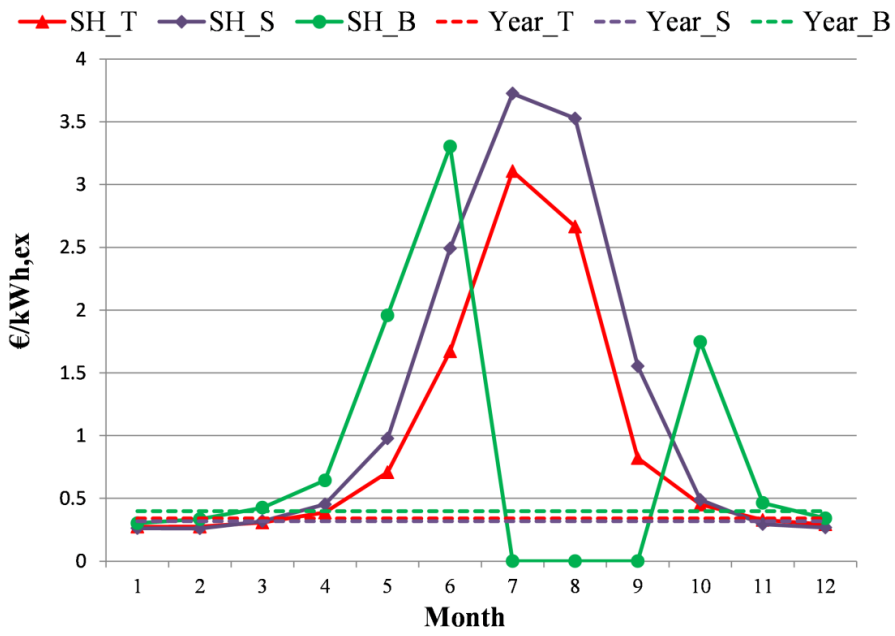

Figure 6-14: *The monthly and yearly exergo-economic costs of space heating in Tampere, Strasbourg and Barcelona.*

The exergo-economic cost of the space heating reached the highest value of 3.73 €/kWh$_{ex}$ in Strasbourg in July due to low space heating demand and high ambient temperature. At the same time, the cost reached the highest value in Tampere as well with 3.11 €/kWh$_{ex}$. In Barcelona, there was no space heating demand from July to September and the specific cost was zero. Figure 6-14 shows that the specific cost reached the highest values in Barcelona and lowest in Tampere over the year. This was caused by the higher space heating demand and cooler reference temperatures in Tampere which leads to higher heat exergy production.

Figure 6-14 presents the specific cost of space heating per kWh of exergy, not energy. Based on the monthly energy levels of the heat exergy flows, the cost transfer coefficient of thermal exergy to energy varied from 0.143 to 0.068 in Tampere, from 0.115 to 0.061 and 0.095 to 0.054 in Strasbourg and Barcelona, respectively. The energy levels of the exergy flows were highest during the cooler months. The annual average specific cost of space heating was the highest in Barcelona with 0.399 €/kWh$_{ex}$ which resulted in 0.036 €/kWh. In Tampere and Strasbourg, the costs were slightly lower in terms of exergy resulting in 0.341 €/kWh$_{ex}$ (0.044 €/kWh) and 0.319 €/kWh$_{ex}$ (0.034 €/kWh), respectively.

In Fig. 15 is presented the exergo-economic cost of DHW in each location on monthly and yearly basis. The DHW profile was assumed to be the same in each location but the specific

cost of DHW were influenced also by the current space heating demand. Due to that, the specific cost reached a value as high as 11.9 €/kWh$_{ex}$ in Barcelona in August when the space heating demand was zero and all costs were allocated only to the DHW. At the same time, the specific costs were 60% lower in Strasbourg and 74% lower in Tampere.

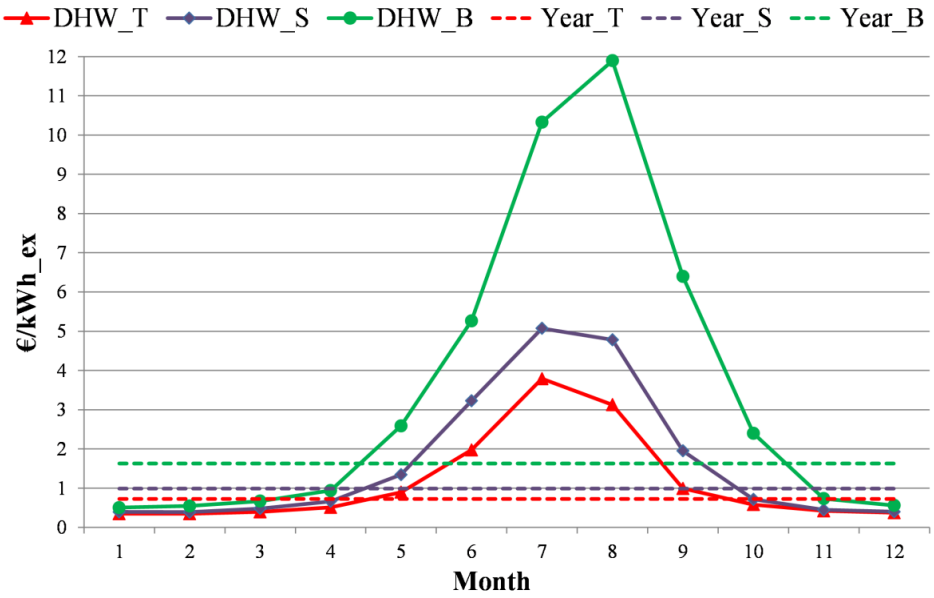

Figure 6-15: *The monthly and yearly exergo-economic costs of DHW in Tampere, Strasbourg and Barcelona.*

On yearly basis, the specific cost of the DHW was the highest in Barcelona with 1.626 €/kWh$_{ex}$ which resulted in 0.111 €/kWh. In Strasbourg and Tampere, the costs were lower resulting in 0.987 €/kWh$_{ex}$ (0.083 €/kWh) and 0.725 €/kWh$_{ex}$ (0.075 €/kWh), respectively.

In this study, the exergo-economic calculation took into account the energy level of the exergy flows in order to allocate more production costs to an energy product with the higher energy level. Due to this, the specific cost of DHW were higher than the specific cost of space heating which had the lower temperature and energy level than the DHW. On the other hand, the specific cost of electricity was the highest among the energy products of the system because of the highest energy level of 1 as electricity is seen as pure exergy. It should be also noted that this study was conducted not taken into account any renewable energy based support or incentive mechanism. However, when comparing different countries, this study took into account the country specific tax and prices in Table 6-5.

Based on the performed exergo-economic analysis it can be concluded that the reasonable unit prices assigned to each energy product of the HRES differ according to the location and climate conditions of the hybrid system. These prices are presented in Table 6-5.

Table 6-5: The average unit prices of the energy products in each location.

Energy product	Barcelona	Strasbourg	Tampere	Unit
Electricity	0.292	0.406	0.404	€/kWh = €/kWh$_{ex}$
Space heating	0.036	0.034	0.044	€/kWh
	0.399	0.319	0.341	€/kWh$_{ex}$
Domestic hot water	0.111	0.083	0.075	€/kWh
	1.626	0.987	0.725	€/kWh$_{ex}$

It can be recognized that the appropriate electricity prices are relatively high compared to the country-specific electricity purchase prices in Table 6-6. This is mainly caused by the high initial investment of the HRES. At the moment, it is not realistic to gain the electricity prices above by selling or self-consuming the produced electricity of the HRES. However, the investment costs of the components can be expected to be reduced in the future while the grid electricity prices are expected to increase. Additionally, a thermally activated cooling device could be added to the system to increase the utility of the system during the summer months and decrease the prices of the heat products.

3.2.1 Sensitivity analysis of exergo-economics

The sensitivity analysis was conducted to investigate the impact of the solar and storage component capacities on the exergo-economic costs. The exergo-economic results in Strasbourg were used as a reference in the analysis. First, the number of the PVT rows was decreased and increased by 33% by removing and adding one row to the original system configuration presented in Section 2. Varying the number of PVT collectors had a strong impact on the monthly and annual specific cost of the electricity as shown in Figure 6-16.

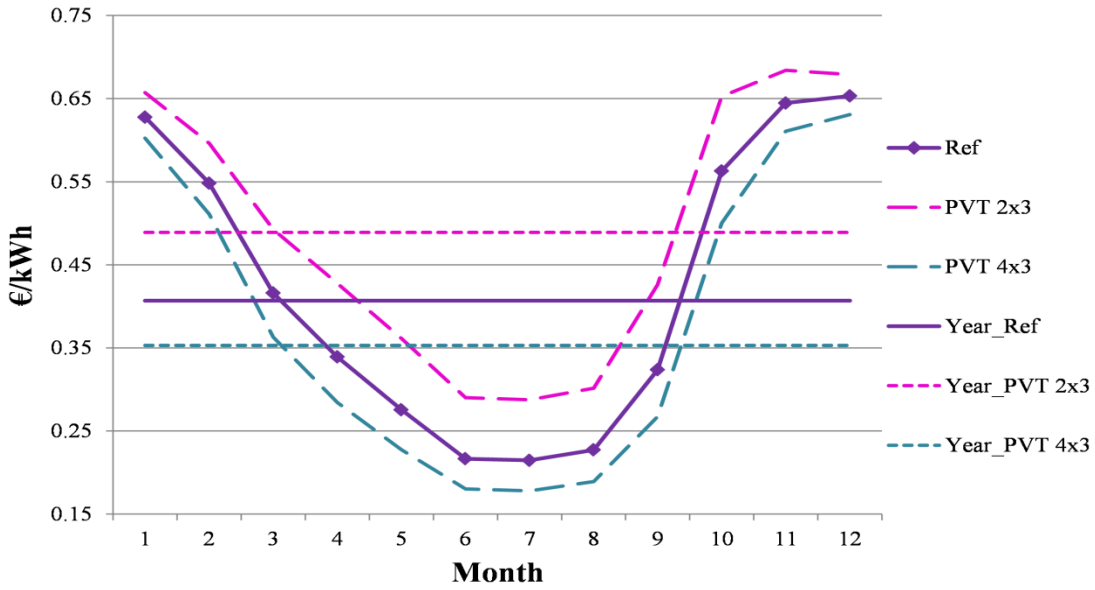

Figure 6-16: *The monthly and yearly exergo-economic costs of electricity produced by the hybrid energy system with different PVT capacities.*

Decreasing the number of PVT collectors increased the monthly and annual specific cost of electricity because the cost-free solar fuel was reduced and compensated by the costly biomass fuel to cover energy demand. Adding the PVT collectors resulted in the opposite results but with a lower magnitude. The smaller PVT field increased the annual specific cost of electricity by 20% while the larger field decreased the cost by 13%. In terms of the space heating and DHW, varying the number of the PVT collectors did not influence the specific cost because these heat products were not the direct output of the PVT field but the thermal storage.

Next, the thermal storage volume was varied by ±25% compared to the reference system resulting in the storage sizes of 1.5 m^3 and 2.5 m^3. The thermal storage is used to facilitate the matching between thermal energy production and demand. Varying the storage size had an impact on the initial investment cost but not on the magnitude of the heat products defined by the building energy use. Due to this, the monthly specific costs of the heat product were increased or decreased only during the summer months when the heating demand was relatively low as shown in Figure 6-17.

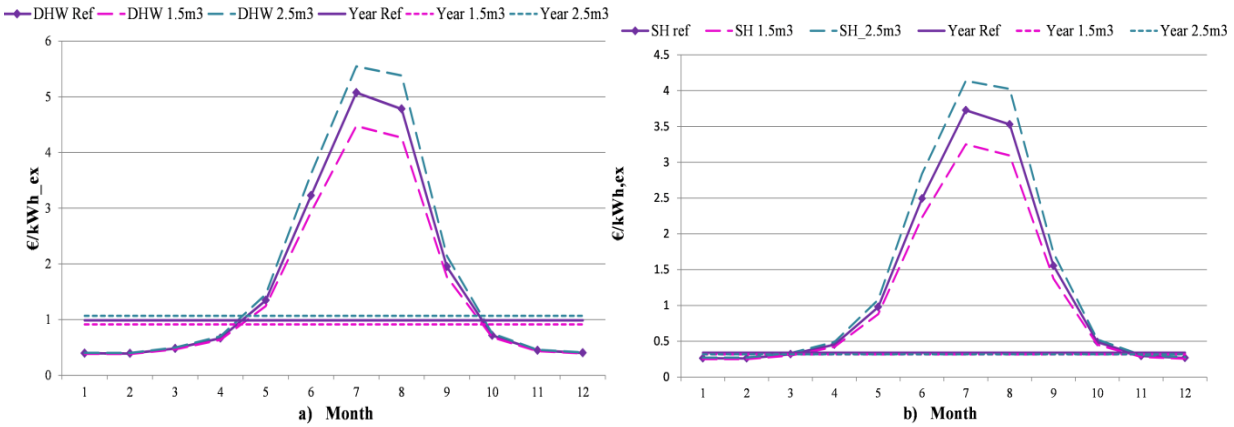

Figure 6-17: *The monthly and yearly exergo-economic costs of a) DHW and b) space heating with different storage capacities.*

In July and August, the specific costs of DHW were 9.3% and 12.6% higher, respectively, if the size was increased. Decreasing the size led to 11.7% and 10.7% lower DHW costs in these months. The variation in the specific cost of space heating was with the same magnitude. The storage size did not influence the specific cost of electricity.

3.3 Comparative results of the HRES to the reference system

Energy, exergy and economic comparison indicators were used to further evaluate the performance of the cogeneration based HRES compared to separated production of heat and power by a reference system. The primary energy savings (PES) were used as an energetic indicator, the relative avoided irreversibility (RAI) as an exergetic indicator, and the simple payback time and net present value as economic indicators.

In terms of PES and RAI indicators, the reference system included an electric grid with an efficiency of 35% for electricity and a natural gas-fired boiler with an efficiency of 80% for heat production. In Figure 6-18 is presented the monthly PES in each location compared to the reference system. The primary energy savings took into account only the reduction in biomass use because solar energy is CO_2 and cost-free primary energy. Figure 18 shows significantly high primary energy savings in each location during the sunniest months from May to August, when the PES was over 60% in each location. The system operation in Barcelona resulted in the highest PES over the year leading to the PES of over 90% from May to September. The PES values were almost the same during the year in Tampere and Strasbourg despite September when the PES was 68% in Strasbourg and 40% in Tampere due to strongly reduced solar irradiation in the northern location.

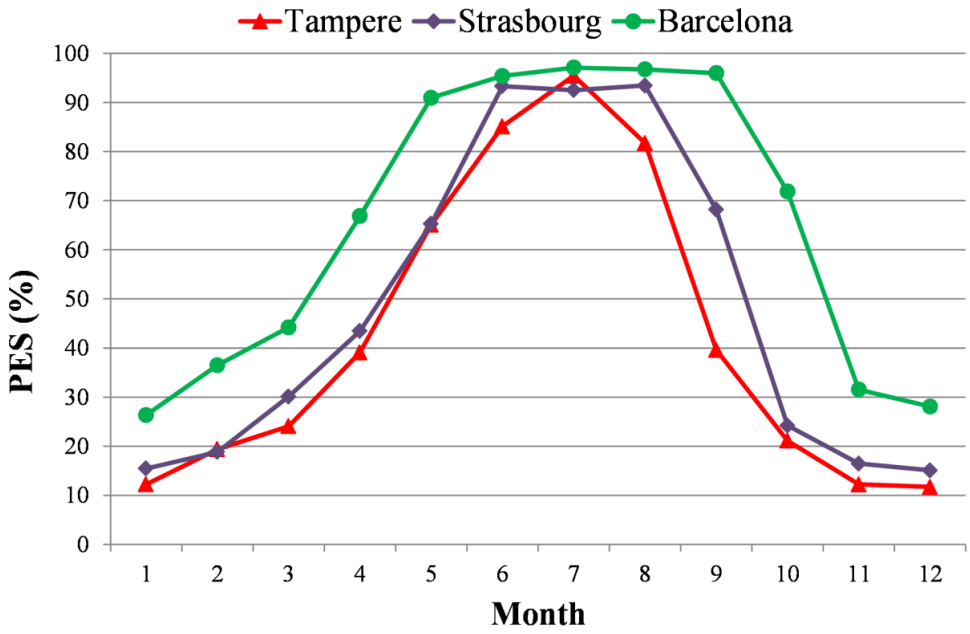

Figure 6-18: *The monthly primary energy savings in each location.*

In each location, the PES was positive and primary energy was saved during the whole year. Based on the results, it can be concluded that hybridization of the fuel-fired micro-CHP system with solar cogeneration reduced strongly primary energy use compared to the reference system. In terms of exergy, the monthly RAI indicator showed the existing irreversibility savings in the HRES compared to the reference system but always at the lower level than primary energy savings. However, in Figure 6-19, the RAI indicator revealed inefficiency of the HRES in Tampere in November when the RAI got a negative value. This indicates that the HRES was not an improvement from the reference system in November. In Tampere and Strasbourg, the RAI indicator was negative or close to zero from November to January. This was mainly caused by the low solar energy production. As a conclusion, the RAI indicator revealed the hidden inefficiency of the HRES operation which was not seen in the PES indicator.

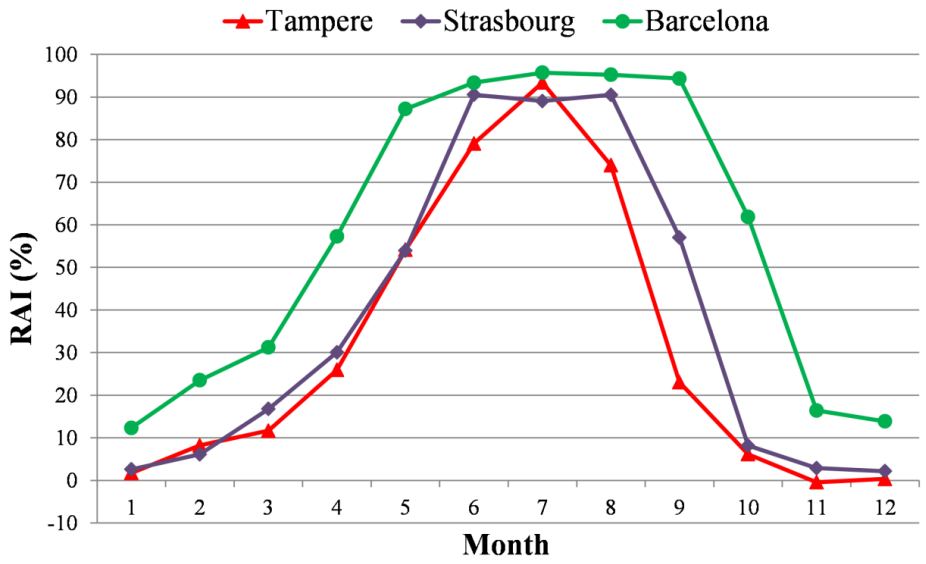

Figure 6-19: *The monthly relative avoided irreversibility in each location.*

Next, the economic indicators were calculated for four different scenarios in each location. The SPT and NPV of the HRES are presented in Table 6-6 with the country-specific parameters used in the calculation. These economic calculations were conducted for the replacement of the reference system by the HRES. The case 1 compared the HRES to the reference system including the electric grid and natural gas boiler, and the case 2 compared to the reference system consisting only of the electric grid. Within the cases, the following two sub-scenarios were considered: a) dynamic electricity balance between the load and production was taken into account, and b) all produced electricity was assumed to be consumed by the building. In the sub-scenario a), the produced electricity was consumed in the building according to the load profile in Section 2.3 and the surplus production was fed to the grid with the country-specific feed-in-tariff presented in Table 6-6. The sub-scenario b) presented an ideal situation to show how the economic indicators were changed if the perfect match between the load and production would be possible.

Table 6-6: The parameters used in the economic comparison to the reference systems and economic results in each location.

	Tampere	Strasbourg	Barcelona	Ref.
Electricity demand	6000 kWh/year	6000 kWh/year	6000 kWh/year	
Heating demand	22475 kWh/year	24571 kWh/year	12901 kWh/year	
DHW	4238 kWh/year	4238 kWh/year	4238 kWh/year	

Electricity price	0.174 €/kWh	0.19 €/kWh	0.224 €/kWh	[185]
Natural gas price	0.087 €/kWh	0.075 €/kWh	0.09 €/kWh	[186, 187]
Wood pellet price	0.27 €/kg	0.25 €/kg	0.23 €/kg	[188]
Feed-in-Tariff	0 €/kWh	0.06 €/kWh	0.05 €/kWh	[189–191]
VAT	24%	20%	21%	
	Tampere	Strasbourg	Barcelona	
RESULTS				
Savings, case 1a	1 830 €/year	1 887 €/year	1 939 €/year	
SPT, case 1a	19.3 years	18 years	17.7 years	
NPV, case 1a	508 €	2 781 €	6 585 €	
Savings, case 1b	2 217 €/ year	2 212 €/year	2 435 €/year	
SPT, case 1b	15.9 years	15.4 years	14.1 years	
NPV, case 1b	8 054 €	9 105 €	3 474 €	
Savings, case 2a	3 361 €/year	4 525 €/year	3 748 €/year	
SPT, case 2a	10.5 years	7.5 years	9.2 years	
NPV, case 2a	30 388 €	54 243 €	38 803 €	
Savings, case 2b	3 747 €/year	4 848 €/year	4 245 €/year	
SPT, case 2b	9.4 years	7 years	8.1 years	
NPV, case 2b	37 934 €	60 567 €	48 494 €	

The economic indicators in Table 6-6 show that the retrofitting of the old system with the considered HRES had economic viability under given circumstances in each location. The NPV was positive in each location after 25 years period. The longest simple payback time was indicated for the case 1a in Tampere resulting in 19.3 years with the NPV of only 508 €. This case took into account the dynamic behavior of the electricity production and demand which is rarely matched with each other without energy storage. In this case, the surplus electricity was sold to the grid with the country-specific feed-in-tariff. The SPT was decreased by 3.4 years if the produced electricity was assumed to be used totally in the building. Additionally, the NPV was increased by 7546 €. In the case 1a, the SPT was 1.3 and 1.6 years shorter in Strasbourg and Barcelona, respectively, than in Tampere due to more favorable economic conditions, such as the feed-in-tariff and VAT.

The economic viability of retrofitting the electricity only based system (case 2) by the HRES resulted in significantly shorter SPT than in the case 1. In Tampere, the SPT of the case 2a was 10.5 years with the NPV of 30388 €. The shortest SPT of the case 2 was indicated in Strasbourg due to lower electricity price combined with low VAT for the initial investment. Assuming the 100% self-consumption in the building resulted only in a small reduction of the SPT. However, the reduction was less significant than between the case 1a and 1b.

The economic results revealed the higher viability of the hybrid system if the produced electricity was used 100% on-site. The electrical energy storage or electric car with advanced and intelligent system control can facilitate the energy management of the system and enable 100% self-consumption but increases the initial investment costs as well.

4. Conclusion

In this paper, a hybrid renewable energy system based on cogeneration from biomass-fuelled Stirling engine micro-CHP unit and photovoltaic-thermal collectors was assessed thermo-economically under three different European climate and economic conditions. The dynamic exergy and exergo-economic analyses were performed and the results were presented on a daily, monthly and yearly basis.

Compared to a yearly analysis, the conducted dynamic exergy analysis gives more detailed insight to the variation of exergy fuels, products and efficiency over the year. The dynamic exergo-economic analysis reveals the high variation in the specific cost of energy products compared to the yearly analysis. This variation is mainly caused by the fluctuating solar energy availability and heat demand of the reference building.

The location of the HRES had an impact on the following issues: the utilization rate of the energy production units within the system, exergy of the heat products, heating demand of the building, economic conditions, payback time, specific costs of energy products, primary energy savings and relative avoided irreversibility. The location of the HRES did not influence significantly the overall exergy efficiency of the system.

First, the results were obtained in terms of monthly fuel exergy, exergy destruction in the components, exergy products and the overall exergy efficiency. The following main findings were done:

- The share of solar exergy was the highest during the summer period in each location. In the southernmost location of Barcelona, the share was also significant during the winter months from November to March covering at worst 26% of fuel exergy in January.
- The micro-CHP caused most of the exergy destruction during the winter months while the PVT dominated the destruction during the summer months. The TES caused 2.5%-6% of the total monthly exergy destruction.
- The hybridization increased significantly cost-free electricity production and facilitated to reduce biomass use and costly exergy destruction during the whole year in each location.
- The overall exergy efficiency of the system varied from 13% to 16% over the year.

The following main findings were done based on the exergo-economic analysis:

- The specific cost of electricity varied strongly in each location over the year with the minimum value as low as 0.189 €/kWh in each location during the summer months and as high as 0.798 €/kWh in Tampere, Finland in November.
- The lowest specific cost of electricity is competitive with the current grid electricity prices in Table 6 which makes the system attractive for the building owner (prosumer).
- The annual specific cost of electricity was 28% lower in Barcelona (0.292 €/kWh) than in Strasbourg (0.406 €/kWh) and Tampere (0.404 €/kWh) due to the higher utilization rate of the PVT and the lower rate of the costly micro-CHP unit, and more favorable economic conditions. The similar utilization rate of the PVT, less favorable economic conditions of Finland and higher exergy of heat products in Finland resulted in the same annual specific cost of electricity in Tampere and Strasbourg.
- The specific cost of the space heating varied over year depending on the heating demand by having the highest value of 3.73 €/kWh_{ex} in July in Strasbourg and the lowest value of 0.26 €/kWh_{ex} in January.
- The DHW had the highest monthly costs of 11.9 €/kWh_{ex} in Barcelona in August due to the highest reference temperature and the lowest space heating demand. The lowest cost were 0.35 €/kWh_{ex} in January in Tampere. The cost of the DHW was higher than space heating due to higher exergy content.

- The specific cost of electricity was sensitive to the number of the PVT collectors but not to the size of the thermal storage. The 33% smaller PVT field increased the annual specific cost by 20% while the 33% larger field decreased the cost by 13%.

Finally, the HRES was compared against two reference systems including the electric grid with or without a gas boiler. Additionally, the self-consumption rate of the produced electricity was taken into account and varied within two reference cases. The following main findings were done:

- The hybridization reduced primary energy use and irreversibility up to 95% compared to the reference system.
- The longest SPT of 19.3 years resulted in Tampere and the shortest in Barcelona of 14.1 years if the comparison was made against the electric grid combined with a natural gas boiler. If only the electric grid was considered as a reference system, the SPT was between 7 to 10.5 years depending on the scenario and location.
- The HRES was economically viable in each case while the NPV resulted to be positive.
- The economic results revealed the higher viability of the HRES if the produced electricity was used 100% on-site.

To enhance the matching of renewable energy production and building energy demand, the upcoming future work should include an investigation of integrating battery storage or electric vehicle into the system with the Time-of-Use tariff. Additionally, the optimization of the energy demand side and the HRES will be performed for each location. More research on advanced and intelligent energy management algorithms is required as well to control better the energy flows in the hybrid renewable energy system.

Acknowledgements

The authors would like to thank Interreg V Rhin supérieur ACA-MODES project for their support and funding of this research.

Nomenclature

A	area, m^2
a	annuity factor
$\dot{C}$	cost rate, €/h
c	specific cost, €/kWh
c_p	specific heat, J/(kg K)
CRF	Capital Recovery Factor
E	electrical energy, kWh
EL	energy level
$\dot{E}x$	exergy rate, kW
Ex	exergy, kWh
H	enthalpy, kJ
h	specific enthalpy, J/kg
I	component specific initial investment, €
i	interest rate
Ir	irreversibility, W
LHV	lower heating value
m	mass, kg
MC	thermal capacity, J/K
n	lifetime, year
NPV	Net Present Value
OM	operating and maintenance
PES	Primary Energy Savings
Q	thermal energy, W, kW
r	discount rate
RAI	Relative Avoided Irreversibility
S	entropy, kJ/K
s	specific entropy, J/kgK
SV	yearly savings, €/year
SPT	Simple Payback Time
T	temperature, K
t	time, h
U	heat transfer coefficient, W/m^2K
Z	initial investment costs, €

Greek symbols

β	temperature coefficient, %/K
η	efficiency
ζ	exergy efficiency

Subscripts

b	boiler
CD	conduction
CV	convection
d	destruction
DHW	domestic hot water
e	environment
eg	electric grid
eng	engine
el	electrical
f	fluid, fuel
g	glass cover
HX	heat exchanger
in	inlet
irr	irradiation
k	k^{th} component
out	outlet
p	product
pv	photovoltaic
q	quality
SH	space heating
sol	solar energy
sys	system
TES	thermal energy storage
th	thermal
0	reference

CHAPTER 7. Home renewable energy management in solar microgrid

1. Introduction

The introduction to the smart and microgrids was presented in Chapter 1. The objective of Chapter 7 is to introduce the main components of a residential solar microgrid and to present an experimental set-up of the residential grid-connected AC microgrid with a central controller. The main components are photovoltaic panels, battery storage system, inverter, local load and energy management system. As a part of this thesis, these components were connected together to realize the experimental set-up at the INSA ICUBE laboratory in Strasbourg to demonstrate an operation of the home renewable energy management system and to collect the operation data of the system. The second objective of Chapter 7 is to compare the operation of the rule-based energy management strategies to the simulation of the optimization-based energy management strategy called a model predictive control.

2. Solar microgrid components

2.1 Photovoltaic panels

Multiple PV panels, introduced in Chapter 1, can be connected in series and parallel to form a PV system with a peak power output from watts to megawatts. Typically, in residential solar microgrids, the power output is within kilowatts depending on the available roof area. The peak power of the PV systems is specified under the Standard Test Conditions (STC). However, these conditions are rarely met in real-world PV installations, and due to this, it can be difficult to estimate the necessary number of PV panels in the system to meet the local loads. Additionally, the increasing PV cell temperature has a significantly high negative impact on the electrical efficiency and power output of the system. This was further studied in Chapter 2 when the PV and PVT operations were compared. The PV cell temperature is influenced by multiple factors, such as solar radiation, wind speed, module materials and the installation conditions [192].

In the literature, several linear and non-linear models have been presented to estimate PV power output as a function of the received solar radiation and cell temperature. Additionally, a system-specific model can be built by using machine learning methods and measured data from

the system [26]. The simple linear model to estimate first the PV cell temperature, T_{pv} (°C), and then the PV power output, P_{pv} (W), is presented as follows [192]:

$$T_{pv} = T_a + \frac{G_{irr}}{G_{NOCT}} \times (T_{NOCT} - 20) \quad (1)$$

where T_a is the ambient temperature G_{irr} is the received solar irradiation for the tilted surface. NOCT refers to the Nominal Operating Cell Temperature conditions that are 800 W/m^2 for solar radiation, 20°C for ambient temperature and 1 m/s for wind speed [26]. After defining the cell temperature, the PV power output is calculated as follows:

$$P_{pv} = N \times P_{STC} \times \frac{G_{irr}}{G_{STC}} \times \left(1 - \delta \times (T_c - 25)\right) \quad (2)$$

where STC refers to the Standard Test Conditions (STC) that are 1000 W/m^2 for solar radiation, 25°C for ambient temperature and 1 m/s for wind speed. The rated peak power P_{STC} is given by the manufacturer in (W) and δ is a maximum power correction factor for temperature [192].

The PV panel electrical efficiency depends linearly on the PV cell temperature, the temperature coefficient β_{pv} and the electrical efficiency at the STC conditions η_{STC} as follows [83, 192]:

$$\eta_{el} = \eta_{STC} \times \left[1 - \beta_{pv}\left(T_{pv} - T_{ref}\right)\right] \quad (3)$$

For a certain solar radiation and PV cell temperature an I-V characteristic curve of the PV cell exists and is presented in Figure 7-1.

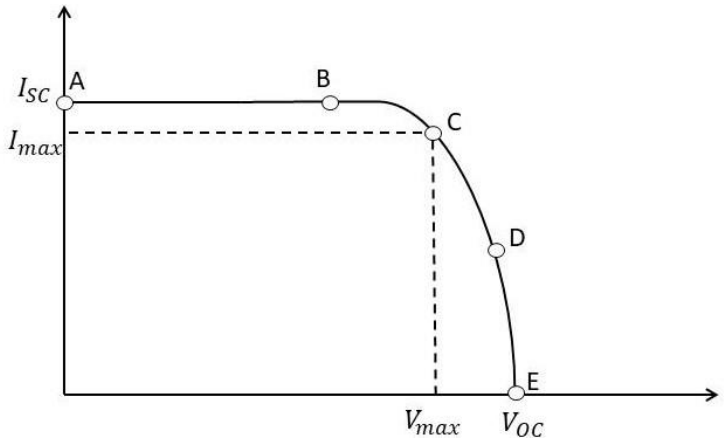

Figure 7-1: *The I-V characteristic curve of the PV cell at a certain solar radiation.*

The operation point of the cell on the current-voltage curve depends on the magnitude of a connected resistive load, and the power of the point is the product of the current and voltage [26]. In the optimal operation point of the I-V curve, the maximum power point can be reached. The current and voltage on the I-V curve change also depending on the solar radiation and cell temperature. Due to this, the maximum power point is constantly moving. The increased radiation level increases the current linearly, and the increased cell temperature decreases the voltage linearly [26]. To maximize the power output of the PV system, the maximum power point tracking methods (MPPT) are used to vary the resistive load. Typically, MPPT technology is integrated into inverters that convert the produced DC power into AC power. The PV system output can be modified by connecting the panels in series and parallel. The parallel connection increases the current, and the series connection increases the voltage of the array. In the solar microgrid, the PV panels can be installed on a building roof or on the ground.

2.2 Battery storage

Due to the fluctuating nature of solar energy production, a battery energy storage system is required in the solar microgrid to store the produced excess electricity to supply later demand during nights or cloudy days. The battery storage supports self-consumption and can generate cost savings by providing energy during a period of high electricity prices. The most common battery types are nickel-cadmium, lead-acid and lithium-ion [26]. The lead-acid batteries are commonly used, but the lithium-ion batteries have high efficiency and are used in the home battery storage systems, such as Tesla Power Wall [193] and Enphase AC battery. During charging of the battery, electrical energy is converted into chemical energy and released by discharging the battery.

An important feature of the battery storage in microgrid applications is the ability to tolerate repetitive deep charging and discharging cycles because this accelerates the battery ageing and degradation [193, 194]. Typically, the batteries are classified by their nominal capacity in kWh and charge/discharge power in W, which indicates the maximal power rate to charge or discharge the battery. The state-of-charge (SOC) battery variable indicates the amount of energy left in the battery as a ratio between the current capacity and the nominal capacity of the battery [26]. On the other hand, the depth of discharge (DOD) indicates the consumed energy capacity. These both indicators can have values between 0 and 1 indicating empty and full

battery. The battery storage has become to the end of its lifetime if it has lost 20% of its nominal capacity. The measure of the lifetime is the number of charge/discharge cycles sustained just before the 20% capacity loss [26].

The installation topology of the home battery system can be alternating current (AC) or direct current (DC) coupled. The AC-coupled battery has an inside built or separated battery inverter to enable AC-coupling and direct feed to the home appliances. On the other hand, the battery can be installed on the DC-side of the building power system with PV panels and a hybrid inverter to convert DC to AC output. In this thesis, the Enphase AC battery system with an internal battery inverter was selected and installed in the laboratory building. The battery has a nominal capacity of 1.2 kWh, and it is presented in Figure 7-11.

2.3 Inverters

The photovoltaic panels produce direct current (DC), which is converted into alternating current (AC) by an inverter. The battery storage system utilizes DC current and requires an inverter as well. The conversion is required because the building appliances work with AC power. The power conversion efficiency of the inverter is usually high from 93% to 98%. The inverters can have different sizes depending on the total power capacity, which can be from watts to megawatts. In the solar microgrid, the PV panels and the battery storage can be connected to the same hybrid inverter which feeds the AC-side or both components can have their inverters. The inverters require a minimum voltage to operate, which normally leads to a requirement to connect about 5 to 8 panels in series to reach the minimum voltage. However, this can be avoided by using micro-inverters separately for each panel.

In this thesis, the Enphase micro-inverters were used to convert each panel output individually from DC to AC power. These micro-inverters include the MPPT technology described in section 2.1. The micro-inverters are installed at the back of each panel, and they enable the monitoring and analysis of the operation on the individual panel and whole system level. The micro-inverters facilitate the installation of a small amount of PV panels because there are no minimum voltage levels to be reached. Additionally, shading on one panel does not influence the whole output of the system as happens with centralized solar or hybrid inverters. This is presented in Figure 7-2.

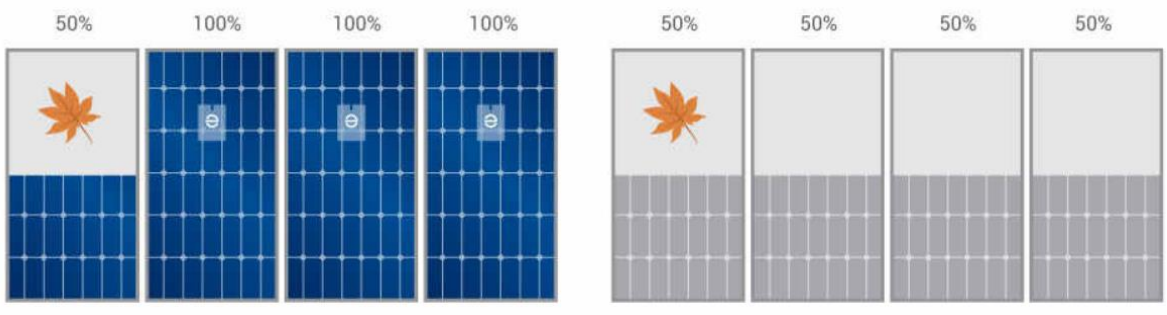

Figure 7-2: *The operation of the micro-inverters compared to centralized inverter [Enphase company]*.

2.4 Configuration typologies

The residential solar microgrid can have different connection topologies depending on the PV system, battery storage system and inverter technology. Figure 7-3a presents the PV and battery systems with two separated inverters of which the battery inverter is bi-directional. In this case, the battery storage is installed on the AC side of the switchboard, and the built-in inverter is included in the battery. The PV array has a centralized solar inverter with MPPT technology. Both inverters feed the AC bus of the building load, and the smart meter is used to connect the microgrid to the power grid. The advantage of this topology is that the sizing and installation are relatively simple, and the battery can be charged from the power grid if necessary. However, as a disadvantage, the power losses of the system increase slightly because of the double DC-AC conversion of the power flows. Figure 7-3b presents the topology with the hybrid inverter for the PV array and DC battery system. This topology reduces the power losses, but the modifications to the system size in terms of the PV and battery capacity are limited due to the fixed sizing of the inverter. Figure 7-3c presents the topology used in this thesis. First, each PV panel is connected to its micro-inverter and then to the AC bus of the building. The Enphase AC battery system includes a built-in bi-directional battery inverter and can be directly installed on the AC side of the building. The main benefit of this topology is relatively easy installation and individual monitoring and operation of each PV panel.

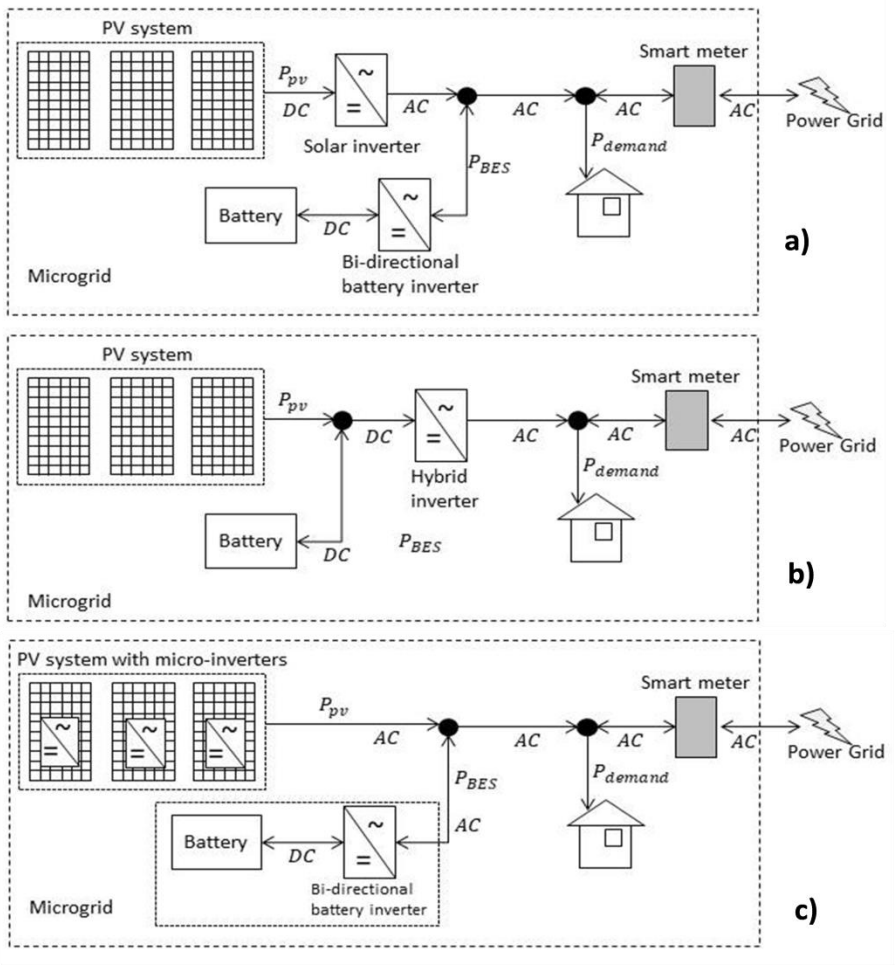

Figure 7-3: *Different solar microgrid topologies.*

2.5 Home renewable energy management system

The energy management system (EMS) is based on smart grid technology to manage energy sources and appliances in the grid. It is required to manage energy flows in the system, which supplies a certain load by more than one energy source in industrial or domestic applications [9, 195]. The energy source can be fluctuating renewable energies, controllable energy sources, energy storage systems or the main power grid. These energy sources form a grid-connected hybrid renewable energy system in the microgrid. The EMS has several functions, such as ensuring, in any case, the continuous energy flow to satisfy the demand, maximizing the use of fluctuating renewable energies, optimizing the system operation according to a certain objective and system constraints, and controlling energy flows between the microgrid and the main power grid by metering [195].

A home renewable energy management system (HREMS) is an optimal management system which manages and monitors energy flows in domestic buildings in terms of renewable energy production, battery storage, electric vehicle (EV) and home appliances [196]. The HREMS strategies optimize the energy flows between the domestic hybrid renewable energy system, the prosumer's load and the main power grid. The aim of the rule-based energy management strategies can be to maximize self-consumption, minimize energy costs according to the Time-of-Use (TOU) tariff regulated by the grid utility company or a hybrid strategy which maximizes self-consumption according to the TOU tariff [194]. The energy management strategies can be based on the optimization approaches as well. In this case, the optimization objective function is formulated to minimize the total energy cost of the microgrid operation over a decision horizon and according to the system constraints [194].

Generally, the HREMS creates an opportunity to shift the prosumer's load to off-peak period. The shifting reduces electricity bills, improves the utilization of the home appliances and facilitates the efficient utilization of the fluctuating renewable energy sources with energy storage in the building [9, 196]. The shifting of the prosumer's load is called demand-side management (DSM), or demand response (DR), and it is managed by the HREMS to generate energy savings and cooperation between the prosumer and utility company. The main idea of the DSM is that the prosumer changes its grid electricity usage from its normal consumption profile according to the changes in the time-dependent electricity price [196]. The aim is to generate cost savings for the prosumer, improve the energy flexibility and efficiency of the building and reduce the peak load in the power grid [197]. The smart meter is used to communicate the real-time electricity price to prosumer to facilitate the shifting of the electrical appliances to the off-peak period [196]. The DSM can follow an incentive- or price-based scheme. Usually, in residential buildings, the price-based Time-of-Use (TOU) scheme is used to shift the controllable load to the low electricity price period [198]. In this case, the hours of a day are divided into two or three periods and priced differently depending on the general demand assumption, such as morning or evening peaks. The incentive-based scheme is typically offered for industrial electricity users to reduce their electricity use against a payment during a certain period, and in the case of failure, they are penalized [198].

The main components related to the HREMS are presented in Figure 7-4.

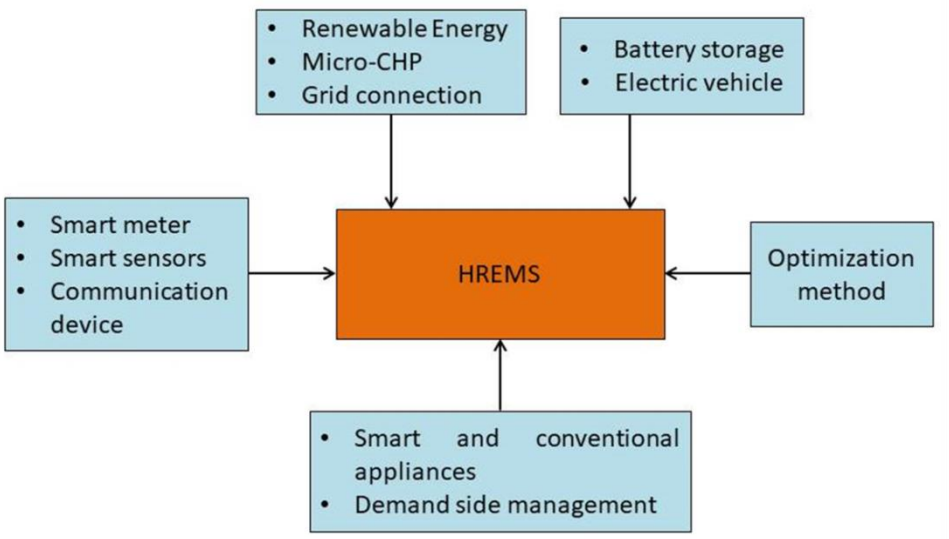

Figure 7-4: *The main components related to the HREMS.*

The most applied fluctuating renewable energy source in the HREMS is solar energy with battery energy storage, of which capacity is optimized based on the photovoltaic panel capacity and load demand. To support solar energy production, different micro-CHP systems can be used to produce simultaneously, in a controllable manner, heat and electricity for onsite use. The smart meter monitors electricity use in a building and communicates it directly with the electricity utility company. The communication device exchange the information between the smart sensors and meter to enable the optimal operation of the battery storage, electric vehicle, appliances and controllable energy production. The most important component of the HREMS is the optimization method which optimizes the decisions in the microgrid based on the current information of the system state or by using the future predictions of the system behavior, such as in the model predictive control method. In Figure 7-5 is presented the energy and information flows around the HREMS to perform the decision optimization.

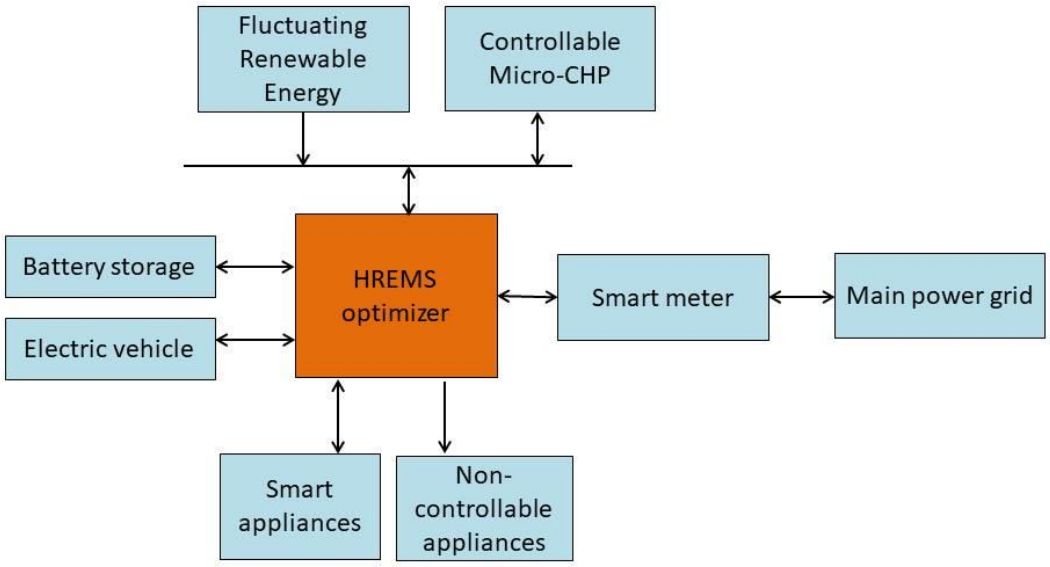

Figure 7-5: *Flow chart of the home renewable energy system connected with RES, grid, storage systems and appliances.*

Next, two different HREMS strategies are presented.

2.5.1 Model predictive control

The following section a direct citation from the ICSREE 2022 conference paper "Kallio S., Siroux M.: A Review – Home Renewable Energy Management Systems in Smart Grids." DOI: 10.1088/1755-1315/1050/1/012001. Published by IOP Publishing in 2022.

"The aim of the HEMS is to solve a load scheduling problem in buildings in terms of defined objectives. The model predictive control (MPC) is used to solve this optimization problem by taking into account future predictions of the most important variables, such as load demands, renewable energy production and real-time energy prices. In this case, the scheduling problem is seen as a receding-horizon optimal control problem [197]. MCP requires an accurate dynamic model of the system, an objective function with constraints to be minimized and an optimization algorithm. The algorithm is often based on mathematical optimization methods, such as linear or non-linear programming. However, heuristics and metaheuristics approaches can also be used as an optimizer if the problem has multiple objectives. MPC is based on the iterative optimization of the dynamic model. The working principle is presented in Figure 7-6 [199]."

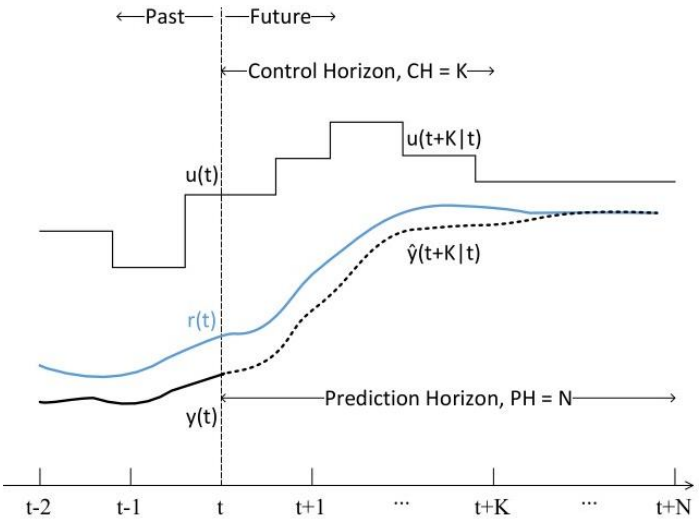

Figure 7-6: *Model predictive control for a certain time horizon [199]*.

The MPC utilizes the system model to generate control predictions for predefined N time steps in the near future called prediction horizon [199], such as 96 time steps (15 min) in the next 24 hours. The control predictions are generated by minimizing the objective function by using the current model state at the time step t and future forecasts, such as PV power prediction. The first predicted control output is applied to the system, and the optimization is performed again for an updated time horizon of the 96 time steps.

Linear programming

One possible method to solve an optimization problem of the MPC is linear programming (LP). The LP is used to maximize or minimize a linear objective function described by the decision variables of the problem [200]. The problem is solved subject to a set of lower and upper bounds, linear equality and/or inequality constraints [200]. In general, the LP model can be presented as follows:

$$\min_{x} f^{T} x \; subject \; to \begin{cases} A \times x \leq b \\ Aeq \times x = beq \\ lb \leq x \leq ub \end{cases} \tag{4}$$

where A and Aeq are matrices and the rest are vectors. The lb and ub indicate for the lower and upper bound, respectively. The LP model defines a feasible region which satisfies the constraints. The optimal solution is the point within the region which minimizes (or maximizes) the objective function.

2.5.2 Reinforcement learning

The following section 2.5.2 is a direct citation from the ICSREE 2022 conference paper "Kallio S., Siroux M.: A Review – Home Renewable Energy Management Systems in Smart Grids." DOI: 10.1088/1755-1315/1050/1/012001. Published by IOP Publishing in 2022.

"Machine learning is a group of methods that learn to identify patterns from historical data. These methods use the patterns to predict or perform decision making. Machine learning has the following three types: supervised learning, unsupervised learning and reinforcement learning [201].

Reinforcement Learning is a physical model-free algorithm that can adapt to its uncertain environment by learning optimal policy of actions through the historical data and interaction with the system. Due to the increasing amount of data and complexity of the systems, the Reinforcement Learning has increased its popularity for HEMS and is seen as a data-driven option for model-based approaches, such as MPC. The RL is used in the DR to schedule and control, for example, the use of renewable energy generation, battery storage and electric vehicle charge/discharge.

Usually, the decision making problem of the single-agent RL algorithm is formalized using a Markov Decision Process (MDP), which can handle multi-stage decision making in a discrete-time framework. The MDP includes four main elements presented in Figure 7-7: a space of states S, a space of actions A, a reward function r to be maximized and transition probabilities between the states P [198]. In MDP, at a discrete-time step t is the agent detects the state S_t of the environment, selects an action A_t which leads to a new state S_{t+1} where a reward is given to the agent [201]. The agent aims to maximize the reward by its actions, and in this way, it learns the optimal policy to control its environment. The most used RL technique is Q-learning [201, 202]."

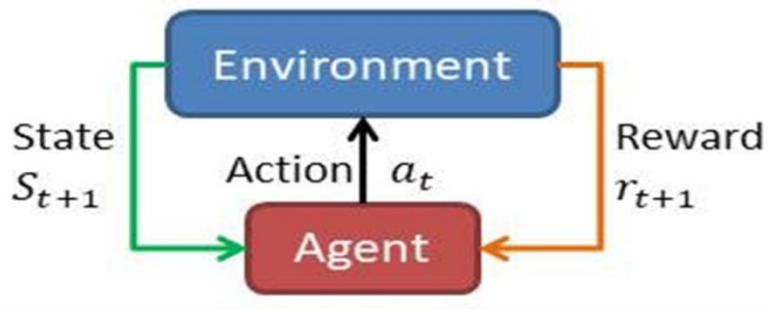

Figure 7-7: *Working principle of the reinforcement learning method.*

3. Experimental set-up of solar microgrid for smart buildings

During this thesis work, a solar microgrid was installed on the roof of the INSA ICUBE laboratory building to demonstrate experimentally home renewable energy management strategies and to collect operational data of the photovoltaic panels coupled with a battery storage system. The grid-connected system was aimed to feed the local load. The adjustable load was demonstrated to present a residential electricity demand profile with certain appliances, such as electrical heater and lighting. In Table 7-1is presented the components, meters and sensors of the experimental set-up.

Table 7-1: The components and sensor of the solar microgrid experimental set-up.

Component	Capacity	Efficiency	Manufacturer
4 x PV panel	4 x 300 W_p	18.3 %	DualSun
AC Lithium-Ion battery	1.2 kWh, 270 W max. charge/discharge	96 %	Enphase
4 x Micro-inverter	235 W – 350 W / inverter	96.5 %	Enphase
Gateway			Enphase
Production meter			Enphase
Consumption meter			Enphase
Electrical load	Max. 700 W		
Weather station, (solar pyranometer, wind anemometer, temperature/humidity sensor)			Davis Instruments

3.1 Materials and methods

The possible installation typologies were discussed in Section 2.4 and the selected typology for this experimental set-up is presented in Figure 7-8.

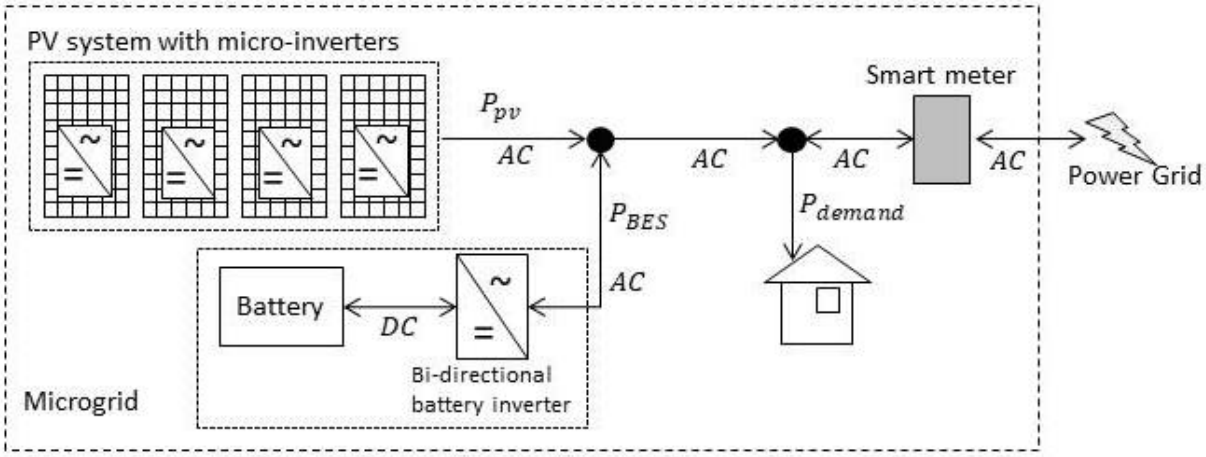

Figure 7-8: *The topology of the solar microgrid experimental set-up.*

The installed PV panel model was selected to be the FLASH Black produced by DualSun [203]. This model has a PERC (Passivated Emitter & Rear Contact) surface and high-performance monocrystalline cells with a reference efficiency of 18.3% and peak power of 300 W_p. The installed panels with the weather station are presented in Figure 7-9.

Figure 7-9: *The installed PV panels at INSA ICUBE laboratory.*

The PV panels were installed with two different mounting systems. The panels in front of the installation were mounted with the Soprasolar Fix Evo Tilt system, which can have a fixed tilt angle of up to 10°. The second mounting system was a frame made for the previous solar tracking research. However, for this installation, the frame was used as a fixed mounting system with a manual angle adjustment. The angle was fixed to 18°.

Each PV panel was connected to its Enphase IQ 7 micro-inverter, which was mounted behind the panel and included the MPPT. The installed inverter is presented in Figure 7-10. The electrical wiring from the inverters was connected to the switchboard of the garage. In Figure 7-11 is presented the switchboard, Enphase Envoy-S Metered gateway and the Enphase AC battery storage system. The Enphase production and consumption meters were integrated into the switchboard to measure the PV production and consumption of the system.

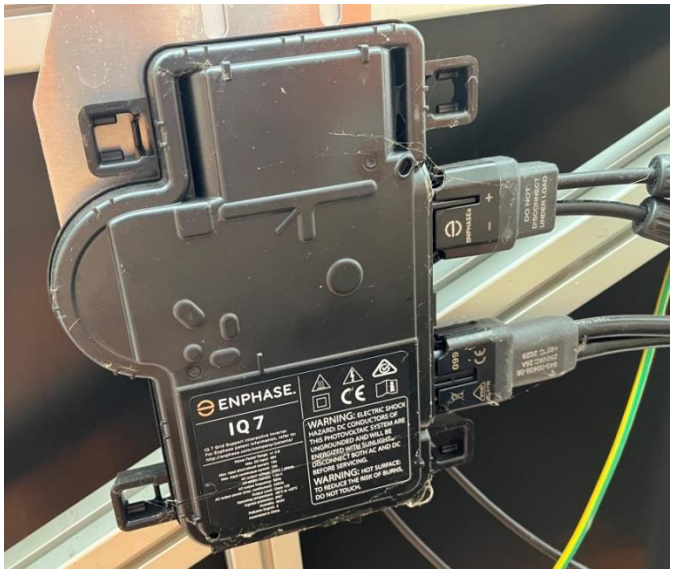

Figure 7-10: *Micro-inverter installed to the back of the panel.*

Figure 7-11: *The installation in the garage with the switchboard, gateway and battery storage.*

The Enphase Envoy-S Metered gateway operated between the system and web-based Enphase Enlighten monitoring and analysis software which is accessible from a computer or mobile device. The user interface of the software is presented in Figure 7-12. The gateway was used to monitor PV production by communicating with micro-inverters, to manage battery charge/discharge cycle and to collect consumption data every 15 min. The gateway forwarded the system data, such as PV power and battery cycle, to the monitoring software via the Internet connection of the garage. The state of each system component was monitored in the software, and the data was downloaded to the excel file for further analysis. The energy management strategy of the system was defined in the software, which sent it to the gateway for the implementation. The system was able to operate under the given Time-of-Use scheme or flat-rate scheme, which aimed to maximize the self-consumption of the PV electricity.

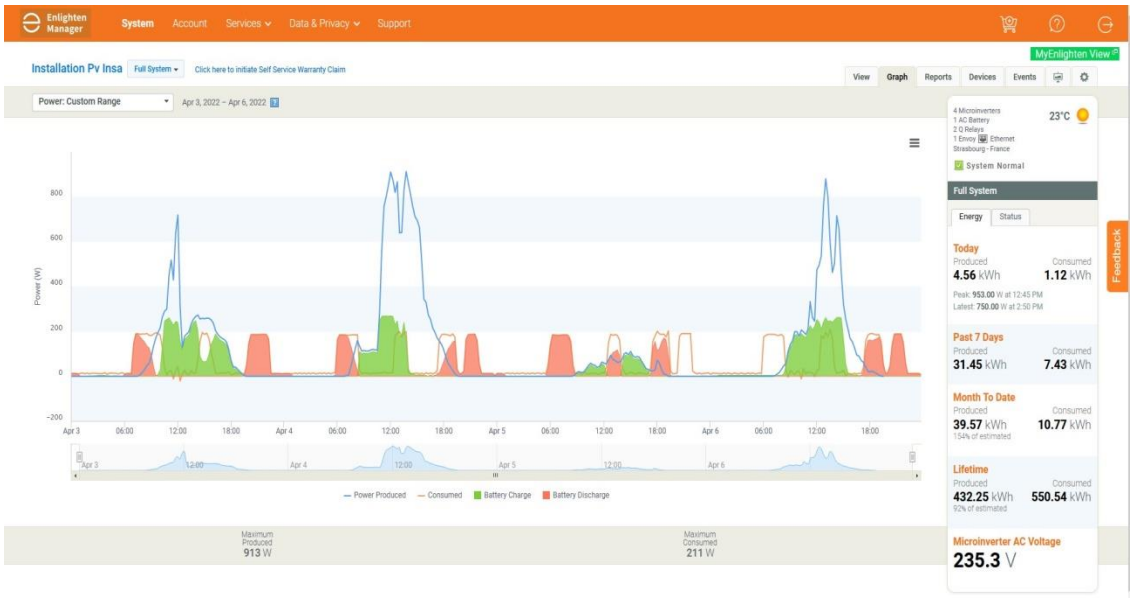

Figure 7-12: *The interface of the web-based monitoring and analysis software.*

The modular Enphase AC Lithium-Ion battery storage had a capacity of 1.2 kWh and a maximum charge/discharge power of 270 W. The battery stored the PV production, fed the electrical load and was able to be charged from the grid during certain night hours managed in the monitoring software.

The sizing of the system was based on the available budget because the electrical load within the garage was adjustable. As the first step, only one modular Enphase AC battery was installed with an option to extend the storage capacity. The maximum charge/discharge power of 270 W narrowed the possibility to store energy during the sunny hours because the total peak power of the PV panels was 1.2 kW, and the battery was able to charge only 270 W. The electrical load was adjusted according to the maximum charge/discharge power.

The Davis Instruments Vantage Pro2 weather station with an anemometer, temperature/humidity sensor and a solar pyranometer presented in Figure 7-13 was installed next to the PV panels to collect the local weather data influencing the daily PV power production. The WeatherLink software and the data logger were used to transfer the data to the computer for further analysis. The data were collected every 15 min interval. The weather station was able to measure many variables, such as global horizontal radiation, ambient temperature, wind speed, relative humidity and dew point temperature. The gathered weather data was used with the collected PV production data to predict the future electricity production of the system. This work is presented in Chapter 8.

Figure 7-13: *The installed weather station. The solar pyranometer is marked with yellow and zoomed.*

The described PV system was used to gather operation data and weather data to model PV power production with the machine learning methods. The workflow to collect the data is presented in Figure 7-14.

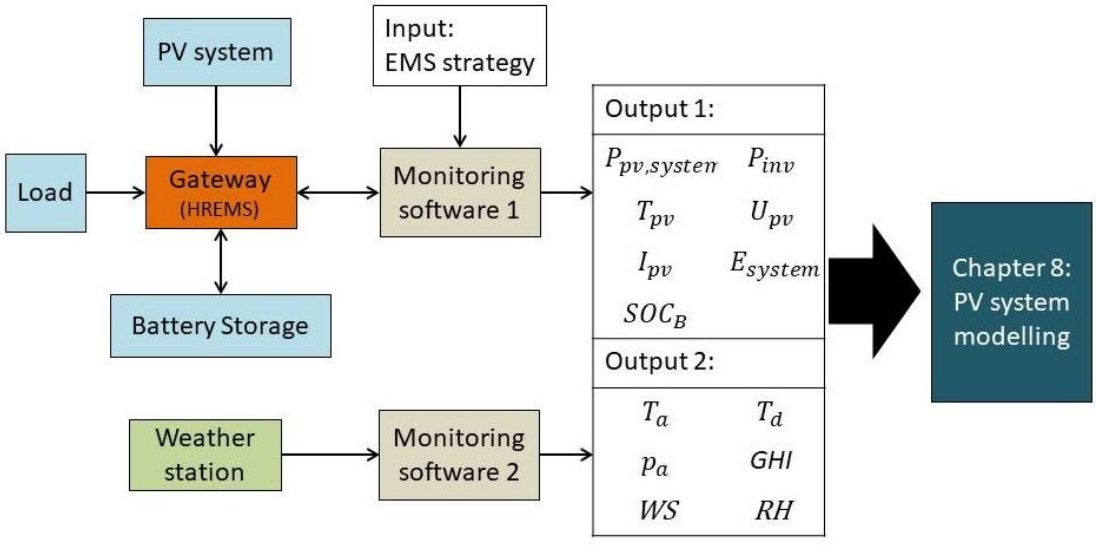

Figure 7-14: *The data gathering workflow of the experimental set-up.*

3.2 Results and discussion

3.2.1 Operation analysis under rule-based EMS strategies

The presented experimental set-up of the PV-battery system was running under two different rule-based energy management strategies: the Time-of-Use (TOU) scheme and the self-consumption strategy. The TOU strategy optimized the use of PV electricity and battery storage depending on the grid electricity price to avoid buying electricity at a high price. The rule-based EMS strategy did not utilize any future information of the PV power production and local load but applied a control command based on the current state of the system. For example, if the battery was not full and the PV production exceeded the load, the battery was charged. The electricity price profile presented in Figure 7-15 was given to the gateway via the monitoring software. The peak price periods were assumed to be from 07:00 to 10:00 o'clock and from 16:00 to 22:00 o'clock with a price of 0.2 €/kWh. The off-peak price was assumed to be 0.12 €/kWh. The self-consumption strategy was operating at a flat rate, and the objective was to maximize self-consumption of the PV electricity. The system was operating under the TOU strategy from 25.-26.4.2022 and under the self-consumption strategy from 17.-18.5.2022. The results are presented in Figure 7-16 and Figure 7-17. The local load was adjusted to be low or high due to available solar radiation. The low demand profile was applied under TOU scheme strategy in Figure 7-16 and the high demand profile under the self-consumption strategy in Figure 7-17.

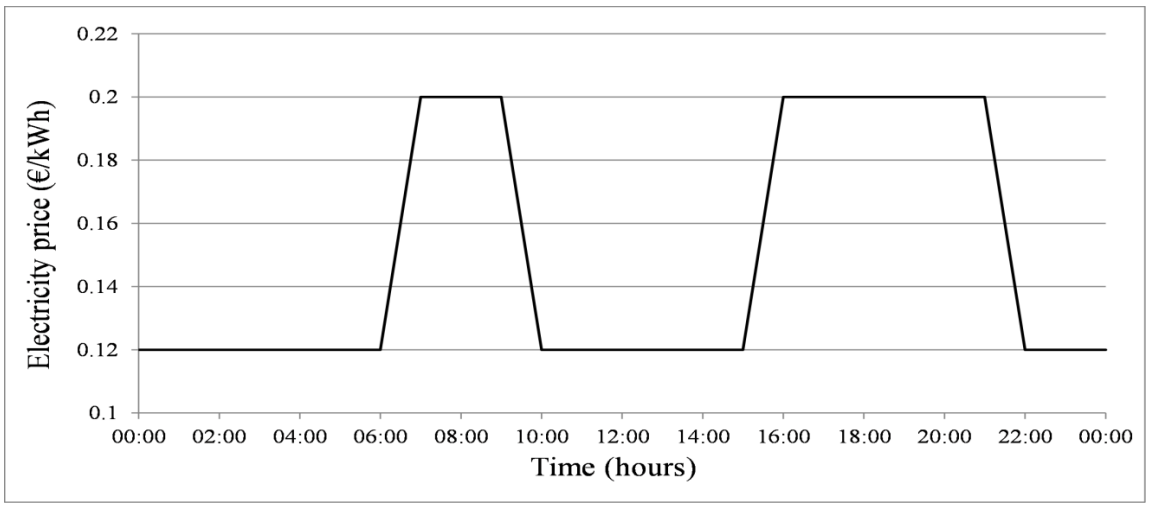

Figure 7-15: *The Time-of-Use scheme*

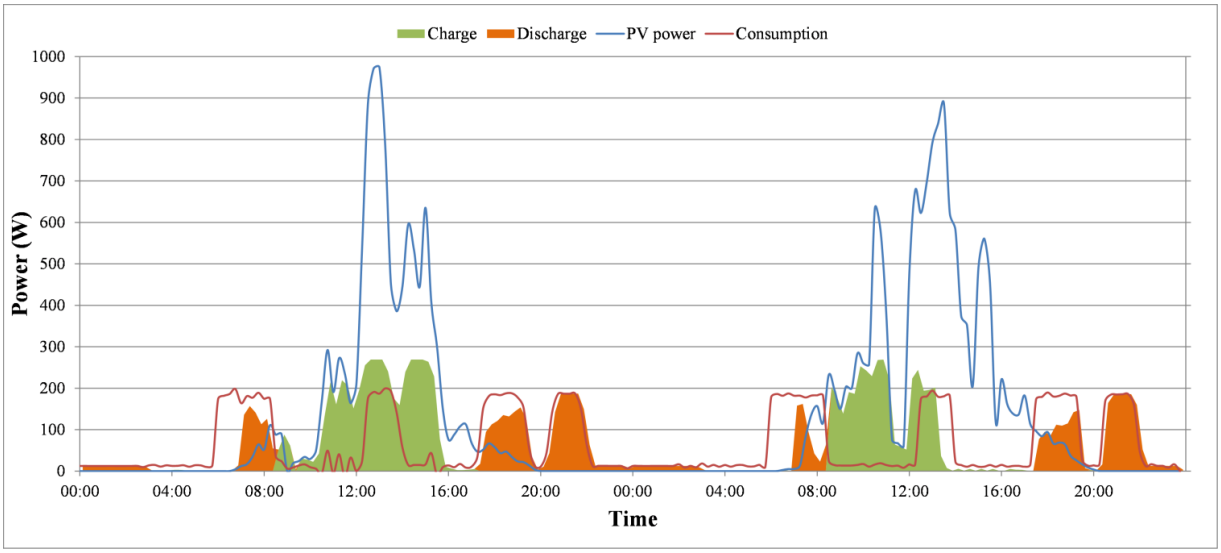

Figure 7-16: *Operation of the PV-battery system under given TOU scheme on 25.-26.4.2022.*

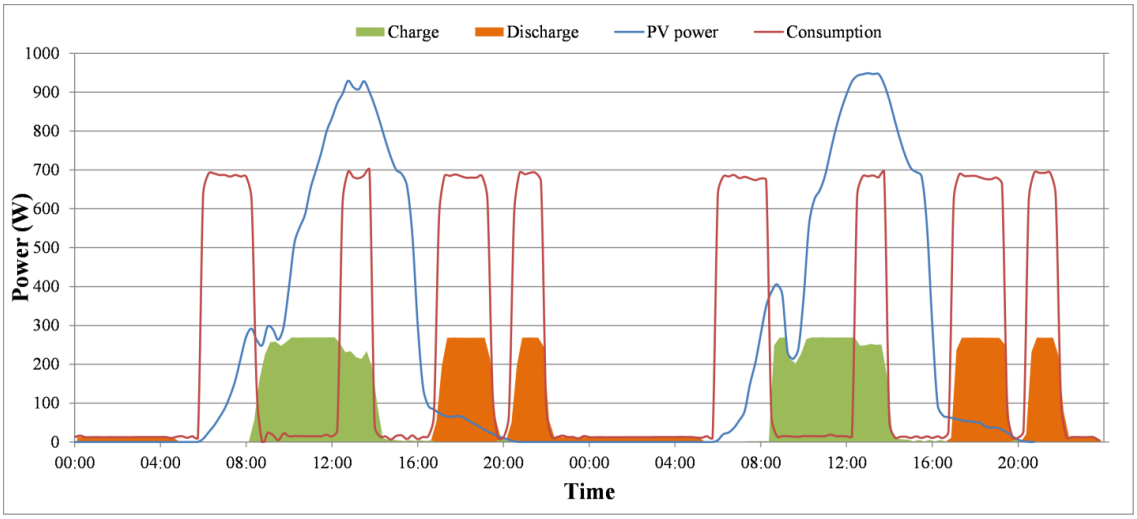

Figure 7-17: *Operation of the PV-battery system under self-consumption strategy on 17.-18.5.2022.*

In Figure 7-16, the gateway optimized the battery charge/discharge according to the given TOU scheme. The consumption peak started each day around 6:00 o'clock, and the grid electricity was used until 7:00 o'clock, when the price peak started. From that moment, the consumption was satisfied by the battery discharge and available PV electricity to avoid high electricity costs. During each day, the PV production was high enough to charge the battery fully and at the same time, satisfy the electricity demand. The evening consumption peak was fully satisfied by the battery charge and PV production. During the night, a small amount of

consumption occurred, which was satisfied by the battery charge until the SOC level of 50% was reached.

In Figure 7-17, the gateway optimized the battery operation by maximizing the self-consumption of PV electricity. Due to the low SOC level, the morning consumption peak was satisfied by the grid and produced PV electricity. When the consumption decreased, the battery was immediately charged fully by the produced PV electricity to maximize the self-consumption. During the evening peak, the battery was discharged almost totally due to the high consumption. The main difference between the results in Figure 7-16 and Figure 7-17 was that the low demand profile allowed discharging the battery next morning during the high price period. The high electricity demand resulted in the empty battery at the end of the day. This could be solved by increasing the battery capacity.

3.2.2 Results of the optimization-based EMS simulation

In Figure 7-18 is presented the simulation results of the energy management strategy based on the model predictive control (MPC) introduced in Section 2.5.1. The results are presented for the first days of Figure 7-17. For the optimal control problem, the objective was to minimize the electricity cost and to have the battery ready for the next day. The optimization was performed in the Matlab software for the 96 time steps and the 24 hours horizon to find out how the MPC strategy differs from the above presented rule-based strategies. The optimization problem was solved by the linear programming method. The objective function was given as follows:

$$Min\ f_{obj} = \sum_{k=1}^{N} \Delta t \times c_{buy}(k) \times P_{from,grid}(k) + \Delta t \times c_{sell}(k) P_{to,grid}(k) - w_f \times E_B(N) \qquad (5)$$

where c is the specific cost of electricity (€/kWh) to buy and sell to the grid, P is the power (W), Δt is a time step (s), w_f is a final weighting factor and E_B is the battery energy at the last time step N. The optimization problem is solved subject to the following constraints:

$$P_{pv}(k) + P_{grid\_buy}(k) + P_{grid\_sell}(k) + P_B(k) = P_{load}(k) \qquad (6)$$

$$P_{grid\_buy}(k), P_{grid\_sell}(k) \leq P_{lim,grid} \qquad (7)$$

$$-270\ W \leq P_B \leq 270\ W \tag{8}$$

To perform the optimization, the MPC requires forecasted information of the PV production and local load. However, as the first step, a perfect forecast of these variables was assumed and the measured profiles in Figure 7-17 were used as forecasts for the MPC. Additionally, the target was to have same battery SOC at the beginning and end of the day. Due to this the final weighting factor w_f was set to be 0.1. This allowed comparing the different EMS strategies and daily costs between the measured and simulated day. The TOU scheme in Figure 7-15 was used in the optimization for c_{buy}, and the selling price c_{sell} of 0.06 €/kWh was applied for the surplus PV production. Additionally, the battery storage was able to sell the stored energy to the grid if necessary.

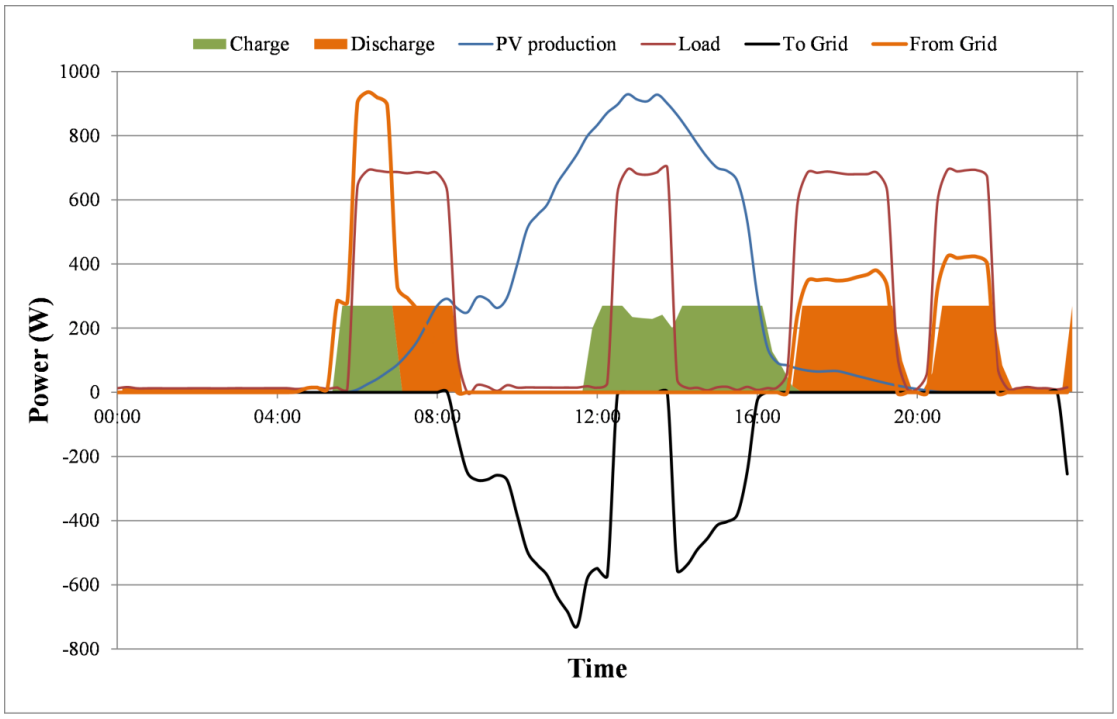

Figure 7-18: *The simulation results of the system under the MPC strategy on 17th of May 2022.*

When comparing the results of the optimal control based EMS strategy to the rule-based strategy in Figure 7-17, the optimal control enabled to charge the battery during the off-peak period just before the high peak period started at 7:00. At the same time, the local load was satisfied by the grid electricity. During the high peak period, the battery was discharged and the high electricity price was avoided. This was allowed because the MPC used the future

information of upcoming high price period from 7:00 to 10:00 o'clock. The rule-based strategy was able to use only the grid electricity to satisfy the morning consumption peak because the battery was almost empty after the previous day. During the day in Figure 7-18, the PV electricity was used later to charge the battery fully again. However, this happened later than in Figure 7-17 because the MPC used the future information of the PV production. Due to this, the prediction of the PV production should be accurate as possible to avoid failing control commands of the battery charge and discharge. Normally, the optimal control signal of the first step is applied to the system and the optimization is performed again with updated forecasts and moving time horizon.

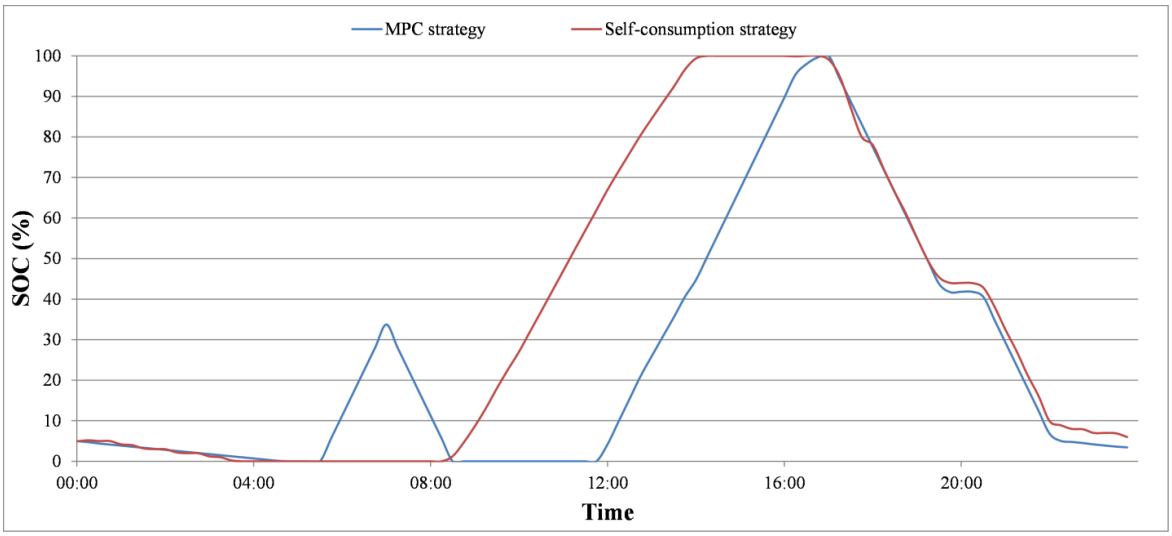

Figure 7-19: *The battery SOC on 17th of May 2022 under the self-consumption and MPC strategy.*

In Figure 7-19 is presented the battery SOC on 17th of May under the self-consumption and MPC strategies. The main difference is that the MPC strategy favored to have zero SOC until the last moment that the battery can be still charged fully. The MPC strategy optimized this moment depending on the PV forecast. The self-consumption strategy charged the battery immediately when possible.

The daily operation cost of the system under the MPC strategy was 0.32 € due to the need of buying electricity from the grid at the morning and evening peaks. During the same day, the self-consumption strategy resulted in the cost of 0.39 € which means that the MPC strategy was able to reduce costs.

As the next step, the MPC strategy should be implemented by performing the optimization at each time step with the system specific PV power prediction model and moving horizon. Additionally, the battery capacity and PV system size could be optimized for a certain load profile when the system is operating under an optimization-based EMS strategy.

4. Conclusion

The main focus of this Chapter was to study experimentally home renewable energy management strategies in the solar microgrid. First, the main components of the solar microgrid were introduced. Next, the experimental set-up of the solar microgrid installed in the INSA ICUBE laboratory was presented. The main purpose of the set-up was to demonstrate experimentally home renewable energy management strategies and to collect operational data of the PV panels coupled with the battery storage system. The collected PV data was used for the modelling purpose in Chapter 8.

The experimental set-up was successfully installed in October 2021 and the data gathering was started. As result, the system operated under two rule-based energy management strategies and different system behaviors were indicated. The optimization-based MPC energy management strategy was implemented in the simulation model of the system. This resulted in the improved operation and the reduced costs because the MPC strategy took into account the future PV production and electricity price.

As the next step, the MPC strategy should be implemented by performing the optimization at each time step with the system specific PV power prediction model and moving horizon. Due to this, the PV power prediction methods based on machine learning are further investigated in Chapter 8.

In future work, the battery capacity and PV system size could be optimized for a certain load profile when the system is operating under an optimization-based EMS strategy with real forecasts and moving horizon. Additionally, the electrical vehicle and fuel-fired micro-cogeneration system can be added to the model. The experimental set-up could be updated with the photovoltaic-thermal collectors and additional AC battery modules to increase the PV storage capacity. Adding the PVT panels would lead to a need for thermal energy storage.

CHAPTER 8. Photovoltaic power prediction for solar microgrid optimal control

Sonja Kallio and Monica Siroux
INSA Strasbourg ICUBE, University of Strasbourg

This article was accepted on 19.05.2022 and will be published in *Energy Reports Special Issue of 2022 The 9th International Conference on Power and Energy Systems Engineering*.

Abstract

In a solar micro-grid, a hybrid renewable energy system generates electricity for a building's onsite use. The battery storage and the main power grid connection are used to facilitate the matching between the demand and production. To control energy flows optimally, an accurate day-ahead prediction of the photovoltaic (PV) panels output is required. However, this is a challenging task due to the fluctuating nature of solar radiation availability. The accuracy of the prediction is influenced by the modelling method and input parameters. In this study, the measured power and weather data is gathered from an experimental installation of PV panels to predict PV output for a 24-hours horizon in 15 min intervals. The multiple linear regression (MLR) and artificial neural network (ANN) methods are considered in the prediction modelling and compared using performance indicators. The micro-inverter technology is used to gather the individual PV panel output in addition to the overall system output. The results show that the modelling methods have different accuracy performances and the ANN model built with the individual PV output data results in the highest accuracy. Utilizing the micro-inverter technology leads to an advantage of having more accurate PV prediction for the control purpose.

1. Introduction

Solar energy is an inexhaustible source of renewable energy. Additionally, it is free of charge and any emissions. However, the availability of solar energy is strongly fluctuating and depends on the changing weather conditions, time of the day and location. That creates significant uncertainty in the power output of solar systems. The photovoltaic panel is a silent device without moving parts and can convert sunlight into electricity through the photovoltaic effect.

The electrical efficiency of the crystalline silicon PV panels varies from 11% to 22% [24]. An increasing amount of distributed PV installations in the building sector enables building owners to act as a prosumer by generating and storing their own electricity onsite or selling it to the grid [101]. A solar microgrid can be used to generate profit for the building owner, and through the optimal control of hybrid renewable energy systems reviewed in [172], the profit and self-consumption can be maximized. However, PV power output has uncontrollable and abrupt nature. Thus, an accurate forecast of the output is required for optimal energy management in the solar microgrid as well as in the other levels of the electric grid [204].

In the literature, different PV power prediction methods have been proposed with different data inputs. The most used methods are deterministic, machine learning (ML) and hybrid techniques [205, 206]. The deterministic methods are based on the physical model of the PV to predict the power output, and the artificial intelligence-based ML methods, such as multiple linear regression (MLR), artificial neural network (ANN) and support vector machine (SVM), aim to form a relationship between input and output without any further knowledge of the system [205]. Kalogirou [26] conducted a comprehensive review on the ANN method in renewable energy systems considering PV systems. Zazoum [207]compared different ML techniques for PV power prediction. He concluded that the ML methods are suitable and fast to predict the PV power of any system.

The scientific literature has aimed to improve the accuracy of the PV power forecasting models in terms of different prediction algorithms and input data. Different sets of weather and PV operation parameters have been investigated to increase the accuracy [208]. However, to the best of the author's knowledge, there is no work focusing on the different ML methods using as an input parameter the PV power data measured by the individual micro-inverters to increase the accuracy of the day-ahead power prediction. In this study, the MLR and ANN prediction models are built for each PV panel and the overall system using the input data measured from the micro-inverter and aggregated system level. The study aims to reveal if using the data of the micro-inverter level can increase the prediction accuracy of the whole PV system.

2. Methodology

A comparative study of different PV power prediction models is conducted. First, the experimental set-up of PV panels is presented with data gathering methods. Next, the monitored data is pre-processed and used to create different data-driven models for the PV power prediction. The first method is a multiple linear regression (MLR) with interaction terms which is compared to a method called Artificial Neural Network (ANN). Both models are regression models, and the monitored data from the PV installation and weather station are used to train and validate the models in the MATLAB environment. The training data was collected from 27.9.2021 to 31.3.2022 and includes large variation of different weather conditions. The different prediction models are built by using as input the weather data and power output data from the micro-inverter and aggregated system level.

2.1 Experimental set-up

The installation of four PV panels in Figure 8-1 was realized on the rooftop of the INSA ICUBE Laboratory in Strasbourg, France (48° N and 7° E) in September 2021. Strasbourg is classified to have an oceanic and semi-continental climate according to the Köppen climate classification [83]. Each PERC (Passivated Emitter & Rear Contact) monocrystalline PV panel has a peak power of 300 W, and micro-inverters are used to convert each panel's DC output to AC power individually. The energy production is maximized by a Maximum Power Point Tracking (MPPT) of each micro-inverter. Two of the panels have a tilt angle of 7°, and the rest is set to an 18° angle. The PV panels were installed on the available roof area which has a clear face with the sun during a part of the day. The shading from the surrounding buildings during the day cannot be avoided. However, the micro-inverter technology enables the independent operation of each panel and partial shading has an impact only on the shaded panels. Using the micro-inverter technology has also several other advantages over traditional inverters discussed in [209].

The four micro-inverters are connected to a gateway which is used to communicate measured system data to the web-based monitoring and analysis software provided by Enphase company [210]. The power output of each panel ($P_{inv,1\text{-}4}$) and the whole system (P_{agg}) is measured every 15 min and uploaded into Excel file from the online software. The installation includes also Lithium-Ion AC battery storage to store the PV production if not used directly in the building. The optimal battery use is managed by the gateway.

In addition to the PV panels, the installation includes a weather station to measure the local weather parameters global horizontal irradiance (GHI), ambient temperature (T_a), dew point temperature (T_d), pressure (pat), wind speed (WS) and relative humidity (RH) in 15 min intervals. A data logger is used to transfer the weather data to a computer for further analysis.

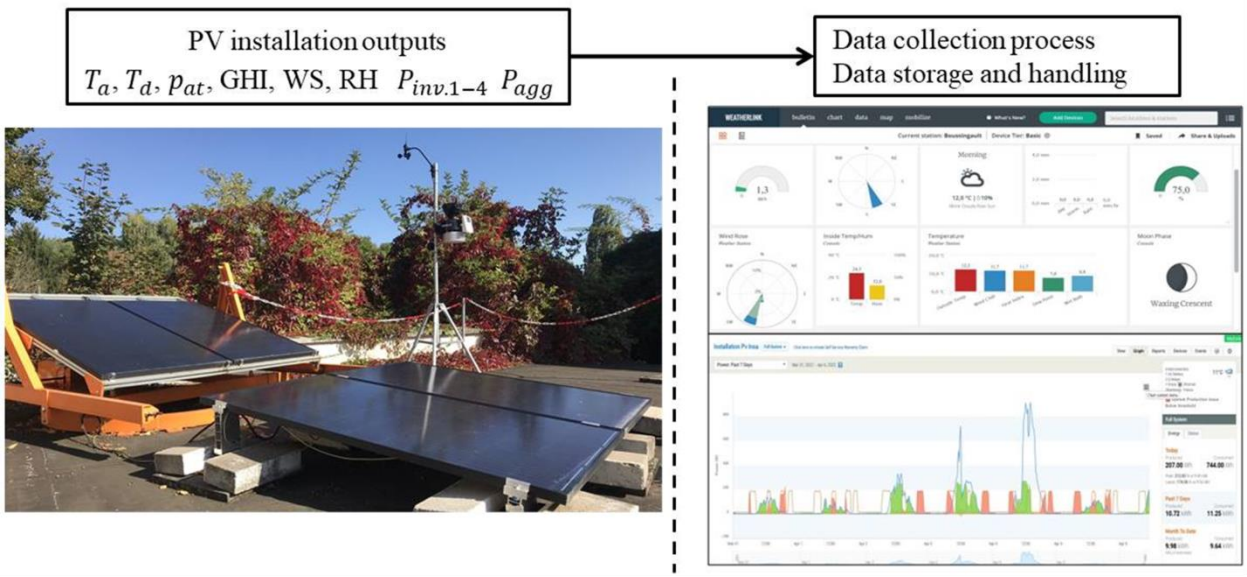

Figure 8-1: *The PV installation with the weather station and data collection process.*

2.2 Correlation analysis

The PV power production correlates with the surrounding weather conditions. The Pearson correlation analysis was used to find out the correlation between the PV power output and individual weather variables. Generally, this analysis method reveals how strong are the linear relationship between the different variables in a given data set. The analysis shows the correlation coefficients that vary from -1 to 1. The magnitude of the absolute value of the coefficient indicates the strength of proportionality between two variables. This indicator is used to select the most significant variables for the prediction model. The high number of parameters can result in lower accuracy of the model.

2.3 Multiple linear regression model

In this study, the measured historical data of both the PV power output and weather variables were used as an input to create a multiple regression model with interaction effects.

The interaction effect occurs when the effect of the independent weather variable on the PV production changes depending on the other weather variables. This interaction is presented as a product of the independent weather variables. The regression model with interaction effects is an extension of the general regression presented as follows [205]:

$$\hat{y} = \beta_0 + \beta_1 x_1 + \beta_2 x_2 + \cdots + \beta_n x_n + \varepsilon \quad (1)$$

where β_0 is the intercept and x represents each independent weather variables. The other β parameters present the slope coefficient of the variable. All β parameters are defined in the model creation process to minimize the error ε. The interaction effects are added to the general form of the multiple regression model as follows:

$$\hat{y} = \beta_0 + \beta_1 x_1 + \beta_2 x_2 + \beta_3 x_1 x_2 \ldots + \beta_n x_n + \beta_l x_n x_m + \varepsilon \quad (2)$$

where x_1x_2 is the interaction between two variables.

2.4 Artificial neural network model

The ANN algorithms are commonly used to solve time series prediction tasks because they have the ability to learn the behavior of variables from historical measurements, such as PV power output and weather data in terms of the PV prediction modelling [211]. The ANN is based on supervised learning, and the prediction performance increases with the amount of historical data used in the training of the model. In addition to the training dataset, a part of the historical dataset is used only for the test and validation of the model to show the generalization capability of the prediction model. The learning or training process is based on continuously improving the weights and biases within the neural network to reach the desired output, which minimizes MSE in Eq. (2) (or RMSE in Eq. (3)) between the actual and predicted output. This is performed by using a learning algorithm, such as gradient descent, error back-propagation or Levenberg-Marquardt [211]. The back-propagation algorithms are the most used and powerful in terms of learning [26]. In this study, the MATLAB software is used to train the ANN model and the limited-memory Broyden-Fletcher-Goldfarb-Shanno quasi-Newton (LBFGS) optimization algorithm is used to minimize the MSE [212].

The number of inputs to the ANN model indicates the "neurons" in the input layer presented in Figure 8-2. The layer structure includes the input layer, a certain number of hidden layers with hidden neurons and the output layer. In the case of PV power prediction, the input layer includes the selected weather variables (x_1, x_2, x_3 …, x_n), and the output is the power prediction. Generally, the ANN model can include any number of hidden layers and neurons. However, the accuracy of the model depends on the right number of layers and neurons. In this study, the Multi-Layer-Feed-Forward Neural Network (MLFFNN) structure is used in which the information flows only in one direction from the input to the output layer. The outputs of the previous layer are the inputs for each neuron on the next layer. The inputs of each neuron are multiplied by weights (w_1, w_2, w_3 …, w_n) and combined using a weighted linear combination [9]. Before the outputs of the neurons are ready, a nonlinear activation function f_{ac}, such as Hyperbolic tangent or Sigmoid function, is applied to the results of the layer. In this study, the Rectified linear unit function is used to perform a threshold operation on the input values to set the values less than zero to be zero [212].

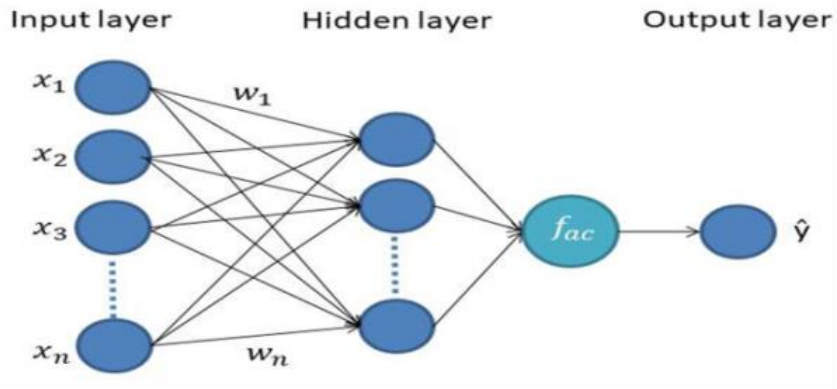

Figure 8-2: *The structure of a simple ANN model with one hidden layer.*

After training, the ANN is a quick method to provide predictions for complex non-linear problems and it can reach good accuracy also with smaller data set used in the training and validation [208].

2.5 Model performance indicators

To conduct a comparative study between different models, certain performance indicators are used to evaluate the accuracy of the prediction models. In addition to a simple absolute error

between the actual and predicted value, the following commonly used performance indicators for the forecasting models are used in this study: Mean Absolute Error (MAE), Mean Squared Error (MSE), Root Mean Square Error (RMSE) and Coefficient of Determination (COD) [208, 213].

$$MAE = \frac{1}{n}\sum_{i=1}^{n}|y_i - \hat{y}_i| \tag{3}$$

$$MSE = \frac{1}{n}\sum_{i=1}^{n}(y_i - \hat{y}_i)^2 \tag{4}$$

$$RMSE = \sqrt{MSE} = \sqrt{\frac{1}{n}\sum_{i=1}^{n}(y_i - \hat{y}_i)^2} \tag{5}$$

$$COD = R^2 = 1 - \frac{\sum (y_i - \hat{y}_i)^2}{\sum (y_i - \bar{y})^2} \tag{6}$$

where n is the number of observations, $\bar{y}$ is the mean value of the observations, y and $\hat{y}$ are the actual and predicted values of the PV power, respectively.

In the regression analysis, the COD is used to present how close the prediction model output is compared to the observed data and it results in values between zero and 1. To evaluate the overfitting of the prediction model, the COD requires the other indicators alongside it. In the evaluating process, the COD should be closer to 1 and the other indicators closer to zero [208].

3. Results and discussion

In this section, the performance results of the MLR and ANN model are presented. The training data was collected from the PV installation between September 2021 and March 2022. In addition to the performance indicators, a representative day in April was selected and the prediction was computed and compared to the actual power output of the system.

3.1 Correlation coefficient analysis

To evaluate the significance of the individual weather variables to the PV power, a correlation coefficient analysis was conducted. The results of the analysis were used to select the most relevant weather variables for the modelling. The weather variables under the investigation

were the ambient temperature T_a, relative humidity RH, dew point temperature T_d, wind speed WS, atmospheric pressure pat, global horizontal irradiance GHI and global tilted irradiation GTI for both panel arrays in the tilt angle of 7° and 18°. The GTI values were calculated based on the measured GHI, number of a day, latitude and tilt angle of the panels. The PV power output P was recorded per panel and overall system. The correlation coefficients between the weather variables and PV power output are presented in Table 8-1.

Table 8-1: The correlation coefficients

Variable	Correlation with PV power
Ambient temperature	0.27
Relative humidity	-0.39
Dew point temperature	0.01
Wind speed	0.15
Atmospheric pressure	0.11
GHI	0.94
GTI_up	0.94
GTI_down	0.94

The highest correlation was recognized between solar irradiation on the horizontal and tilted surface (GHI and GTI) and the PV power. The coefficient for each solar irradiation variable was 0.94. The second highest significance was shown by the RH followed by the ambient temperature. The impact of the RH was negative, which decreased PV power when the RH increased. This was caused by the increased amount of water vapor particles in the air reducing the solar insolation such as dust. The dew point temperature T_d showed the lowest significance by the value of 0.01 and was excluded from the modelling. The other variables in Table 8-1 were included in the prediction modelling by MLR and ANN.

3.2 Multiple linear regression model performance

To predict the PV power, an MLR model was trained in the MATLAB software environment. The performance indicators presented in Section 2.5 were used to evaluate the accuracy of the model.

First, the regression model was trained with the weather data and the aggregated PV power output of the system. Next, the PV power output data of each micro-inverter was used to predict the output of each panel. The predictions of each panel were summed up to have a prediction of the whole system. The performance of the prediction models generated by the aggregated PV output data and by the individual micro-inverter data was compared.

The overall performance results in Table 8-2 show that the MLR, which was based on the micro-inverter data, showed better performance with 13.86 MAE, 1438 MSE, 37.92 RMSE and 0.938 COD than the model based on the aggregated PV power data with 16.32 MAE, 2160 MSE, 46.48 RMSE and 0.907 COD. The results revealed that a more accurate prediction model was achieved if the micro-inverter data was used first to model each panel output and then summed up to have PV power prediction for the whole system. This method can help to predict more accurately the PV power of the system if all the panels are not positioned equally to the sun during the day, for example, if some shading occurs.

The MLR model based on the micro-inverter data was used to predict the PV power for the representative day in April, shown in Figure 8-3a. This day was not used in the training dataset. Figure 8-3b presents the correlation between the actual and predicted values. In this case, the model was able to perform as follows: 43.4 MAE, 7552 MSE, 86.9 RMSE and 0.91 COD.

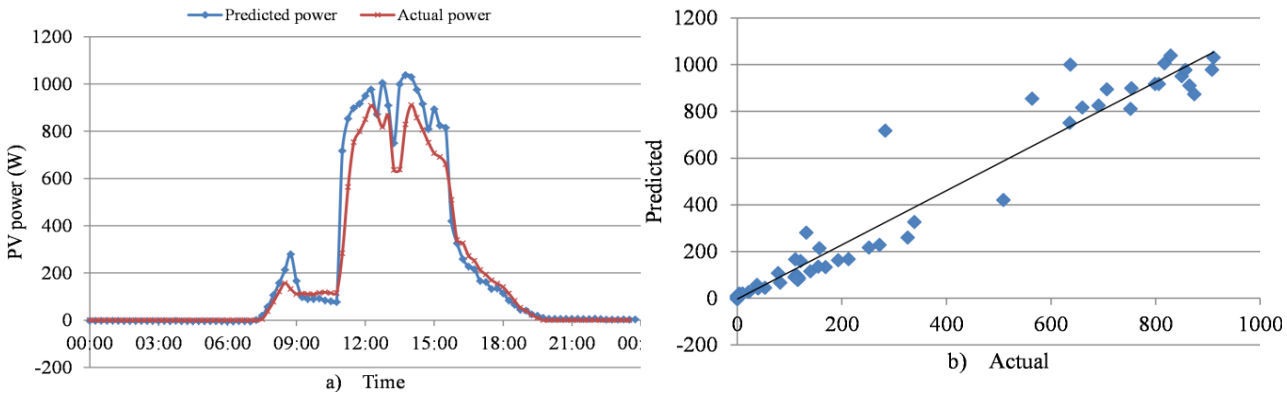

Figure 8-3: *a) The predicted and actual PV power using the micro-inverter based MRL model. b) Actual vs. predicted PV power correlation with the linear trendline from the MRL model.*

3.3 Artificial Neural Network model performance

The same dataset, as for the MLR model, was used to train an ANN model. Again both aggregated and micro-inverter based PV power data were used to train the model to see if the micro-inverter data can be used to have a more accurate prediction model for the installation.

The overall performance results in Table 8-2 show that the ANN model, which was based on the micro-inverter data, showed again better performance with 9.87 MAE, 930 MSE, 30.497 RMSE and 0.9596 COD than the model based on the aggregated PV power data with 13.34 MAE, 1517 MSE, 38.96 RMSE and 0.935 COD. However, in both cases, the ANN model showed the better overall performance than the MLR models.

The ANN model based on the micro-inverter data was used to predict the PV power for the representative day in April, shown in Figure 8-4a. Figure 8-4b presents the correlation between the actual and predicted values. The model was able to perform as follows: 32.26 MAE, 4632 MSE, 68.06 RMSE and 0.9471 COD.

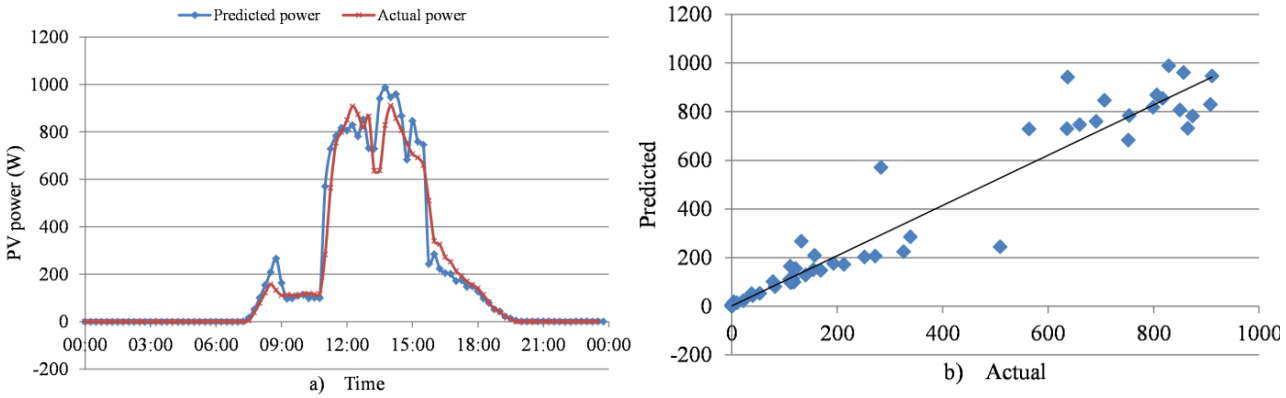

Figure 8-4: *a) The predicted and actual PV power using the micro-inverter based ANN model. b) Actual vs. predicted PV power correlation with the linear trendline from the ANN model.*

Table 8-2: The overall performance comparison of the models based on the different methods and PV data input.

Model		Performance indicator			
		MAE	MSE	RMSE	COD (R^2)
Multiple regression	Overall	16.32	2161	46.485	0.9074
	Micro-inv.	13.86	1438	37.919	0.9376

ANN	Overall	13.34	1517	38.96	0.935
	Micro-inv.	9.87	930	30.497	0.9596

4. Conclusion

In this paper, the PV panel installation using micro-inverter technology was realized in INSA ICUBE Laboratory in Strasbourg to build a PV power prediction model using two different methods: multiple linear regression and artificial neural network. The weather station was used to collect the weather data. The correlation analysis was used to select the most significant weather parameters correlating with the PV power output. The parameters were the ambient temperature, relative humidity, pressure, wind speed and solar irradiation.

In addition to the two different modelling methods, the prediction models were built using two different approaches to collect the PV power output data from the installation. First, the aggregated PV power was used in the modelling process. Next, the PV power data, detected by each individual micro-inverter, was used to model each PV panel output to get a more accurate model of the whole system.

The results showed that the overall performance of the ANN models was better than the MLR models resulting in lower MAE, RMSE and MSE and higher COD. Additionally, the results revealed that building a model of each panel by using the PV power data from the micro-inverters resulted in more accurate prediction models. Due to this, it is recommended to use the micro-inverter technology in the PV installations to facilitate the prediction of the system output power.

For future work, the PV prediction model based on the ANN and micro-inverter data will be enhanced by collecting more data from the installation. The comparison between different models will be extended with other methods, such as Support Vector Machine, Fuzzy prediction and Regression Tree. Additionally, the prediction model will be used in the model predictive control of a hybrid renewable energy system.

Acknowledgements

The authors would like to thank Interreg V Rhin supérieur for their support and funding of this research.

GENERAL CONCLUSION AND PERSPECTIVES

1. Conclusions

To reduce primary energy use and to design more rational energy systems for buildings, deeper and more critical research on the energy efficiency of the available energy technologies is required. The exergy method combines the first and second laws of thermodynamics by defining the quantity and quality of a certain energy amount. The quality aspect can reveal hidden inefficiency of energy systems that cannot be identified by the quantity-based energy analysis alone. Analyzing and optimizing the renewable energy fueled micro-cogeneration and hybrid energy systems by the exergy method have been the main focus of this thesis. Due to this, a comprehensive literature review of the exergy method and hybrid renewable energy systems based on micro-cogeneration was carried out. The review showed that the scientific community does not have a common agreement to apply the exergy method to the hybrid energy systems in the domestic microgrids in different locations due to the dependence of the analysis on the varying reference environment. Selecting the reference temperature has a strong impact on the results of the exergy analysis, and the same reference temperature cannot be applied to different locations at the same time. In this thesis, a method to derive comparable exergy analysis results between different locations was proposed. Based on the literature review on the micro-sized hybrid renewable energy systems, a novel hybrid system for building microgrids was proposed including solar and biomass-based micro-cogeneration systems with energy storage.

To answer the research questions stated in the introduction of this thesis, the exergy method was used to analyze two system components of the hybrid renewable energy system: the PVT collectors and biomass-fueled Stirling engine micro-cogeneration system. The exergy-based design optimization was performed on a single and multi-stage PVT collector (Chapters 2 and 3) in terms of electrical and thermal exergy efficiency. Based on the results, the exergy analysis brought new information on the efficiency and design variables compared to the energy approach. The thermal exergy efficiency was maximized by decreasing the coolant mass flow rate and by increasing the coolant inlet temperature, which are both opposite if compared to maximizing the thermal energy efficiency which led to high mass flow rate and low inlet temperature. As a drawback, the higher operating temperature decreases linearly the electrical efficiency. However, it is more rational to have a higher outlet temperature of the collector than a

high amount of energy at a low temperature. The results showed also that the electrical output of the PVT collector, which maximized the thermal exergy output, was still competitive compared to the PV panel output. The exergy analysis applied to the biomass-fueled ÖkoFEN Stirling engine micro-CHP unit in Chapter 4 revealed a high thermal inefficiency resulting in 7.6% thermal exergy efficiency compared to the energy analysis, which resulted in 98% thermal energy efficiency. Great and costly exergy destruction was caused by using the high-quality biomass fuel to produce low quality heat up to 75°C. The thermal exergy efficiency and relative avoided irreversibility were increased by increasing the inlet temperature of the system. This result highly recommends combining the micro-CHP with heat storage to increase the inlet temperature. Compared to a reference system, the micro-CHP was an improvement and recommended.

In this thesis, the question about the suitable reference temperature in the exergy analysis and comparison of the results between different weather conditions was solved by using a monthly average ambient temperature of each location. This resulted in a fair comparison but still presented the variation of the conditions over a year.

To answer the research questions related to the exergo-economic analysis in the hybrid renewable energy system, the PVT collectors and biomass-fueled micro-CHP system were coupled with heat storage to form a novel hybrid system for buildings. The system aimed to provide 100% renewable energy with fluctuating and controllable energy sources for a residential microgrid. The dynamic energy, exergy and exergo-economic analysis were conducted on the system model under three different climate conditions to evaluate its exergo-economic performance and to define the specific costs of the energy products. Exergo-economics is a more rational costing method than conventional energy-economics because it combines the value of a certain energy quantity with the monetary value. Additionally, it is a suitable costing method for the system which produces different energy products with different exergy content. The hybridization of solar and biomass technologies reduced the specific cost of electricity and offered continuous energy production to support the energy independence of the microgrid. The different weather conditions had an impact on the specific costs of the energy products due to varying solar energy availability and exergy content of the heat products which depends on the ambient temperature. The solar availability reduced the costs and the high ambient temperature reduced the heat exergy. As conclusion, the defined exergo-economic cost of electricity can be

compared with the available grid electricity price to evaluate the economic viability of the system. The specific cost of electricity varied strongly over a year and the yearly average prices were 0.29 €/kWh in Barcelona, 0.41 €/kWh in Strasbourg and 0.4 €/kWh in Tampere.

In the framework of the ACA-MODES project, the complex hybrid energy systems require advanced control methods to operate optimally. The model predictive control (MPC) resulted in the lower operation cost of the experimental solar microgrid than the rule based energy management method. However, this optimal control method requires future forecasts of uncertain variables, such as photovoltaic power production, to optimize the next control signal of the system. In this thesis, the machine learning methods were investigated in Chapter 8 to build a PV power prediction model. The experimental data from the solar microgrid was used to train the models. As a conclusion, the artificial neural network with the data from the PV micro-inverters resulted in the most accurate model.

2. Perspectives

In future work, the hybrid renewable energy system will be further studied in the component and system level.

In terms of the PVT collectors, the model of the multi-stage collector will be developed to present the coolant fluid temperature between the collectors. Additionally, a hybrid solar system combining, for example, the flat plate PVT collector in series with a concentrated PVT collector should be investigated.

In terms of the biomass fueled micro-CHP unit, the laboratory experiment with thermal storage connection will be conducted. Additionally, the component level exergy analysis should be conducted to indicate the place of the highest exergy destruction in the unit.

In terms of the hybrid renewable energy system, the optimization of the system components, such as PVT field and energy storage, should be performed. The deeper analysis of the solar support impact on the economic viability of the fuel-fired micro-cogeneration installation should be conducted. Additionally, the integration of an electric vehicle to the HRES of the residential microgrid with the optimal energy management system and forecast models should be developed. The HRES should be also extended with thermally activated cooling device to enlarge heat use during the summer period and evaluate exergo-economic performance of the

tri-generation system. It would be also interesting to investigate other fuel-fired micro-CHP units, such as organic Rankine cycle, integrated with solar technologies.

The developed ANN model for the PV power prediction will be developed by collecting more data from the experimental set-up and different models will be trained, such as Support Vector Machine, Fuzzy prediction and Regression Tree, to be compared. The prediction model could be developed to predict electricity and heat production of the PVT collector.

3. 1st authored journal publications

Kallio S., Siroux M.; Energy Analysis and Exergy Optimization of Photovoltaic-Thermal Collector. *Energies.* **2020**, *13*, 5106.

Kallio S., Siroux M.; Exergy optimization of a multi-stage solar micro-cogeneration system. *IET Renewable Power Generation.* **2021**.

Kallio S., Siroux M.; Hybrid renewable energy systems based on micro-cogeneration. *Energy Reports.* **2021**, *8*, 762-769.

Kallio S., Siroux M.; Exergy and Exergo-economic analysis of a hybrid renewable energy system under different climate conditions. *Renewable Energy.* **2022**, *194*, 396-414

Kallio S., Siroux M.; Photovoltaic power prediction for solar micro-grid optimal control. *Energy Reports.* Accepté le **19/05/2022**.

4. Conference publications

Kallio S., Siroux M.; Exergo-economics of Hybrid Renewable Energy System. Congrès Société Francaise de Thermique (SFT 2021), 31 Mai – 3 Juin, 2022, Valenciennes, France

Kallio S., Siroux M.: A Review – Home Renewable Energy Management Systems in Smart Grids. 7th International conference on Sustainable and Renewable Energy Engineering (ICSREE2022), Mai 5-7, 2022, Barcelona, Spain.

Sawant P., Braasch C., Koch M., Bürger A., Kallio S.; An energy-economic analysis of real-world hybrid building energy systems. The conference of Carbon Neutral Cities (CISBAT 2021), Septembre 8-10, Lausanne, Switzerland.

Kallio S., Siroux M., Voronca S.; Energy and exergy analysis of a biomass-fuelled micro-CHP unit. 34th International Conference on Efficiency, Cost, Optimization, Simulation and Environmental Impact on Energy Systems (ECOS 2021), 27 Juin – 2 Juillet 2021, Taormina, Italy.

Kallio S., Siroux M.; Multi-objective design optimization of a hybrid renewable energy system.

Congrès Société Francaise de Thermique (SFT 2021), Juin 1-3, 2021, Belfort, France

Kallio S., Siroux M.: A Review – Renewable energy based micro-cogeneration and hybrid energy systems. 6th International conference on Sustainable and Renewable Energy Engineering (ICSREE2021), Mai 5-7, 2021, Strasbourg, France.

Kallio S., Siroux M.; Energy and exergy analysis of a photovoltaic-thermal system under two different climate conditions. 33rd International Conference on Efficiency, Cost, Optimization, Simulation and Environmental Impact of Energy Systems (ECOS 2020), Juin 29-Juillet 3, 2020, Osaka, Japan.

References

[1] TRION-climate e.V. RAPPORT TRINATIONAL CLIMAT-ENERGIE. 2019; 1–22.

[2] Rousselot M, Da Rocha FP. *Energy efficiency trends in buildings in the EU*, https://www.odyssee-mure.eu/publications/other/odex-indicators-database-definition.pdf (2021, accessed 4 March 2022).

[3] Torio H, Schmidt D. *'Exergy Assessment Guidebook for the Built Environment' Low Exergy Systems for High-Performance Buildings and Communities Operating Agent for the ECBCS Executive Committee Support Services Unit, on behalf of the Contracting Parties of the Internatio-nal E*, www.ecbcs.org (2011, accessed 24 November 2020).

[4] Rosen MA. Exergy and economics: Is exergy profitable? *Exergy, An Int J* 2002; 2: 218–220.

[5] Eurostat. Eurostat. *Online publication, eurostat*, https://ec.europa.eu/eurostat/statistics-explained/index.php?title=Energy_efficiency_statistics#Primary_energy_consumption_and_distance_to_2020_and_2030_targets (2020, accessed 19 January 2022).

[6] Simon F. Energy consumption continues to rise in Europe: Eurostat. *Euractiv*, https://www.euractiv.com/section/energy/news/energy-consumption-continues-to-rise-in-europe-eurostat/ (accessed 6 November 2020).

[7] Eurostat. Energy statistics - an overview, https://ec.europa.eu/eurostat/statistics-explained/index.php?title=Energy_statistics_-_an_overview (accessed 4 March 2022).

[8] H. F. The path of the smart grid. *IEEE power energy mag- azine* 2010; 8: 18–28.

[9] Balakrishnan R, Geetha V. Review on home energy management system. *Mater Today Proc* 2021; 47: 144–150.

[10] Zia MF, Elbouchikhi E, Benbouzid M. Microgrids energy management systems: A critical review on methods, solutions, and prospects. *Applied Energy* 2018; 222: 1033–1055.

[11] Hatziargyriou N. *Microgrids: Architectures and Control*. 2014. Epub ahead of print 2014. DOI: 10.1002/9781118720677.

[12] Padinger R, Aigenbauer S, Schmidl C. Best practise report on decentralized biomass fired CHP plants and status of biomass fired small-and micro scale CHP technologies. *IEA Bioenergy*; 32.

[13] Martinez S, Michaux G, Salagnac P, et al. Micro-combined heat and power systems (micro-CHP) based on renewable energy sources. *Energy Convers Manag* 2017; 154: 262–285.

[14] Pereira JS, Ribeiro JB, Mendes R, et al. ORC based micro-cogeneration systems for residential application - A state of the art review and current challenges. *Renewable and Sustainable Energy Reviews* 2018; 92: 728–743.

[15] Parliament TE. *DIRECTIVE 2004/8/EC of the European Parliament and of the Council of 11 February 2004 on the promotion of cogeneration based on a useful heat demand in the internal energy market and amending Directive 92/42/EEC*. Official Journal of the European Union, 2004.

[16] Dong L, Liu H, Riffat S. Development of small-scale and micro-scale biomass-fuelled CHP systems - A literature review. *Applied Thermal Engineering* 2009; 29: 2119–2126.

[17] Maghanki MM, Ghobadian B, Najafi G, et al. Micro combined heat and power (MCHP) technologies and applications. *Renew Sustain Energy Rev* 2013; 28: 510–524.

[18] Angrisani G, Roselli C, Sasso M. Distributed microtrigeneration systems. *Progress in Energy and Combustion Science* 2012; 38: 502–521.

[19] Roselli C, Sasso M, Sibilio S, et al. Experimental analysis of microcogenerators based on different prime movers. *Energy Build* 2011; 43: 796–804.
[20] Murugan S, Horák B. A review of micro combined heat and power systems for residential applications. *Renewable and Sustainable Energy Reviews* 2016; 64: 144–162.
[21] Jia Y, Alva G, Fang G. Development and applications of photovoltaic–thermal systems: A review. *Renew Sustain Energy Rev* 2019; 102: 249–265.
[22] Kannan N, Vakeesan D. Solar energy for future world: - A review. *Renew Sustain Energy Rev* 2016; 62: 1092–1105.
[23] Solar GIS, Global Horizontal Irradiation (GHI), https://solargis.com/maps-and-gis-data/download/world (accessed 28 February 2022).
[24] Wang J, Han Z, Guan Z. Hybrid solar-assisted combined cooling, heating, and power systems: A review. *Renewable and Sustainable Energy Reviews* 2020; 133: 110256.
[25] Herez A, El Hage H, Lemenand T, et al. Review on photovoltaic/thermal hybrid solar collectors: Classifications, applications and new systems. *Sol Energy* 2020; 207: 1321–1347.
[26] Kalogirou SA. *Solar Energy Engineering*. Elsevier, 2009.
[27] Ferreira AC, Silva J, Teixeira S, et al. Assessment of the Stirling engine performance comparing two renewable energy sources: Solar energy and biomass. *Renew Energy* 2020; 154: 581–597.
[28] Ferreira AC, Nunes ML, Teixeira JCF, et al. Thermodynamic and economic optimization of a solar-powered Stirling engine for micro-cogeneration purposes. *Energy* 2016; 111: 1–17.
[29] Farzanehnia A, Sardarabadi M. Exergy in Photovoltaic/Thermal Nanofluid-Based Collector Systems. *Exergy Its Appl - Towar Green Energy Prod Sustain Environ*. Epub ahead of print 2019. DOI: 10.5772/intechopen.85431.
[30] Tamayo Vera J, Laukkanen T, Sirén K. Performance evaluation and multi-objective optimization of hybrid photovoltaic-thermal collectors. *Sol Energy* 2014; 102: 223–233.
[31] Joshi SS, Dhoble AS. Photovoltaic -Thermal systems (PVT): Technology review and future trends. *Renewable and Sustainable Energy Reviews* 2018; 92: 848–882.
[32] Aste N, Leonforte F, Del Pero C. Design, modeling and performance monitoring of a photovoltaic-thermal (PVT) water collector. *Sol Energy* 2015; 112: 85–99.
[33] Wegener M, Malmquist A, Isalgué A, et al. Biomass-fired combined cooling, heating and power for small scale applications – A review. *Renewable and Sustainable Energy Reviews* 2018; 96: 392–410.
[34] Zabalaga PJ, Cardozo E, Campero LAC, et al. Performance analysis of a stirling engine hybrid power system. *Energies*; 13. Epub ahead of print 2020. DOI: 10.3390/en13040980.
[35] Rank., https://www.rank-orc.com/rank-micro-2/ (accessed 2 November 2020).
[36] Liu M, Shi Y, Fang F. Combined cooling, heating and power systems: A survey. *Renewable and Sustainable Energy Reviews* 2014; 35: 1–22.
[37] Alanne K, Saari A. Sustainable small-scale CHP technologies for buildings: The basis for multi-perspective decision-making. *Renewable and Sustainable Energy Reviews* 2004; 8: 401–431.
[38] Brett DJL, Brandon NP, Hawkes AD, et al. Fuel cell systems for small and micro combined heat and power (CHP) applications. In: *Small and Micro Combined Heat and Power (CHP) Systems: Advanced Design, Performance, Materials and Applications*. Elsevier Inc., 2011, pp. 233–261.

[39] Zhu S, Yu G, Jongmin O, et al. Modeling and experimental investigation of a free-piston Stirling engine-based micro-combined heat and power system. *Appl Energy* 2018; 226: 522–533.
[40] Mascuch J, Novotny V, Spale J, et al. Experience from set-up and pilot operation of an in-house developed biomass-fired ORC microcogeneration unit. *Renew Energy* 2021; 165: 251–260.
[41] Ellamla HR, Staffell I, Bujlo P, et al. Current status of fuel cell based combined heat and power systems for residential sector. *Journal of Power Sources* 2015; 293: 312–328.
[42] Perna A, Minutillo M. Residential cogeneration and trigeneration with fuel cells. In: *Current Trends and Future Developments on (Bio-) Membranes*. Elsevier, 2020, pp. 197–239.
[43] Di Florio G, Macchi EG, Mongibello L, et al. Comparative life cycle assessment of two different SOFC-based cogeneration systems with thermal energy storage integrated into a single-family house nanogrid. *Appl Energy* 2021; 285: 116378.
[44] Farhad S, Hamdullahpur F, Yoo Y. Performance evaluation of different configurations of biogas-fuelled SOFC micro-CHP systems for residential applications. *Int J Hydrogen Energy* 2010; 35: 3758–3768.
[45] Chang H, Wan Z, Zheng Y, et al. Energy analysis of a hybrid PEMFC–solar energy residential micro-CCHP system combined with an organic Rankine cycle and vapor compression cycle. *Energy Convers Manag* 2017; 142: 374–384.
[46] Calise F. Design of a hybrid polygeneration system with solar collectors and a Solid Oxide Fuel Cell: Dynamic simulation and economic assessment. *Int J Hydrogen Energy* 2011; 36: 6128–6150.
[47] Hedström L, Wallmark C, Alvfors P, et al. Description and modelling of the solar-hydrogen-biogas-fuel cell system in GlashusEtt. *J Power Sources* 2004; 131: 340–350.
[48] González A, Riba JR, Puig R, et al. Review of micro- and small-scale technologies to produce electricity and heat from Mediterranean forests' wood chips. *Renewable and Sustainable Energy Reviews* 2015; 43: 143–155.
[49] Romero Rodríguez L, Salmerón Lissén JM, Sánchez Ramos J, et al. Analysis of the economic feasibility and reduction of a building's energy consumption and emissions when integrating hybrid solar thermal/PV/micro-CHP systems. *Appl Energy* 2016; 165: 828–838.
[50] Pearce JM. Expanding photovoltaic penetration with residential distributed generation from hybrid solar photovoltaic and combined heat and power systems. *Energy* 2009; 34: 1947–1954.
[51] Mundada AS, Shah KK, Pearce JM. Levelized cost of electricity for solar photovoltaic, battery and cogen hybrid systems. *Renewable and Sustainable Energy Reviews* 2016; 57: 692–703.
[52] Awad A, Bazan P, German R. Optimized Operation of PV/T and Micro-CHP Hybrid Power Systems. *Technol Econ Smart Grids Sustain Energy*; 1. Epub ahead of print 2016. DOI: 10.1007/s40866-016-0004-3.
[53] ÖkoFEN. Pellematic Condens_e, https://www.oekofen.com/en-gb/pellematic-condens_e/ (accessed 25 January 2021).
[54] Auñón-Hidalgo JA, Sidrach-de-Cardona M, Auñón-Rodríguez F. Performance and CO2 emissions assessment of a novel combined solar photovoltaic and thermal, with a Stirling engine micro-CHP system for domestic environments. *Energy Convers Manag* 2021; 230:

113793.
[55] Kotowicz J, Uchman W. Analysis of the integrated energy system in residential scale: Photovoltaics, micro-cogeneration and electrical energy storage. *Energy* 2021; 227: 120469.
[56] Wang K, Pantaleo AM, Oyewunmi OA, et al. Flexible PVT-ORC hybrid solar-biomass cogeneration systems: the case study of the university sports centre in Bari, Italy. 2019, pp. 1–9.
[57] Settino J, Morrone P, Algieri A, et al. Integration of an Organic Rankine Cycle and a Photovoltaic Unit for Micro-Scale CHP Applications in the Residential Sector. In: *Energy Procedia*. Elsevier Ltd, 2017, pp. 597–604.
[58] Facão J, Palmero-Marrero A, Oliveira AC. Analysis of a solar assisted micro-cogeneration ORC system. *Int J Low-Carbon Technol* 2008; 3: 254–264.
[59] Wall G. Exergy. *Encycl Energy* 2004; 593–606.
[60] Sciubba E, Wall G. A brief Commented History of Exergy From the Beginnings to 2004. *Int J Thermodyn* 2007; 10: 1–26.
[61] Gibbs JW. Graphical methods in the thermodynamics of fluids. *Trans Connect Acad* 1873; 1: 309–342.
[62] Ibrahim Dincer MAR. *Exergy: Energy, Environment and Sustainable Development*. Elsevier Ltd, https://books.google.com/books?hl=en&lr=&id=FrUolHxhGVYC&oi=fnd&pg=PP1&dq=%5B1%5D+Ibrahim+Dincer,+Marc+Rosen,+Exergy:+energy,+environment+and+sustainable+development,+Newnes,+2012.&ots=9Imjb34j5b&sig=cXh5HJXc_s3eGFXdzv4iXrLEiDs#v=onepage&q=%5B1%5D Ibrah (2013, accessed 24 January 2017).
[63] Moran MJ, Sciubba E. Exergy Analysis: Principles and Practice. *J Eng Gas Turbines Power* 1994; 116: 285.
[64] Evola G, Costanzo V, Marletta L. Exergy analysis of energy systems in buildings. *Buildings*; 8. Epub ahead of print 2018. DOI: 10.3390/buildings8120180.
[65] Tsatsaronis G. Definitions and nomenclature in exergy analysis and exergoeconomics. *Energy* 2007; 32: 249–253.
[66] Rosen MA, Dincer I. Effect of varying dead-state properties on energy and exergy analyses of thermal systems. *Int J Therm Sci* 2004; 43: 121–133.
[67] Chow TT, Pei G, Fong KF, et al. Energy and exergy analysis of photovoltaic-thermal collector with and without glass cover. *Appl Energy*. Epub ahead of print 2009. DOI: 10.1016/j.apenergy.2008.04.016.
[68] Tiwari A, Dubey S, Sandhu GS, et al. Exergy analysis of integrated photovoltaic thermal solar water heater under constant flow rate and constant collection temperature modes. *Appl Energy* 2009; 86: 2592–2597.
[69] Gonçalves P, Gaspar AR, Da Silva MG. Comparative energy and exergy performance of heating options in buildings under different climatic conditions. *Energy Build* 2013; 61: 288–297.
[70] Pons M, Neumann RJ Von, Cedex O. On the Reference State for Exergy when Ambient Temperature Fluctuates *. 2009; 12: 113–121.
[71] Fujisawa T, Tani T. Annual exergy evaluation on photovoltaic-thermal hybrid collector. *Sol Energy Mater Sol Cells* 1997; 47: 135–148.
[72] Evola G, Marletta L. Exergy and thermoeconomic optimization of a water-cooled glazed hybrid photovoltaic/thermal (PVT) collector. *Sol Energy* 2014; 107: 12–25.

[73] Ibrahim Dincer MAR. *Exergy: Energy, Environment and Sustainable Development*. Second edi. Elsevier Ltd, https://books.google.ca/books?hl=en&lr=&id=FrUolHxhGVYC&oi=fnd&pg=PP1&ots=9Kgkg26l93&sig=gWFjnVM8kMgzMsaJx9R2I-YZHrU#v=onepage&q&f=false (1999).
[74] Blanco HT. *Comparison and optimization of building energy supply systems through exergy analysis and its perspectives*, http://verlag.fraunhofer.de (2012, accessed 25 January 2022).
[75] Jeter SM. Maximum conversion efficiency for the utilization of direct solar radiation. *Sol Energy* 1981; 26: 231–236.
[76] Petela R. Exergy of undiluted thermal radiation. *Sol Energy* 2003; 74: 469–488.
[77] Bejan A. *Advanced Engineering Thermodynamics, 4th edition*. John Wiley & Sons, 2016.
[78] Pons M. Exergy analysis of solar collectors, from incident radiation to dissipation. *Renew Energy* 2012; 47: 194–202.
[79] Ertesvåg IS. Exergetic comparison of efficiency indicators for combined heat and power (CHP). *Energy* 2007; 32: 2038–2050.
[80] Wall G. *EXERGY-A USEFUL CONCEPT WITHIN RESOURCE ACCOUNTING 1*, http://exergy.se.
[81] Andlauer B. *Optimisation systémique de micro-cogénérateurs intégrés au bâtiment*, https://pastel.archives-ouvertes.fr/pastel-01073341.
[82] Goran Wall MG. Life Cycle Exergy Analysis of Solar Energy Systems. *J Fundam Renew Energy Appl*; 05. Epub ahead of print 2014. DOI: 10.4172/2090-4541.1000146.
[83] Kallio S, Siroux M. Energy Analysis and Exergy Optimization of Photovoltaic-Thermal Collector. *Energies* 2020; 13: 5106.
[84] Naked Energy Virtu PVT, https://venfeld.com/wp-content/uploads/2020/10/VirtuPVTSpecification.pdf (accessed 2 November 2020).
[85] Tsatsaronis G. Thermoeconomic analysis and optimization of energy systems. *Prog Energy Combust Sci* 1993; 19: 227–257.
[86] Sciubba E. Exergo-economics: Thermodynamic foundation for a more rational resource use. *Int J Energy Res* 2005; 29: 613–636.
[87] Valdimarsson P. BASIC CONCEPTS OF THERMOECONOMICS.
[88] Rosen MA. A Concise Review of Kernel Methods. In: *3rd Int. Conf. Ener. & Envir. (IASME/WSEAS)*. 2008, pp. 136–144.
[89] Tsatsaronis G. Thermoeconomic analysis and optimization of energy systems. *Prog Energy Combust Sci* 1993; 19: 227–257.
[90] Rosen MA, Dincer I. Exergy–cost–energy–mass analysis of thermal systems and processes. *Energy Convers Manag* 2003; 44: 1633–1651.
[91] Lazzaretto A, Tsatsaronis G. SPECO: A systematic and general methodology for calculating efficiencies and costs in thermal systems. *Energy* 2006; 31: 1257–1289.
[92] Wang J, Li M, Ren F, et al. Modified exergoeconomic analysis method based on energy level with reliability consideration: Cost allocations in a biomass trigeneration system. *Renew Energy* 2018; 123: 104–116.
[93] Sciubba E. Beyond thermoeconomics? The concept of Extended Exergy Accounting and its application to the analysis and design of thermal systems. *Exergy, An Int J* 2001; 1: 68–84.
[94] Beausoleil-Morrison I. *An Experimental and Simulation-Based Investigation of the Performance of Small-Scale Fuel Cell and Combustion-Based Cogeneration Devices*

Serving Residential Buildings Energy Conservation in Buildings and, www.ecbcs.org. (2008).

[95] Bouvenot JB, Latour B, Siroux M, et al. Dynamic model based on experimental investigations of a wood pellet steam engine micro CHP for building energy simulation. *Appl Therm Eng* 2014; 73: 1041–1054.

[96] Bouvenot JB, Andlauer B, Stabat P, et al. Gas Stirling engine μcHP boiler experimental data driven model for building energy simulation. *Energy Build* 2014; 84: 117–131.

[97] Uchman W, Kotowicz J, Remiorz L. An experimental data-driven model of a micro-cogeneration installation for time-domain simulation and system analysis. *Energies* 2020; 13: 2759.

[98] González-Pino I, Pérez-Iribarren E, Campos-Celador A, et al. Modelling and experimental characterization of a Stirling engine-based domestic micro-CHP device. *Energy Convers Manag* 2020; 225: 113429.

[99] Martinez S, Michaux G, Salagnac P, et al. Numerical Investigation of Energy Potential and Performance of a Residential Building- Integrated Solar - Chp System. 2018, pp. 1–20.

[100] Brottier L, Bennacer R. Thermal performance analysis of 28 PVT solar domestic hot water installations in Western Europe. *Renew Energy* 2020; 160: 196–210.

[101] Barbu M, Darie G, Siroux M. Analysis of a residential photovoltaic-thermal (PVT) system in two similar climate conditions. *Energies* 2019; 12: 1–18.

[102] Barbu M, Siroux M, Darie G. Numerical model and parametric analysis of a liquid based hybrid photovoltaic thermal (PVT) collector. *Energy Reports*. Epub ahead of print 4 August 2021. DOI: 10.1016/J.EGYR.2021.07.058.

[103] da Silva RM, Fernandes JLM. Hybrid photovoltaic/thermal (PV/T) solar systems simulation with Simulink/Matlab. *Sol Energy* 2010; 84: 1985–1996.

[104] Zhou C, Liang R, Zhang J. Optimization design method and experimental validation of a solar pvt cogeneration system based on building energy demand. *Energies*; 10. Epub ahead of print 2017. DOI: 10.3390/en10091281.

[105] Wang K, Pantaleo AM, Herrando M, et al. Spectral-splitting hybrid PV-thermal (PVT) systems for combined heat and power provision to dairy farms. *Renew Energy* 2020; 159: 1047–1065.

[106] Herrando M, Ramos A, Freeman J, et al. Technoeconomic modelling and optimisation of solar combined heat and power systems based on flat-box PVT collectors for domestic applications. *Energy Convers Manag* 2018; 175: 67–85.

[107] Chow TT. Performance analysis of photovoltaic-thermal collector by explicit dynamic model. *Sol Energy* 2003; 75: 143–152.

[108] Herez A, El Hage H, Lemenand T, et al. Parabolic trough photovoltaic/thermal hybrid system: Thermal modeling and parametric analysis. *Renew Energy* 2021; 165: 224–236.

[109] Gonçalves P, Angrisani G, Roselli C, et al. Energy and exergy-based modeling and evaluation of a micro-combined heat and power unit for residential applications. In: *3 Microgen*. 2013.

[110] Taie Z, West B, Szybist J, et al. Detailed thermodynamic investigation of an ICE-driven, natural gas-fueled, 1 kWe micro-CHP generator. *Energy Convers Manag* 2018; 166: 663–673.

[111] Alomar OR, Ali OM. Energy and exergy analysis of hybrid photovoltaic thermal solar system under climatic condition of North Iraq. *Case Stud Therm Eng* 2021; 28: 101429.

[112] Kallio S, Siroux M. Exergy optimization of a multi-stage solar micro-cogeneration system. *IET Renew Power Gener*. Epub ahead of print 2021. DOI: 10.1049/RPG2.12372.
[113] Abdul-Ganiyu S, Quansah DA, Ramde EW, et al. Techno-economic analysis of solar photovoltaic (PV) and solar photovoltaic thermal (PVT) systems using exergy analysis. *Sustain Energy Technol Assessments* 2021; 47: 101520.
[114] Mahian O, Mirzaie MR, Kasaeian A, et al. Exergy analysis in combined heat and power systems: A review. *Energy Conversion and Management* 2020; 226: 113467.
[115] Wang J, Li S, Zhang G, et al. Performance investigation of a solar-assisted hybrid combined cooling, heating and power system based on energy, exergy, exergo-economic and exergo-environmental analyses. *Energy Convers Manag* 2019; 196: 227–241.
[116] Wang J, Chen Y, Lior N. Exergo-economic analysis method and optimization of a novel photovoltaic/thermal solar-assisted hybrid combined cooling, heating and power system. *Energy Convers Manag*; 199. Epub ahead of print 1 November 2019. DOI: 10.1016/j.enconman.2019.111945.
[117] Chen Y, Xu J, Zhao D, et al. Exergo-economic assessment and sensitivity analysis of a solar-driven combined cooling, heating and power system with organic Rankine cycle and absorption heat pump. *Energy* 2021; 230: 120717.
[118] Calise F, Dentice d'Accadia M, Piacentino A. Exergetic and exergoeconomic analysis of a renewable polygeneration system and viability study for small isolated communities. *Energy* 2015; 92: 290–307.
[119] Zhang X, Zhao X, Smith S, et al. Review of R&D progress and practical application of the solar photovoltaic/thermal (PV/T) technologies. *Renew Sustain Energy Rev* 2012; 16: 599–617.
[120] Lee JH, Hwang SG, Lee GH. Efficiency improvement of a photovoltaic thermal (PVT) system using nanofluids. *Energies* 2019; 12: 491.
[121] Han X, Chen X, Wang Q, et al. Investigation of CoSO4-based Ag nanofluids as spectral beam splitters for hybrid PV/T applications. *Sol Energy* 2019; 177: 387–394.
[122] Walshe J, Carron PM, McLoughlin C, et al. Nanofluid Development Using Silver Nanoparticles and Organic-Luminescent Molecules for Solar-Thermal and Hybrid Photovoltaic-Thermal Applications. *Nanomaterials* 2020; 10: 1201.
[123] Yazdanpanahi J, Sarhaddi F, Mahdavi Adeli M. Experimental investigation of exergy efficiency of a solar photovoltaic thermal (PVT) water collector based on exergy losses. *Sol Energy* 2015; 118: 197–208.
[124] Feidt M. Two Examples of Exergy Optimization Regarding the 'Thermo-Frigopump' and Combined Heat and Power Systems Two Examples of Exergy Optimization Regarding the 'Thermo-Frigopump' and Com-bined Heat and Power Systems Two Examples of Exergy Optimization Regarding the 'Thermo-Frigopump' and Combined Heat and Power Systems. *Entropy, MDPI* 2013; 15: 544–558.
[125] Feidt M, Costea M. Energy and Exergy Analysis and Optimization of Combined Heat and Power Systems. Comparison of Various Systems. *Energies* 2012; 5: 3701–3722.
[126] Calise F, Figaj R, Vanoli L. Experimental and Numerical Analyses of a Flat Plate Photovoltaic/Thermal Solar Collector. *Energies* 2017; 10: 491.
[127] Bhattarai S, Oh JH, Euh SH, et al. Simulation and model validation of sheet and tube type photovoltaic thermal solar system and conventional solar collecting system in transient states. *Sol Energy Mater Sol Cells* 2012; 103: 184–193.
[128] Dubey S, Tiwari GN. Analysis of PV/T flat plate water collectors connected in series. *Sol*

Energy 2009; 83: 1485–1498.
[129] Abdul-Ganiyu S, Quansah DA, Ramde EW, et al. Investigation of solar photovoltaic-thermal (PVT) and solar photovoltaic (PV) performance: A case study in Ghana. *Energies* 2020; 13: 2701.
[130] Tamayo Vera J, Laukkanen T, Sirén K. Multi-objective optimization of hybrid photovoltaic-thermal collectors integrated in a DHW heating system. *Energy Build* 2014; 74: 78–90.
[131] Ouhsiane L, Siroux M, El Ganaoui M, et al. Multi-Objective Optimization of Hybrid PVT Solar Panels. *Proc Conf Ind Commer Use Energy, ICUE* 2019; 2018-Octob: 2–7.
[132] Conti P, Schito E, Testi D. Cost-benefit analysis of hybrid photovoltaic/thermal collectors in a nearly zero-energy building. *Energies*; 12. Epub ahead of print 2019. DOI: 10.3390/en12081582.
[133] Sobhnamayan F, Sarhaddi F, Alavi MA, et al. Optimization of a solar photovoltaic thermal (PV/T) water collector based on exergy concept. *Renew Energy* 2014; 68: 356–365.
[134] Wohlfeil A. CARNOT Toolbox. FH Aachen. *CARNOT Toolbox*, https://fh-aachen.sciebo.de/index.php/s/0hxub0iIJrui3ED (2019, accessed 14 December 2020).
[135] McAdams WH. *Heat transmission*. 3rd editio. New York: McGraw-Hill, 1954.
[136] Guarracino I, Mellor A, Ekins-Daukes NJ, et al. Dynamic coupled thermal-and-electrical modelling of sheet-and-tube hybrid photovoltaic/thermal (PVT) collectors. *Appl Therm Eng* 2016; 101: 778–795.
[137] Touafek K, Khelifa A, Adouane M. Theoretical and experimental study of sheet and tubes hybrid PVT collector. *Energy Convers Manag* 2014; 80: 71–77.
[138] Hollands KGT, Unny TE, Raithby GD, et al. Free Convective Heat Transfer Across Inclined Air Layers. *Am Soc Mech Eng* 1975; 189–193.
[139] Incropera F. *Fundamentals of heat and mass transfer*. John Wiley and Sons, 2011.
[140] Deb K. *Multi-Objective Optimization using Evolutionary Algorithms*. Chichester, England: John Wiley and Sons, 2001.
[141] Ilmatieteen laitos. Kuukausitilastot - Ilmatieteen laitos, https://www.ilmatieteenlaitos.fi/kuukausitilastot (accessed 12 August 2020).
[142] Prevision-meteo.ch. Relevés mensuels de Strasbourg pour l'année en cours, https://www.prevision-meteo.ch/climat/mensuel/strasbourg (accessed 12 August 2020).
[143] Doroudchi E, Alanne K, Okur Ö, et al. Approaching net zero energy housing through integrated EV. *Sustain Cities Soc* 2018; 38: 534–542.
[144] Khelifa A, Touafek K, Moussa H Ben. Approach for the modelling of hybrid photovoltaic–thermal solar collector. *IET Renew Power Gener* 2015; 9: 207–217.
[145] Sahota L, Tiwari GN. Review on series connected photovoltaic thermal (PVT) systems: Analytical and experimental studies. *Sol Energy* 2017; 150: 96–127.
[146] Liang R, Zhou C, Pan Q, et al. Performance evaluation of sheet-and-tube hybrid photovoltaic/thermal (PVT) collectors connected in series. *Procedia Eng* 2017; 205: 461–468.
[147] Tiwari GN, Meraj M, Khan ME. Exergy analysis of N-photovoltaic thermal-compound parabolic concentrator (N-PVT-CPC) collector for constant collection temperature for vapor absorption refrigeration (VAR) system. *Sol Energy* 2018; 173: 1032–1042.
[148] Giwa A, Yusuf A, Dindi A, et al. Polygeneration in desalination by photovoltaic thermal systems: A comprehensive review. *Renewable and Sustainable Energy Reviews* 2020;

130: 109946.
[149] Anand B, Shankar R, Murugavelh S, et al. A review on solar photovoltaic thermal integrated desalination technologies. *Renew Sustain Energy Rev* 2021; 141: 110787.
[150] Ma T, Li M, Kazemian A. Photovoltaic thermal module and solar thermal collector connected in series to produce electricity and high-grade heat simultaneously. *Appl Energy* 2020; 261: 114380.
[151] Kazemian A, Parcheforosh A, Salari A, et al. Optimization of a novel photovoltaic thermal module in series with a solar collector using Taguchi based grey relational analysis. *Sol Energy* 2021; 215: 492–507.
[152] Sarhaddi F. Exergy analysis of a weir-type cascade solar still connected to PV/T collectors. *IET Renew Power Gener* 2018; 12: 1336–1344.
[153] Eborx. European Solar Irradiation, http://www.eborx.com/download/en/data/European-Solar-Irradiation-kWh-m2.pdf.
[154] Fan W, Kokogiannakis G, Ma Z. A multi-objective design optimisation strategy for hybrid photovoltaic thermal collector (PVT)-solar air heater (SAH) systems with fins. *Sol Energy*. Epub ahead of print 2018. DOI: 10.1016/j.solener.2018.02.014.
[155] Alanne K, Söderholm N, Siŕen K. Implementation and validation of combustion engine micro-cogeneration routine for the simulation program IDA-ICE. *IBPSA 2009 - Int Build Perform Simul Assoc 2009* 2009; 33–40.
[156] Cheekatamarla P, Abu-Heiba A. A Comprehensive Review and Qualitative Analysis of Micro-Combined Heat and Power Modeling Approaches. *Energies* 2020; 13: 3581.
[157] Lombardi K, Ugursal VI, Beausoleil-Morrison I. Proposed improvements to a model for characterizing the electrical and thermal energy performance of Stirling engine micro-cogeneration devices based upon experimental observations. *Appl Energy* 2010; 87: 3271–3282.
[158] Balli O, Ekici S, Karakoc HT. Achieving a more efficient and greener combined heat and power system driven by a micro gas turbine engine: Issues, opportunities, and benefits in the presence of thermodynamic perspective. *Int J Energy Res* 2021; er.6398.
[159] Gong M, Wall G. Exergy Analysis of the Supply of Energy and Material Resources in the Swedish Society. *Energies* 2016; 9: 707.
[160] Energy Education, University of Calgarus, https://energyeducation.ca/encyclopedia/Nuclear_power_plant (accessed 22 January 2021).
[161] Bajpai P, Dash V. Hybrid renewable energy systems for power generation in stand-alone applications: A review. *Renewable and Sustainable Energy Reviews* 2012; 16: 2926–2939.
[162] Shivarama Krishna K, Sathish Kumar K. A review on hybrid renewable energy systems. *Renewable and Sustainable Energy Reviews* 2015; 52: 907–916.
[163] Gu W, Wu Z, Bo R, et al. Modeling, planning and optimal energy management of combined cooling, heating and power microgrid: A review. *Int J Electr Power Energy Syst* 2014; 54: 26–37.
[164] Calise F, Dentice d'Accadia M, Figaj RD, et al. A novel solar-assisted heat pump driven by photovoltaic/thermal collectors: Dynamic simulation and thermoeconomic optimization. *Energy* 2016; 95: 346–366.
[165] Buonomano A, Calise F, Cappiello FL, et al. Dynamic analysis of the integration of electric vehicles in efficient buildings fed by renewables. *Appl Energy* 2019; 245: 31–50.
[166] European Comission. Energy performance of buildings directive,

https://ec.europa.eu/energy/topics/energy-efficiency/energy-efficient-buildings/energy-performance-buildings-directive_en.
[167] EU Building Factsheets, https://ec.europa.eu/energy/eu-buildings-factsheets_en.
[168] Sadineni SB, Madala S, Boehm RF. Passive building energy savings: A review of building envelope components. *Renewable and Sustainable Energy Reviews*; 15. Epub ahead of print 2011. DOI: 10.1016/j.rser.2011.07.014.
[169] Palomba V, Borri E, Charalampidis A, et al. Implementation of a solar-biomass system for multi-family houses: Towards 100% renewable energy utilization. *Renew Energy* 2020; 166: 190–209.
[170] European Comission. European Comissions, Energy Efficiency Directive 2012/27/EU, https://eur-lex.europa.eu/legal-content/EN/TXT/PDF/?uri=CELEX:32012L0027&from=EN.
[171] Figaj R. Performance assessment of a renewable micro-scale trigeneration system based on biomass steam cycle, wind turbine, photovoltaic field. *Renew Energy* 2021; 177: 193–208.
[172] Kallio S, Siroux M. Hybrid renewable energy systems based on micro-cogeneration. *Energy Reports* 2022; 8: 762–769.
[173] Mouaky A, Rachek A. Energetic, exergetic and exergeoeconomic assessment of a hybrid solar/biomass poylgeneration system: A case study of a rural community in a semi-arid climate. *Renew Energy* 2020; 158: 280–296.
[174] Hafner B, Plettner J, Wemhöner C, et al. *CARNOT Blockset Version 1.0*. 1999.
[175] Equa. IDA Indoor Climate and Energy, https://www.equa.se/en/ida-ice.
[176] Jordan U, Vajen K. Influence of the DHW profile on the Fractional Energy\rSavings: A Case Study of a Solar Combi-System. *Sol Energy* 2000; 69(Suppl.): 197–208.
[177] Jordan U, Vajen K. DHWcalc: Program to generate Domestic Hot Water profiles with statistical means for user defined conditions. In: *Proceedings of the Solar World Congress 2005: Bringing Water to the World, Including Proceedings of 34th ASES Annual Conference and Proceedings of 30th National Passive Solar Conference*, pp. 1525–1530.
[178] BDEW. Standardlastprofile Strom, https://www.bdew.de/energie/standardlastprofile-strom/ (accessed 18 December 2020).
[179] Kottek, M. & Rubel F (2012). Updated Köppen-Geiger climate classification, http://koeppen-geiger.vu-wien.ac.at/present.htm.
[180] ASHRAE. ASHRAE IWEC, https://www.ashrae.org/technical-resources/bookstore/ashrae-international-weather-files-for-energy-calculations-2-0-iwec2.
[181] Equa. ASHRAE IWEC weather files, http://www.equaonline.com/ice4user/new_index.html.
[182] Calise F, Cappiello FL, Dentice d'Accadia M, et al. Thermo-economic optimization of a novel hybrid renewable trigeneration plant. *Renew Energy* 2021; 175: 532–549.
[183] Wang J, Mao T, Wu J. Modified exergoeconomic modeling and analysis of combined cooling heating and power system integrated with biomass-steam gasification. *Energy* 2017; 139: 871–882.
[184] Tap water price, https://www.waternet.nl/en/service-and-contact/tap-water/costs/.
[185] Strom Report. Electricity Prices in Europe, https://strom-report.de/electricity-prices-europe/#electricity-prices-household-map (accessed 24 November 2021).
[186] Eurostat Statistics Explained. Natural gas prices for household consumers, https://ec.europa.eu/eurostat/statistics-

explained/index.php?title=File:Natural_gas_prices_for_household_consumers,_second_half_2020_(EUR_per_kWh)_v1.png (accessed 24 November 2021).
[187] Kaasuenergia S. Kaasulämmityksen hinnasto omakotitaloille, https://suomenkaasuenergia.fi/wp-content/uploads/2018/02/SK-Oy-ja-AK-Oy-Kotikulta-ja-Bio-Kotikulta-hinnasto.pdf (accessed 24 November 2021).
[188] Calderón C. European Bioenergy Outlook. In: *greenGrain project conference*. 2016, p. 15.
[189] Selectra. Autoconsumo con excedentes, https://selectra.es/autoconsumo/info/tarifas (accessed 24 November 2021).
[190] Commission de Régulation de l'Énergie. Le tarif de rachat photovoltaïque en 2021, https://news.dualsun.com/aide-fiscalite/tarif-rachat-photovoltaique/ (accessed 24 November 2021).
[191] Motiva. Ylijäämäsähkön myynti, https://www.motiva.fi/ratkaisut/uusiutuva_energia/aurinkosahko/aurinkosahkojarjestelman_kaytto/ylijaamasahkon_myynti (accessed 24 November 2021).
[192] Pantic LS, Pavlović TM, Milosavljević DD, et al. The assessment of different models to predict solar module temperature, output power and efficiency for Nis, Serbia. *Energy* 2016; 109: 38–48.
[193] Truong CN, Naumann M, Karl RC, et al. Economics of residential photovoltaic battery systems in Germany: The case of tesla's powerwall. *Batteries*; 2. Epub ahead of print 2016. DOI: 10.3390/batteries2020014.
[194] Azuatalam D, Paridari K, Ma Y, et al. Energy management of small-scale PV-battery systems: A systematic review considering practical implementation, computational requirements, quality of input data and battery degradation. *Renew Sustain Energy Rev* 2019; 112: 555–570.
[195] Olatomiwa L, Mekhilef S, Ismail MS, et al. Energy management strategies in hybrid renewable energy systems: A review. *Renewable and Sustainable Energy Reviews* 2016; 62: 821–835.
[196] Zhou B, Li W, Chan KW, et al. Smart home energy management systems: Concept, configurations, and scheduling strategies. *Renew Sustain Energy Rev* 2016; 61: 30–40.
[197] Leitao J, Gil P, Ribeiro B, et al. A Survey on Home Energy Management. *IEEE Access* 2020; 8: 5699–5722.
[198] Vázquez-Canteli JR, Nagy Z. Reinforcement learning for demand response: A review of algorithms and modeling techniques. *Applied Energy* 2019; 235: 1072–1089.
[199] Zhang H, Seal S, Wu D, et al. Data-driven Model Predictive and Reinforcement Learning Based Control for Building Energy Management: a Survey, http://arxiv.org/abs/2106.14450 (2021, accessed 30 November 2021).
[200] Winston W, Goldberg J. *Operations Research, Applications and Algorithms*. Fourth Edi. Thomson, www.duxbury.com (2004, accessed 11 May 2022).
[201] Antonopoulos I, Robu V, Couraud B, et al. Artificial intelligence and machine learning approaches to energy demand-side response: A systematic review. *Renew Sustain Energy Rev* 2020; 130: 109899.
[202] Wei Y, Zhang X, Shi Y, et al. A review of data-driven approaches for prediction and classification of building energy consumption. *Renew Sustain Energy Rev* 2018; 82: 1027–1047.
[203] DualSun, https://dualsun.com/en/ (accessed 4 October 2021).

[204] Gupta P, Singh R. PV power forecasting based on data-driven models: a review. *https://doi.org/101080/1939703820211986590* 2021; 14: 1733–1755.
[205] Abubakar Mas'ud A. Comparison of three machine learning models for the prediction of hourly PV output power in Saudi Arabia. *Ain Shams Eng J* 2022; 13: 101648.
[206] Theocharides S, Theristis M, Makrides G, et al. Comparative Analysis of Machine Learning Models for Day-Ahead Photovoltaic Power Production Forecasting. *Energies 2021, Vol 14, Page 1081* 2021; 14: 1081.
[207] Zazoum B. Solar photovoltaic power prediction using different machine learning methods. *Energy Reports* 2022; 8: 19–25.
[208] Alshafeey M, Csáki C. Evaluating neural network and linear regression photovoltaic power forecasting models based on different input methods. *Energy Reports* 2021; 7: 7601–7614.
[209] Mundada AS, Nilsiam Y, Pearce JM. A review of technical requirements for plug-and-play solar photovoltaic microinverter systems in the United States. *Sol Energy* 2016; 135: 455–470.
[210] Enphase, https://enphase.com/fr-fr (accessed 8 March 2022).
[211] Dolara A, Grimaccia F, Leva S, et al. Comparison of Training Approaches for Photovoltaic Forecasts by Means of Machine Learning. *Appl Sci 2018, Vol 8, Page 228* 2018; 8: 228.
[212] Matlab. Regression Neural Network, https://fr.mathworks.com/help/stats/regressionneuralnetwork.html (accessed 5 April 2022).
[213] Nageem R, Jayabarathi R. Predicting the Power Output of a Grid-Connected Solar Panel Using Multi-Input Support Vector Regression. *Procedia Comput Sci* 2017; 115: 723–730.

Appendices

Appendix A: Simulink model of the PVT collector

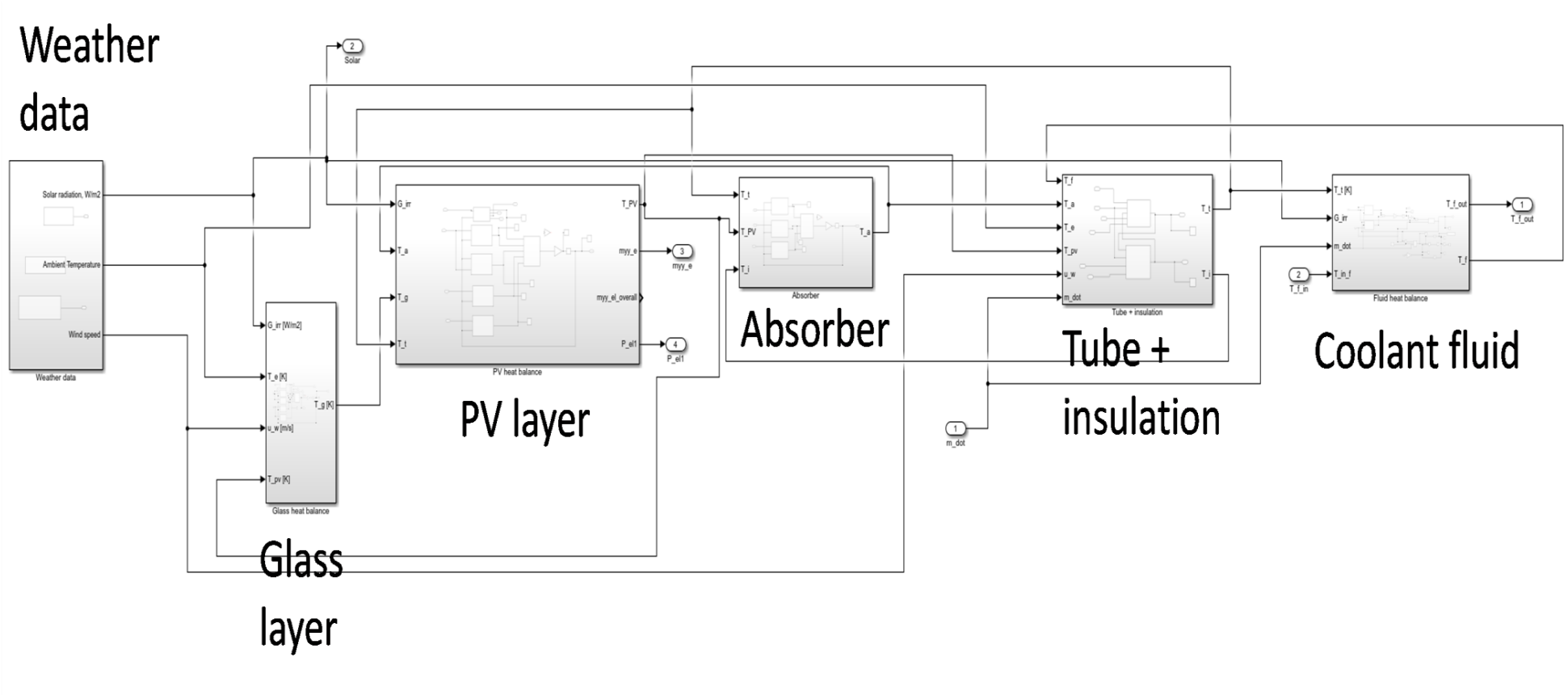

Figure A.1: Simulink layout of the PVT model.

Appendix B: Simulink model of the hybrid renewable energy system

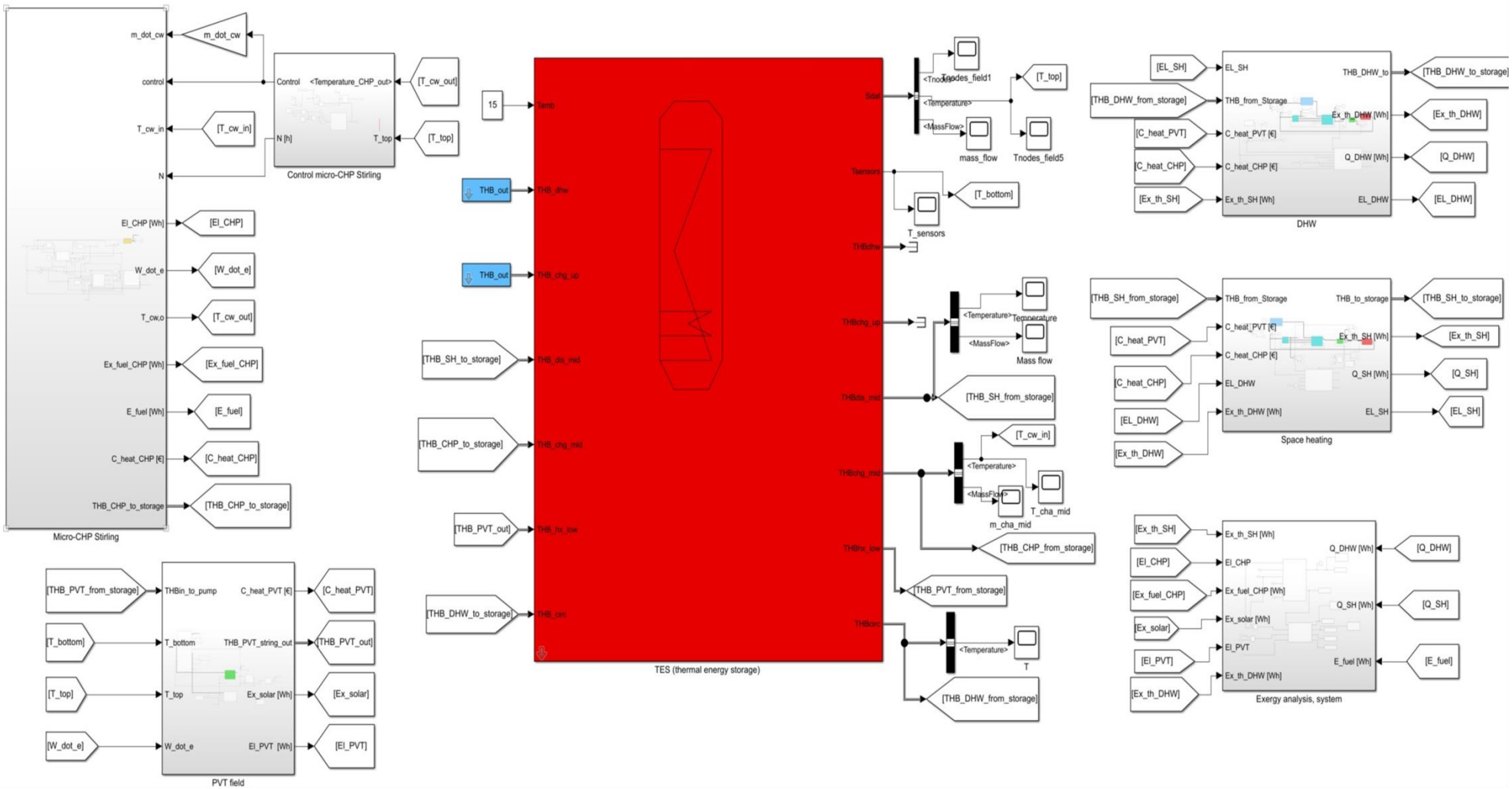

Figure B.1: Simulink layout of the HRES model built and used in Chapter 6.

Appendix C: Optimal control and simulation of the solar microgrid

C.1 Model parameters

```
%% The optimal control algorithm of Chapter 7 implemented in the section
%  3.2.2 Results of the optimization-based EMS simulation

% Parameters:
FWeight = 0.1;          % Final weight on energy storage
timeStep = 15;          % [min] Time step for optimization in 24 hours horizon
dt = timeStep*60;       % [s]
N = 96;                 % Number of the time steps
t_vec = (1:N)'*dt;      % Time vector for the plotting
t_hour = t_vec/3600;    % Time vector in hours
E_batt = 1.2*3.6e6;              % [J] Enphase battery capacity of the experimental
setup 1.2 kWh
E_batt_int = 0.05*E_batt;        % [J] Battery capacity at the beginning of the day
batt_bounds.Emax = 1*E_batt;     % [J] Max energy stored to the battery
batt_bounds.Emin = 0*E_batt;     % [J] Min energy stored to the battery
batt_bounds.Pmin = -270;         % [W] Max battery charge/discharge power
batt_bounds.Pmax = 270;          % [W] Min battery charge/discharge power

Ppv = pv_perfect_forecast;         % pv_perfect_forecast = pv production from the
experimental on 17th of May 2022.
Pload = Pload_perfect_forecast;    % Pload_perfect_forecast = electrical load from
the experimental on 17th of May 2022.

% Optimizing the battery charge/discharge
[Pgrid_b,Pgrid_s,Pbatt,E_batt] =
Optimisation_problem_Ch7(N,dt,Ppv,Pload,E_batt_int,C_buy,C_sell,FWeight,batt_bounds);

% Plot the results:
figure(1);
subplot(2,1,1);
grid on;
plot(t_hour,Ebatt/battEnergy*100); grid on;
xlabel('Time'); ylabel('SOC [%]')

subplot(2,1,2);
plot(t_hour,Ppv,t_hour,Pbatt,t_hour,Pgrid_b,t_hour,Pgrid_s,t_hour,Pload);
grid on;
legend('PV','Battery','From Grid','To Grid','Load')
xlabel('Time'); ylabel('Power [W]');
```

C.2 Optimization function

```
% Creating of the optimization function to minimize operating costs Eq. (5) of
Chapter
% 7.

function [Pgrid_b,Pgrid_s,P_batt,E_batt] =
Optimisation_problem_Ch7(N,dt,Ppv,Pload,E_batt_int,C_buy,C_sell,FWeight,batt_bounds)
```

```
prob = optimproblem('ObjectiveSense','minimize');

% Decision variables with lower and upper bounds of the grid connection and
% battery storage
Pgrid_sell = optimvar('Pgrid_sell',N,'LowerBound',-1500,'UpperBound',0);
Pgrid_buy = optimvar('Pgrid_buy',N,'LowerBound',0,'UpperBound',1500);
P_battVar =
optimvar('P_battVar',N,'LowerBound',batt_bounds.Pmin,'UpperBound',batt_bounds.Pmax);
E_battVar =
optimvar('E_battVar',N,'LowerBound',batt_bounds.Emin,'UpperBound',batt_bounds.Emax);

% Objective function aims to minimize the costs
prob.Objective = dt*C_buy'*Pgrid_buy + dt*C_sell'*Pgrid_sell - FWeight*E_battVar(N);

% Optimization constraints for the energy balance of the battery and to
% satisfy power balance of the system all the time.
prob.Constraints.energyBalance = optimconstr(N);
prob.Constraints.energyBalance(1) = E_battVar(1) == E_batt_int;
prob.Constraints.energyBalance(2:N) = E_battVar(2:N) == E_battVar(1:N-1) -
P_battVar(1:N-1)*dt;
prob.Constraints.powerBalance = Ppv + Pgrid_buy + Pgrid_sell + P_battVar == Pload;

% Solve the linear programming problem and arrange the results over the
% time horizon.
[values] = solve(prob);

Pgrid_b = values.Pgrid_buy;
Pgrid_s = values.Pgrid_sell;
P_batt = values.P_battVar;
E_batt = values.E_battVar;
```

Appendix D: Training of the machine learning models

The multiple linear regression (MLR) and artificial neural network (ANN) models of Chapter 8 were trained in the Matlab Regression Learner app. The following code of the function was automatically generated after the model training process implemented via the app. The following code presents the function to train the MLR model with the collected data presented in Chapter 8.

```
function [trainedModel, validationRMSE] = trainRegressionModel(trainingData)
% [trainedModel, validationRMSE] = trainRegressionModel(trainingData)
% Returns a trained regression model and its RMSE. This code recreates the
% model trained in Regression Learner app. Use the generated code to
% automate training the same model with new data, or to learn how to
% programmatically train models.
%
%  Input:
%      trainingData: A table containing the same predictor and response
%       columns as those imported into the app.
%
%  Output:
%      trainedModel: A struct containing the trained regression model. The
%       struct contains various fields with information about the trained
```

```
%       model.
%
%      trainedModel.predictFcn: A function to make predictions on new data.
%
%      validationRMSE: A double containing the RMSE. In the app, the Models
%       pane displays the RMSE for each model.
%
% Use the code to train the model with new data. To retrain your model,
% call the function from the command line with your original data or new
% data as the input argument trainingData.
%
% For example, to retrain a regression model trained with the original data
% set T, enter:
%   [trainedModel, validationRMSE] = trainRegressionModel(T)
%
% To make predictions with the returned 'trainedModel' on new data T2, use
%   yfit = trainedModel.predictFcn(T2)
%
% T2 must be a table containing at least the same predictor columns as used
% during training. For details, enter:
%   trainedModel.HowToPredict

% Auto-generated by MATLAB on 21-Jun-2022 14:59:12


% Extract predictors and response
% This code processes the data into the right shape for training the
% model.
inputTable = trainingData;
predictorNames = {'Ta', 'RH', 'WS', 'p', 'GHI', 'GTI_up', 'GTI_down'};
predictors = inputTable(:, predictorNames);
response = inputTable.P;
isCategoricalPredictor = [false, false, false, false, false, false, false];

% Train a regression model
% This code specifies all the model options and trains the model.
concatenatedPredictorsAndResponse = predictors;
concatenatedPredictorsAndResponse.P = response;
linearModel = fitlm(...
    concatenatedPredictorsAndResponse, ...
    'interactions', ...
    'RobustOpts', 'off');

% Create the result struct with predict function
predictorExtractionFcn = @(t) t(:, predictorNames);
linearModelPredictFcn = @(x) predict(linearModel, x);
trainedModel.predictFcn = @(x) linearModelPredictFcn(predictorExtractionFcn(x));

% Add additional fields to the result struct
trainedModel.RequiredVariables = {'GHI', 'GTI_down', 'GTI_up', 'RH', 'Ta', 'WS',
'p'};
trainedModel.LinearModel = linearModel;
trainedModel.About = 'This struct is a trained model exported from Regression Learner
R2021b.';
```

```
trainedModel.HowToPredict = sprintf('To make predictions on a new table, T, use: \n
yfit = c.predictFcn(T) \nreplacing ''c'' with the name of the variable that is this
struct, e.g. ''trainedModel''. \n \nThe table, T, must contain the variables returned
by: \n  c.RequiredVariables \nVariable formats (e.g. matrix/vector, datatype) must
match the original training data. \nAdditional variables are ignored. \n \nFor more
information, see <a href="matlab:helpview(fullfile(docroot, ''stats'',
''stats.map''), ''appregression_exportmodeltoworkspace'')">How to predict using an
exported model</a>.');

% Extract predictors and response
% This code processes the data into the right shape for training the
% model.
inputTable = trainingData;
predictorNames = {'Ta', 'RH', 'WS', 'p', 'GHI', 'GTI_up', 'GTI_down'};
predictors = inputTable(:, predictorNames);
response = inputTable.P;
isCategoricalPredictor = [false, false, false, false, false, false, false];

% Perform cross-validation
KFolds = 5;
cvp = cvpartition(size(response, 1), 'KFold', KFolds);
% Initialize the predictions to the proper sizes
validationPredictions = response;
for fold = 1:KFolds
    trainingPredictors = predictors(cvp.training(fold), :);
    trainingResponse = response(cvp.training(fold), :);
    foldIsCategoricalPredictor = isCategoricalPredictor;

    % Train a regression model
    % This code specifies all the model options and trains the model.
    concatenatedPredictorsAndResponse = trainingPredictors;
    concatenatedPredictorsAndResponse.P = trainingResponse;
    linearModel = fitlm(...
        concatenatedPredictorsAndResponse, ...
        'interactions', ...
        'RobustOpts', 'off');

    % Create the result struct with predict function
    linearModelPredictFcn = @(x) predict(linearModel, x);
    validationPredictFcn = @(x) linearModelPredictFcn(x);

    % Add additional fields to the result struct

    % Compute validation predictions
    validationPredictors = predictors(cvp.test(fold), :);
    foldPredictions = validationPredictFcn(validationPredictors);

    % Store predictions in the original order
    validationPredictions(cvp.test(fold), :) = foldPredictions;
end

% Compute validation RMSE
isNotMissing = ~isnan(validationPredictions) & ~isnan(response);
validationRMSE = sqrt(nansum(( validationPredictions - response ).^2) /
numel(response(isNotMissing) ));
```